National and Kapodistrian
University of Athens
Faculty of Biology
Department of Botany

Mechanisms of subcellular membrane trafficking

Subtitle: The unexpected pleiotroptic functional role of cytoplasmic tails of the Fur transporters

Ph.D. THESIS

Georgia F Papadaki

BIOLOGIST

ATHENS 2021

Εθνικό και Καποδιστριακό
Πανεπιστήμιο Αθηνών
Τμήμα Βιολογίας
Τομέας Βοτανικής

Μηχανισμοί υποκυτταρικής διακίνησης μεμβρανικών πρωτεϊνών

Υπότιτλος: Ο πλειοτροπικός λειτουργικός ρόλος των κυταροπλασματικών άκρων των μεταφορέων της οικογένειας Fur

ΔΙΔΑΚΤΟΡΙΚΗ ΔΙΑΤΡΙΒΗ

Παπαδάκη Φ Γεωργία

Βιολόγος

ΑΘΗΝΑ 2021

«Η έγκριση της Διδακτορικής Διατριβής από το Τμήμα Βιολογίας της Σχολής Θετικών Επιστημών του ΕΚΠΑ δεν υποδηλώνει αποδοχή των απόψεων του συγγραφέα (Ν. 5343/1932, άρθρο 202)»

Advisory Committee

G. Diallinas, Professor, University of Athens (Supervisor)

B. André, Professor, Université Libre de Bruxelles

E. Mikros, Professor, University of Athens

Examining Committee

G. Diallinas, Professor, University of Athens (Supervisor)

B. André, Professor, Université Libre de Bruxelles

E. Mikros, Professor, University of Athens

C. Vorgias, Professor, University of Athens

D. Hatzinikolaou, Associate Professor, University of Athens

E. Frillingos, Professor, University of Ioannina

C. Gournas, Associate Researcher, National Centre for Scientific Research "Demokritos"

This research has been financed by the Stavros Niarchos Foundation (SNF)

Τριμελής Συμβουλευτική Επιτροπή

Γ. Διαλλινάς, Καθηγητής Πανεπιστημίου Αθηνών (Επιβλέπων)

B. André, Καθηγητής, Université Libre de Bruxelles

Ε. Μικρός, Καθηγητής Πανεπιστημίου Αθηνών

Επταμελής Εξεταστική Επιτροπή

Γ. Διαλλινάς, Καθηγητής Πανεπιστημίου Αθηνών (Επιβλέπων)

B. André, Καθηγητής, Université Libre de Bruxelles

Ε. Μικρός, Καθηγητής Πανεπιστημίου Αθηνών

Κ. Βοργιάς, Καθηγητής Πανεπιστημίου Αθηνών

Δ. Χατζηνικολάου, Αναπληρωτής Καθηγητής Πανεπιστημίου Αθηνών

Ε. Φριλίγγος, Καθηγητής Πανεπιστημίου Ιωαννίνων

Χ. Γουρνάς, Ερευνητής Γ', ΕΚΕΦΕ "Δημόκριτος"

Η παρούσα έρευνα έχει χρηματοδοτηθεί από το Ίδρυμα Σταύρος Νιάρχος (ΙΣΝ)

This dissertation is dedicated to my favorite person,
my grandmother

ΠΕΡΙΛΗΨΗ

Οι μεταφορείς, είναι διαμεμβρανικές πρωτεΐνες μέσω των οποίων πραγματοποιείται η διακίνηση θρεπτικών συστατικών, μορίων σηματοδοτών ή άλλων ουσιών εντός και εκτός του κυττάρου. Αυτό τις καθιστά απαραίτητα μόρια για την επικοινωνία του κυττάρου με το περιβάλλον. Τα τελευταία χρόνια, γενετικά, βιοχημικά και βιοφυσικά δεδομένα που προέρχονται από τη μελέτη αρκετών μεταφορέων, συνέβαλλαν στην κατανόηση των σχέσεων δομής-λειτουργίας και των μηχανισμών αναγνώρισης και μεταφοράς υποστρώματος. Παρά τις εξελικτικές, δομικές και λειτουργικές διαφορές τους, όλοι οι μεταφορείς χρησιμοποιούν έναν κοινό μηχανισμό εναλλασσόμενης πρόσβασης, όπου μια θέση πρόσδεσης υποστρώματος εναλάσσεται μεταξύ πολλαπλών διαμορφώσεων προκειμένου να μεταφέρει ένα υπόστρωμα από τη μία πλευρά της μεμβράνης στην άλλη. Αυτός ο βασικός μηχανισμός που διεξάγεται από δυναμικές κινήσεις του κύριου διαμεμβρανικού σώματος και υποβοηθείται από την ευελιξία υδρόφιλων βρόχων, συναντάται σε διάφορες παραλλαγές, γνωστές ως rocker-switch, rocking-bundle και μηχανισμός elevator.

Μία από τις μεγαλύτερες οικογένειες δευτερογενών μεταφορέων είναι η υπεροικογένεια amino acid/polyamine/organocation (APC), η οποία περιλαμβάνει μεταφορείς που λειτουργούν ως συμμεταφορείς διαλυτής ουσίας-κατιόντος και αντιμεταφορείς διαλυτών ουσιών με μεγάλη ποικιλία υποστρωμάτων. Η οικογένεια Nucleobase Cation Symporter 1 (NCS1) αποτελεί μία από τις πιο καλά μελετημένες υποοικογένειες της APC υπεροικογένειας, και εκπρόσωποί της συναντώνται σε προκαρυωτικούς οργανισμούς, μύκητες και μερικά φυτά. Αυτό οφείλεται στην πληθώρα γενετικών και βιοχημικών δεδομένων που αφορούν μέλη της οικογένειας σε μύκητες, καθώς και σε εκτεταμένες δομικές και βιοφυσικές μελέτες ενός βακτηριακού ομολόγου, του συμμεταφορέα υδαντοΐνης/Na^+, Mhp1. Η οικογένεια NCS1 δεν έχει αντιπροσώπους στα θηλαστικά, κάτι που την καθιστά ιδανική για τη στόχευση ειδικών φαρμάκων κατά των μικροβιακών παθογόνων. Οι μεταφορείς της οικογένειας NCS1 αποτελούνται από 12 διαμεμβρανικά τμήματα (ΔΤ) με δομή α-έλικας, που συνδέονται με σχετικά μικρές ενδιάμεσες αλληλουχίες και έχουν κυτταροπλασματικά αμινο- και καρβοξυτελικά άκρα. Τα ΔΤ1-10 οργανώνονται σε μια δομή ανεστραμμένης επανάληψης ανά 5 (5-helix intertwined inverted repeat; 5HIRT) που ονομάζεται αλλιώς και LeuT-fold, και συναντάται σε μεταφορείς πολλών διαφορετικών οικογενειών που εμπλέκονται στη μεταφορά νευροδιαβιβαστών, σακχάρων, αμινοξέων ή φαρμάκων. Τα δύο τελευταία διαμεμβρανικά τμήματα (11 και 12) μερικών μεταφορέων που έχουν παρόμοια δομή με τον LeuT, φαίνεται να εμπλέκονται

στον ολιγομερισμό, παρά στο μηχανισμό λειτουργίας τους αυτό καθαυτό. Παρόλα αυτά, δεν υπάρχουν επαρκή δεδομένα για το δομικό ή/και λειτουργικό τους ρόλο.

Μεταφορείς που ανήκουν στην οικογένεια NCS1 στους μύκητες, είναι από τους πιο καλά μελετημένους σε γενετικό, βιοχημικό και κυτταρικό επίπεδο. Δομικά μοντέλα μυκητιακών μεταφορέων NCS1 βασίζονται σε πολλές διακριτές κρυσταλλικές δομές του βακτηριακού ομολόγου Mhp1 και υποστηρίζονται από γενετικές μελέτες που προκαθόρισαν τη θέση δέσμευσης του υποστρώματος και τα πιθανά στοιχεία που δρουν σαν πύλες, καθορίζοντας την εξειδίκευση. Πιο συγκεκριμένα, ένα σημαντικό εύρημα που προέρχεται από έρευνα του εργαστηρίου μας πάνω στους μυκητιακούς μεταφορείς της NCS1 οικογένειας (τόσο σε μέλη της Fcy όσο και της Fur υποοικογένειας) είναι ότι η εξειδίκευση δεν καθορίζεται μόνο από κατάλοιπα που βρίσκονται στο σημείο πρόσδεσης του υποστρώματος (ΔΤ1, ΔΤ3, ΔΤ6 ή ΔΤ8) αλλά και από δυναμικές κινήσεις του τμήματος ΔΤ9-ΔΤ10 που δρα σαν εξωκυτταρική πύλη.

Σε αυτή τη διατριβή, παρέχουμε πειραματικά και *in silico* δεδομένα που αποδεικνύουν ότι η ενδοκύτωση, η λειτουργία και περιέργως η εξειδίκευση του FurE, ενός μεταφορέα του *Aspergillus nidulans* που ανήκει στην NCS1 οικογένεια και μεταφέρει ουρακίλη-αλλαντοΐνη και ουρικό οξύ, εξαρτάται από δυναμικές αλληλεπιδράσεις των άμινο- και καρβοξυτελικών άκρων μεταξύ τους και με το βασικό σώμα του μεταφορέα. Πιο συγκεκριμένα, τα καρβοξυτελικά άκρα εμπλέκονται σε ενδομοριακές δυναμικές αλληλεπιδράσεις που είναι απαραίτητες για την εκλεπτυσμένη ρύθμιση των πυλών που ελέγχουν την επιλογή των υποστρωμάτων. Πραγματοποιώντας Μοριακές Δυναμικές (ΜΔ) και αναλύσεις μεταλλαγών στο γονίδιο του μεταφορέα, υποθέσαμε ότι αυτό συμβαίνει μέσω αλληλεπιδράσεων των κυτταροπλασματικών ουρών με ενδοκυττάριες θηλιές, οι οποίες με τη σειρά τους επηρεάζουν τη διαδικασία διαλογής υποστρωμάτων μέσω των πυλών στην εξωκυττάρια πλευρά της πλασματικής μεμβράνης. Επιπρόσθετα, τα αποτελέσματά μας έδειξαν ότι αυτές οι αλληλεπιδράσεις εξαρτώνται άμεσα από το pH.

Στη συνέχεια, αξιοποιώντας τις πληροφορίες από εκτεταμένες αναλύσεις ΜΔ, πραγματοποιήσαμε συστηματική και στοχευμένη λειτουργική ανάλυση μεταλλαγών στο μόριο του μεταφορέα FurE, προκειμένου να χαρακτηρίσουμε το μονοπάτι μετατόπισης του υποστρώματος κατά τη διάρκεια της μετάβασής του από τις διακριτές διαμορφώσεις του. Επιπροσθέτως, παρέχουμε πειραματικά στοιχεία που δείχνουν πως η ταυτότητα των αμινοξέων που απαρτίζουν τα δύο τελευταία ΔΤ του FurE, δεν καθορίζει την κατάλυση της μεταφοράς. Ωστόσο, ένα συντηρημένο κατάλοιπο τυροσίνης είναι απολύτως απαραίτητο για τη σωστή στόχευση του μεταφορέα στην πλασματική μεμβράνη.

Στο τελευταίο μέρος αυτής της δουλειάς, συνδυάζουμε βιοφυσικές τεχνικές και υπολογιστικές μεθόδους για να καταλάβουμε σε βάθος το μηχανισμό που διέπει το λειτουργικό

ρόλο των κυτταροπλασματικών άκρων στη διαλογή και μεταφορά του υποστρώματος, κάτι που φαίνεται να αντικατοπτρίζει ένα γενικότερο μηχανισμό που χαρακτηρίζει τους μεταφορείς της APC υπεροικογένειας. Το σύνολο της διατριβής αυτής, υποστηρίζει την ευρύτερη ιδέα ότι το μέγεθος των άκρων των ευκαρυωτικών μεταφορέων αυξήθηκε κατά τη διάρκεια της εξέλιξης, προσδίδοντας περισσότερους διακριτούς τρόπους ρύθμισης της λειτουργίας τους.

ABSTRACT

Transporters are membrane proteins that mediate the import and export of nutrients, metabolites, signaling molecules or drugs in and out of cells, and thus are essential for their communication with the environment. In the recent years, genetic, biochemical and biophysical data for several transporters have come to provide us with new knowledge concerning structure-function relationships and mechanisms of substrate recognition and transport. Despite their evolutionary, structural and functional differences all transporters use an alternating-access mechanism where a substrate binding site, in allosteric co-operation with gating domains, alternates between multiple conformations for receiving and delivering specific substrate(s) from one side of the membrane to the other. This basic mechanism, carried out by dynamic movements of the main transmembrane body and assisted by the flexibility of interconnecting hydrophilic loops, exists in different variations, known as the rocker-switch, the rocking-bundle or the elevator sliding mechanisms.

One of the largest families of transporters is the amino acid/polyamine/organocation (APC) superfamily, which includes members that function as solute:cation symporters and solute:solute antiporters with varying specificities. The Nucleobase Cation Symporter 1 (NCS1) family consists one of the best-studied subfamilies of the APC superfamily and is present in prokaryotes, fungi and some plants. This is due to a plethora of genetic and biochemical findings concerning fungal members of the family, as well as, extensive structural and biophysical data concerning a bacterial homologue, namely the benzyl-hydantoin/Na^+ Mhp1 symporter. Absence of NCS1 homologues in mammals makes this family an ideal, highly specific gateway to target nucleobase-specific drugs to microbial pathogens. NCS1 proteins consist of 12 transmembrane α-helical segments (TMS) interconnected with rather short loops and cytosolic N- and C-termini. TMSs 1-10 are arranged as a 5-helix intertwined inverted repeat (5HIRT), the so called LeuT-fold, also found in different transporter families involved in neurotransmitter, sugar, amino acid or drug transport. The last two TMSs (11 and 12) in all LeuT-like proteins seem to be crucial for the oligomerization state of some NCS1-similar transporters, rather than being involved in the mechanism of transport. However, formal evidence for their structural and/or functional role is missing.

Fungal NCS1 proteins are among the best-studied transporters at a genetic, biochemical and cellular level. Structural models of fungal NCS1 transporters, based on several distinct crystal structures of the bacterial homologue Mhp1 are fully supported by genetic studies that identify the substrate binding site and putative gating elements determining specificity. More specifically, a major novel finding that has originated from our work on fungal NCS1 transporters (both on Fur and Fcy

members) is that substrate specificity is determined not only by residues of the substrate binding site (TMS1, TMS3, TMS6 or TMS8), but also by dynamic movements of the TMS9-TMS10 region, acting as an outward-facing gate.

In work described herein, we provide experimental and *in silico* evidence that the turnover, function, and interestingly, the specificity of an *Aspergillus nidulans* NCS1 homologue, namely the FurE uracil-allantoin-uric acid transporter, depends on dynamic interactions of the N- and C-terminal cytoplasmic regions with each other and the main body of the transporter. We specifically show that the N- and C-terminal domains of FurE are involved in intramolecular dynamics critical for the fine regulation of the mechanism of gating that controls substrate selection. Using Molecular Dynamics (MD) and mutational analysis we postulate that this occurs via interactions of the cytoplasmic tails with the cytoplasmic loops, which in turn affect the gating process at the extracellular side of the plasma membrane (PM) in a pH-dependent manner.

Next, using the information from extensive MD analysis, we performed a targeted systematic mutational and functional analysis to characterize the substrate translocation trajectory in FurE, during its transition from the outward-open to the inward-open conformation. Additionally, we provide experimental evidence that the nature of the amino acid residues of the last two transmembrane domains of FurE is not critical for the transport catalysis. However, a single tyrosine residue is absolutely necessary for the proper trafficking of the transporter to the plasma membrane.

Finally, in the last part of this work we wanted to combine biophysical techniques and computational modeling in order to better understand the mechanism underlying the functional role of cytoplasmic tails in substrate selection and translocation, which seems to reflect a more general mechanism that controls APC transporters. In general, our work supports the emerging concept that the size of eukaryotic transporter termini increased during evolution and adds more and different modes of regulation.

Keywords: *Aspergillus nidulans;* fungi; FurE; genetics; gating; transport; folding; cytoplasmic termini; substrate; specificity

ACKNOWLEDGEMENTS

There are many people whom I would like to thank for their direct or indirect contribution to this thesis but first and foremost, my supervisor Prof. George Diallinas. Counting more than five years, I have never met anyone who is more involved and caring. Always available for support and guidance whenever you needed him, in the fastest way possible! I thank him for trusting me, for giving me the opportunity to fail at times, to expand my skills and my limits and supporting me as my career goals evolved through these years. He certainly gave me a lot and I can dive into the future with more confidence and courage, no matter what I do.

To my thesis advisory committee, I would like to thank them for challenging my knowledge and guiding me as my thesis developed. Individually, I would like to thank Prof Emmanuel Mikros for the great collaboration all these years and Prof Bruno André, for his help and for actually being the first person I presented my work as a student, long before taking the decision to continue as a PhD candidate.

I would also like to thank my external committee, Prof. Dimitris Hatzinikolaou who I met the first day I started my undergraduate thesis and his presence was always delightfully unique; Prof. Constantinos E. Vorgias who was more than willing to help me in a rather stressful period and I am really grateful; Dr Christos Gournas who is not only an excellent scientist, but also a person and we are very lucky to have him back in Athens; and last but not least Prof. Stathis Frillingos for accepting to be part of this work and for his helpful contribution.

I am indebted to Dr Sotiris Amillis for his constructive scientific guidance, for always being there and for being part of this work even from the very beginning. I owe special thanks to all the people who laid a little stone to carry out this work: Emmanuel Mikros, George Lambrinidis, Andreas Zamanos and Iliana Zantza. I would also like to express my gratitude to Stavros Niarchos Foundation, as without their financial support throughout all these years, it would have been impossible to conduct this research.

I wish to acknowledge Prof. Per Ljungdahl, who I very much appreciate and has helped me a lot before even starting this journey as well as all the people in his lab: Antonio, Andreas, Fitz, Kicki, Mel who made me realize how important is to have the most amazing, crazy and fun lab mates! This brings me to all the people in our lab that I have worked with in the past: Georgia S., Khoar, George, Olga, Yiannis Theologidis and especially Sofia Balaska; as well as the younger members Vaggelis, Marco, Valentina, Pothos and Konstantina. Thank you all for all the unforgettable moments -in and out of the lab- we spent together. I specially thank everyone from the Microbiology team and Nancy for being available and willing to help me or advise me every time I needed them and for all the fun we had during these years.

I am deeply grateful to the best partners in crime, my current lab mates! Sofia, Anzie, and Mariangela. We shared great moments of laughter, tears, anger and laughter again. You helped me a lot and I will always remember you as my best team!! Going a bit further, only a corridor away, I want to thank two beautiful creatures, Irene and Andreas B. for the great lunch meetings and the crazy moments we shared, especially the past year. You are unique people and I definitely owe you more than a few windsurf lessons. I can’t wait to call you doctors soon, soon!!

Ioanna, no words can describe how much I appreciate you and how much you have helped me all these years poulaki, but you do know... Marco, I have no idea what brought us together but I feel super lucky to have met you! Both of you may be away but every time is like we were never apart. Sofia and Spyros, we have shared so many unforgettable moments in such a short period of time that it's really hard to believe! Not a single time have I felt uncomfortable, fed up or scared of anything when I'm with you. I admire and love you guys! Maria D., same goes for you, you are one of a kind and I really appreciate our moments! Grigoria, George, Vivi and Maria S., I cherish all the hours we spent talking, playing and…playing again! I truly wish you the best in the new journeys you begun or will begin soon cause you deserve it. You are all special and I am very lucky to have you. Of course, I could not fail to mention my friends Arietta, Athina, Tonia, Dimos, Danai, Manos for all the great moments we spent all these years and I wish them all the best in what lies ahead.

Last but not least, a big thank you to my parents Filippos & Mania, my sister Myrto, my aunt and of course my favorite person, my beloved grandmother. You were always there supporting me and enduring me when I was all grumpy. What I appreciate the most though, is that every time you made me laugh with my heart and this gave me great strength to keep going.

Well, as a final note I want to say that the last year was definitely something! Hopefully, 2020 made us realize that we should not take anything for granted, that people come and go but fortunately for me, I have met quite a few that will definitely stay and I cannot be more grateful.

-Here is to spreading kindness and creativity around!

gfp.

Contents

ABBREVIATIONS

ADHD	Attention Deficit Hyperactivity Disorder
ALL	Allantoin
APC	Amino acid-polyamine-organoCation Superfamily
ATP	Adenosine Triphosphate
BiFC	Bifluorescence Complementation Assays
CHS	Cholesterol Hemisuccinate
CIAP	Calf Intestine Alkaline Phosphatase
Cryo-EM	Transmission Electron Cryomicroscopy
ΔACZ	uapAΔ uapCΔ azgAΔ strain
DEER	Double Electron-Electron Resonance
DTT	Dithiothreitol
DUBs	De-ubiquitinating enzymes
EDTA	Ethylenediaminetetraacetic Acid
EL	Extracellular Loop
EPR	Electron Paramagnetic Resonance
ER	Endoplasmic Reticulum
ERG	Ergosterol
EtOH	Ethanol
FRET	Fluorescence Resonance Energy Transfer
GFP	Green Fluorescent Protein
*gpd*Ap	Glyceraldehyde-3-phosphate Dehydrogenase Promoter
h	Hour
IL	Internal Loop
K_m	Michaelis-Menten constant
L	Loop
LID	Loop Interacting Domain
MD	Molecular Dynamics
MFS	Major Facilitator Superfamily
Min	Minute
MM	Minimal Media
mRFP	Monomeric Red Fluorescent Protein
MTSSL	Methanethiosulfonate-functionalized nitroxide
NAT	Nucleobase Ascorbate Transporter
NCS1	Nucleobase Cation Symporter family 1
NCS2	Nucleobase Cation Symporter family 2
NMR	Nuclear Magnetic Resonance
NSS	Neurotransmitter:Sodium Symporter
^{o}C	Celsius degrees
OCD	obsessive-compulsive disorder
ORF	Open Reading Frame
paba	p-aminobenzoic acid
panto	D-pantothenic acid
PC	phosphatidylcholine
PCR	Polymerase Chain Reaction
PEG	Polyethylene Glycol
PELDOR	Pulsed Electron-Electron Double Resonance
PIP2	Phosphatidylinositol (4,5)-biphosphate lipids
PM	Plasma Membrane
POPI	phosphatidylinositol lipids
ribo	Riboflavin
RMSD	Root-Mean-Square Deviation
ROI	Region of Interest
Rpm	Rounds per minute
RT	Room Temperature
SD	Synthetic Minimal Dextrose
SDS	Sodium Dodecyl Sulfate
SDS-PAGE	Sodium Dodecyl Sulfate Polyacrylamide Gel Electrophoresis
sec	Second

SLC	Solute Carrier
SSS	Solute Sodium Symporter
TCA	Trichloroacetic Acid
TCDB	Transporter Classification Database
Tm	Melting Temperature
TMS	Transmembrane segment
UA	Uric Acid
Ub	Ubiquitin
Ura	Uracil
UV	Ultraviolet
WT	Wild type
XAN	Xanthine
YFP	Yellow Fluorescent Protein
YPD	Yeast Extract Peptone Dextrose
5FC	5-fluorocytosine
5FU	5-fluorouracil
5HIR	Five-Helix Inverted Repeat

CHAPTER 1

INTRODUCTION

1.1 The genus *Aspergillus* & the model fungus *Aspergillus nidulans*

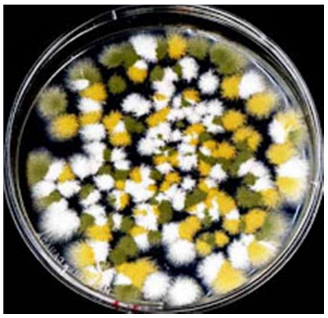

Figure 1.1 *Color mutants of Aspergillus nidulans grown in a petri dish (courtesy of R. Fischer, http://www.fgsc.net/).*

Aspergillus nidulans is a homothallic, filamentous fungus of the genus Aspergilli under the phylum of Ascomycota, one of the largest phyla of the Fungi Kingdom. Counting more than 64000 species, it includes a wide range of fungi, from unicellular yeasts to fairly large moulds and truffles (Kirk et al., 2008). Phylogenetic studies divide the phylum of Ascomycota in three subphyla: the Pezizomycotina (Ascomycotina) that contains *Aspergillus nidulans* along with most of Ascomycetes that produce ascocarps, the Saccharomycotina that contains most of the true yeast and the basal group Taphrinomycotina (Kirk et al., 2008; Lutzoni et al., 2004). The primary morphological feature that distinguishes members of Ascomycota is the formation of the ascus, a saclike cell which contains eight ascospores, formed by one meiosis and a subsequent mitotic division. Filamentous Ascomycetes are characterized by a compartmentalized mycelium with distinctive walls that generate from the hyphal periphery and are called septa. A small circular pore in the center of the septa allows cytoplasm, nuclei, organelles and metabolites to migrate from one hyphal compartrment to the next (Alexopoulos et al., 1996). The term 'homothallic' refers to the absence of mating types due to the ability of a single organism to reproduce sexually.

The genus of Aspergilli was first described in 1729 by the Italian priest and botanist Pietro Antonio Micheli and was named after an instrument called Aspergillum, which was used in the Roman Catholic clergy to sprinkle holy water over the heads of the faithful. Several species of the genus are of medical and commercial importance. Particularly, *A. niger* is used for citric acid, amylase, invertase and other enzymes production and *A. oryzae* has been used in food fermentation especially in the East Asian cuisines. However, some species function as opportunistic pathogens causing a group of diseases known as Aspergilloses. For instance, *A. fumigatus* is the most frequent cause of invasive fungal infection in immunosuppressed individuals; *A. flavus* produces a toxic chemical compound (aflatoxin B1) that can contaminate grains before harvest or during storage. *Aspergillus nidulans*, belongs in subphylum Pezizomycotina, class Eurotiomycetes, order Eurotiales, family Aspergillaceae (Houbraken et al., 2014; Kirk et al., 2008). As many other fungal species, it was

initially named after its asexual stage (anamorph) and then correlated to a sexual stage (teleomorph) with a different genus name. Since 1905 the Botanical Code has allowed dual nomenclature for the same organism but when the sexual phase is discovered, this name takes precedence. For this reason, *Aspergillus nidulans* is indexed as *Emericella nidulans* within GenBank after *Emericella,* the name of the cleitothecium which is the fruiting body of the sexual reproductive stage of Pezizomycotina.

1.1.1 Life cycle of A. nidulans

Aspergillus nidulans has a complex life cycle that can be divided into three reproductive sub-cycles: the asexual, the sexual and the parasexual.

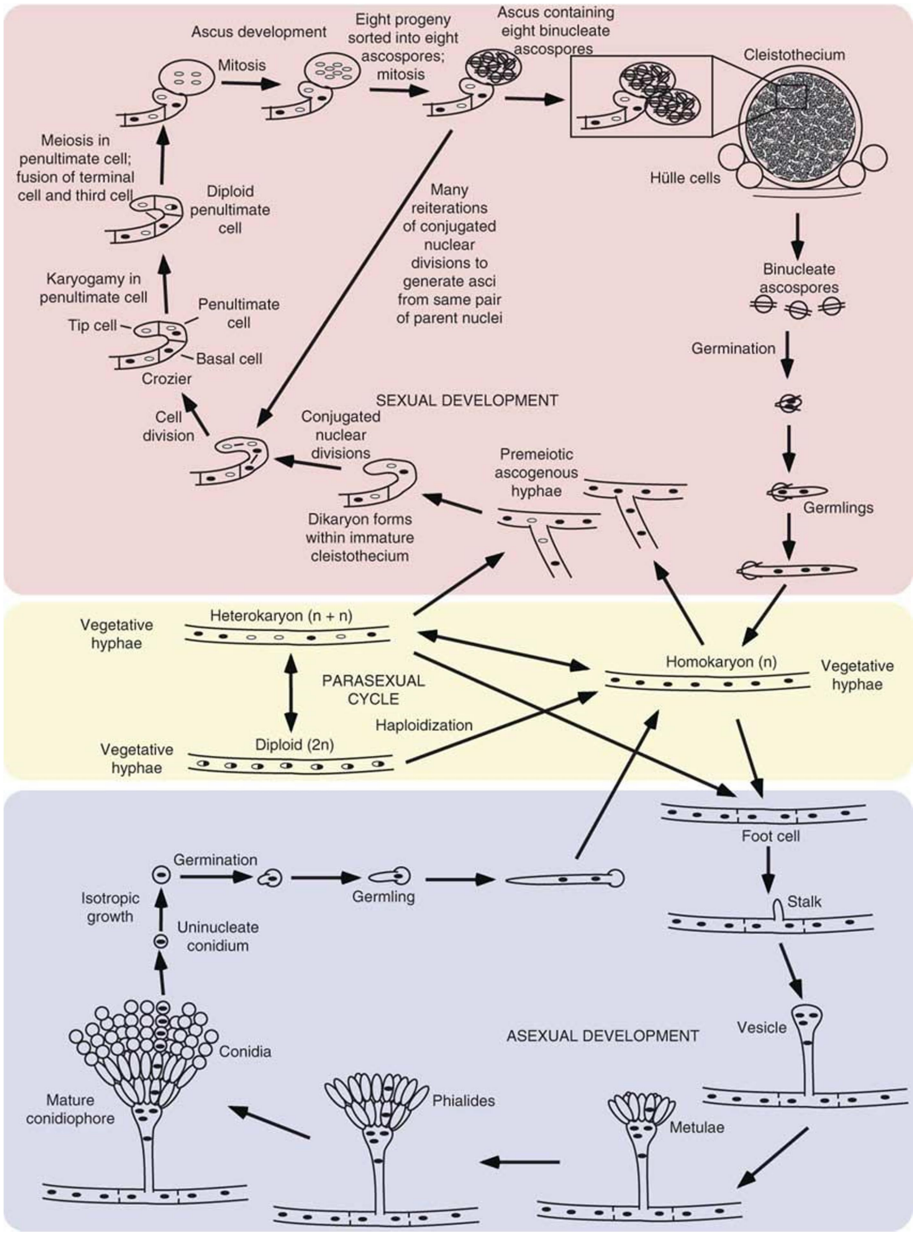

Figure 1.2 *Diagrammatic representation of A. nidulans life cycle (Todd et al., 2007).*

In the asexual reproductive cycle a single, uninucleate cell called conidiospore, germinates and produces multicellular hyphae. Under favorable for development environmental conditions (i.e. air, light) some hyphal cells differentiate into footcells from which long stalks (70 μM) emerge. At their end, a vesicle is formed which produces a layer of metulae, each of them produces 2-3 phialidae which in turn produce mitotically long chains of conidiospores. The conidiospores are dispersed and initiate another asexual cycle (Bayram et al., 2010; Todd et al., 2007).

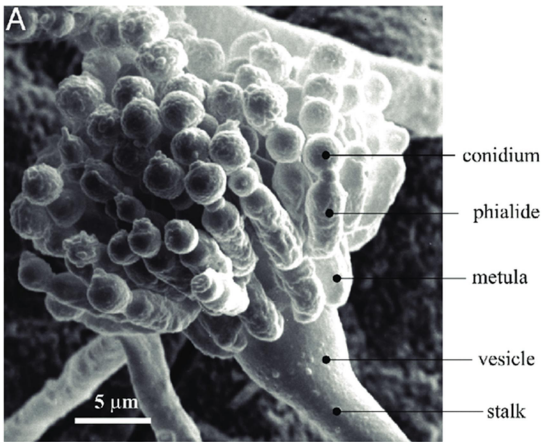

Figure 1.3 *Scanning micrograph of a conidiophore with nomenclature of the different specialized cells (Peñalva et al., 2012).*

The sexual cycle can be triggered under various stress conditions, such as lack of nutrient supply or environmental stress. In this case, two individual hyphae may fuse to form a heterokaryon (contains nuclei from both parental strains). The end of an ascogenous heterokaryon can comprise a final uninucleate tip cell, a binucleate penultimate cell and a uninucleate basal cell. Enlargement of the penultimate cell and eventually fusion of the two haploid nuclei (karyogamy), leads to the formation of a transient diploid zygote that undergoes meiotic and mitotic divisions. The four nuclei produced are mitotically divided, producing eight ascospores in the ascus. The nucleus in each ascospore undergoes mitosis, resulting in mature binucleate ascospores. The terminal and basal cells fuse to generate a binucleate cell which will eventually form a second ascus by repeating the process (Todd et al., 2007). All the asci are dispersed in cleistothecia which are surrounded by thick-walled nursing Hülle cells. A mature cleistothecium can contain more than 10,000 binucleate ascospores that lead to the reinitiation of the vegetative growth and the continuation of the lifecycle.

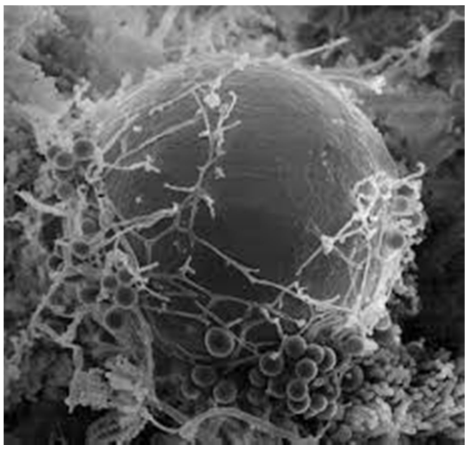

Figure 1.4 *Image of an A. nidulans cleistothecium as seen by scanning electron microscopy (https://www.aspergillus.org.uk/, courtesy of R. Fischer).*

In the parasexual cycle and at the stage of the heterokaryon formation two haploid nuclei are fused with a probability of 10^{-6} to form relatively stable heterozygous diploid nuclei. These vegetative nuclei can give rise to a

mitotically dividing mycelium via the asexual cycle. Haploid and diploid mycelia share the same architecture, but the first contain half the number of nuclei.

1.1.2 A. nidulans as a model organism

Aspergillus nidulans has been established as a model system for the study of genetics since the 1940s by Guido Pontecorvo, and already in 1953 and 1983 genetic crossing techniques and transformation protocols were developed, while in 2005 its genome was sequenced in collaboration between the Broad Institute and Monsanto (Galagan et al., 2005). With a total size of 30 million base pairs, it has eight chromosomes containing around 9,500 protein-coding genes with many auxotrophic, drug resistance and color markers. Its genes can be cloned, expressed under the control of regulatable promoters, deleted at will, disrupted or altered. The conidiospores are in haploid form, which enables the direct screening of mutants or transformants by plating on appropriate media but also heterokaryons and stable diploids can be produced under stress, enabling the complementation analysis for mutations. Moreover, *Aspergillus nidulans* grows rapidly on inexpensive media under a variety of nutritional conditions and produces conidia or ascospores that can be stored for long periods of time at low temperatures. The morphology of the colonies formed on solid media (shape, colour and sporulation) can provide vital information on the essentiality of the studied genes. Additionally, chimeric protein molecules tagged with fluorescent epitopes can be easily constructed with molecular cloning and expressed stably in *A. nidulans* transformants, for further *in vivo* observation under epifluorescence microscopy. Finally, *A. nidulans* is closely related to many other *Aspergillus* species which are of medical and industrial interest, such as *A. flavus, A. oryzae, A. niger* and *A. fumigatus,* that are exploited experimentally using technologies developed for *A. nidulans* (Scazzocchio, 2006).

1.2 Transport proteins: Channels vs Transporters

Biological membranes define the boundaries of the cells and ensure the controlled communication between the cytosol and the extracellular environment, features that make them indispensable for their survival. The inner membranes of the endoplasmic reticulum (ER), Golgi apparatus, mitochondria and other membrane bounded organelles of eukaryotic cells maintain the characteristic differences between the contents of each organelle and the cytosol (Alberts, 1994). Nevertheless, they all share a common general structure that consists of a thin, continuous lipid bilayer, proteins and carbohydrates.

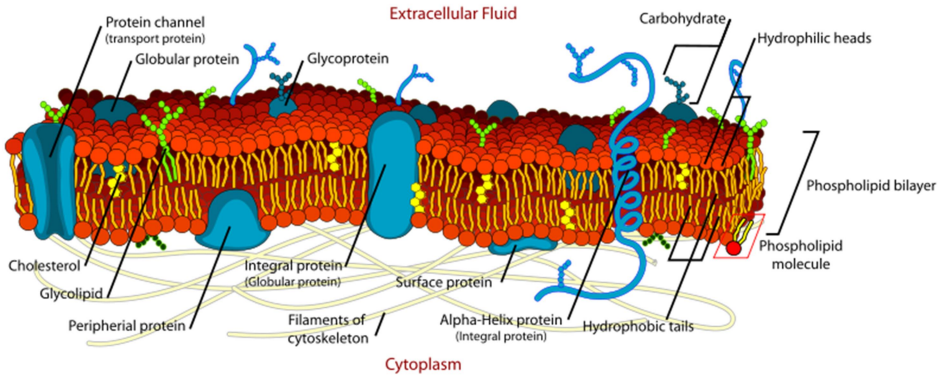

Figure 1.5 *Components of biological membranes (http://cellbiology.med.unsw.edu.au).*

The permeability properties of the membrane are determined by their lipid and protein components. In general, the lipid bilayer is penetrated by very few small non-polar molecules (e.g. ethanol and some lipophilic drugs) but is nearly impermeable to ions and most metabolites and solutes. The movement of those molecules across the membrane is assisted by specialized membrane proteins or protein complexes that are of major importance, especially if we consider that they are encoded in 30% of the eukaryotic genome (Engel and Gaub, 2008) and that membranes contain up to 80% w/w of proteins (Luckey, 2008).

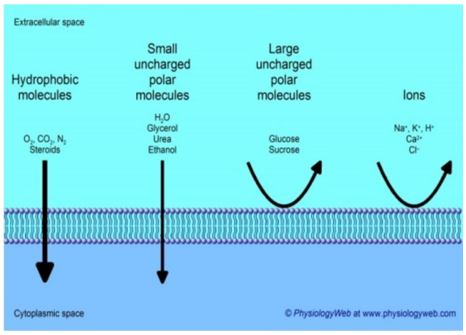

Figure 1.6 *Lipid bilayer permeability.*

A *transport system* can be distinguished into *passive* or *active* depending on whether the transport is in the direction of or against the electrochemical gradient respectively. Passive transport does not require energy consumption and may be through the lipid bilayer (simple diffusion), mediated by a channel (passive diffusion) or through a facilitator protein, often called uniporter or simply transporter (facilitated diffusion).

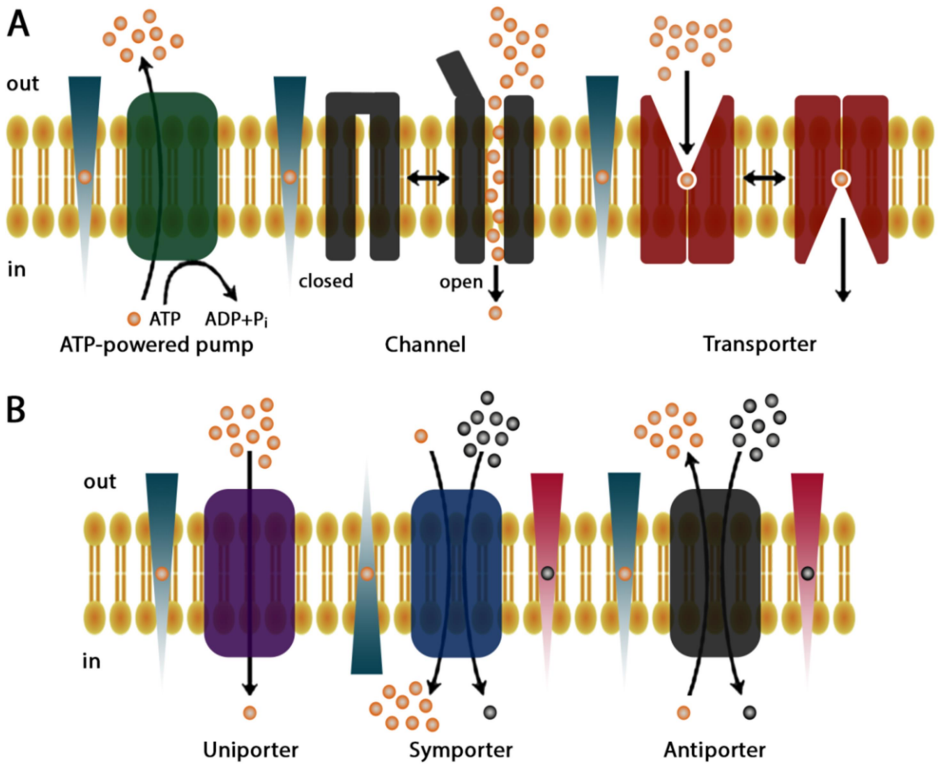

Figure 1.7 A. *Types of membrane transport proteins include the ATP-driven transporters, channels and transporters.* ***B.*** *Different types of transporters. Concentration gradients are indicated by the triangles with the tip pointing towards the side of the membrane with the lower solute concentration (modified from Bosshart and Fotiadis, 2019).*

Channels form a hydrophilic pore that extends across the lipid bilayer and allows small molecules (usually ions) to flow rapidly through them, with an approximate rate of 10^6-10^7 ions/sec. Uncontrollable movement of ions and other molecules would prove catastrophic for the cells, thus channels possess *selectivity filters* composed of residues specific for the molecules transported through them (Moran et al., 2015). Specific *gating* elements exist on both sides of the membrane, controlling the accessibility of the selectivity filters and eventually the channel pore. The external signals responsible for the opening and closing of the gates include changes in transmembrane voltage, binding of ligands or lipids and mechanical stress. In some cases, ion channels can possess additional *hydrophobic gating* that is tunable to local changes in the diameter and/or hydrophilicity of the channel pore due to liquid-vapour transitions of water within the pore (Aryal et al., 2015; Gadsby, 2009).

In contrast to channels, *transporters* (also referred as *carriers*) do not possess a continuous pore and do not seem to use channel-like gating mechanisms to control substrate translocation across the membrane. Instead, they bind their substrate(s) at one side of the membrane and undergo a series of induced-fit conformational changes that bring the substrate-binding site on the

other side of the membrane, where the substrate is released. Thus, transporters might be considered as *topological enzymes* characterized by a major substrate binding site, a rate of transport catalysis and a specificity profile, which can all be determined by Michaelis-Menten kinetic measurements. Transporters can be subdivided into primary or secondary based on the the mechanism of energy acquisition.

Primary active transporters use as source of energy the adenosine-triphosphate (ATP) hydrolysis, light absorption or electron force to shuttle substrates against their concentration gradients. Secondary transporters, couple the favorable energy of the electrochemical gradient of one solute (e.g. an ion) to the transmembrane movement of another. They can be antiporters, which catalyze the exchange of one or more substances for another, or symporters, which transport two or more substances in the same direction. Most transporters, despite their distinct evolutionary origins, structure and function, consist of a hydrophobic main body made of 4-14 transmembrane domains and cytoplasmic (most commonly) or extracellular (less frequently) hydrophilic N- and C-terminal regions. Given their role in cell nutrition, detoxification, homeostasis communication and signaling, transporters of all kinds are essential for life, and consequently their malfunction is related to several diseases (e.g. cystic fibrosis, cancer, neurological diseases; Sonders et al., 2005; Turk and Wright, 2004).

1.2.1 Regulation of transporter endocytosis

Transmembrane proteins -including nutrient transporters, ion channels and signaling receptors- are subject to tight regulation, allowing cells to adapt to their constantly changing environment. This is a vital need for the cells as they must respond to stress conditions or different nutrient needs in order to survive. Such a control occurs at the level of protein trafficking, including secretion towards the plasma membrane, direct vacuolar sorting, endocytosis, endosomal recycling and turnover in the vacuole/lysosome. Other control points include autophagy, Golgi-to-endosome traffic, Golgi complex quality control which will not be discussed in detail. Ubiquitylation is a key regulatory signal promoting the internalization of fungal and mammalian membrane proteins via endocytosis, which will then be re-routed for degradation in the vacuole through a series of trafficking steps.

Ubiquitylation is a post-translational modification, where ubiquitin is covalently and reversibly linked to a target protein by the formation of an isopeptide bond between the amino group of a lysine residue of the protein and the C-terminal glycine of ubiquitin. Ubiquitin (Ub) is a highly conserved protein that can be found in all eukaryotic organisms and cell types and consists of 76 amino acids. It is conjugated to the protein target via three sequential enzymatic reactions, catalyzed by three distinct enzymes. Firstly, a ubiquitin-activating enzyme (E1) activates Ub in an

ATP-dependent reaction. Next, Ub is transferred to a ubiquitin-conjugating enzyme (E2) and finally to a ubiquitin ligase of the HECT family (E3), which catalyzes the transfer of Ub to the substrate. Alternatively, Ub can be directly transferred from E2 to the substrate with the help of an E3 enzyme of the RING family, acting as a platform for substrate recognition (Dupré et al., 2004; Lauwers et al., 2010; Miranda and Sorkin, 2007). Target proteins can be modified with a single Ub molecule on one (mono-ubiquitylation) or several lysines (multi-ubiquitylation). Additionally, given the fact that Ub itelf carries conserved lysine residues (K6, K11, K27, K29, K33, K48, K63), Ub molecules can be ligated to one another forming ubiquitin chains (poly-ubiquitylation). For example, K48-linked poly-Ub chains target proteins for degradation by the 26S proteasome and K63-linked poly-Ub chains are involved in various cellular processes such as DNA repair, stress responses and endocytic trafficking of PM proteins (Ohtake et al., 2018).

In yeast, for most transmembrane cargoes studied, the E3 ubiquitin ligase that mediates ubiquitylation is Rsp5, an enzyme that belongs to the Nedd4 HECT family and its homologue in *A. nidulans* is HulA (Gournas et al., 2010; Hein et al., 1995; Springael et al., 1999). Various adaptor proteins have been reported to mediate the physical interaction of ubiquitin ligases with their substrates, being an additional layer of specificity in the ubiquitylation cascade. α-arrestins is a family of these proteins, that consists of 13 known members in *S. cerevisiae* with six related proteins in human (Patwari and Lee, 2012). The Ub ligase can bind to the [L/P]PxY motifs of the α-arrestins through three WW domains, while many target proteins are able to functionally interact with multiple α-arrestins (Lin et al., 2008; Nikko and Pelham, 2009). In *A. nidulans*, the arrestin-like protein, ArtA, is responsible for the $HulA^{Rsp5}$-dependent ubiquitylation and endocytosis of many purine transporters such as the NAT/NCS2 UapA transporter, AzgA (purines) and PrnB (L-proline) (Karachaliou et al., 2013). Ubiquitylation is a reversible modification, and Ub molecules are recycled after cleavage of the isopeptide bond by specific proteases, named de-ubiquitinating enzymes (DUBs), such as Doa4 in *S. cerevisiae* or CreB in *A. nidulans* (Lockington and Kelly, 2001; Swaminathan et al., 1999).

1.3 Secondary Active Transporters

1.3.1 The Major Facilitator Superfamily (MFS)

The Major Facilitator Superfamily (MFS) is an evolutionary old, diverse and one of the largest superfamily of secondary transporters across the kingdom of life (Marger and Saier, 1993; Pao et al., 1998). According to the Transporter Classification Database (TCDB; http://www.tcdb.org/; Saier et al., 2014; Wang et al., 2020; Yan, 2015), a total of 105 distinct families are phylogenetically classified

within the MFS. These transporters operate by uniport, symport or antiport mechanisms that take advantage of the electrochemical gradient of the co-transported ion or the concentration of the ligand to initiate the transport cycle. Some of the substrates of the MFS transporters are sugars, drugs, neurotransmitters, amino acids, vitamins, organic and inorganic ions and many other small compounds, and thus are of great physiological and clinical importance.

The MFS fold consists of 12 transmembrane segments (TMSs) that are arranged in two symmetrically related bundles connected by a cytosolic loop that can often be ordered. The two bundles consist of six TMSs each and they themselves are related by a pseudo two-fold axis of symmetry of three TMSs. The first crystal structure describing this fold was that of the lactose-H^+ symporter LacY (Abramson, 2003), whose mechanism of proton/sugar symport has been studied extensively and the key residues involved in the translocation trajectory are well-characterized.

Some of the bacterial MFS structures known are these of the glycerol-3-phosphate-phosphate antiporter GlpT (Radestock and Forrest, 2011), the multidrug transporter EmrD (Yin et al., 2006), the xylose/proton symporter XylE (Sun et al., 2012) etc. Fewer eukaryotic MFS transporter structures are known but some recently resolved include the *Piriformospora indica* phosphate transporter PiPT (Pedersen et al., 2013), the plant nitrate transporter NRT1.1 (Sun et al., 2014) and the human glucose transporter GLUT1 (Deng et al., 2014).

The bacterial lactose permease LacY as the most deeply studied example of MFS

The lactose permease of *E. coli*, LacY, catalyzes the symport of galactoside:H^+ and it is one of the most studied members of the MFS family since the 70s. However, the first crystal structure was not released until three decades later (Abramson, 2003) and today there are many structures available in different conformations. The transporter consists of 12 α-helical TMSs organized into two pseudo-symmetrical six-helix bundles named the N- and the C-terminal bundles, similar to other MFS transporters. The two domains are connected by a long cytoplasmic loop between TMSs 6 and 7. The substrate and proton binding sites are located in the middle of the protein at the apex of a hydrophilic cavity, with the residues participating in the sugar binding located mostly in the N-terminal while the ones for the proton binding in the C-terminal bundle (Smirnova et al., 2011).

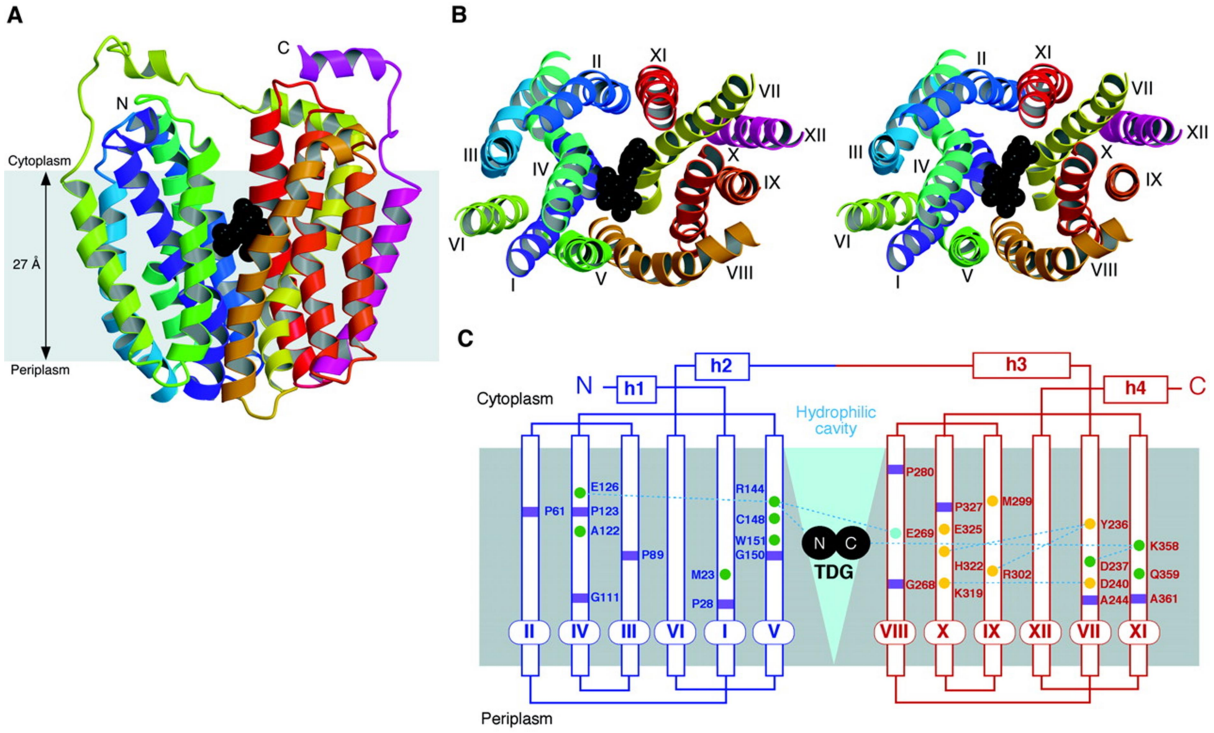

Figure 1.8 Overall structure of LacY. A. *Ribbon representation of LacY viewed parallel to the membrane.* ***B.*** *Stereo view of LacY viewed along the membrane normal from the cytoplasmic side.* ***C.*** *Schematic secondary structure of LacY where the N- and C-terminal domains are colored in blue and red respectively. Residues at the kinks in the transmembrane helices are marked in purple rectangles; residues involved in substrate binding and proton translocation are marked as green and yellow circles respectively (Adapted from Abramson, 2003).*

1.3.2 The Amino acid-Polyamine-organoCation (APC) Superfamily

The second largest family of secondary transporters is the Amino acid-Polyamine-organoCation (APC) superfamily, which includes members that function as solute:cation symporters and solute:solute antiporters. Currently, 18 families are categorized in this superfamily, with members specific for nucleobases, amino acids, metal ions, purines, pyrimidines, vitamines, peptides etc (Jack et al., 2000; Västermark and Saier, 2014). Most members share a common basic core of 10 TMSs that form a five-helix inverted repeat (5HIR), also known as the 5+5 or LeuT-fold, however some are known to display a 7+7 TMS fold. Among the 5+5 members, most contain two extra TMSs at their N- or C-terminal part, but in some cases there are four extra C-terminal TMSs or one extra TMS before every inverted repeat unit. This structural diversity implies that multiple hairpin and domain duplication events occurred during the evolution of this family (Västermark and Saier, 2014). The substrate binding site is located near the center of the transporter between prominent kinks in TMS1 and its symmetry-related pair TMS6 and they share a common mechanism of transport and gating reflected in the alternating access model. Some of the families included in this superfamily are the Nucleobase:Cation Symporter family 1 (NCS1), the Nucleobase Ascorbate

Transporter/Nucleobase:Cation Symporter 2 family (NAT/NCS2), the Solute:Sodium Symporter (SSS) family and the Neurotransmitter:Sodium Symporter (NSS) family.

1.3.2.1 The Neurotransmitter:Sodium Symporter (NSS) family

The Neurotransmitter:Sodium Symporter (NSS) family includes members that use sodium and chloride electrochemical gradients to catalyse the transport of a wide array of substrates, including biogenic amines (serotonin, dopamine, norepinephrine), amino acids (GABA, glycine, proline, taurine) and osmolytes (betaine, creatine); (Masson et al., 1999; Nelson, 2002). Notably, a subset of this family are the biogenic amine transporters such as the dopamine transporter (DAT), the norepinephrine transporter (NET) and the serotonin transporter (SERT), which are targets for additive substances such as cocaine, amphetamine and many antidepressants, while their malfunction leads to multiple disorders including depression, Parkinson's disease, orthostatic intolerance, epilepsy, attention deficit hyperactivity disorder (ADHD) or obsessive-compulsive disorder (OCD); (Amara and Sonders, 1998; Hahn and Blakely, 2002; Krogsgaard-Larsen et al., 2000; Mazei-Robison and Blakely, 2006; Ozaki et al., 2003; Richerson and Wu, 2004).

The bacterial amino acid transporter LeuT

The best studied member of the NSS family is the bacterial amino acid symporter from *Aquifex aerolicus*, LeuT, with several crystallographic and biochemical data available. LeuT is in fact the role model of the APC superfamily, establishing a common fold among its members and providing important details on the mechanism of substrate binding and transport. It is a Na^+ coupled, non-polar amino acid symporter and even though it was named after leucine, it is specific for several aliphatic/aromatic amino acids including glycine, alanine, methionine and tyrosine and can also bind without transporting tryptophan (Singh and Pal, 2015).

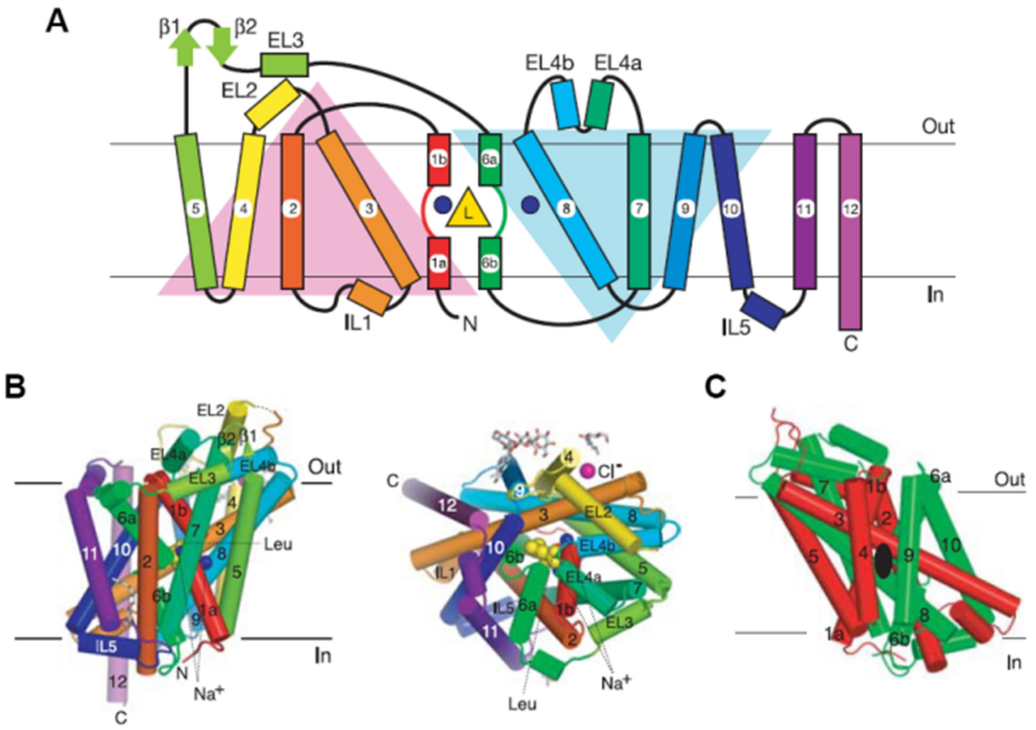

Figure 1.9 A. *The LeuT topology. The position of leucine and the two sodium ions are depicted as a yellow triangle and blue circles respectively.* ***B.*** *Stereoview in the plane of the membrane and from the extracellular side.* ***C.*** *The pseudo-two-fold axis of symmetry that relates TM1–TM5 (red) and TM6–TM10 (green). The pseudo-two-fold rotation axis is depicted as a black ellipsoid (Yamashita et al., 2005).*

The first crystal structure of LeuT (Yamashita et al., 2005) revealed that the protein consists of 12 α-helical transmembrane segments (TMS1-TMS12) with numerous loops and helices on the intra- and extracellular surfaces. The core domain of TMSs 1-10 is organized in an internal structural repeat, relating TMSs 1-5 and TMSs 6-10 by an antiparallel pseudo two-fold axis located in the plane of the membrane. The first TMSs in each repeat (1 and 6) which are the most conserved among the human transporter homologues, present an antiparallel orientation and most importantly, are not continuous helices. On the contrary, they have breaks in the helical structure at approximately halfway across the membrane bilayer, exposing main-chain carbonyl oxygen and nitrogen atoms for hydrogen bonding and ion coordination. TMSs 3 and 8 are also related by the pseudo two-fold axis and along with TMSs 1 and 6 comprise the substrate and sodium binding sites. The rest TMSs (2, 4, 5, 7, 9, 10) support the protein core and more specifically, TMSs 2 and 7 uphold TMSs 1 and 6 respectively, while a prominent V-shaped structure formed by TMSs 4 and 5 and its inverted pseudo two-fold formed by TMSs 9 and 10, hold TMSs 3 and 8 like pincers. The last two transmembrane segments (TMS11 and TMS12) are implicated in the dimerization of the transporter. Two Na^+ binding sites have been identified and located at the unwound regions of TMS1 and TMS6, having key roles

in stabilizing the core of the transporter and the leucine binding. The transport mechanism predicted for LeuT is the rocking-bundle alternating-access model (see §1.4.3).

The dopamine transporter (DAT)

One of the eukaryotic transporters whose X-ray structure has been determined, is the *Drosophila melanogaster* dopamine transporter (dDAT), which was captured in an inhibitor-bound, outward-open conformation (Penmatsa et al., 2013). With more than 50% sequence identity with its mammalian counterparts, dDAT is a powerful tool to study NSS pharmacology and transport mechanisms. The structure of dDAT is similar to that of its prokaryotic relative LeuT (Yamashita et al., 2005) with 12 transmembrane segments of which TMSs 1-5 and 6-10 are related by inherent pseudosymmetry. Residues in TMS1 and TMS6 interact with the ligand and ions via their mid-helix breaks, connecting the bonding networks of all three ions and the inhibitor. A bend in TMS3 contributes to the hydrophobic pocket where the ligand is located. One cholesterol molecule is wedged in a groove between TMS5 and TMS7, modulating the movement of TMS1a during the transport cycle. Moreover, the crystal revealed some features that are important for the neurotransmitter transport, such as a kink at a proline residue located in the center of TMS12 that causes the second half of the tail to turn away from the transporter. This feature implies that the potential oligomerization of the NSS transporters is not assisted by the last TMSs as in the case of LeuT. In fact, even though previous studies indicate that NSS transporters form oligomers (Sitte, 2004; Torres et al., 2003), the crystal of dDAT is a monomer. Additionally, the extracellular loop 2 (EL2) seems to play a critical role in the proper localization of the transporter in the PM, with numerous predicted N-linked glycosylation sites and a disulfide bond. Altogether, the core of dDAT resembles that of LeuT. However, there are some distinctions that include a latch-like C-terminal helix that interacts extensively with the cytoplasmic face of the transporter, a kink in TMS12 halfway across the membrane and a cholesterol molecule located within a groove formed by TMs 1a, 5 and 7.

Studies on the human homologue hDAT revealed that the N-terminal region of the transporter is very important for the efflux process in NSS proteins and questions on the mechanism underlying the DAT-mediated reverse transport remain unclear, due to lack of structural information (Hamilton et al., 2014; Khelashvili et al., 2015a; Razavi et al., 2018). As the amino acid sequence of the N-terminus is not conserved among its homologues or any protein with known fold, *ab initio* structure prediction tools and extensive atomistic MD simulations were combined and revealed two distinct structural elements: a beta sheet motif and a α-helical segment. Phosphorylation and interactions not only with specific membrane lipids but also with the internal loops (ILs) of the

transporter and the N-terminal region proved to be critical for the efflux phenotype (Hamilton et al., 2014; Khelashvili et al., 2015a; Razavi et al., 2018).

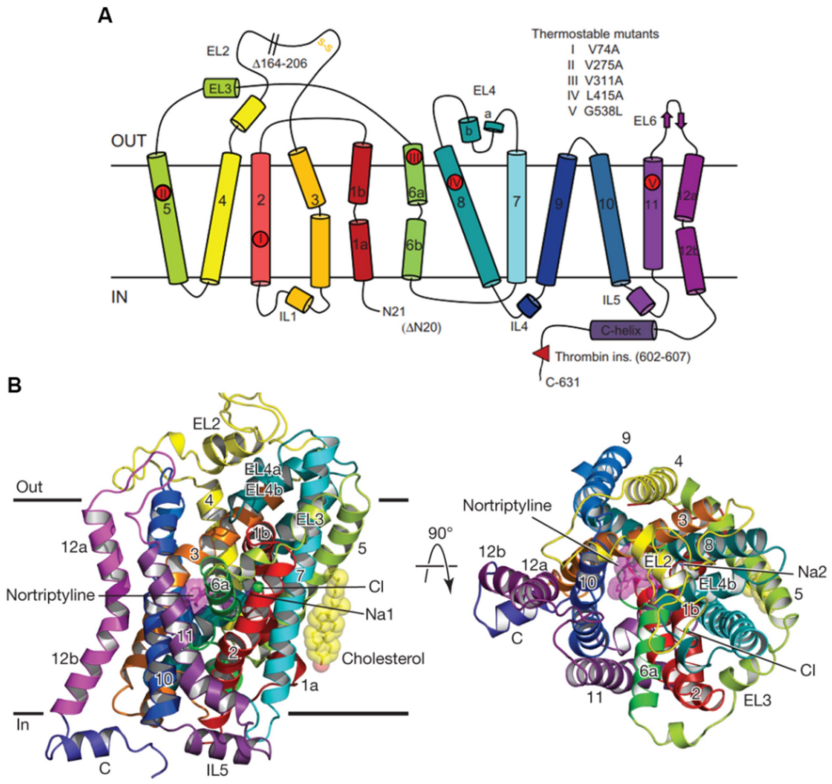

Figure 1.10 A. *Topology of dDAT crystallization construct. Red circles labeled in roman numerals represent residues mutated to improve thermal stability. The first 20 residues at the N-terminus were deleted. EL2 was truncated from residue 164 to 206. C-terminal truncation was generated post-expression and purification by introducing a thrombin site (-LVPR|GS-) at position 602 into the intact C-terminus.* ***B.*** *Structure of dDAT viewed parallel to the membrane and from the extracellular face. (Penmatsa et al., 2013).*

The serotonin transporter (SERT)

The X-ray structure of the human serotonin transporter was determined in an inhibitor-bound, outward-open conformation (Coleman et al., 2016), defining the mechanism of antidepressant action and providing information for potential drug design. Akin to LeuT and DAT, SERT has 12 transmembrane domains with TMSs 1-5 and 6-10 related by a pseudo-2-fold axis. Similar to dDAT, the intracellular face of the transporter is capped by IL1, IL5 and the C-terminal region, with the latter having a pronounced kink halfway across the membrane and a cholesterol hemisuccinate (CHS) molecule bound near TMS12a. Oligomerization of the SERT was experimentaly suggested (Kilic and Rudnick, 2000), however in detergent the transporter is a monomer. In contrast with dDAT, the TMS9 of SERT is shifted towards TMS12 and TMS11 extends further into the putative membrane

environment, providing a larger cavity for allosteric ligands. Moreover, interaction of cholesterol with the lipid molecules may reinforce the conformation of TMS12. The C-terminal region of SERT mimics dDAT with a similar hinge and helix region (Coleman et al., 2016).

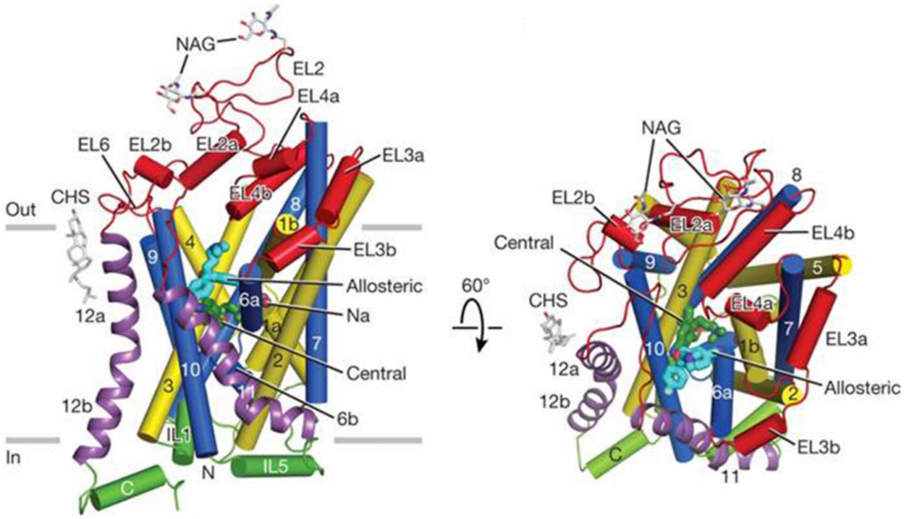

Figure 1.11 *Architecture of the human serotonin transporter SERT viewed parallel to the membrane and from the extracellular side of the membrane (Coleman et al., 2016).*

1.3.2.2 The Solute Sodium Symporter (SSS) family

Solute Sodium Symporters (SSS) family includes a large number of proteins that co-transport Na^+ with sugars, amino acids, inorganic ions or vitamins (Turk and Wright, 2004). Members of this family are of great importance for human physiology and disease, as malfunction in glucose and iodide uptake can lead to congenital metabolic disorders.

The bacterial glucose/galactose transporter vSGLT

The first member of the SSS family that was cloned was the intestinal sodium glucose/galactose symporter from *Vibrio parahaemolyticus*, vSGLT. The crystal structure of vSGLT (Faham et al., 2008) revealed 14 α-helical TMSs with both termini facing the cytoplasm. TMSs 2-6 and 7-11 (i.e. the 5+5 core in this case) are related by a 153° rotation parallel to the membrane plane and represent the core domain of the transporter. TMSs 2-4, 7-9 and 11 contribute in the side chain interactions for ligand selectivity, and the rest seven TMSs stabilize these central helices. A significant structural feature is the two breaks in the symmetrically related TMSs 2 and 7, which has been implicated in transport mechanisms of several co-transporters. Given the functional homology between the bacterial and humans SGLTs, the vSGLT structure should provide a very useful tool in the rational design of drugs for the treatment of diabetes.

1.3.2.3 The Nucleobase:Cation Symporter-2 (NCS2) family

The Nucleobase Ascorbate Transporter/Nucleobase:Cation Symporter 2 (NAT/NCS2) family includes bacterial, fungal and plant H^+ or Na^+ symporters, specific for purines, pyrimidines and related analogues. Notably, the mammalian L-ascorbate/Na^+ transporters SVCT1 and SVCT2 also belong in the NAT/NCS2 family, which was first defined by the cloning and characterization of the uric acid-xanthine transporters UapA and UapC of *A. nidulans* and the uracil transporters UraA and PyrP of *Escherichia coli* (Diallinas and Gournas, 2008; Gournas et al., 2008). Crystal structures of NAT/NCS2 transporters revealed that members of this family contain 14 transmembrane segments with 7+7 inverted repeat fold.

The bacterial uracil transporter UraA

The H^+/uracil symporter from *E. coli*, UraA, has a known crystal structure (Lu et al., 2011; Yu et al., 2017) which appears to differ from that of other members of the APC superfamily and functions as a dimer (Yu et al., 2017). It consists of 14 transmembrane segments that are mostly α-helical, however two short antiparallel β-strands in TMS3 and TMS10 break the continuity of this structure. The 14 TMSs are arranged into two structural repeats as two groups of 7 (TMSs 1-7 and TMSs 8-14), rotated to each other in a 180° axis parallel to the membrane. Also, the TMSs can be divided in two distinct domains: the core domain consisting of TMSs 1-4 and 8-11, and the gate domain consisting of TMSs 5-7 and 12-14. The substrate binding site is located between TMSs 1, 3, 8 and 9.

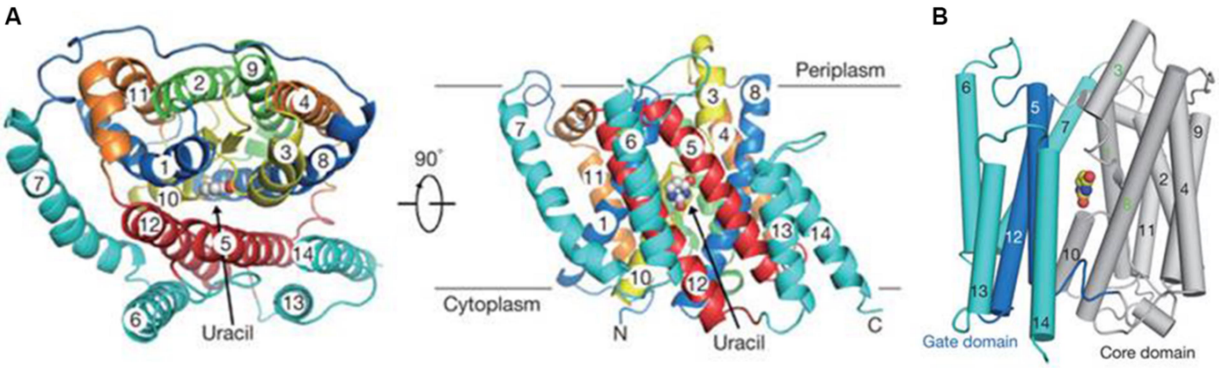

Figure 1.12 The UraA crystal structure. A. *Top and side views of the UraA structure. Bound uracil is shown.* ***B.*** *The gate and core domains of UraA, highlighted in blue and grey color respectively (adapted from Lu et al., 2011).*

The fungal uric acid-xanthine transporter UapA

UapA from *A. nidulans* is specific for the uptake of the purines xanthine and uric acid but does not transport hypoxanthine or adenine (Diallinas and Scazzocchio, 1989). Recently, the crystal structure of UapA was determined (Alguel et al., 2016), revealing a homodimer formation. The overall

structure of UapA contains 14 TMSs organized into a 7+7 fold divided in a core domain (TMSs 1-4 and 8-11) and a gate domain (TMSs 5-7 and 12-14), a structure similar to that of UraA however with longer loop regions between the TMSs. Interestingly, TMSs 3 and 10 extend halfway through the protein and are followed by short β-strands and random coils in the center of the transporter. The dimer is formed with the participation of TMSs 12, 13 and 14 of the gate domain with TMS13 fitting into a cleft formed by the opposite monomer. Genetic, cellular and biochemical studies reveal a critical role of dimerization in UapA trafficking and turnover (Martzoukou et al., 2015). The substrate binding site is located approximately halfway across the membrane in a cleft formed by the half helices of TMSs 3 and 10.

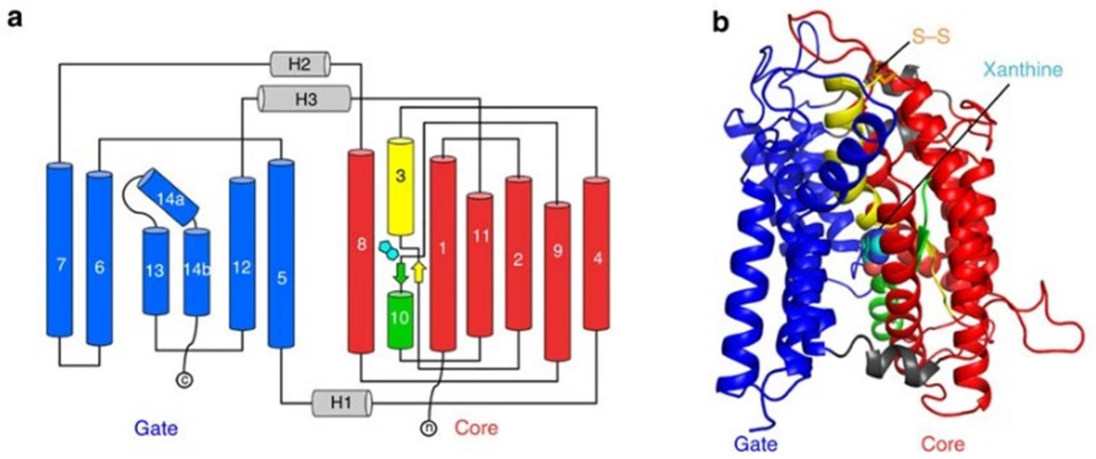

Figure 1.13 Structure of UapA. A. *Topology diagram of UapA and* ***B.*** *ribbon representation of the UapA monomer. The gate domain is shown in blue while most of the core domain is shown in red (adapted from Alguel et al., 2016).*

1.3.2.4 The Nucleobase:Cation Symporter-1 (NCS1) family

A major subfamily of the APC superfamily is the Nucleobase Cation Symporter 1 family (NCS1) present in prokaryotes, fungi and some plants. NCS1 proteins use proton or sodium gradient to transport purines, pyrimidine nucleobases and nucleosides, hydantoins and related compounds. Its absence from mammals makes this family an ideal, highly specific gateway to target nucleobase-specific drugs to microbial pathogens (Gavriil et al., 2018; Lougiakis et al., 2016; Sioupouli et al., 2017). Fungal members of this family are among the best-studied transporters at a genetic, biochemical and cellular level mostly from *A. nidulans* and *Saccharomyces cerevisiae* and are further classified into two sub-families: the Fcy-like and the Fur-like transporters with five and seven members respectively. Most probably, Fur and Fcy originated independently from prokaryotes through horizontal gene transfer and repeated duplications lead to their increased number of copies,

allowing the evolution of novel functions and specificities (Harry de Koning, George Diallinas, 2000; Krypotou et al., 2015a; Pantazopoulou and Diallinas, 2007).

The Fcy-like family members share a 29-37% amino acid sequence identities and in Fungi the family consists of five members (FcyA-FcyE), conserved in all 23 Aspergilli with known genomic sequences. The *S. cerevisiae* homologue Fcy2p was characterized as a high-affinity, high-capacity adenine/hypoxanthine/guanine/cytosine H^+ symporter (Brethes et al., 1992). In *A. nidulans*, the FcyB protein is a high-affinity, low-capacity transporter specific for the same substrates (Krypotou et al., 2012; Vlanti and Diallinas, 2008).

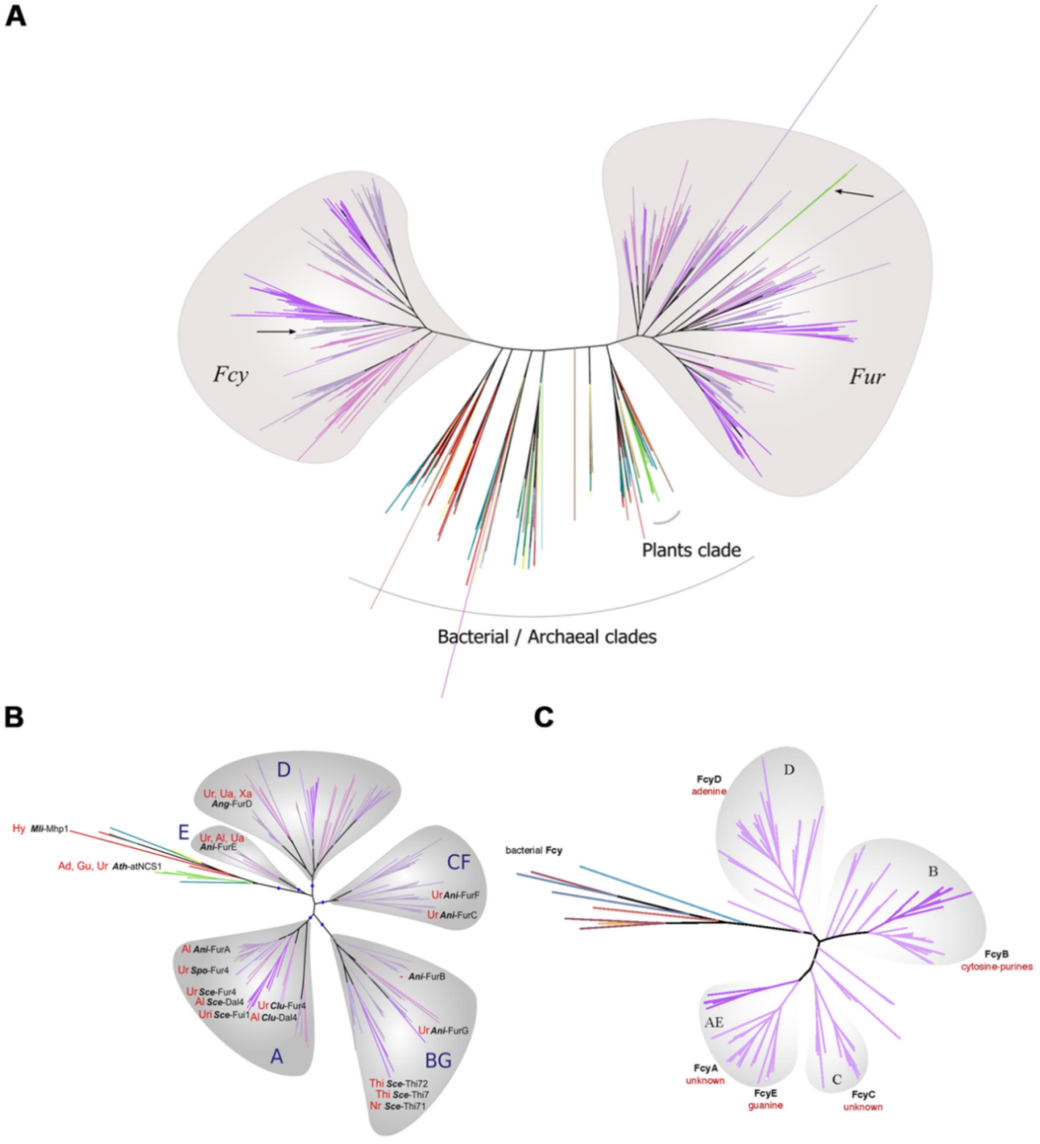

Figure 1.14 Phylogenetics of NCS1 transporters. *Maximum Likelihood phylogenetic tree of* ***A.*** *all 2248 sequences from 1093 species of NCS1 proteins* ***B.*** *Fur family of transporters (190 sequences) and* ***C.*** *Fcy family of transporters (102 sequences). Purple lines correspond to Fcy and Fur fungal proteins, green lines to plant proteins and Actinobacteria, Proteobacteria and Firmicutes are in red, blue and yellow lines respectively (Papadaki et al., 2018).*

The Fur-like subfamily consists of seven members (FurA-FurG), of which two have been functionally characterized as allantoin (FurA) or uracil (FurD) transporters (Amillis et al., 2007; Hamari et al., 2009). FurA shares a 37% sequence identity with its homologue in *S. cerevisiae*, Fur4p which was characterized as a high-affinity, high-capacity uracil/H^+ symporter (Wagner et al., 1998).

The Mhp1 transporter

The benzyl-hydantoin/Na^+ symporter Mhp1 from *Microbacterium liquefaciens* is the only member of the NCS1 family that is captured throughout a complete transport cycle and more specifically in outward-open, outward-occluded and inward-open conformations (Shimamura et al., 2008; Weyand et al., 2008), providing important information on the mechanism underlying transport catalysis. Mhp1 is structurally similar to LeuT and other members of the APC superfamily with 12 α-helical TMSs of which the first ten constitute the conserved motif of the LeuT-fold. More specifically, TMSs 1, 2, 6 and 7 form the four-helix bundle and TMSs 3, 4, 8, and 9 the hash motif. TMS5 and TMS10 link the four-helix bundle with the hash motif and the latter with the C-terminal TMSs 11 and 12 respectively, and appear to participate in significant movements during transition from one state to the other. The substrate binding site is located between TMSs 1, 3, 6 and 8.

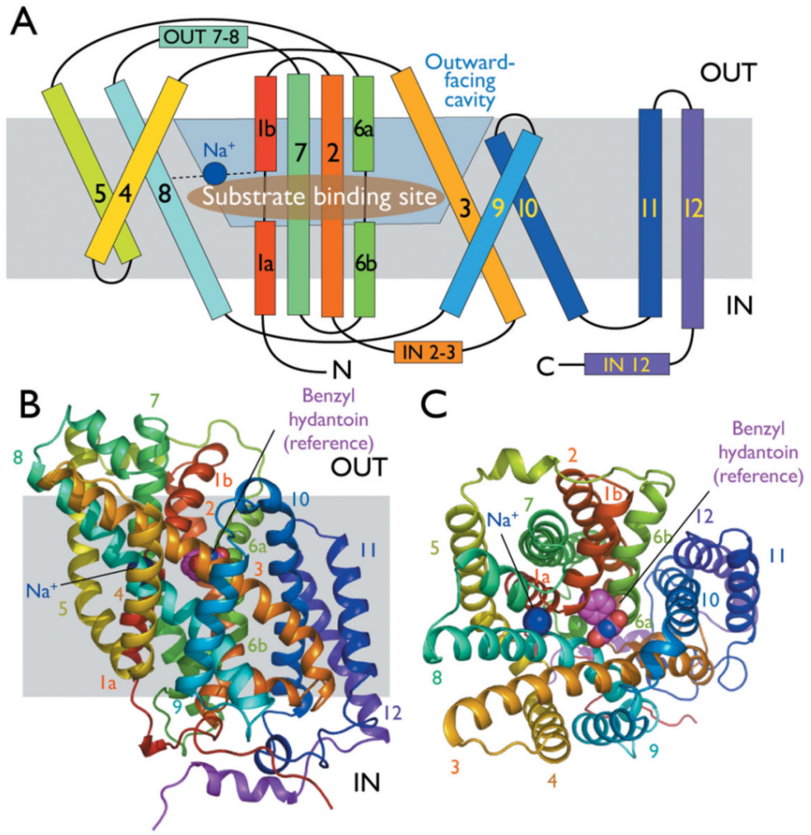

Figure 1.15 Structure of Mhp1. A. *Mhp1 topology. The positions of the substrate and the cation binding sites are depicted as a brown ellipsoid and blue circle, respectively. The Mhp1 structure viewed* ***B.*** *in the plane and* ***C.*** *from the outside of the membrane (Weyand et al., 2008).*

1.4 Transport mechanisms: the alternating access model

The conceptual framework of the alternating-access model was proposed already in the mid-1950s (Mitchell, 1990, 1957; Patlak, 1957, 1956), to explain the mode of action of membrane transporters that mediate the passive or active transport of solutes. The keystone of this mechanism is the transition of the transporter between different conformational states in which the substrate-binding site is exposed to opposite sides of the membrane in an alternating fashion. A plethora of crystal structures of transporters of different families, captured in multiple functional states have been available during the past decade, which along with biophysical and computational approaches shed light in the molecular mechanisms of transporters and describe three distinct mechanisms: the the rocker-switch, the rocking-bundle or the elevator mechanism.

1.4.1 The rocker-switch mechanism

In the simple rocker-switch mechanism, two symmetrically related bundles surround the substrate binding site of the transporter which is located approximately halfway across the membrane. During a transport cycle, the protein moves and exposes the binding site on one side of the membrane. After substrate binding, the protein opens to the other side of the membrane with a rocker-switch like movement around the region of the binding site and the substrate is released. This mechanism is mostly proposed for the Major Facilitator Superfamily (MFS) with a 6+6-fold structure, and was first described for the permease LacY of *E. coli.* Crystal structures obtained for transporters of this family further supported this model.

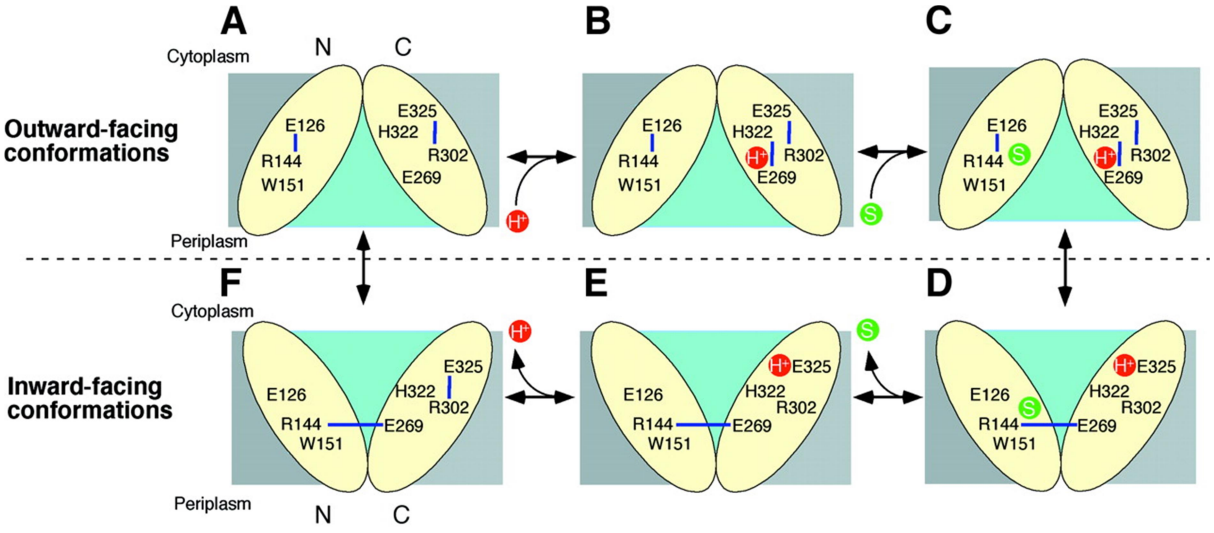

Figure 1.16 *A possible lactose/proton symport mechanism. N- and C-terminal domains are shown as yellow ovals. Key residues are labeled; hydrogen bonds are shown as blue lines. The proton and the substrate are shown as red and green circles, respectively; the hydrophilic cavity is represented as a light blue area (Abramson, 2003).*

1.4.2 The elevator mechanism

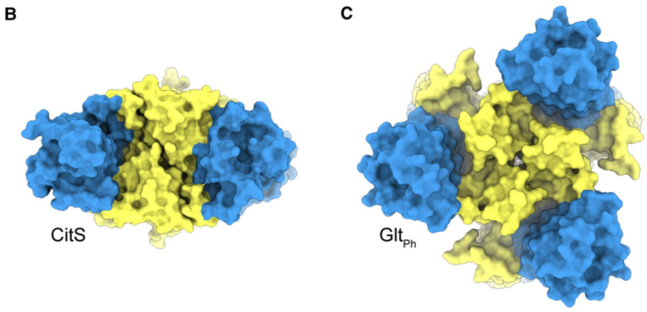

Figure 1.17. *Oligomeric state of elevator transporters. Transport domain is in blue and scaffold domain in yellow (Garaeva and Slotboom, 2020).*

In this model, transporters are made up of two distinct bundles: a moving one called the transport domain and a fixed one called the scaffold domain. During a transport cycle, the transport domain and the substrate binding site that is fully or largely confined to it, slide through the lipid bilayer as a rigid body against the scaffold domain. Eventually, the substrate is carried across the membrane by only one of the two domains. In many cases, the transport domain contains structural elements named helical hairpins (HPs) that form gates, which when open allow the access of the substrate and must be closed to enable the elevator movement. The scaffold domain is responsible for the subunit contacts in the oligomerization state of the transporters, something very common in this family. The first elevator-type mechanism was described for the glutamate transporter homologue Glt_{Ph} from *Pyrococcus horikoshii* (DeChancie et al., 2011; Reyes et al., 2009) and characterizes mostly transporters with a 7+7-fold.

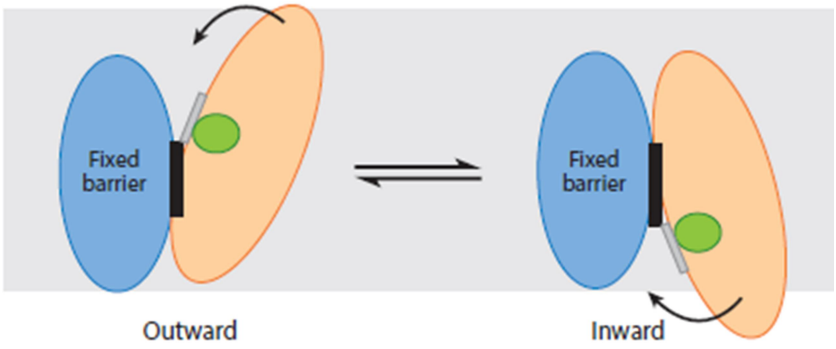

Figure 1.18. *Schematic representation of the elevator mechanism of transport. The substrate (green sphere) binds to one of the domains, which moves against a structurally dissimilar immobile domain to physically translocate the substrate to the other side of a fixed barrier. Substrate binding and release in each state are likely facilitated by local gating transitions, primarily in the moving domain (gates are depicted here as a thick line over the substrate; adapted from Drew and Boudker, 2016).*

1.4.3 The rocking-bundle mechanism

In the rocking-bundle mechanism, substrate binding between two structurally distinct domains is directly coupled with the movement of outer and inner gates around the centrally located substrate binding site (Forrest and Rudnick, 2009). The acquisition of an inward-open structure of LeuT (Krishnamurthy and Gouaux, 2012) along with outward-open and intermediate occluded structures

helped us understand the transport mechanism in more detail. In the LeuT fold, two distinct bundles are formed: the so called scaffold domain that consists of TMS3-TMS4 and TMS8-TMS9 and the core domain that consists of TMS1-TMS2 and TMS6-TMS7 (Yamashita et al., 2005). Initially, the transporter is open to the extracellular, with its binding site accessible to the ligand. Proper binding of the substrate leads to the transition from the outward-open to the occluded state, with TMSs 1b and 6a moving towards TMS3 and TMS10 and with the bending of TMS2 and TMS7. The tight packing of the core against the scaffold domain via extracellular loop 4 closes the outer cavity and these changes seem to precede the rocking movements of the core bundle that leads to the inward-occluded conformation. A significant outward movement of the intracellular gate of TMS1a enables the cytosolic release of the substrate, leading to the inward-open conformation of the transporter.

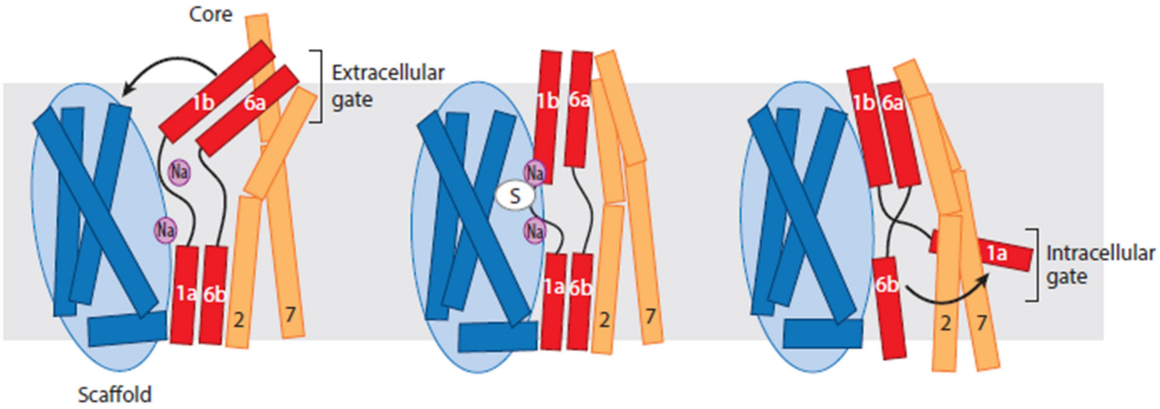

Figure 1.19 *Schematic representation of the rocking-bundle-type rearrangement of the core domain (red and light orange) against the scaffold domain (blue). Adapted from (Drew and Boudker, 2016).*

1.5 Aims of this study

Structure determination of eukaryotic and especially mammalian/human transporters is still very challenging and this is why structural models based on bacterial homologues is mostly used in order to understand the mechanism of transport function and the role of specific transporters in human health and disease. Nonetheless, it has become evident that structural differences such as the long termini of eukaryotic transporters that appeared later in evolution and offer an expanded set of functional properties are not shared by their bacterial homologues. Thus, speculations on the function of human/mammalian transporters based on prokaryotic homologs alone may lead to erroneous conclusions and misinterpretations. This in turn suggests that there is need for direct assessment of structure-function relationships in eukaryotic transporters.

The goal of the current study is to establish the elements critical for substrate specificity, endocytosis and folding of *Aspergillus nidulans* NCS1/FurE transporter through structure function approaches and provide a mechanistic rationale on how cytosolic termini affect specificity through the regulation of selective gating. More specifically, we present genetic, biochemical and *in silico* evidence supporting that the cellular expression and function of FurE transporter is determined via dynamic intramolecular interactions that involve both cytoplasmic regions and we delimit distinct motifs crucial for endocytosis, transport activity, substrate specificity and folding. Data arising from this study will hopefully reinforce and expand the current knowledge concerning transporters function in general and not only in *A. nidulans*.

CHAPTER 2

MATERIALS AND METHODS

2.1 Strains, culture media, growth and storage conditions

2.1.1 Strains used in this study

All strains used in this study carry the mutation veA1 that allows sporulation and are included in Table 2.1.

Table 2.1 List of strains used in this study.

Strain genotype	References
pabaA1	Wild-type reference strain
ΔuapA UapC::pyrG ΔazgA ΔFcyB::argB ΔFurD::riboB ΔFurA::riboB ΔcntA pabaA1 pantoB100	(Krypotou and Diallinas, 2014a)
ΔuapA UapC::pyrG ΔazgA ΔFcyB::argB ΔFurD::riboB ΔFurA::riboB ΔcntA pabaA1	(Krypotou and Diallinas, 2014a)
uapAΔ uapCΔ::AFpyrG azgAΔ fcyBΔ::argB furDΔ::AFriboB furAΔ::AFriboB cntAΔ::AFriboB pantoB100 pabaA1 pBS-uapAp-FcyB-pabaA1	(Krypotou et al., 2012)
uapA-gfp::argB ΔuapA ΔuapC::AfpyrG ΔazgA pabaA1	(Pantazopoulou and Diallinas, 2007)
pBS-azgA-gfp argB ΔuapA ΔuapC::AfpyrG ΔazgA argB2 pabaA1	(Karachaliou et al., 2013)
ΔuapA ΔuapC::AfpyrG ΔazgA pabaA1	(Pantazopoulou and Diallinas, 2007)
ΔuapA UapC::pyrG ΔazgA ΔFcyB::argB ΔFurD::riboB ΔFurA::riboB ΔcntA pabaA1 pantoB100 pGEM-gpdAp-FurE-GFP pantoB	(Krypotou et al., 2015)
uapAΔ uapCΔ::AFpyrG azgAΔ fcyBΔ::argB furDΔ::AFriboB furAΔ::AFriboB cntAΔ::AFriboB pantoB100 pabaA1 pGEM-gpdAp-FurD-ΔC-GFP-trpC-pantoB	This study
uapAΔ uapCΔ::AFpyrG azgAΔ fcyBΔ::argB furDΔ::AFriboB furAΔ::AFriboB cntAΔ::AFriboB pantoB100 pabaA1 pGEM-gpdAp-FurA-ΔC-GFP-trpC-pantoB	This study
uapAΔ uapCΔ::AFpyrG azgAΔ fcyBΔ::argB furDΔ::AFriboB furAΔ::AFriboB cntAΔ::AFriboB pantoB100 pabaA1 pGEM-gpdAp-FurE-ΔC-GFP-trpC-pantoB	This study
ΔuapA UapC::pyrG ΔazgA ΔFcyB::argB ΔFurD::riboB ΔFurA::riboB ΔcntA pabaA1 pantoB100 pGEM-gpdAp-FurE-K252F pantoB	(Krypotou et al., 2015)
ΔuapA UapC::pyrG ΔazgA ΔFcyB::argB ΔFurD::riboB ΔFurA::riboB ΔcntA pabaA1 pantoB100 pGEM-gpdAp-FurE-K252F-ΔC pantoB	This study
uapAΔ uapCΔ::AFpyrG azgAΔ fcyBΔ::argB furDΔ::AFriboB furAΔ::AFriboB cntAΔ::AFriboB pantoB100 pabaA1 pGEM-gpdAp-FurE-ΔN/ΔC-GFP-trpC-pantoB	This study
uapAΔ uapCΔ::AFpyrG azgAΔ fcyBΔ::argB furDΔ::AFriboB furAΔ::AFriboB cntAΔ::AFriboB pantoB100 pabaA1 pGEM-gpdAp-FurE ΔN27-29-GFP-trpC-panB	This study
uapAΔ uapCΔ::AFpyrG azgAΔ fcyBΔ::argB furDΔ::AFriboB furAΔ::AFriboB cntAΔ::AFriboB pantoB100 pabaA1 pGEM-gpdAp-FurE ΔN24-29-GFP-trpC-panB	This study
uapAΔ uapCΔ::AFpyrG azgAΔ fcyBΔ::argB furDΔ::AFriboB furAΔ::AFriboB cntAΔ::AFriboB pantoB100 pabaA1 pGEM-gpdAp-FurE ΔN30-32-GFP-trpC-panB	This study
uapAΔ uapCΔ::AFpyrG azgAΔ fcyBΔ::argB furDΔ::AFriboB furAΔ::AFriboB cntAΔ::AFriboB pantoB100 pabaA1 pGEM-gpdAp-FurE ΔN33-35-GFP-trpC-panB	This study
uapAΔ uapCΔ::AFpyrG azgAΔ fcyBΔ::argB furDΔ::AFriboB furAΔ::AFriboB cntAΔ::AFriboB pantoB100 pabaA1 pGEM-gpdAp-FurE ΔN36-38-GFP-trpC-panB	This study
uapAΔ uapCΔ::AFpyrG azgAΔ fcyBΔ::argB furDΔ::AFriboB furAΔ::AFriboB cntAΔ::AFriboB pantoB100 pabaA1 pGEM-gpdAp-FurE R108A-GFP-trpC-panB	This study
uapAΔ uapCΔ::AFpyrG azgAΔ fcyBΔ::argB furDΔ::AFriboB furAΔ::AFriboB cntAΔ::AFriboB pantoB100 pabaA1 pGEM-gpdAp-FurE K188A-GFP-trpC-panB	This study
uapAΔ uapCΔ::AFpyrG azgAΔ fcyBΔ::argB furDΔ::AFriboB furAΔ::AFriboB cntAΔ::AFriboB pantoB100 pabaA1 pGEM-gpdAp-FurE Y265A-GFP-trpC-panB	This study
uapAΔ uapCΔ::AFpyrG azgAΔ fcyBΔ::argB furDΔ::AFriboB furAΔ::AFriboB cntAΔ::AFriboB	This study

Strain genotype	References
pantoB100 pabaA1 pGEM-gpdAp-FurE K355A-GFP-trpC-panB	
uapAΔ uapCΔ::AFpyrG azgAΔ fcyBΔ::argB furDΔ::AFriboB furAΔ::AFriboB cntAΔ::AFriboB pantoB100 pabaA1 pGEM-gpdAp-FurE T359A-GFP-trpC-panB	This study
uapAΔ uapCΔ::AFpyrG azgAΔ fcyBΔ::argB furDΔ::AFriboB furAΔ::AFriboB cntAΔ::AFriboB pantoB100 pabaA1 pGEM-gpdAp-FurE ΔC498-500-GFP-trpC-panB	This study
uapAΔ uapCΔ::AFpyrG azgAΔ fcyBΔ::argB furDΔ::AFriboB furAΔ::AFriboB cntAΔ::AFriboB pantoB100 pabaA1 pGEM-gpdAp-FurE ΔC501-503-GFP-trpC-panB	This study
uapAΔ uapCΔ::AFpyrG azgAΔ fcyBΔ::argB furDΔ::AFriboB furAΔ::AFriboB cntAΔ::AFriboB pantoB100 pabaA1 pGEM-gpdAp-FurE ΔC504-506-GFP-trpC-panB	This study
uapAΔ uapCΔ::AFpyrG azgAΔ fcyBΔ::argB furDΔ::AFriboB furAΔ::AFriboB cntAΔ::AFriboB pantoB100 pabaA1 pGEM-gpdAp-FurE ΔC507-509-GFP-trpC-panB	This study
uapAΔ uapCΔ::AFpyrG azgAΔ fcyBΔ::argB furDΔ::AFriboB furAΔ::AFriboB cntAΔ::AFriboB pantoB100 pabaA1 pGEM-gpdAp-FurE ΔC510-512-GFP-trpC-panB	This study
uapAΔ uapCΔ::AFpyrG azgAΔ fcyBΔ::argB furDΔ::AFriboB furAΔ::AFriboB cntAΔ::AFriboB pantoB100 pabaA1 pGEM-gpdAp-FurE ΔC513-515-GFP-trpC-panB	This study
uapAΔ uapCΔ::AFpyrG azgAΔ fcyBΔ::argB furDΔ::AFriboB furAΔ::AFriboB cntAΔ::AFriboB pantoB100 pabaA1 pGEM-gpdAp-FurE ΔC516-518-GFP-trpC-panB	This study
uapAΔ uapCΔ::AFpyrG azgAΔ fcyBΔ::argB furDΔ::AFriboB furAΔ::AFriboB cntAΔ::AFriboB pantoB100 pabaA1 pGEM-gpdAp-FurE ΔC522-524-GFP-trpC-panB	This study
uapAΔ uapCΔ::AFpyrG azgAΔ fcyBΔ::argB furDΔ::AFriboB furAΔ::AFriboB cntAΔ::AFriboB pantoB100 pabaA1 pGEM-gpdAp-FurE W39A-GFP-trpC-panB	This study
uapAΔ uapCΔ::AFpyrG azgAΔ fcyBΔ::argB furDΔ::AFriboB furAΔ::AFriboB cntAΔ::AFriboB pantoB100 pabaA1 pGEM-gpdAp-FurE Q59A-GFP-trpC-panB	This study
uapAΔ uapCΔ::AFpyrG azgAΔ fcyBΔ::argB furDΔ::AFriboB furAΔ::AFriboB cntAΔ::AFriboB pantoB100 pabaA1 pGEM-gpdAp-FurE T63A-GFP-trpC-panB	This study
uapAΔ uapCΔ::AFpyrG azgAΔ fcyBΔ::argB furDΔ::AFriboB furAΔ::AFriboB cntAΔ::AFriboB pantoB100 pabaA1 pGEM-gpdAp-FurE S64A-GFP-trpC-panB	This study
uapAΔ uapCΔ::AFpyrG azgAΔ fcyBΔ::argB furDΔ::AFriboB furAΔ::AFriboB cntAΔ::AFriboB pantoB100 pabaA1 pGEM-gpdAp-FurE R123A-GFP-trpC-panB	This study
uapAΔ uapCΔ::AFpyrG azgAΔ fcyBΔ::argB furDΔ::AFriboB furAΔ::AFriboB cntAΔ::AFriboB pantoB100 pabaA1 pGEM-gpdAp-FurE R193A-GFP-trpC-panB	This study
uapAΔ uapCΔ::AFpyrG azgAΔ fcyBΔ::argB furDΔ::AFriboB furAΔ::AFriboB cntAΔ::AFriboB pantoB100 pabaA1 pGEM-gpdAp-FurE F196A-GFP-trpC-panB	This study
uapAΔ uapCΔ::AFpyrG azgAΔ fcyBΔ::argB furDΔ::AFriboB furAΔ::AFriboB cntAΔ::AFriboB pantoB100 pabaA1 pGEM-gpdAp-FurE K199A-GFP-trpC-panB	This study
uapAΔ uapCΔ::AFpyrG azgAΔ fcyBΔ::argB furDΔ::AFriboB furAΔ::AFriboB cntAΔ::AFriboB pantoB100 pabaA1 pGEM-gpdAp-FurE D261A-GFP-trpC-panB	This study
uapAΔ uapCΔ::AFpyrG azgAΔ fcyBΔ::argB furDΔ::AFriboB furAΔ::AFriboB cntAΔ::AFriboB pantoB100 pabaA1 pGEM-gpdAp-FurE R264A-GFP-trpC-panB	This study
uapAΔ uapCΔ::AFpyrG azgAΔ fcyBΔ::argB furDΔ::AFriboB furAΔ::AFriboB cntAΔ::AFriboB pantoB100 pabaA1 pGEM-gpdAp-FurE N347A-GFP-trpC-panB	This study
uapAΔ uapCΔ::AFpyrG azgAΔ fcyBΔ::argB furDΔ::AFriboB furAΔ::AFriboB cntAΔ::AFriboB pantoB100 pabaA1 pGEM-gpdAp-FurE S384A-GFP-trpC-panB	This study
uapAΔ uapCΔ::AFpyrG azgAΔ fcyBΔ::argB furDΔ::AFriboB furAΔ::AFriboB cntAΔ::AFriboB pantoB100 pabaA1 pGEM-gpdAp-FurE F385A-GFP-trpC-panB	This study
uapAΔ uapCΔ::AFpyrG azgAΔ fcyBΔ::argB furDΔ::AFriboB furAΔ::AFriboB cntAΔ::AFriboB pantoB100 pabaA1 pGEM-gpdAp-FurE S386A-GFP-trpC-panB	This study
uapAΔ uapCΔ::AFpyrG azgAΔ fcyBΔ::argB furDΔ::AFriboB furAΔ::AFriboB cntAΔ::AFriboB pantoB100 pabaA1 pGEM-gpdAp-FurE d438-440-GFP-trpC-panB	This study
uapAΔ uapCΔ::AFpyrG azgAΔ fcyBΔ::argB furDΔ::AFriboB furAΔ::AFriboB cntAΔ::AFriboB pantoB100 pabaA1 pGEM-gpdAp-FurE d441-443-GFP-trpC-panB	This study
uapAΔ uapCΔ::AFpyrG azgAΔ fcyBΔ::argB furDΔ::AFriboB furAΔ::AFriboB cntAΔ::AFriboB pantoB100 pabaA1 pGEM-gpdAp-FurE d444-447-GFP-trpC-panB	This study
uapAΔ uapCΔ::AFpyrG azgAΔ fcyBΔ::argB furDΔ::AFriboB furAΔ::AFriboB cntAΔ::AFriboB pantoB100 pabaA1 pGEM-gpdAp-FurE d466-468-GFP-trpC-panB	This study
uapAΔ uapCΔ::AFpyrG azgAΔ fcyBΔ::argB furDΔ::AFriboB furAΔ::AFriboB cntAΔ::AFriboB	This study

Strain genotype	References
pantoB100 pabaA1 pGEM-gpdAp-FurE d469-471-GFP-trpC-panB	
uapAΔ uapCΔ::AFpyrG azgAΔ fcyBΔ::argB furDΔ::AFriboB furAΔ::AFriboB cntAΔ::AFriboB pantoB100 pabaA1 pGEM-gpdAp-FurE d475-477-GFP-trpC-panB	This study
uapAΔ uapCΔ::AFpyrG azgAΔ fcyBΔ::argB furDΔ::AFriboB furAΔ::AFriboB cntAΔ::AFriboB pantoB100 pabaA1 pGEM-gpdAp-FurE d478-480-GFP-trpC-panB	This study
uapAΔ uapCΔ::AFpyrG azgAΔ fcyBΔ::argB furDΔ::AFriboB furAΔ::AFriboB cntAΔ::AFriboB pantoB100 pabaA1 pGEM-gpdAp-FurE d481-483-GFP-trpC-panB	This study
uapAΔ uapCΔ::AFpyrG azgAΔ fcyBΔ::argB furDΔ::AFriboB furAΔ::AFriboB cntAΔ::AFriboB pantoB100 pabaA1 pGEM-gpdAp-FurE d484-486-GFP-trpC-panB	This study
uapAΔ uapCΔ::AFpyrG azgAΔ fcyBΔ::argB furDΔ::AFriboB furAΔ::AFriboB cntAΔ::AFriboB pantoB100 pabaA1 pGEM-gpdAp-FurE d487-489-GFP-trpC-panB	This study
uapAΔ uapCΔ::AFpyrG azgAΔ fcyBΔ::argB furDΔ::AFriboB furAΔ::AFriboB cntAΔ::AFriboB pantoB100 pabaA1 pGEM-gpdAp-FurE d490-492-GFP-trpC-panB	This study
uapAΔ uapCΔ::AFpyrG azgAΔ fcyBΔ::argB furDΔ::AFriboB furAΔ::AFriboB cntAΔ::AFriboB pantoB100 pabaA1 pGEM-gpdAp-FurE Y484M-GFP-trpC-panB	This study
uapAΔ uapCΔ::AFpyrG azgAΔ fcyBΔ::argB furDΔ::AFriboB furAΔ::AFriboB cntAΔ::AFriboB pantoB100 pabaA1 pGEM-gpdAp-FurE Y484F-GFP-trpC-panB	This study
uapAΔ uapCΔ::AFpyrG azgAΔ fcyBΔ::argB furDΔ::AFriboB furAΔ::AFriboB cntAΔ::AFriboB pantoB100 pabaA1 pGEM-gpdAp-FurE S23C-GFP-trpC-panB	This study
uapAΔ uapCΔ::AFpyrG azgAΔ fcyBΔ::argB furDΔ::AFriboB furAΔ::AFriboB cntAΔ::AFriboB pantoB100 pabaA1 pGEM-gpdAp-FurE T38C-GFP-trpC-panB	This study
uapAΔ uapCΔ::AFpyrG azgAΔ fcyBΔ::argB furDΔ::AFriboB furAΔ::AFriboB cntAΔ::AFriboB pantoB100 pabaA1 pGEM-gpdAp-FurE T63C-GFP-trpC-panB	This study
uapAΔ uapCΔ::AFpyrG azgAΔ fcyBΔ::argB furDΔ::AFriboB furAΔ::AFriboB cntAΔ::AFriboB pantoB100 pabaA1 pGEM-gpdAp-FurE G112C-GFP-trpC-panB	This study
uapAΔ uapCΔ::AFpyrG azgAΔ fcyBΔ::argB furDΔ::AFriboB furAΔ::AFriboB cntAΔ::AFriboB pantoB100 pabaA1 pGEM-gpdAp-FurE L187C-GFP-trpC-panB	This study
uapAΔ uapCΔ::AFpyrG azgAΔ fcyBΔ::argB furDΔ::AFriboB furAΔ::AFriboB cntAΔ::AFriboB pantoB100 pabaA1 pGEM-gpdAp-FurE K188C-GFP-trpC-panB	This study
uapAΔ uapCΔ::AFpyrG azgAΔ fcyBΔ::argB furDΔ::AFriboB furAΔ::AFriboB cntAΔ::AFriboB pantoB100 pabaA1 pGEM-gpdAp-FurE A266C-GFP-trpC-panB	This study
uapAΔ uapCΔ::AFpyrG azgAΔ fcyBΔ::argB furDΔ::AFriboB furAΔ::AFriboB cntAΔ::AFriboB pantoB100 pabaA1 pGEM-gpdAp-FurE P354C-GFP-trpC-panB	This study
uapAΔ uapCΔ::AFpyrG azgAΔ fcyBΔ::argB furDΔ::AFriboB furAΔ::AFriboB cntAΔ::AFriboB pantoB100 pabaA1 pGEM-gpdAp-FurE A383C-GFP-trpC-panB	This study
uapAΔ uapCΔ::AFpyrG azgAΔ fcyBΔ::argB furDΔ::AFriboB furAΔ::AFriboB cntAΔ::AFriboB pantoB100 pabaA1 pGEM-gpdAp-FurE L502C-GFP-trpC-panB	This study
uapAΔ uapCΔ::AFpyrG azgAΔ fcyBΔ::argB furDΔ::AFriboB furAΔ::AFriboB cntAΔ::AFriboB pantoB100 pabaA1 pGEM-gpdAp-FurE T63C/A383C-GFP-trpC-panB	This study
uapAΔ uapCΔ::AFpyrG azgAΔ fcyBΔ::argB furDΔ::AFriboB furAΔ::AFriboB cntAΔ::AFriboB pantoB100 pabaA1 pGEM-gpdAp-FurE T38C/K188C -GFP-trpC-panB	This study
uapAΔ uapCΔ::AFpyrG azgAΔ fcyBΔ::argB furDΔ::AFriboB furAΔ::AFriboB cntAΔ::AFriboB pantoB100 pabaA1 pGEM-gpdAp-FurE S23C/G112C-GFP-trpC-panB	This study
uapAΔ uapCΔ::AFpyrG azgAΔ fcyBΔ::argB furDΔ::AFriboB furAΔ::AFriboB cntAΔ::AFriboB pantoB100 pabaA1 pGEM-gpdAp-FurE S23C/L187C-GFP-trpC-panB	This study
uapAΔ uapCΔ::AFpyrG azgAΔ fcyBΔ::argB furDΔ::AFriboB furAΔ::AFriboB cntAΔ::AFriboB pantoB100 pabaA1 pGEM-gpdAp-FurE S23C/A266C-GFP-trpC-panB	This study
uapAΔ uapCΔ::AFpyrG azgAΔ fcyBΔ::argB furDΔ::AFriboB furAΔ::AFriboB cntAΔ::AFriboB pantoB100 pabaA1 pGEM-gpdAp-FurE S23C/P354C-GFP-trpC-panB	This study
uapAΔ uapCΔ::AFpyrG azgAΔ fcyBΔ::argB furDΔ::AFriboB furAΔ::AFriboB cntAΔ::AFriboB pantoB100 pabaA1 pGEM-gpdAp-FurE S23C/L502C-GFP-trpC-panB	This study
MATa ura3 pDDGFP-2 empty vector	This study
MATa ura3 pDDGFP-2 FurE NS cDNA	This study
MATa ura3 pDDGFP-2 FurE NS cDNA S23C	This study
MATa ura3 pDDGFP-2 FurE NS cDNA T38C	This study
MATa ura3 pDDGFP-2 FurE NS cDNA T63C	This study

Strain genotype	References
MATa ura3 pDDGFP-2 FurE NS cDNA L187C	This study
MATa ura3 pDDGFP-2 FurE NS cDNA K188C	This study
MATa ura3 pDDGFP-2 FurE NS cDNA A266C	This study
MATa ura3 pDDGFP-2 FurE NS cDNA P354C	This study
MATa ura3 pDDGFP-2 FurE NS cDNA A383C	This study
MATa ura3 pDDGFP-2 FurE NS cDNA L502C	This study
MATa ura3 pDDGFP-2 FurE NS cDNA T38C/K188C	This study
MATa ura3 pDDGFP-2 FurE NS cDNA S23C/G112C	This study
MATa ura3 pDDGFP-2 FurE NS cDNA S23C/L187C	This study
MATa ura3 pDDGFP-2 FurE NS cDNA S23C/A266C	This study
MATa ura3 pDDGFP-2 FurE NS cDNA S23C/P354C	This study
MATa ura3 pDDGFP-2 FurE NS cDNA S23C/L502C	This study

2.1.2 Culture media and growth conditions

Two different types of media were used for the growth of fungal cultures, the complete medium and the minimal medium. The complete medium contained all the elements required for fungal growth, thus enabling all strains to grow normally and independently of their auxotrophies. The minimal medium contained the minimum nutrients for fungal growth. That is salt solution, carbon source (glucose, fructose or sucrose), nitrogen source and the appropriate auxotrophies, according to the requirements of each strain. Composition of all media and solutions used are shown in Table 2.2 and Table 2.3 respectively. Depending on the purpose of the culture, growth media were used in a liquid or a solid form. For the latter, 1-2% agar was added before autoclaving.

Table 2.2 Composition of culture media for the growth of *A. nidulans* (Cove, 1966; Scazzocchio et al., 1982).

	Complete Medium (CM)	Minimal Medium (MM)	Sucrose Medium (SM)
H_2O_{dist}	1 L	1 L	1 L
Salt solution	20 mL	20 mL	20 mL
Vitamine solution	10 mL	-	-
D-Glucose/D-Fructose	10 g	10 g/1 g	10 g
Casamino acids	1 g	-	-
Bactopeptone	2 g	-	-
Yeast extract	1 g	-	-
Sucrose	-	-	342.3 g

Table 2.3 Solutions used in *A. nidulans* culture media of Table 2.2.

Salt solution		Vitamine solution		Trace elements*	
H_2O_{dist}	1 L	H_2O_{dist}	1 L	$Na_2B_4O_7$ x $10H_2O$	40 mg
KCl	26 g	p-aminobenzoic acid	20 mg	$CuSO_4$ x $5H_2O$	400 mg
$MgSO_4$ $7H_2O$	26 g	biotin	1 mg	FeO_4P x $4H_2O$	714 mg
KH_2PO_4	76 g	D-pantothenic acid	50 mg	$MnSO_4$ x $1H_2O$	728 mg
Chloroform	2 mL	riboflavin	50 mg	Na_2MoO_4 x $2H_2O$	800 mg
Trace elements*	50 mL	pyridoxine	50 mg	$ZnSO_4$ x $7H_2O$	8 mg

2.1.3 Storage conditions

For long term storage, fungi strains can be preserved in glycerol stocks at -80°C. For this purpose, conidiospores from a CM plate were harvested in 1 mL of 1:1 glycerol:PBS [NaCl 8 g, KCl 0,2 g, Na_2PO_4 1,44 g, KH_2PO_4 0,24 g, pH 7.4 with 1 N HCl] in a sterile eppendorf tube. For short term storage, agar plates were stored at 4°C to avoid serious loss of fungal viability.

2.2 Genetic crosses and progeny analysis

Genetic crosses of strains were performed based on Todd et al., 2007. More specifically, petri dishes containing MM and the appropriate auxotrophies were inoculated with the two parental strains, in pairs and with a distance of 1 cm between them. After incubation at 37°C for 2-3 days, small parts of media in the contact area of the two colonies were removed with a sterile toothpick and transferred in a small petri dish containing nitrate as a sole nitrogen source and only the supplements required from both parental strains (if any). Therefore, only heterokaryons were able to produce the missing supplements and grow. This plate was then tightly sealed and incubated for at least 2 weeks at 37°C, in order to form cleistothecia.

After this period, the plates were unsealed and single cleistothecia (usually 8) were isolated using a sterile toothpick. Hülle cells, aerial hyphae and any conidiophores were removed by rolling on an agar plate and the cleistothecium was burst open by mechanical forces and the ascospores were released in an eppendorf tube containing 1 mL of sterile water. Different dilutions of the suspension from one recombinant cleistothecium were plated in order to obtain single colonies, which were then selected and analyzed for their genetic background. For the characterization of unknown strains in *A. nidulans*, growth tests are performed, comparing their growth with that of well-studied control strains in different conditions of temperature, pH, nitrogen or carbon sources, supplements, toxic

analogues and antibiotics. Further genetic analysis is usually required for their complete genetic characterization by the use of polymerase chain reaction (PCR) or epifluorescence microscopy.

2.3 Nucleic acid manipulations

2.3.1 Preparation of genomic DNA

Genomic DNA extraction from *A. nidulans* was performed as described in FGSC (http://www.fgsc.net). More specifically, CM culture plates were incubated for 3-4 days at 37°C and ¼ of the plate was harvested in 25 mL of MM containing NH_4^+ as a nitrogen source and all the supplements required. Liquid cultures were then incubated overnight at 37°C, 140 rpm. The next day, the culture was filtered through a blutex, dried and immediately frozen in liquid nitrogen. The mycelia were pulverized in a mortar with a pestle in the presence of liquid nitrogen; ~200 mg of the fine powder were transferred in a 2 mL eppendorf tube, resuspended in 800 mL of DNA extraction buffer [0.2 M Tris-HCl pH 8.0, 1% SDS, 1 mM EDTA pH 8.0], mixed by vortexing and incubated on ice for 20 min. Next, 800 µL of phenol were added and after vigorous shaking the sample was centrifuged (1200 rpm, 5 min) and the upper phase was transferred to a new 2 mL eppendorf tube. Equal volume of chloroform was added and the steps of mixing and centrifugation were repeated. As previously, the upper aqueous phase was transferred in a new eppendorf tube and DNA was precipitated by adding equal volume of isopropanol and 1/10 volume of CH_3COONa, followed by mild agitation and centrifugation (1200 rpm, 5 min). The supernatant was discarded, the pellet washed with 200 µL of 70% EtOH without mixing and after centrifugation (1200 rpm, 2 min) EtOH was removed with a pipette. The pellet was dried for 5-10 min at 50°C, resuspended in 80-100 µL of sterile H_2O_{dist} containing 0.2 mg/mL RNaseA and incubated at 37°C for 30 min. The quality and quantity of the extracted DNA was checked by agarose gel electrophoresis of 2-3 µL of the DNA solution.

Agarose gel electrophoresis was used for the analysis of size and conformation of DNA in a sample, quantification of DNA and the separation and extraction of DNA fragments. For the gel preparation, 0,8% or 1.2% agarose was dissolved in 1x TAE buffer [242 g Tris-Base, 57.1 mL glacial CH3COOH, 100 mL 0.5 M EDTA pH 8.0 for 1L 50x buffer] by warming up the solution in the microwave. After cooling, 0.5 mg/mL ethidium bromide (EthBr) was added and the solution was poured into a casting tray and left to harden. After sample loading, gels were run at 100 V, exposed to UV light with a UV transilluminator and DNA bands were visualized due to the intercalating fluorescent dye (EthBr).

2.3.2 Molecular cloning

The first step of molecular cloning is the preparation of the cloning vector and the DNA fragment of interest (insert). In particular, the insert was amplified by PCR using primers that added the desired restriction sites to its termini and was subsequently digested with the corresponding restriction endonucleases. A cloning vector that contained recognition sequences for the same restriction enzymes in its multiple cloning site was selected and subjected to digestion in order to generate sticky ends complementary to those of the digested insert (Sambrook and Russell, 2001). Restriction enzymes were from Takara Bio or Minotech (Lab Supplies Scientific SA, Hellas). The digested vector and the insert were purified from agarose gel using the Nucleospin Extract II Kit (Macherey-Nagel). The corresponding DNA bands were quickly excised from the gel under low-strength UV light exposure to avoid DNA damage, transferred into an eppendorf tube and processed as described in the manufacturer instructions.

In cases where the termini of the resulting linearized plasmid were complementary (e.g. when cloning with one restriction enzyme), the digested vector was incubated at 37^{o}C for 15 min with 1 µL of Calf Intestine Alkaline Phosphatase CIAP (TaKaRa) before being loaded to the agarose gel. Removal of the 5'-terminal phosphate groups is necessary in order to avoid self-ligation of the linearized vector and also improves ligation efficiency by diminishing the background of transformed bacterial colonies that carry "empty" vectors (Sambrook and Russell, 2001).

Generation of recombinant DNA was mediated by DNA ligase, an enzyme that covalently links the complementary sticky ends together. The purified vector and insert were mixed at a 1:3 concentration ratio along with 1 µL of T4 DNA ligase (TaKaRa) and 1x ligase buffer in 10 µL total volume. The reaction was incubated at 25^{o}C for 1.5 h and was then used to transform *E. coli* competent cells.

2.4 Polymerase Chain Reaction (PCR)

2.4.1 Standard PCR reactions

Conventional PCR reactions were performed using KAPA Taq DNA polymerase (Kapa Biosystems). A high fidelity KAPA HiFi HotStart Ready Mix (Kapa Biosystems) polymerase was used in order to lower error frequency, in the cases that the amplified fragment would be used for molecular cloning or transformation. Components and conditions of the PCR reactions are described in the Tables 2.5 and 2.6, according to manufacturer instructions.

Table 2.5 *Composition of conventional and high fidelity PCR reactions.*

Components	Final Concentration	
	Conventional	High Fidelity
10x polymerase buffer*	1x	-
dNTPs	200 µM of each	-
2x Polymerase Ready mix	-	1x
Forward primer	0.4 µM	0.4 µM
Reverse primer	0.4 µM	0.4 µM
DNA polymerase	KapaTaq 1 µL	-
DNA template	10-20 ng	10 ng
H_2O_{dist}	up to 25 µL	up to 25 µL

*with 1.5 mM $MgCl_2$

Table 2.6 *Conditions used for conventional, high fidelity and site-directed mutagenesis PCR reactions.*

Steps	Conventional		High Fidelity		Mutagenesis	
	°C	Duration	°C	Duration	°C	Duration
1	95	5 min	95	3 min	95	3 min
2	95	30 sec	98	20 sec	98	30 sec
3	T_m*-5	30 sec	60-75	15 sec	60-75	1 min
4	72	1 min/kb	72	15-16 sec/kb	72	5 min
5	steps 2-4	x25 cycles	steps 2-4	X30 cycles	steps 2-4	x18 cycles
6	72	10 min	72	10 min	72	10 min
7	12	∞	12	∞	12	∞

*The formula used for estimating the T_m of the primers is: T_m=69.3+0.41(%GC)-650/L-(%mismatch)

2.4.2 In vitro site-directed mutagenesis PCR

For site-directed mutagenesis, a pair of complimentary primers was designed for each mutation. The primers were long (35-40 nucleotides) with >50% GC-content and the mutation was located in the middle of the sequence, so that annealing to the complementary sequence of the template DNA would not be severely affected by the mismatch. Codon substitutions were designed in a way that the least possible number of mismatches would occur, by taking advantage of the redundancy of the genetic code, while the resulting codons would be frequently encountered in *A. nidulans* genome. Furthermore, designed mutations, if possible, led to the introduction of a restriction site that would enable direct diagnostic digestion after mutagenesis. High fidelity PCR reactions for *in vitro* site-directed PCR mutagenesis were carried out using KAPA HiFi HotStart Ready Mix (Kapa Biosystems) polymerase. Components and conditions for this type of PCR are described in Tables 2.5 and 2.6.

After amplification, the PCR product was incubated at 37°C for 2 h with 1 µL of the restriction enzyme *Dpn*I (TaKaRa), which cleaves methylated (GA^m|TC) DNA strands so that parental non-

mutated plasmids were fragmented. The resulting solution was used to transform *E. coli* competent cells. Plasmid DNA from the ampicillin-resistant colonies was prepared, diagnostic digestion with the appropriate restriction endonucleases was performed and the sample was sent for sequencing. Finally, plasmids with the desired mutation were transformed in *A. nidulans.*

2.5 Preparation and transformation of *Escherichia coli*

E. coli DH5a cells were prepared by streaking from the glycerol stock on an LB agar plate and incubating at 37^{o}C overnight. 5 mL LB medium were inoculated with a single colony from the plate and were incubated for 16 h at 37^{o}C, 200 rpm. An aliquot of 0.5 mL of the saturated culture was used to inoculate 400 mL LB medium in a 1 L conical flask and was incubated at 37^{o}C, 260 rpm until an OD_{600} of 0.45-0.55 had been reached. The culture was then centrifuged at low speed (4.500 g, 5 min, 4^{o}C) and the supernatant was discarded. The cell pellet was resuspended in 0.4x original volume of ice-cold transformation buffer I (30 mM CH_3COOK, 10 mM $CaCl_2$, 50 mM $MnCl_2$, 100 mM $RbCl_2$, 15% glycerol, pH 5.8 with 1 M CH_3COOH) and incubated on ice for 5 min. The cells were collected by centrifugation at (4500 g, 5 min, 4^{o}C), resuspended in 1/25 original volume of ice-cold transformation buffer II (10 mM MOPS pH6.5, 75 mM $CaCl_2$, 10 mM $RbCl_2$, 15% glycerol, pH 6.5 with 1 M KOH) and then incubated on ice for 15-60 min. Aliquots of 200 µL were distributed in sterile eppendorf tubes and frozen in liquid nitrogen. The competent cells were then stored at -80^{o}C.

Transformation of *E. coli* was performed by addition of 0.01-0.5 µg of plasmid DNA in 200 µL of defrosted *E. coli* competent cells, mixing and incubating on ice for 30 min. The cells were then subjected to heat shock by incubation at 42^{o}C for 90 sec and immediate incubation on ice for 2 min. After this, 1 mL of liquid LB medium was added and the cells were incubated at 37^{o}C for 1 h, to allow expression of the ampicillin resistance gene of the plasmid. Cell pellet was collected by centrigufation (13.000 rpm, 30 sec), resuspended in ~100 µL of LB medium and spread on LB agar plates containing 100 µg/mL ampicillin. After overnight incubation at 37^{o}C, colonies were selected and further analysed.

2.6 *Aspergillus nidulans* DNA transformation

Aspergillus nidulans transformation was performed as previously described in (Koukaki et al., 2003). In particular, conidiospores were harvested from a full grown CM culture plate and filtered through blutex. 100 mL minimal media with the appropriate supplements and nitrogen source were inoculated with the spore solution and were incubated at 37^{o}C for 4-5 h, 140 rpm. Aliquots of the

culture were regularly observed under the microscope for the appearance of germ tubes. Once conidia were at the germinative phase, incubation was stopped and the culture was transferred into sterile falcons and centrifuged (4000 rpm, 10 min). The pellet was resuspended in 20 mL of Solution I (1.2 M $MgSO_4$, 10 mM orthophosphate pH 5.8) and was poured into a sterile 250 mL conical flask. About 0.2 g of lysing enzymes from *Trichoderma harzianiae* were added for the disruption of the cell wall and release of the protoplasts. The spore suspension was incubated for 2 h at 30^{o}C, 60 rpm. Protoplasts were concentrated by centrifugation (4000 rpm, 10 min) and washed with 10 mL Solution II (1 M sorbitol, 10 mM Tris-HCl pH 7.5, 10 mM $CaCl_2$). The pellet was then resuspended in Solution II at a volume depending on the number of transformations desired. Protoplasts were distributed in eppendorf tubes and plasmid DNA was added in final concentration of 1.5-2 μg followed by ¼ of the total volume Solution III (60% w/v PEG6000, 10 mM Tris-HCl pH 7.5, 10 mM $CaCl_2$). A control tube without DNA was included in order to evaluate whether the protoplasts and the solutions used were free of contaminations. Tubes were incubated on ice for 15 min and 1 mL of Solution III was added, mixed and incubated for another 15 min at room temperature (RT). The tubes were then centrifuged (6000 rpm, 10 min), protoplasts were washed with 1 mL of Solution II, centrifuged as before and resuspended in 200 μL of Solution II. Protoplasts were transferred into 15 mL sterile falcons containing 4 mL of melted Top Sucrose Minimal Media (0.45% agar, 20 mL salt solution, 10 g D-glucose, 342,4 g sucrose for 1 L) and after mild agitation plated on SM-agar plates (sucrose minimal media; 1% agar). The SM bottom plates were supplemented with vitamins and nitrogen sources as required, depending on the selection marker carried in the plasmid/DNA cassette. Plates were incubated at 37^{o}C for 4-5 days and transformants were isolated by streaking on minimal media and analyzed further by growth tests.

2.7 Protein extraction and purification

Filtered conidiospores from a full plate were used to inoculate 100 mL of minimal media containing nitrate and necessary supplements. The liquid cultures were incubated for 14-16 h at 25^{o}C and then filtered through blutex, squeezed between two papers to remove excessive liquid and immediately frozen in liquid nitrogen. The mycelia were pulverized 5-6 times in a mortar with a pestle in the presence of liquid nitrogen, and ~400 mg of the fine powder were collected in a 2 mL eppendorf tube.

For Total Protein Extraction, the mycelia powder was resuspended in 800 μL of ice cold precipitation buffer [50 mM Tris-HCl pH 8.0, 50 mM NaCl, 12.5% (v/v) trichloroacetic acis (TCA), 1 mM PMSF, 1x Protease Inhibitors Cocktail (PIC)], vortexed and incubated for 10-30 min on ice. The

pellet was collected by centrifugation (13000 rpm, 10 min, 4°C). The pellet was resuspended once in ice-cold EtOH 100% and twice in ice cold acetone and the sample was centrifuged (13000 rpm, 5 min, 4°C) after each step. After the final centrifugation, the supernatant was discarded and the pellet was air-dried at 60°C for 30 min. The pellet was then resuspended in 500-600 μL of Extraction Buffer I [100 mM Tris-HCl pH 8.0, 50 mM NaCl, 1% (v/v) SDS, 1 mM EDTA, 1 mM PMSF, 1x PIC] and centrifuged (13000 rpm, 15 min, 4°C). The supernatant was transferred in a pre-frozen eppendorf tube and was stored at -80°C for further use.

The determinaton of protein concentration in the samples was done using the Bradford method (Bradford, 1976). The protein-dye complex causes a shift in the dye absorption maximum from 465 nm to 595 nm. The amount of absorption produced is proportional to the protein concentration. 1 mL Bradford Reagent [100 mg Coomassie Brillant Blue G-250, 50 mL 100% EtOH, 100 mL H_3PO_4, 850 mL H_2O] were transferred in a cuvette and 2 μL of the protein sample were added and vertexed briefly. Prior to reading the absorbance, 1 mL of this reagent was used to calibrate the spectrophotometer. The optical density (OD) of the protein sample in this reagent was then read at 595 nm. Each sample was analyzed twice and the protein concentrations were determined by comparing the average of the obtained OD values against BSA standard curve, generated by plotting the average of various absorbances versus various (known) concentrations of BSA.

SDS-page and western blot

For the SDS-page electrophoresis, 25-50 mg of proteins (estimated by Bradford assays) were incubated with 4x sample buffer [40% (v/v) glycerol, 250 mM Tris-Hcl pH 6.8, 0.02% (w/v) bromophenol blue, 8% (v/v) SDS, 20% (v/v) β-mercaptoethanol] for 30 min at 37°C (for membrane proteins), loaded and separated in an 8-10% (w/v) polyacrylamide gel with the use of Mini-PROTEAN Tetracell (Bio-Rad) tank filled up with Running Buffer [25 mM Tris, 192 mM Glycine, 0.1% w/v SDS] at 80 V through the stacking gel and 100 V through the separating gel. After electrophoresis, the SDS-gel was equilibrated in Transfer Buffer for 20 min. In the meantime, the PVDF membrane (Macherey-Nagel, Lab Supplies Scientific SA, Hellas) was activated by soaking in 100% methanol for 1 min. For the transfer, the gel was then placed in a cassette on top of a sponge and two filter papers (Whatman), followed by the membrane, two more filter papers and another sponge. The cassette was inserted in a blotting apparatus filled with cold Transfer Buffer [25 mM Tris, 192 mM Glycine, 20% Methanol]. Electric current was applied at 100 V for 1.5-2 h, forcing the proteins to migrate on the membrane. After transfer, the membrane was stored in TBS-T Buffer [10 mM Tris-Hcl pH 7.5, 150 mM NaCl] at 4°C.

For the blocking, the membrane was soaked in 2% (w/v) non-fat dry milk in TBS-T buffer was used for 1 h in room temperature (RT) with gentle agitation. For the immunodetection, a primary mouse anti-GFP monoclonal antibody (Roche Diagnostics, Hellas) and a mouse anti-actin monoclonal (C4) antibody (MP Biomedicals Europe) both diluted at 1:2000 according to manufacturer's instructions were used. The membrane was incubated for 2 h, RT under gentle agitation. After 3 x 10 min washing in TBS-T with vigorous shaking to remove non-specifically bound antibody, the membrane was incubated with a secondary goat anti-mouse IgG HRP-linked antibody (Cell Signaling Technology Inc, Bioline Scientific SA, Hellas), diluted in blocking solution at 1:3000 for 1 h, RT, with gentle shaking. After that, the membrane was washed again as previously and blots were developed in a dark room with Kodak developing reagents using the LumiSensor Chemiluminescent HRP Substrate kit (Genoscript USA) according to the manufacturer's instructions and SuperRX Fuji medical X-Ray films (FujiFILM Europe).

2.8 Epifluorescence microscopy and quantification

Samples for inverted fluorescence microscopy were prepared as previously described (Gournas et al., 2010; Karachaliou et al., 2013; Valdez-Taubas et al., 2004). In particular, sterile 35 mm l-dishes with glass bottom (Ibidi, Germany) containing liquid minimal media supplemented with $NaNO_3$ and 0.1% glucose (for experiments with the strong glyceraldehyde-3-phosphate dehydrogenase *gpdAp* promoter) or fructose (for experiments with the *alcAp* promoter) were inoculated from a spore solution and incubated for 16-22 hours at 25^{o}C. For the observation of proteins expressed by the *alcAp* promoter, 0.4% v/v ethanol in derepressing media for 2 hours or overnight was added in order to achieve full induction of expression. The samples were observed on an Axioplan Zeiss phase contrast epifluorescent microscope and the resulting images were acquired with a Zeiss-MRC5 digital camera using the AxioVs40 V4.40.0 software. Image processing, contrast adjustment and color combining were made using Adobe Photoshop CS3 software or ImageJ software.

For quantifying transporters endocytosis, Vacuolar Surface (Total surface of vacuoles containing GFP/hypha) and Vacuolar GFP Fluorescence (Total fluorescence intensity of vacuoles containing GFP/hypha) were measured using the Area Selection Tool of ICY application. Turkey's Multiple Comparison Test (One-Way ANOVA) was performed to test the statistical significance of the results for 5 Regions of Interest (ROIs), using Graphpad Prism 3. Images were further processed and annotated in Adobe Photoshop CS3.

2.9 Kinetic analysis of transporters

Kinetic analysis of transporters activity was measured by estimating uptake rates of [^{3}H]-uracil uptake, as previously described in Koukaki et al., 2005 and Papageorgiou et al., 2008. Briefly, conidiospores from a fresh CM culture plate were harvested in 25 mL of minimal media containing nitrate and all the necessary supplements, filtered through a blutex and incubated at 37^{o}C, 140 rpm for 4 h.

In *Aspergillus nidulans*, [^{3}H]-uracil uptake was assayed at 37^{o}C in germinating conidiospores, just prior of germ tube emergence. The culture was centrifuged (4000 rpm, 10 min) and conidiospores were resuspended in minimal media without nitrogen source and supplements, at final concentration 10^7 conidiospores/μL. The resulting spore solution was distributed in 1.5 mL eppendorf tubes (75 μL in each tube) and these were equilibrated for 10 min at 37^{o}C in the heat block. Initial velocities were measured at 1 min and at 4 min of incubation with 25 μL of radioactive substrate. Reactions were terminated by adding 1000-fold excess of ice-cold non-radiolabelled substrate. To remove non-incorporated radioactivity, the spore suspension was washed with ice-cold minimal media (12500 rpm, 5 min). The supernatant was removed by sunction and the pellet was finally resuspended in 1 mL of scintillation solution (666 mL toluol, 2.66 g PPO, 0.066 g POPOP, 333 mL Triton-X-100). The eppendorf tubes were inserted in scintillation vials and radioactivity was measured in a scintillation counter.

Initial velocities were corrected by subtracting background uptake values obtained in the simultaneous presence of 1000-fold excess of non-radiolabelled substrate. The background uptake level did not exceed 15-20% of the total counts obtained in wild-type strains. The K_m (concentration for obtaining V_m/2) of transporters was obtained directly by performing and analyzing (Prism3) uptakes at various concentrations. All experiments were carried out in triplets.

2.10 Standard UV mutagenesis

Complete medium culture plates were incubated for 4 days at 37^{o}C. Conidiospores from 4 full plates were harvested in a sterile falcon containing 20 mL H_2O-Tween (0.02%) and vortexed. The solution was then filtered through blutex in a new falcon and H_2O-Tween was added until final volume of 40 mL. After vortexing, the solution was separated in two and a final volume of 80 mL of the spore solution was equally distributed in 15-20 petri dishes, so that a very thin layer covered the bottom. The petri dishes were then exposed to UV light for 3 min 45 sec (the exposure time of the UV lamp was standardized after plotting a viability curve), all equally distanced from the UV light source. The

solution from all petri dishes was quickly collected in two new falcons and centrifuged (4000 rpm, 10 min). Only 20 mL of the supernatant were kept, and the rest were discarded. The pellets from both falcons were resuspended in the 20 mL and the final solution was poured into minimal medium containing the appropriate nitrogen source for the selection of suppressors, auxotrophies and 0.5% agar. After vortexing, 4 mL of the TOP agar with the spores overlaid 20 already dried petri dishes containing minimal medium with the same supplements but 1% agar. After stabilization, all the petri dishes were incubated in 25^{o}C for 5-8 days. Specific mutants were isolated after streaking, due to their ability to grow in the presence the specific nitrogen source. DNA extraction of the suppressors, PCR and finally sequencing of the whole gene of interest, helped us locate the mutations caused by the UV exposure.

2.11 Yeast manipulations

2.11.1 Media and storage conditions

Standard Yeast Growth Media was used, including yeast extract-peptone-dextrose (YPD) medium and ammonia-based synthetic minimal dextrose (SD) medium. In more detail, as carbon source 2% Glucose or 0.1% Glucose and 2% Galactose were added for the non-inductive or the inductive medium respectively. As nitrogen sources, 30 mM $(NH_4)_2SO_4$ or 10 mM proline were used and the final concentrations of substances added to the solid or liquid media were 0.18 mM uracil and 0.55 mM L-lysine. The pH was adjusted at pH 5.6 and for the solid plates, 1-2% agar was added. The *furE-gfp* gene and all the mutants were expressed under the control of GAL promoter.

2.11.2 Transformation

For the yeast transformation 1 mL of saturated yeast cultures in YPD media at 30^{o}C (overnight) were collected in a microfuge tube for each transformation. In 50-100 µL of the supernatant, 30 µL of 2 mg/mL carrier DNA were added and the pellet was resuspended with pipet tip. Next, 1 µg of plasmid, 0.5 mL of Plate Mixture [Sterile 45% PEG 4000, 1 M LiOAc, 1 M Tris-HCl pH 7.5, 0.5 M EDTA] and 100 mL DTT (1 M) were added and the sample was vortexed after each step. After benchtop incubation for 6-8 h (RT), cells were heat shocked for 15 min at 42^{o}C and collected by centrifugation (13000 rpm, 1 min). The supernatant was discarded with a pipet and the pellet resuspended in 500 µL of sterile water, 200 µL of which were plated in SD plates and incubated at 30^{o}C.

2.11.3 Protein extraction

For the total protein extracts, 1 mL of cells grown to the early log phase (YPD grown cells OD_{600} =1 or SD grown cells OD_{600}=0.8) were collected with centrifugation (13000 rpm, 1 min), resuspended in 250

µL of ice-cold NaOH 2 M and incubated on ice for 5-10 min. Next, 250 µL of 50% TCA solution was added, vortexed to mix and incubated on ice as much as possible. The lysed cells were pelleted by centrifugation (13000 rpm, 5 min), the protein pellet was rinsed with 100 µL of 1 M Tris Base without resuspension and fully drained with pipet. The pellet was then dissolved in 50 µL of Sample Buffer [4% SDS, 0.1 M Tris pH 6.8, 4 mM EDTA, 20% Glycerol, 2% 2-Mercaptoethanol, 0.02% Bromophenol Blue] and stored at -20^{o}C for further use.

2.11.4 Epifluorescence microscopy

For the epifluorescence microscopy observation, cells were grown up to OD_{600}=0.6-0.8 in inductive media (2% Galactose and 0.1% Glucose) and 8 µL were laid on microscope slides, fixed with the cover slip and observed at RT.

CHAPTER 3

RESULTS

3.1 Substrate specificity of the FurE transporter is determined by cytoplasmic terminal region interactions

Adapted from Papadaki GF, Amillis S, Diallinas G. ***Genetics.*** *2017. 207(4):1387-1400.*

3.1.1 C-terminally truncated Fur transporters show increased protein stability, modified apparent substrate specificities and transport kinetics

In previous studies, we have shown that Fur transporters are differentially sensitive to endocytic turnover in response to two well-characterized endocytic triggers, the excess of substrate or the presence of a primary nitrogen source (Gournas et al., 2010; Krypotou et al., 2015). In order to investigate the basis of the differential response of Fur transporters to endocytosis, we constructed and functionally analyzed strains expressing C-terminally truncated versions of FurA, FurD and FurE transporters. We also constructed a C-terminally truncated version of a specific allele of FurE, FurE K252F, which increases dramatically FurE mediated transport activity and thus permits better assessment of FurE function (Krypotou et al., 2015). Based on the fact that all Fur proteins contain several lysine residues at their C-terminal region that might act as candidates for ubiquitylation, all the truncated versions of transporters lacked the three most terminally located lysine residues.

Note that all *furE* gene versions were C-terminally tagged with the *gfp* ORF, expressed from the strong *gpd*A promoter (Punt et al., 1991) and introduced by standard genetic transformation in an *A. nidulans* strain called Δ7, which lacks all genes encoding nucleobase related transporters (*uapAΔ uapCΔ azgAΔ furDΔ furAΔ fcyBΔ cntAΔ*). The Δ7 strain has an intact endogenous *furE* gene, but it is very little expressed under standard conditions and does not contribute to detectable transport of its physiological substrates (UA, ALL) or to sensitivity in 5FU (Krypotou et al., 2015).

Figure 3.1A shows a growth test of selected transformants and isogenic control strains on UA, ALL or nitrate plus the toxic nucleobase analogues known to be transported by the Fur transporters. The wild-type positive control grows on UA or ALL and is sensitive to all the toxic analogues tested, whereas the negative control strain Δ7 has the opposite phenotype. Strains expressing the corresponding truncated versions of FurD, FurE, or FurE-K252F (i.e., FurD-ΔC, FurE-ΔC, or FurE-K252F-ΔC) showed distinct growth phenotypes when compared to their non-truncated equivalents. The strain expressing the truncated FurD transporter shows stronger growth on UA and allantoin, but is more resistant to 5FC. More impressively, the strain expressing the truncated FurE

transporter could not grow at all on UA, despite retaining full capacity to grow on allantoin or being sensitive to 5FU, 5FC, or 5FUd. In contrast, no apparent growth differences could be detected between strains expressing FurA or FurA-ΔC.

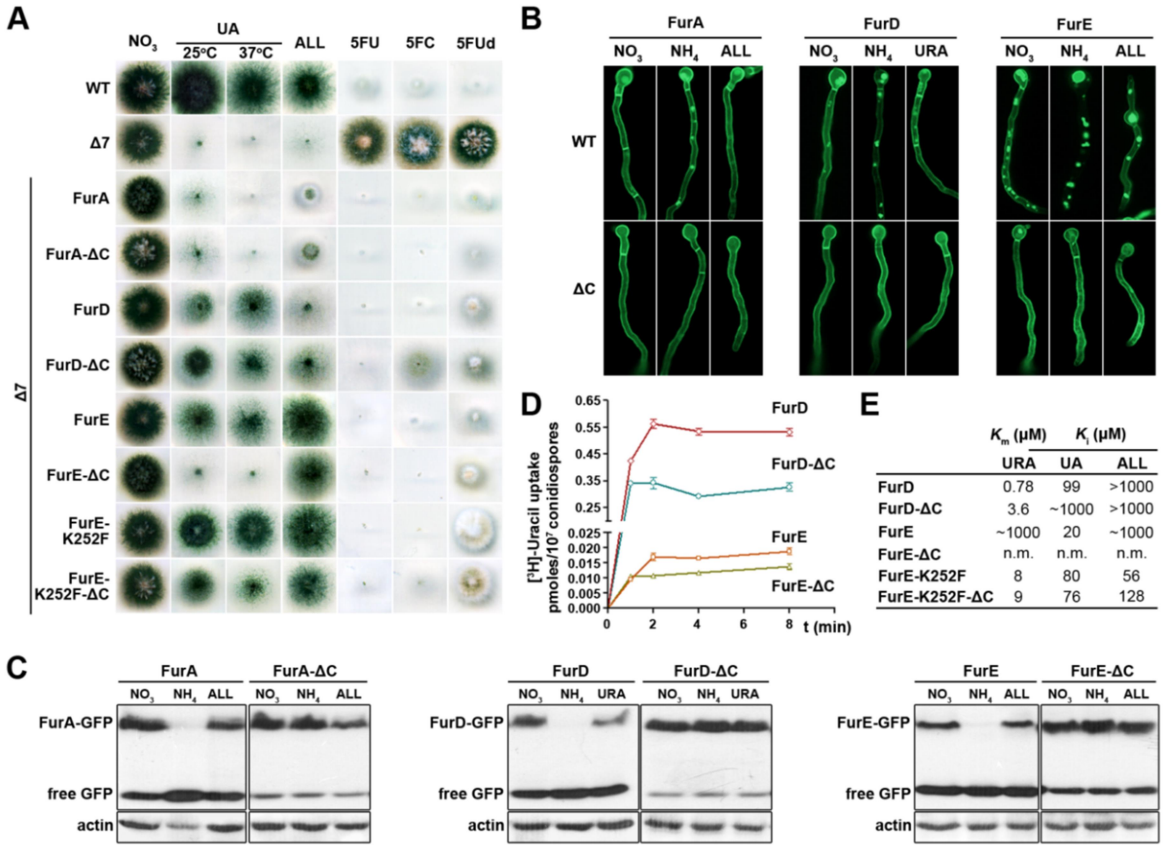

Figure 3.1 Functional characterization of truncated Fur transporters. A. *C-terminally-truncated Fur transporters show modified apparent substrate specificities. Growth test of strains expressing, from the strong gpdAp promoter, non-truncated (WT) and truncated Fur-GFP transporters. The test is performed at 37°C on MM media containing as sole nitrogen source nitrate (control), UA, or ALL, or on nitrate media containing a nucleobase toxic analogue (5FU, 5FC, or 5FUd). The growth on UA is recorded at both 37 and 25°C.* ***B.*** *C-terminally-truncated Fur transporters do not undergo endocytosis. Subcellular localization of the same strains as analyzed by in vivo inverted epifluorescence microscopy. Samples are grown for 18 h at 25°C under control (MM with nitrate as N source), substrate-elicited (ALL or URA) or ammonium-elicited endocytic conditions (addition of substrate or ammonium for the last 2 hr of the culture). Notice that different Fur transporters have distinct sensitivities to endocytosis, but truncation of the C-terminus stabilizes the Fur-GFP chimeras in all cases.* ***C.*** *C-terminally-truncated Fur transporters show dramatically reduced turnover. Western blot analysis of total protein extracts of strains expressing WT and truncated Fur-GFP versions, using anti-GFP (upper panel) or anti-actin (control, lower panel) antibody. Growth conditions are as in (B). Free GFP levels reflect vacuolar degradation of Fur-GFP proteins.* ***(D and E)*** *C-terminally-truncated Fur transporters show modified transport kinetics.* ***D.*** *Time course of [^{3}H]-uracil uptake by truncated and non truncated transporters. Standard deviation is depicted with error bars.* ***E.*** *$K_{i/m}$ values (μM) for truncated and non truncated FurD and FurE transporters determined using [^{3}H]-uracil uptake competition. Results are averages of three measurements for each concentration point. Standard deviation was <20%.*

Epifluorescence microscopy (Figure 3.1B) revealed that all the truncated Fur versions were stabilized in the PM under all conditions that elicit endocytosis. As a consequence very little, if any, fluorescence is associated within the vacuoles, unlike what is observed for the non-truncated Fur versions. Western blot analysis (Figure 3.1C) confirmed that the steady-state levels of truncated Fur proteins are similar and remain high in all conditions tested, including conditions triggering endocytosis. This contrasts with the picture of the non truncated Fur proteins, where the relevant steady-state levels show a dramatic reduction in the presence of ammonium and a significant drop in the presence of substrate (allantoin or uracil), when compared to non endocytic conditions (i.e. NO_3^-). The increased stability of the truncated versions could, in principle, explain the observation that FurD-ΔC grows better on UA or ALL compared to the wild type FurD, but could not explain the increased resistance to 5FC of the former vs the latter. More importantly, the increased stability of FurE-ΔC contrasted with its specific inability to transport UA. Thus, the apparent changes in the specificity of FurD and FurE could not be rationalized on a quantitative basis of increased protein levels.

Additionally, the transport activity of the truncated and non truncated FurD and FurE transporters was measured directly by standard uptake assays using radiolabeled uracil (Krypotou and Diallinas, 2014). FurA activity could not be measured as there is no commercially available radiolabeled allantoin. Figure 3.1D shows that FurD-ΔC and FurE-ΔC had similar initial uptake rates albeit 40-50% reduced steady-state accumulation of uracil compared to the wild type transporters. In Figure 3.1E the K_m or K_i values for uracil, UA or ALL were determined. Specifically, the FurD truncation reduced the affinity for uracil (4.6-fold) and UA (>10-fold), but did not seem to affect the very low affinity for ALL. Truncation of FurE-K252F did not affect the affinity for uracil and UA, but led to a moderate 2.5-fold reduction in ALL binding. Overall, these results showed that truncation of the C-tail of Fur transporters not only increased their stability in the plasma membrane (PM), but also led to differential modification of the relevant transport kinetics, in addition to changes in specificity.

The molecular rationale behind the unexpected observation that deletion of the C-terminal part of at least FurD and FurE led to a modification of the apparent substrate specificity of these transporters, became the major theme of the following work.

3.1.2 Genetic suppressors of the C-terminal truncation restore substrate specificity in FurE

In order to better understand how the C-terminal region might affect FurE specificity, we selected genetic suppressors that restore the ability of FurE-mediated growth on uric acid, by directly selecting for revertants on media containing UA as a sole nitrogen source, after standard UV

mutagenesis of the strain expressing FurE-ΔC. We obtained more than 50 revertants able to grow on UA and the *furE-ΔC* ORF of 45 of them was amplified by PCR and sequenced. In nearly all cases, we detected a single-codon change, and mutations were located in several transmembrane segments (TMSs 3, 7, 8, 9 and 10), in external loops L5 or L7 and in the N-terminal region. Growth tests of the revertants showed that they were all able to grow on UA, ALL and were sensitive to the toxic nucleobase analogues (Figure 3.2A upper panel). Interestingly, T133V and to a less degree some of the other mutants (e.g. Y392N, Y392E, V343I), could moderately grow on xanthine which normally is not a substrate of either FurE or FurE-ΔC. Notably, the suppressor mutations did not affect the proper localization of FurE-ΔC in the plasma membrane (Figure 3.2A lower panel) suggesting that they did not affect the folding or the overall stability of the transporter.

Comparative uptake assays further showed that most suppressors have little effect on the generally low rate of steady state accumulation of radiolabeled uracil (Figure 3.2B). The most prominent exception was mutation T133V in TMS3, which led to a >10-fold increase in uracil uptake, and to a lower degree mutations I371P (TMS9) and Y392C (TMS10), which led to 3- to 6-fold increases. This was not justified by an analogous increase in FurE protein steady-state levels as revealed from western blot analysis of two selected suppressor mutants (Figure 3.2C). Due to the generally low uptake rates of most suppressors, we could not test whether suppressors reestablished UA transport by increasing its binding. The K_i for UA could be measured only in mutant FurE-T133-ΔC (Figure 3.2D), with an affinity constant of 32 μM for UA and 57 μM for uracil. Even though these values are not directly comparable to FurE-ΔC, similar affinity constants (29 μM for UA and 49 μM for uracil) have been obtained in the strain expressing FurE-T133V non-truncated version, suggesting that the effect of this mutation is independent of the C-terminal segment.

Overall, the functional analysis of suppressors showed that the relevant mutations do not affect significantly the expression, folding, transport activity of uracil and turnover of FurE-ΔC, but specifically modify the ability of FurE-ΔC to transport uric acid. This observation suggested that suppressors might not affect the basic functional elements of FurE, including its major substrate binding site, but rather affect peripheral domains acting as selectivity filters or gating elements controlling access to the binding site, as has been previously shown to be the case for the UapA uric acid-xanthine transporter (Diallinas, 2016, 2014; Papageorgiou et al., 2008), but also for FurD (Krypotou et al., 2015).

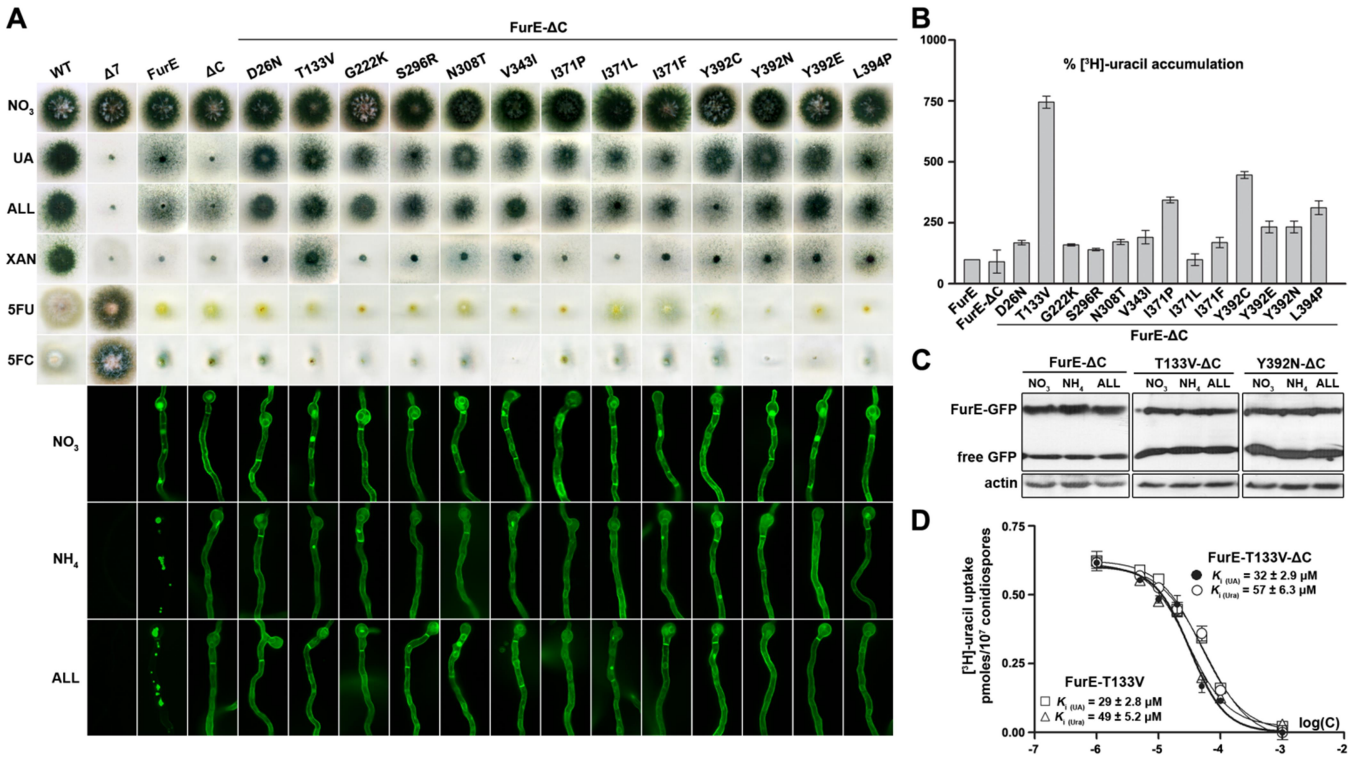

Figure 3.2 *Functional characterization of FurE-ΔC suppressors.* ***A. (upper panel)*** *Growth tests of FurE-ΔC suppressors and control strains grown in MM containing nitrate (control), UA, ALL, or XAN as N sources, or on nitrate media containing 5FU or 5FC. All growth tests shown were performed at 37°C.* ***(lower panel)*** *Subcellular localization of FurE-ΔC suppressors. Notice that some suppressor mutations lead to partial retention of FurE-ΔC in internal structures resembling ER (open rings), or to moderate sorting in the vacuole, but still the majority of FurE is sorted in the PM.* ***B.*** *Comparative [3H]-uracil accumulation in strains expressing FurE-ΔC suppressor mutations and control strains (FurE and FurE-ΔC). Standard deviation is depicted with error bars.* ***C.*** *Steady-state protein levels of selected FurE-ΔC suppressors showing increased apparent transport activity. Free GFP levels reflect vacuolar degradation of the intact Fur-GFP proteins.* ***D.*** *Dose response curve of [3H]-uracil uptake by FurE-T133V or FurE-T133V-ΔC in the presence of increasing concentration of non radiolabeled uracil or UA, respectively. Results are averages of three measurements for each concentration point. Standard deviation was <20%.*

3.1.3 Suppressors reveal the critical role of distinct gating elements in FurE function and specificity

We have previously constructed and validated structural models of FurA, FurD and FurE based on the crystal structures available for the bacterial benzyl-hydantoin Mhp1 homologous transporter. Validation included substrate docking, Molecular Dynamics (MDs) and mutational analysis. These models identified the putative binding site of relative substrates and revealed the importance of TMS10, which acts as an external gate critical for the high specificity of FurD (Krypotou et al., 2015).

Herein, we mapped all suppressor mutations in the predicted model (Figure 3.3) and based on it, we classified them in three types. Type I concerned suppressors that were proximal to the substrate binding residues and include T133V (TMS3) and V342I (TMS8) which are very close to the major substrate binding residues Trp130 and Gln134 or Asn341, respectively. Thr133 seems to be an

essential element of the major binding site, whereas Val341 lies “one step down” in the theoretical trajectory, from the binding site to the cytoplasm. Type II suppressors concerned S296 (TMS7), I371 (TMS9) and Y392, L394 in TMS10 that has been shown to act as an outward-facing gate in MhpI (Kazmier et al., 2014; Simmons et al., 2014). Finally, Type III suppressors concerned residues located in flexible loops, distantly from the binding-site. These were N26 in the N-terminal region, G222 and N308 in the extraellular loops L5 and L7 respectively.

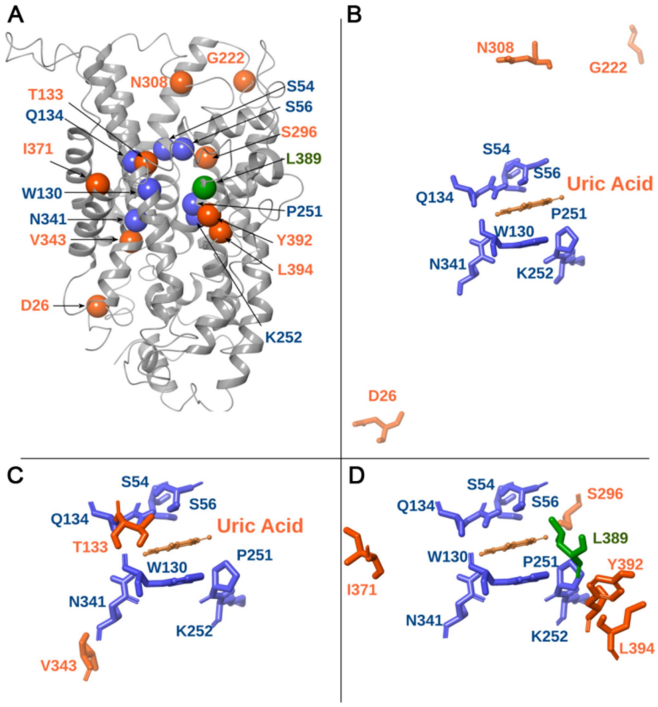

Figure 3.3 Location of suppressor mutations in the 3D model structure of FurE. A. *The residues altered are depicted as orange spheres, in relation to residues in the substrate-binding site (blue spheres) and a critical residue in the putative outer gate (green sphere) (Krypotou et al., 2015).* ***B-D.*** *Topology of amino acids modified in Type III, Type I and Type II suppressors respectively.*

3.1.4 The N- and C-terminal cytoplasmic segments of FurE come into close proximity in the absence of substrate

Given that one of the suppressors was located in the N-terminal region of FurE, we also constructed and studied an N-terminally truncated version of FurE transporter lacking the first 21 amino acids (FurE-ΔN) and a mutant lacking both its terminal regions (FurE-ΔN/ΔC). In the first case, FurE-ΔN led to specific apparent loss of UA transport without affecting transport of the other substrates, mimicking the phenotype of the C-terminally truncated transporter. Microscopic analysis showed that the FurE-ΔN version was stably localized in the PM under all conditions eliciting endocytosis (Figure 3.4). On the other hand, the doubly truncated FurE version showed growth on UA in addition to allantoin and was sensitive to toxic analogs, an apparent specificity profile that was similar to wild-type FurE (Figure 3.4). FurE-ΔN/ΔC was stably localized in the PM and did not respond to endocytosis. In other words, simultaneous truncation of both cytoplasmic terminal regions seemed to restore the wild-type FurE transport function.

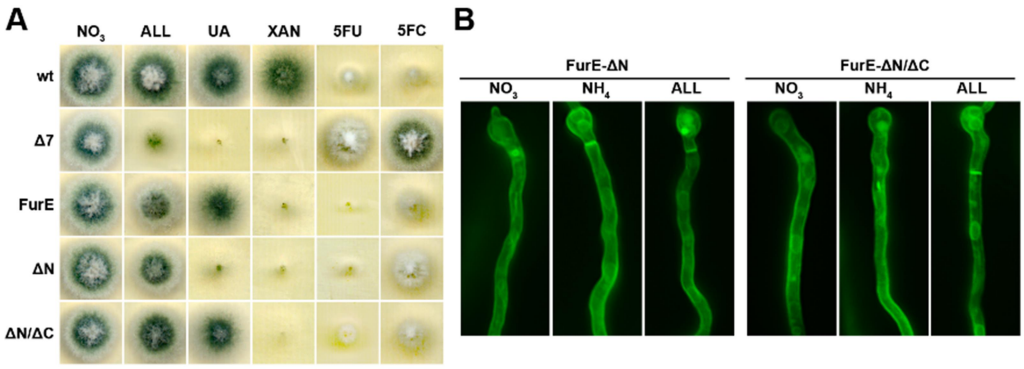

Figure 3.4 *Functional analysis of FurE-ΔN and the doubly truncated FurE-ΔN/ΔC.* ***A.*** *Growth tests of mutants and control strains (WT, Δ7, FurE). All growth tests shown were performed at 37°C.* ***B.*** *Subcellular localization of FurE-ΔN and FurE-ΔN/ΔC mutants analyzed by in vivo epifluorescence microscopy.*

The similarity of phenotypes arising from truncations of either the N- or the C-terminal regions prompted us to test whether these two domains interact and whether this interaction is part of a mechanism regulating FurE function and stability. For this reason, we employed intramolecular bifluorescence complementation assays (BiFC). Figure 3.5A shows that YFP was reconstituted in the case of the doubly chimeric YFP_n-FurE-YFP_c molecule in the PM, whereas expression of each chimera by itself (FurE-YFP_c or FurE-YFP_n) did not produce any detectable fluorescent signal. Interestingly, in the presence of substrates (e.g. allantoin) added for increasing time periods, the fluorescent signal was practically lost in a time-dependent manner (Figure 3.5B). This observation suggested that during the active transport of its substrates, FurE terminal regions are not constantly in close proximity reconstituting split-YFP.

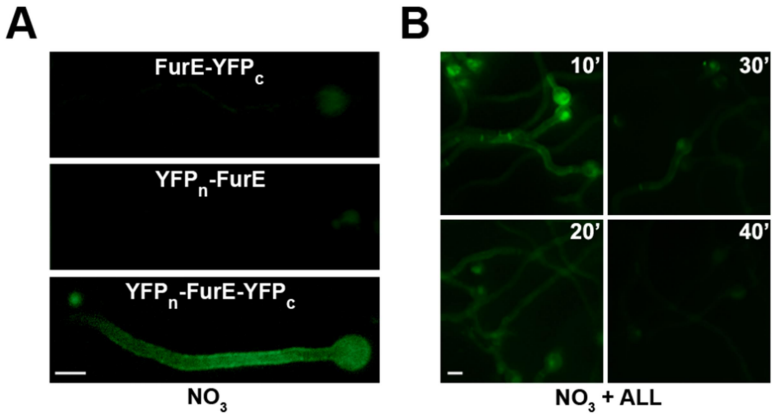

Figure 3.5 A. *Isogenic strains expressing YFP_n-FurE-YFP_c, FurE-YFP_c or YFP_n-FurE were analyzed by in vivo epifluorescence microscopy. Expression of FurE-YFP_c or YFP_n-FurE did not lead to a detectable fluorescent signal, whereas expression of YFP_n-FurE-YFP_c led to clear cortical fluorescence, compatible with reconstitution of the two parts of YFP in the doubly chimeric transporter, apparently expressed in the PM.* ***B.*** *Addition of ALL in the strain expressing YFP_n-FurE-YFP_c prior to microscopic examination, reduced and eventually turned off the fluorescent signal in a time-dependent manner. Scale bars: 5 μm.*

3.2 Cytosolic termini of the FurE transporter contain distinct elements that regulate function and specificity

Adapted from Papadaki GF, Lambrinidis G, Zamanos A, Mikros E, Diallinas G. ***J. Mol. Biol.*** *2019. 431, 3827–3844.*

Thus far, we have provided genetic evidence that the turnover, function and interestingly specificity of the *A. nidulans* NCS1 homologue, namely the FurE transporter, are regulated by dynamic interactions of its cytoplasmic terminal regions with each other and the main body of the transporter (Papadaki et al., 2017). We further dissected the function of both N- and C-terminal domains which are involved in intramolecular dynamics that are critical for the fine regulation of the gates and subsequently for substrate selection.

3.2.1 The N-terminus of FurE is essential for ER-exit, transport activity and endocytic turnover

The N-terminal region of FurE includes an absolutely conserved sequence in the Fur subfamily and in several prokaryotic NCS1 homologues, including the structurally studied Mhp1 transporter. This sequence forms the motif: **N**-X-**D**/S-**L**-X-**P** (Figure 3.6A) which will, from now on, be called Loop Interacting Domain (LID) motif, in accordance with a previous publication referring to it (Keener and Babst, 2013). Conserved amino acids in *Aspergilli* and in all fungal homologues are marked in blue and in red respectively.

We have previously characterized the function of a truncated version of FurE lacking the first 21 amino acid residues from its N-terminal region (FurE-ΔN21), tagged C-terminally with the GFP epitope. FurE-ΔN21 was insensitive to signals that elicit endocytosis such as the presence of ammonium or excess of substrate and consequently remained stable in the PM (Gournas et al., 2010; Karachaliou et al., 2013; Papadaki et al., 2017). Most interestingly, the strain expressing the truncated transporter lost its capacity specifically for uric acid transport and not for its other substrates, allantoin and uracil, as judged from relevant growth tests (Figure 3.6B). In order to investigate the function of LID and relate it to the already established role of the distal part of the N-terminus (1-21) in endocytosis and substrate specificity, we constructed and analyzed two new truncated FurE versions. The first lacked the entire N-terminal region (FurE-ΔN38) and the second only the first 11 amino acid residues (FurE-ΔN11), retaining the LID sequence. FurE-ΔN38 was found to be retained in the ER membrane and consequently had no apparent transport activity (Figure 3.6B, C). In contrast, FurE-ΔN11 possessed normal apparent transport activity and substrate specificity as judged by growth tests, but also showed partial resistance to endocytic internalization, when compared to the wild-type FurE and FurE-ΔN21 (Figure 3.6B, C).

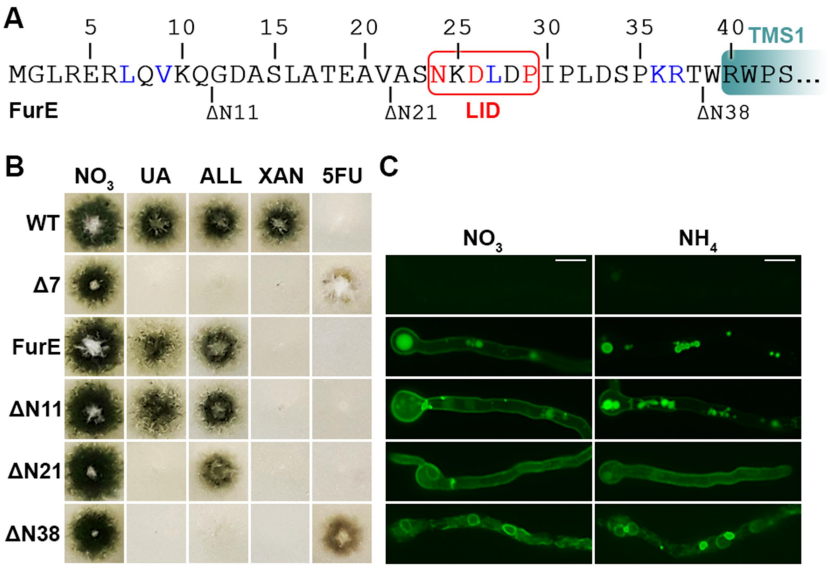

Figure 3.6 A. *Schematic representation of the cytosolic N-terminal region of FurE, depicting the limits of deletions ΔN11, ΔN21 and ΔN38, and the conserved LID motif (boxed in red). Conserved amino acids in Aspergilli and in all fungal homologues are marked in blue and in red respectively.* ***B.*** *Growth test analysis of a standard wild-type (WT) A. nidulans strain, a Δ7 strain and isogenic Δ7 transformants expressing functional GFP-tagged FurE versions. The test was performed on minimal media (MM) containing nitrate (NO_3), uric acid (UA), allantoin (ALL), xanthine (XAN) as sole nitrogen sources, and NO_3 plus the toxic nucleobase analogue 5-fluorouracil (5FU), at 37°C and pH 6.8.* ***C.*** *In vivo epifluorescence microscopy of the same strains grown until the stage of young hyphae (16-18 h in MM plus NO_3). In the right panel ammonium tartrate (NH_4^+) was added 2h before microscopic observation. NH_4^+-elicited endocytosis is visible as reduced fluorescent signal from the cell periphery concomitant with the appearance of cytosolic structures which correspond to vacuoles and endosomes (Krypotou et al., 2015; Papadaki et al., 2017). Scale bars: 5 μm.*

Comparing the effects of the three truncated versions (FurE-ΔN11, FurE-ΔN21 and FurE-ΔN38), it seems that the distal part of 11 residues of the N-terminus is partly critical for endocytosis, but redundant for transport activity or specificity, whereas segment 12-21 contributes significantly to endocytosis, but is also crucial for substrate specificity (compare truncations ΔN11 to ΔN21 in respect to endocytosis and growth on uric acid). Finally, segment 22-38 proved critical for ER-exit (compare truncations ΔN21 to ΔN38 in respect to subcellular localization). This analysis however was not sufficient to define the role of the LID, as ΔN38 deletion was not sorted to the PM.

3.2.2 The LID motif of FurE is dispensable for PM localization, transport activity and endocytic turnover, but crucial for substrate specificity

In order to further dissect the role of the LID, present in the middle part of the N-terminus (residues 21-29) we substituted its conserved residues with alanines (N24A, D26A, D26A/L27A and P29A). Figure 3.7A shows that LID mutations retained the FurE-mediated growth on uric acid and allantoin and conferred sensitivity to 5-fluorouracil (5FU), similar to that of an isogenic strain expressing wild-type FurE. Surprisingly, mutations N24A, D26A and especially D26A/L27A conferred growth on

xanthine, which normally is not transported by FurE. In other words, Ala substitutions did not seem to affect transport activity in general, but replacements of these specific residues enlarged the set of substrates transported to include xanthine.

In terms of subcellular localization, none of the mutations seemed to affect the proper sorting of FurE in the plasma membrane and neither affected its sensitivity to NH_4^+-elicited endocytosis (Figure 3.7B). We then compared the rate of [^{3}H]-uracil uptake in the different mutants, and observed an insignificant (D26A) or a ~2-2.5-fold increase (N24A, D26A/L27A, P29A) compared to that of the wild type. Given that mutants N24A, D26A and D26/L27A conferred growth on xanthine, we also tested whether this was due to an increase in the affinity for this substrate by performing competitive inhibition assays that measure radiolabeled uracil accumulation in the presence of excess xanthine (1 mM). Our results showed that only in the double mutant D26A/L27A, uracil uptake was inhibited to >50% by xanthine (Figure 3.7C).

The very low affinity transport of the novel substrate of N24A, D26A and D26A/L27A mutants is characteristic of mutations modifying the gating mechanism (Diallinas, 2016; Papageorgiou et al., 2008), suggesting that the LID sequence affects substrate specificity in a similar way.

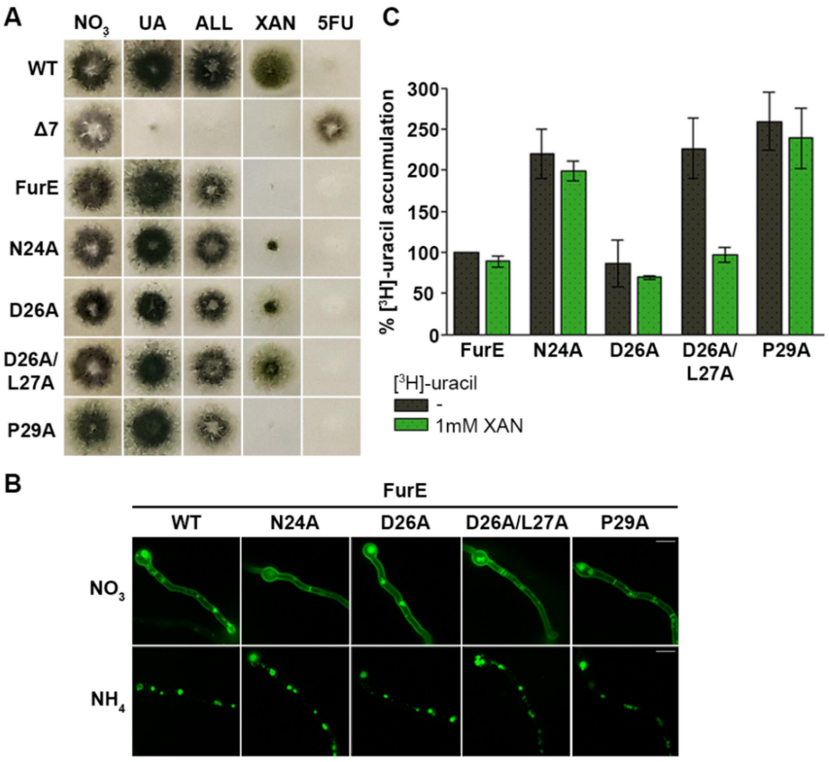

Figure 3.7 A. *Growth tests of the control strains, and strains expressing GFP-tagged FurE mutations in the LID motif (N24A, D26A, D26A/L27A, and P29A).* ***B.*** *Subcellular localization of the FurE mutants. Noticeably, none of the LID mutations affected the PM localization of FurE (NO_3 panel) or its endocytosis elicited by NH_4^+. Scale bars: 5 μm.* ***C.*** *Comparative [^{3}H]-uracil accumulation (0.5 μM) and competition assays in the presence of excess (1 mM) of xanthine in strains expressing FurE, FurE-N24A, FurE-D26A, FurE-D26A/L27A or FurE-P29A. Results shown are averages of three independent assays. Standard deviation is depicted with error bars.*

3.2.3 A tripartite role of the FurE N-terminus in endocytosis, substrate specificity and ER-exit

Next, we wanted to obtain a deeper view on the amino acid residues that are crucial for endocytosis versus those that are important for substrate specificity or ER-exit. For this purpose, we

systematically mutated the entire N-terminus of FurE by triple alanine substitutions. The only triple mutations that led to an apparent loss of FurE-mediated transport, as judged by lack of growth on allantoin or uric acid and resistance to 5FU, were those affecting residues 30-32 and 36-38 (Figure 3.8A). Epifluorescence microscopy showed that these two mutations led to retention of the transporter in the ER membrane, while all other mutants were properly located in the PM and in some vacuoles, similarly to wild-type FurE (Figure 3.8B, NO_3 panels).

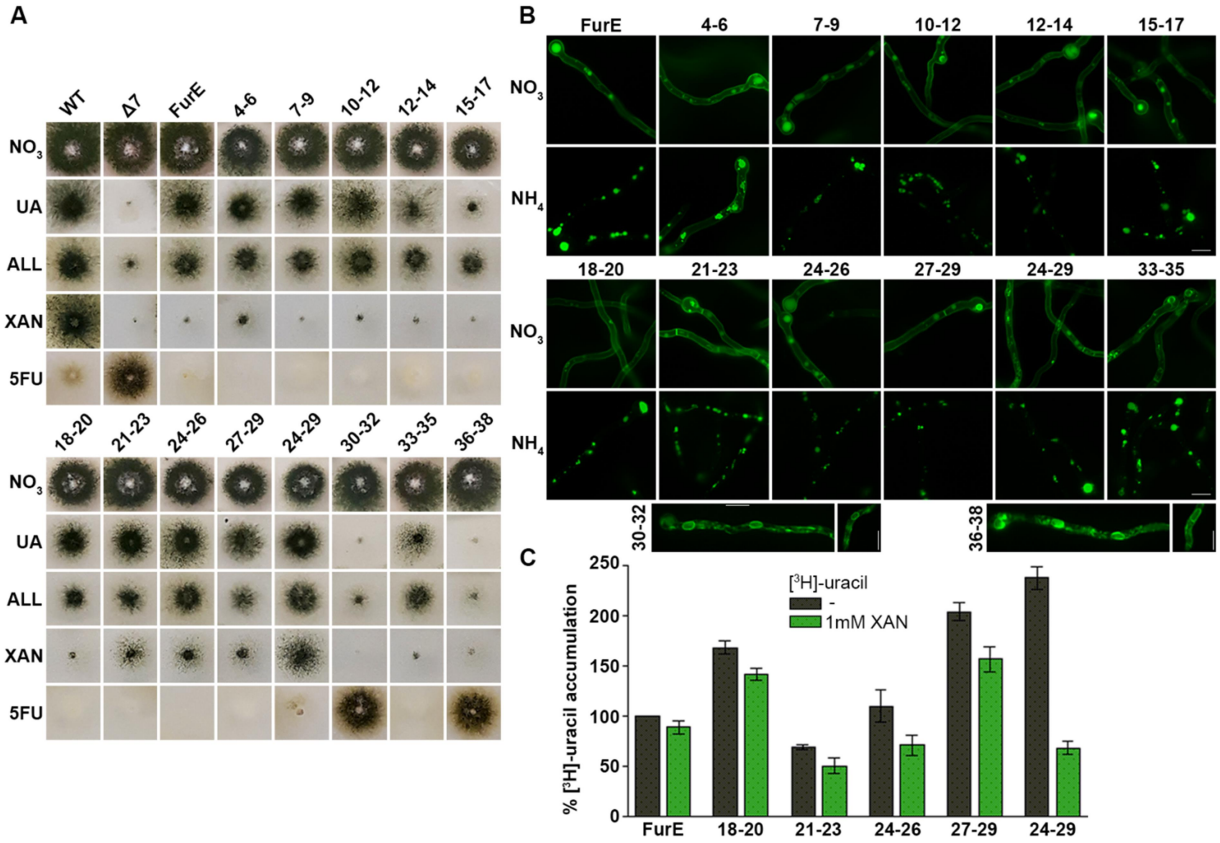

Figure 3.8 A. *Growth tests and* ***B.*** *Epifluorescence microscopy of control strains and FurE mutants expressing triple Ala substitutions in the FurE N-terminus. Each mutant is named after the position of residues replaced. Scale bars: 5 μM.* ***C.*** *Uptake assays measuring accumulation and competition assays by excess substrate of the different strains carrying triple mutations. Standard deviation is depicted with error bars. Details are as in Figure 3.7C.*

A minor reduction of growth on allantoin was observed in mutants 21-23 and 27-29 compared to the wild-type, however these mutants were still highly sensitive to 5FU, suggesting that their transport activity was generally not affected. Notably, the triple mutations concerning residues 21-23, 24-26, 27-29 and mostly the hexavalent substitution 24-29, conferred growth on xanthine which is not a substrate of FurE transporter (Figure 3.8A). This suggests that residues 24-29 of the LID are critical for substrate specificity. Additionally, growth on uric acid was reduced progressively in mutants 10-12, 12-14, 15-17 and moderately in 33-35 (Figure 3.8A), meaning that segments close to LID contribute differently to the substrate selection.

Given that several N-terminal triple Ala substitutions conferred growth on xanthine, we tested whether this was due to an increase in the binding affinity for this substrate or due to a modification in selective gating. Hence, we performed a standard competition assay measuring radiolabeled uracil accumulation in the presence of excess of non-radiolabeled xanthine in mutants 18-20, 21-23, 24-26, 27-29 and 24-29 (Figure 3.8C). Accumulation of radiolabeled uracil was significantly increased in 27-29 and 24-29 (~20-25% of wild-type FurE), but little affected in 21-23, 24-26 or 18-20 (see gray bars). The fact that the capacity for uracil uptake is not reflected in differences in growth (e.g. sensitivity to 5FU) is normal, as modifications in transport capacities lower than 70-75% do not become apparent in growth tests. Estimation of the level of inhibition of radiolabeled uracil accumulation by excess xanthine suggested that the mutations studied do not significantly modify the binding affinity for xanthine, despite a trend towards increased inhibition for uracil uptake (mostly in mutant 24-29). Thus, growth on xanthine of FurE mutants seems not to be due to increased xanthine binding, but rather to an alteration of the gating process, as also previously suggested for the single Ala replacements in the LID region. We also tested whether apparent loss of uric acid uptake in the mutant concerning positions 15-17 (i.e. S15A/L16A, as residue 17 was already an alanine in the wild-type) was due to reduced binding affinity for uric acid. Our results showed that the K_i of uric acid for uracil transport competition remained similar to that found for the wild-type FurE (K_i ~20 μM), suggesting that the defect in the S15A/L16A mutant is uric acid transport *per se*, rather than reduction of the affinity for uric acid binding (results not shown). In respect to sensitivity to endocytosis, the only alanine triplet that led to reduced internalization was the one in residues 4-6 (Figure 3.8B, NH_4^+ panels). This was in contrast to the total block of endocytosis observed when deleting residues 1-21 and resembled the partial insensitivity observed when deleting residues 1-11 (Figure 3.6C).

Overall, the above mutational analysis showed that the most distal residues of the N-tail 4-6 and 12-21 are additively essential to endocytosis, the middle N-terminal residues affect specificity (mutations in residues 24-29 led to gain of xanthine transport and mutations in residues 12-17 reduced uric acid transport), whereas residues proximal to TMS1 (30-32 and 36-38) are mostly essential for ER-exit by affecting the proper folding of the transporter.

3.2.4 Genetic evidence suggests functional interaction of LID with elements of the substrate translocation mechanism

A very useful tool to further understand how the N-terminus might affect substrate specificity was the direct selection of revertants that re-established the capacity for FurE-mediated growth on uric acid, by performing UV mutagenesis of the strain S15A/L16A. In total 24 mutants were purified and

characterized in respect to their growth phenotypes on purines and to amino acid changes that occurred in *furE* ORF. In Figure 3.9A it is shown that all suppressor mutations characterized conferred growth phenotypes practically identical to that of the isogenic strain expressing wild-type FurE (left panel) and did not affect the proper localization of FurE in the plasma membrane (right panel).

We also performed radiolabeled uracil uptake or competition assays in mutants A74V, G291S, S295P, S296R and N308T, as previously described. Most of them showed a ~50-70% reduced uptake capacity compared to the wild-type FurE (Figure 3.9B). Importantly, mutants that resulted in increased growth on xanthine (mostly G291S and N308T) also showed increased binding affinity for xanthine as indicated by the higher level of competition for uracil accumulation compared to the wild-type FurE, suggesting that the specific defect in uric acid transport in the original mutant (15-17) might be partially restored by an increase in substrate affinity.

All mutations identified, concerned five amino acid changes: A74V in TMS2, G291S, S295P, S296R in TMS7, and N308T in loop L7 (Figure 3.9C). Given that 24 random mutations concerned 5 residues and that 20 out of 24 residues were located in the same region, we can assume that the defect caused by the original S15A/L16A mutation (i.e. loss of uric acid transport) is “allosterically” transmitted in the dynamics of TMS7 and this in turn affects substrate translocation in a very specific manner.

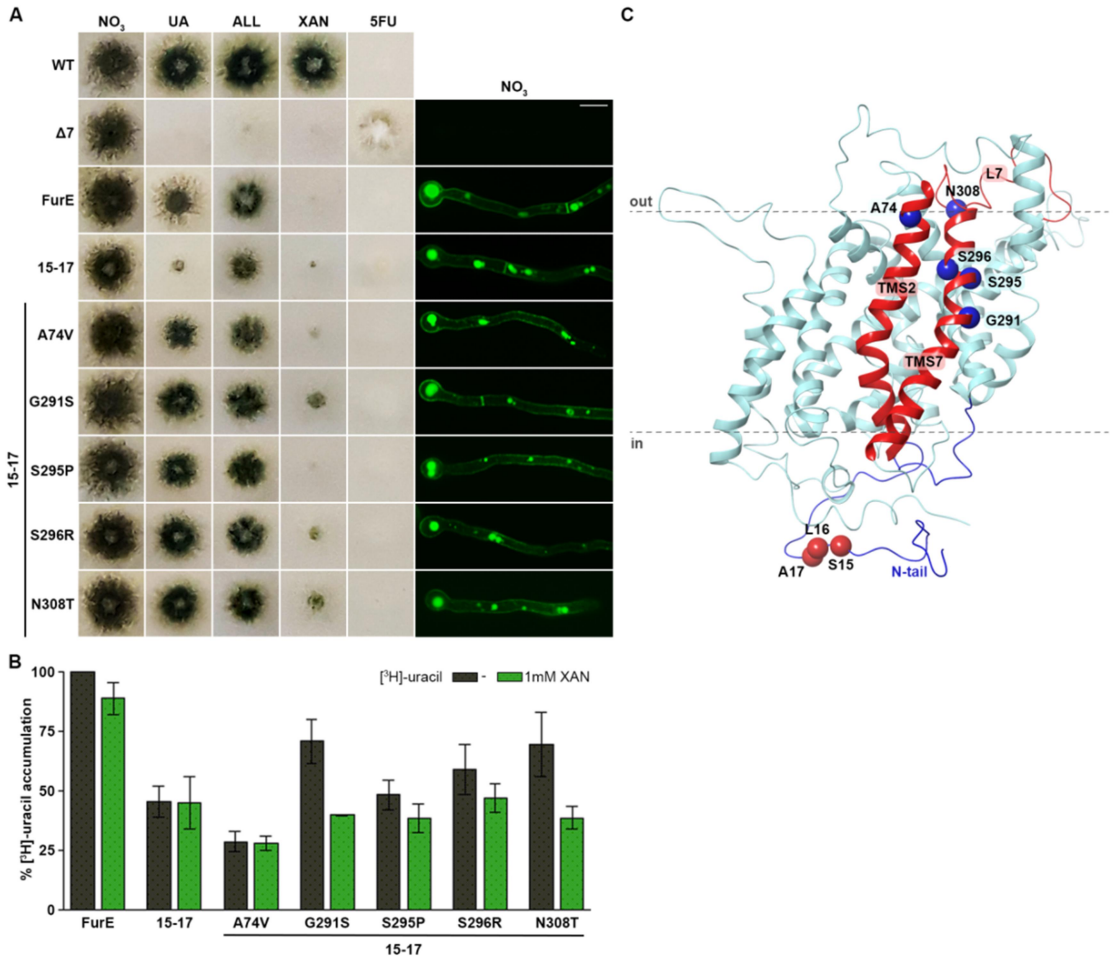

***Figure 3.9 A**. Growth tests (left panel) and subcellular localization (right panel) of the control strains, FurE-S15A/L16A mutant (named 15-17) and its suppressor strains. Notice that all suppressors were normally localized in the PM and all regained the ability of wild-type, FurE-mediated growth on UA. Scale bar: 5 μm. **B.** Relative accumulation of radiolabeled uracil and competition assays in the presence of excess substrate in different suppressors. Details are as in Figure 3.7C. Standard deviation is depicted with error bars. **C.** Topology of the suppressor mutations (blue spheres) compared to the original N-terminal S15A/L16A mutation (red spheres).*

3.2.5 Rationally targeted loop mutations and modeling support that LID interacts dynamically with internal loops to control specificity

The next question to address, was how truncations of segments or amino acid substitutions in the cytosolic N- and C-terminal regions (Papadaki et al., 2017) might be sensed by the core part of the transporter, where the substrate translocation trajectory is located.

From the crystal structure of Mhp1, it was already known that the 20 amino acid region upstream TMS1 that includes LID, is an extended conformation that runs parallel to the membrane along all cytoplasmic loops. Based on this observation, (Keener and Babst, 2013) have proposed that the N-terminus of the homologous Fur4p transporter in *S. cerevisiae*, and in particular its LID, might functionally and dynamically interact with several cytoplasmic loops when the transporter acquires

an outward-facing conformation. This interaction might be disrupted by the alternation of the transporter to its inward-facing conformation, elicited by substrate binding. The authors further proposed that dissociation of the LID from the loops renders the N-terminus accessible for Rsp5/Nedd4-type ubiquitylation and degradation, which in turn would explain the phenomenon of transport activity-dependent turnover of Fur4p. Thus, LID is acting as a conformational-sensitive degron that drives turnover under conditions that lead to partial misfolding of Fur4p. However, their hypothesis was not supported by targeted mutations in the LID motif which in their case led to no detectable effect on Fur4p stability or function. Most interestingly, (Razavi et al., 2018) showed recently that the N-terminus of the mammalian dopamine transporter (hDAT), which is a structural homologue of NCS1 transporters, interacts dynamically with specific internal loops and the C-terminus, affecting its function. Based on these reports, we tried to obtain evidence as to whether the LID of FurE interacts with the cytosolic loops of the transporter, subsequently affecting the dynamics of substrate gating and eventually transport specificity.

To identify possible interactions of the N-terminus with internal loops we built and validated, via MDs, a novel FurE structural model using as templates the occluded (PDB 4D1B) and the inward (PDB 2X79) structures of Mhp1 (Figure 3.10A). This model predicted a number of specific and possibly dynamic contacts of residues of the N-terminus with residues of internal loops (IL) and the C-terminus (shown in Figure 3.10B). The main interactions identified were: Asn24 (LID) with Arg108 (L2), Asp26 (LID) with Lys355 (L8), Asp28 (LID) with Lys188 (L4), and residues 32-38 of the N-terminus with Tyr265 (L6). Additionally, Lys188 in L4 seems to interact with the LID (Asp28) and with L8 (Thr359). Finally, residues 32-34 of the N-terminus (Leu-Asp-Ser) seem to also interact with the C-terminus, and in particular with Met505, and possibly Asp506 and Asp507. Overall, the LID is predicted to interact with L2, L4 and L8, while its downstream region that is proximal to TMS1 (residues 32-38) with L6 and the C-terminus.

In case the above proposed interactions were true, relative mutations in specific loop residues might also affect specificity. To experimentally validate this assumption, we constructed and functionally analyzed the following relative loop mutations: R108A in L2, K188A in L4, Y265A in L6, K355A and T359A in L8. The growth phenotypes and the subcellular localization of the corresponding FurE mutants are shown in Figure 3.10C.

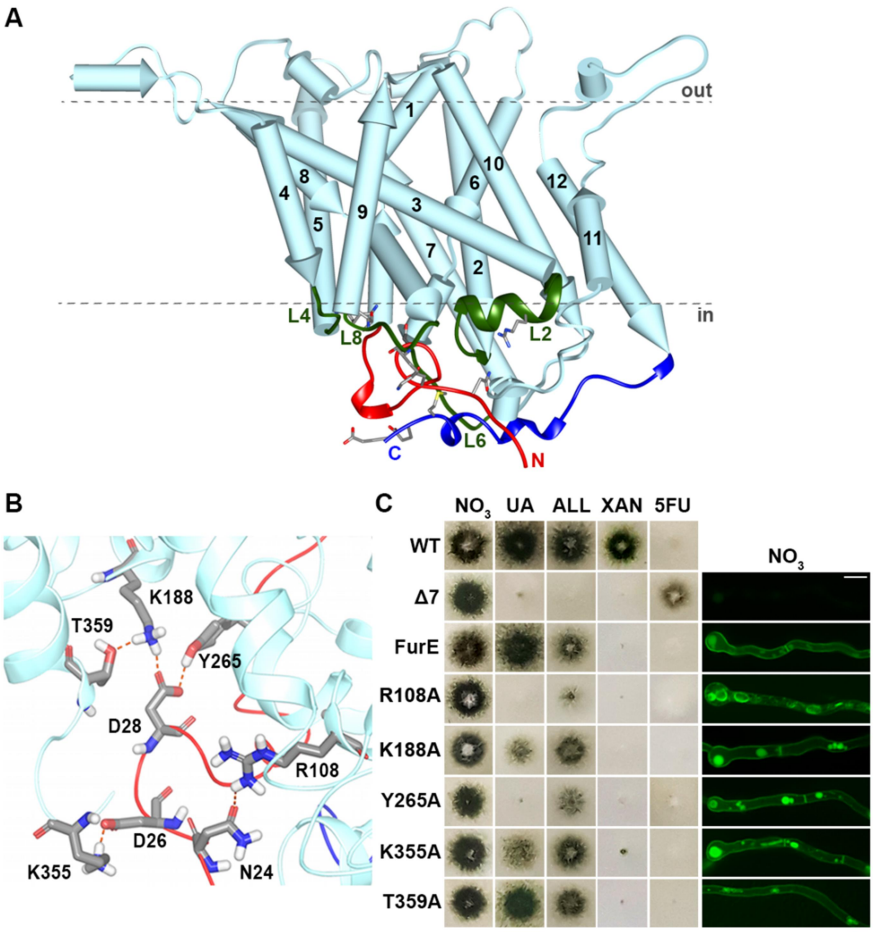

Figure 3.10 A. *FurE model. Notice the close topological distance of the N-terminal region (red) with internal cytosolic loops L2, L4, L6, L8 (green) and the C-tail (blue).* ***B.*** *Putative major interactions of N-terminal LID with internal cytosolic loops L2, L4 and L8.* ***C.*** *Growth phenotypes (left panel) and subcellular localization (right panel) of loop mutants R108A (L2), K188A (L4), Y265A (L6), K355A and T359A (L8). Scale bar: 5 μm.*

Mutation R108A resulted in total ER-retention causing significant FurE misfolding, thus, no conclusion on the role of Arg108 in specificity could be drawn. The rest of the mutants were normally localized at the PM and retained an apparent normal capacity to transport 5FU. Interestingly, Y265A resulted in very little allantoin and no uric acid transport, while mutants K188A and K355A had a reduced ability to transport allantoin and uric acid. T359A showed wild-type transport level for both substrates. In other words, Lys188 (L2), Y265 (L6) and Lys355 (L8) are indeed crucial for determining the wild-type rather broad specificity profile of FurE. Noticeably however, while mutations in the LID enlarged the set of compounds transported to include xanthine, mutations in loops L2, L6 or L8 restricted the set of substrates to 5FU, and in some cases also to allantoin. This suggests that LID-loop interactions are complex and thus the outcome of different Ala substitutions is difficult to predict. The case of R108A, which led to apparent transporter misfolding, probably highlights that

mutations in internal loops are more important for the proper folding and function than mutations in LID residues that seem to solely affect specificity.

3.2.6 LID motif is crucial for determining pH-dependent specificity of FurE

Considering that FurE is a proton symporter (Krypotou et al., 2015), we decided to test whether its function, and specifically that of the LID, would be differentially affected by the proton or cation gradient of the membrane. To that end, we tested FurE-mediated growth phenotypes on relevant substrates or toxic analogues in different pHs, as well as in the presence of a strong Na^+ gradient and we came across a notable pH-dependence of FurE activity.

In particular, as it is reflected in growth phenotypes in Figure 3.11, wild-type FurE had a significantly reduced apparent transport activity at pH 5.0, as judged by the reduced growth on uric acid and allantoin of the relevant strain. However, it could still efficiently transport uracil as seen by sensitivity to 5FU. At pH 8.0, FurE conferred normal growth on uric acid and allantoin, as well as 5FU sensitivity. Unexpectedly though, it led to significant growth on xanthine which normally is not a substrate at pH 6.8 or 5.0. Thus, the overall picture is that FurE has a previously unnoticed pH-dependent substrate profile. At low pH it efficiently transports solely 5FU (and apparently uracil), at neutral pH it additionally transports uric acid and allantoin while at basic pH additionally transports xanthine. The presence of Na^+ gradient had no effect on the apparent function of wild-type FurE or the different FurE mutants.

Interestingly, the FurE LID mutants also showed distinct pH-dependent phenotypes. At pH 5.0 most LID mutants (N24A, D26A, D26A/L27A, 24-26 and to a lower degree P29A) grew well on uric acid unlike the strain expressing the wild-type FurE, while their ability to grow on allantoin or uracil remained similar to that of the wild-type at pH 6.8. In other words, at low pH LID mutants regain wild-type transport capacity for uric acid, but not for allantoin. At pH 8.0 these mutants conserved the wild-type FurE capacity for xanthine transport, which was also apparent at pH 6.8.

Altogether, these findings revealed that at low pH wild-type FurE functions as a highly specific 5FU (uracil) transporter, incapable for transporting other structurally related substrates, whereas at basic pH FurE becomes an efficient broad-specificity promiscuous transporter, transporting uracil, uric acid, allantoin and xanthine.

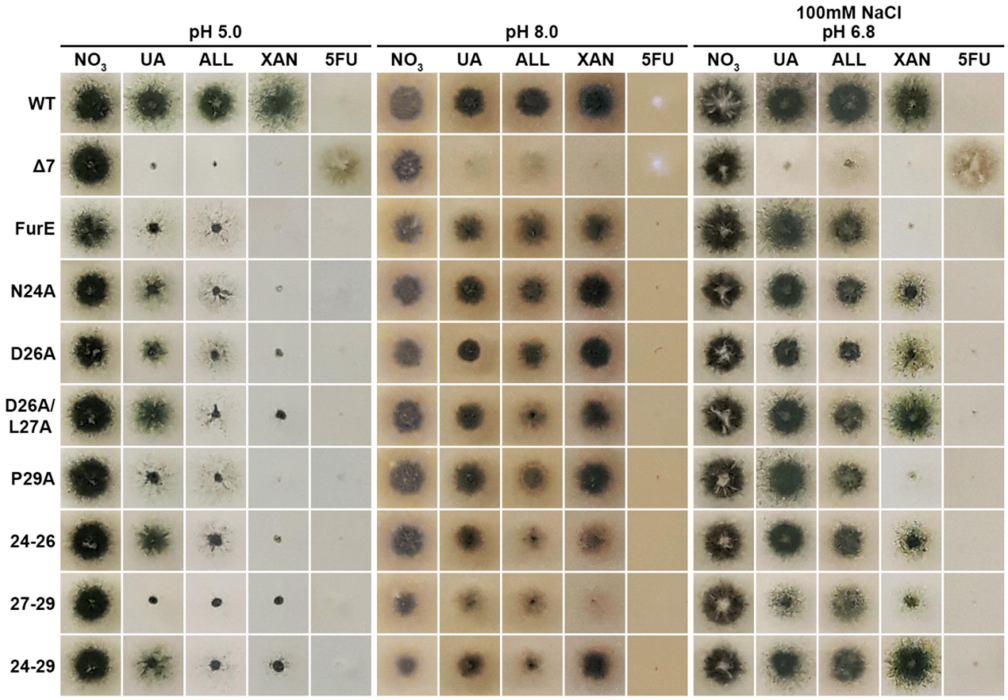

Figure 3.11 *Growth tests of control strains and LID mutations in pH 5.0, 8.0 and in pH 6.8 but in the presence of high Na^+ gradient. pH-dependence of specificity mutations suggests that ion coupling affects LID interactions and gating.*

3.2.7 Molecular Dynamics of FurE reveal pH-dependent interactions of the LID with intracellular loops affect gating

In order to gain better insight on the interactions between LID and intracellular facing loops, a detailed structural study was undertaken by running specific MD calculations that would provide evidence of the flexibility of the LID and the stability of the hydrogen bonds observed in the model. The accurate lipid bilayer composition is necessary for a successful MD simulation of a transmembrane protein. In our case, the lipid bilayer used was composed of 40% phosphatidylcholine 16:1/18:1 (PC), 20% Ergosterol (ERG), and 40% phosphatidylinositol lipids (POPI), based on data available for the composition of fungal PM. To specifically address the pH-dependent specificity of FurE, we selected different POPIs to emulate different pH environments. For the acidic pH (5.0) lipid models, POPIs with overall charge -1 (not phosphorylated inositol) were selected. For the neutral pH (6.8), 20% POPI and 20% monophosphorylated POPI on position 4 or 5 of inositol with overall charge -3 were mixed (POPI14 or POPI15 equally distributed). Finally, for the basic pH (8.0) we have selected 20% POPI and 20% di-phosphorylated POPI on position 4 and 5 of inositol (POPI24 or POPI25 equally distributed), with overall charge -4. In addition, we ran Molecular Dynamic Simulations of the FurE mutant version where residues 24-28 of the LID were substituted by Ala, using the lipid bilayer simulation for the neutral pH. FurE was embedded on each lipid bilayer,

and solvated by explicit water molecules (TIP3P) and 100 ns of simulation have been calculated in all four cases.

The MD simulations suggested that N-terminus exhibits a dynamic behavior for the part between residues 20-29 (that is the LID), while the proximal to TMS1 part (residues 30-40) displays sparse flexibility. The RMSD of the backbone depicted in Figure 3.12A shows that in all cases except at pH 5.0, the LID was flexible after the first 30 ns of the simulation period. Figure 3.12B-E illustrates the significant motion of the LID and the rather fixed position of the downstream residues 30-40, which remained in close proximity mostly with L8 but also with L2 and L10. Interestingly, although the LID mutant (24-28) was simulated using the lipid bilayer for neutral pH (6.8), it displayed different and more flexible dynamic behavior compared to the wild type, which exhibited only minor deviation from the initial structure for more than the first part of the calculation. The highest RMSD in the simulation was attained at pH 8.0, reaching 15 Å for most of the calculated time period. This might be due to the higher number of interactions of Lys25 with lipid molecules (Figure 3.13A), in addition to the role of other positively charged residues, such as Lys188 and Arg360, which seem to attract PIP2 molecules due to the higher negative charge of the phosphorylated phosphatidylinositol, thus facilitating the displacement of the LID (Figure 3.13B). The apparent stability of the segment of residues 30-40 was in good agreement with the experimentally defined structures of Mhp1. The comparison between the two crystal structures, outward-open (2JLN) and inward-open (2X79) presented in Figure 3.14 shows that only the segment upstream from the small bend at Pro15 is re-oriented in the inward position, thus relaxing the interaction between LID and L8 as TMS8 is also slightly bent, similar to what has been shown for LeuT (Krishnamurthy and Gouaux, 2012). Although there are important differences between Mhp1 and LeuT in the mechanism of substrate translocation, it appears that the interruption of the contact between the N-terminus and L8 is common in both cases. Our results suggest that FurE displays the tendency to follow a motion more similar to that observed in Mhp1.

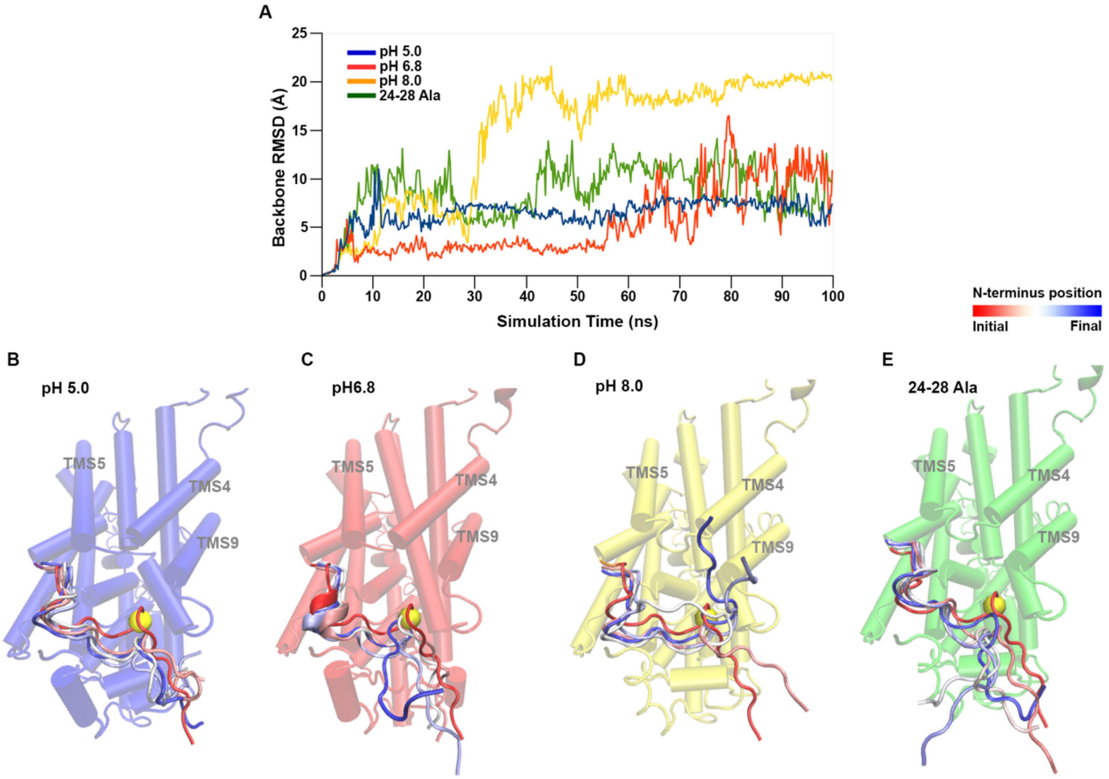

Figure 3.12 Molecular Dynamics of FurE and the LID mutant at different pHs. A. *RMSD of all Cα atoms of the LID residues 20-40 in respect to the initial structure (blue: pH=5.0, red: pH=6.8, yellow: pH=8 and green: 24-28 Ala mutant).* ***B-E.*** *Schematic representation of FurE cytoplasmic view together with the conformational transition of the LID residues. Snapshots were taken every 25 ns along the transition pathway and are illustrated in color code (red for the initial and blue for the final position). Proline 29 showing the residue of the LID most flexible part is labeled as a yellow sphere.*

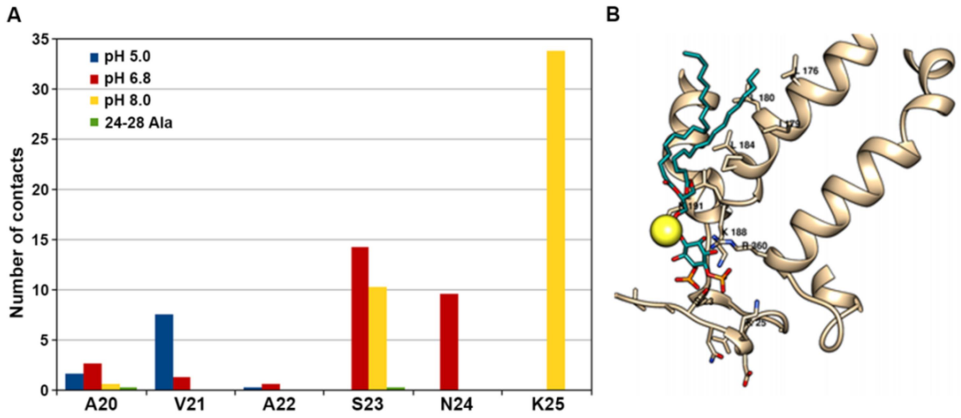

Figure 3.13 A. *Number of contacts with lipids of different N-terminal residues in all four MD simulations (blue: pH 5.0, red: pH 6.8, yellow: pH 8.0, green: 24-28 Ala mutant).* ***B.*** *Final structure of the MD simulation at pH 8.0 showing the interactions between the 4,5-phosphorylated phosphatidylinositol lipid with FurE. More specifically the polar head forms salt bridges with K188, R360 and K25 and a hydrogen bond with S23. A positively charged sodium ion is also attracted in the vicinity of the above interactions (yellow sphere). The hydrophobic tail of the lipids interacts all along the TMS4 with several lipophilic residue side chains.*

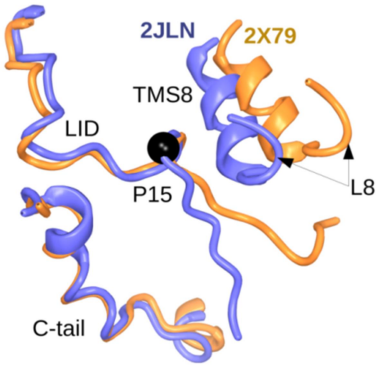

Figure 3.14 *Superposition of the N-terminus in the outward-open structure (PDB 2JLN; blue) onto the inward-open structure (PDB 2X79; orange) of Mhp1 transporter. The L8 loop and TMS8, which participate in interactions with the LID are shown.*

In order to better visualize and further understand the specific motions of the different helices during the MD simulation we have investigated a) the RMSD of each individual helix, b) the corresponding tilt compared to the Z-axis, and c) the distance of each axis center to that of TMS2, which is the TMS with the less motion. The calculations showed that in all cases, TMSs 4, 5, 9 and 10 have a higher propensity to bend, specifically at the loops L4 and L9. The RMSD for the initial position calculated during the MD simulation showed that all four TMSs move away from the initial structure between 2 to 5 Å (Figure 3.15A-D). Differences between the four simulations were more pronounced in the case of TMS5, where the wild-type FurE at pH 8.0 and the LID mutant at pH 6.8 showed larger deviations than those of the wild-type at pHs 5.0 and 6.8.

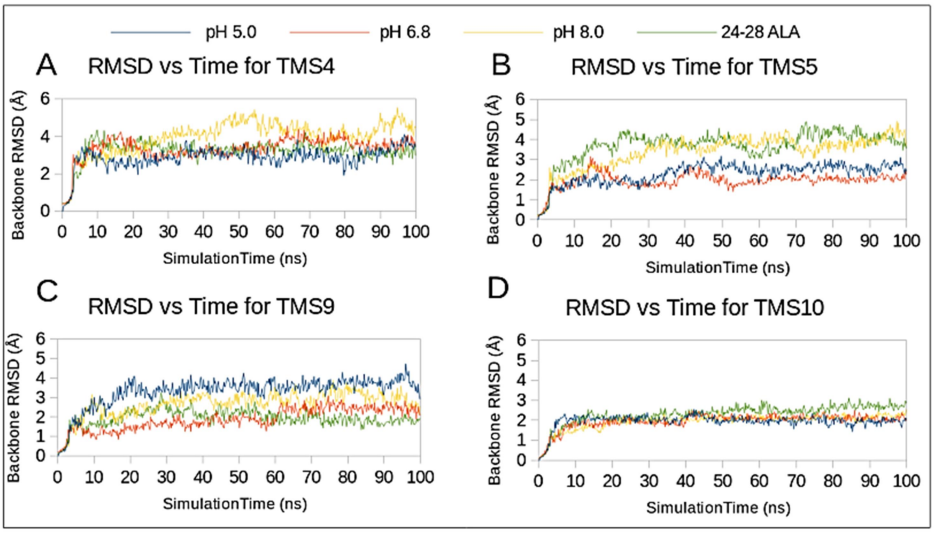

Figure 3.15 *MD simulations monitoring the motion of TMS4, 5, 9 and 10.* ***A-D.*** *RMSD of all Ca atoms of the specific helix residues in respect to the initial structure versus time.*

Similarly, highest deviations of the initial value are observed for the tilt of the helices compared to the Z-axis in the case of TMS5, with the LID mutant tilting in the opposite direction compared to the three different pH simulations (Figure 3.16 E-H).

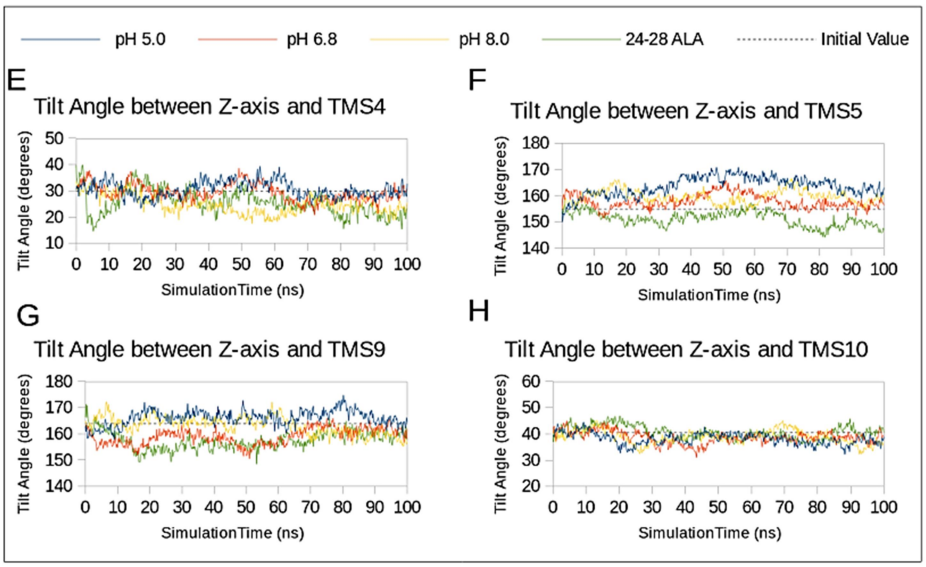

Figure 3.16 *MD simulations monitoring the motion of TMS4, 5, 9 and 10.* ***E-H.*** *Tilt Angle between Z-axis and the specific helix.*

Finally, when comparing the distance of the axis between the four TMSs 4, 5, 9 and 10 with TMS2, again the highest variation was observed in the case of TMS5, where the mutant displays the highest deviation from the initial value while the pH 5.0 simulation remains almost stable (Figure 3.17I-L). Importantly, the specific propensity is clearer when comparing the TMS 5 and TMS9 with the inward open structure of Mhp1.

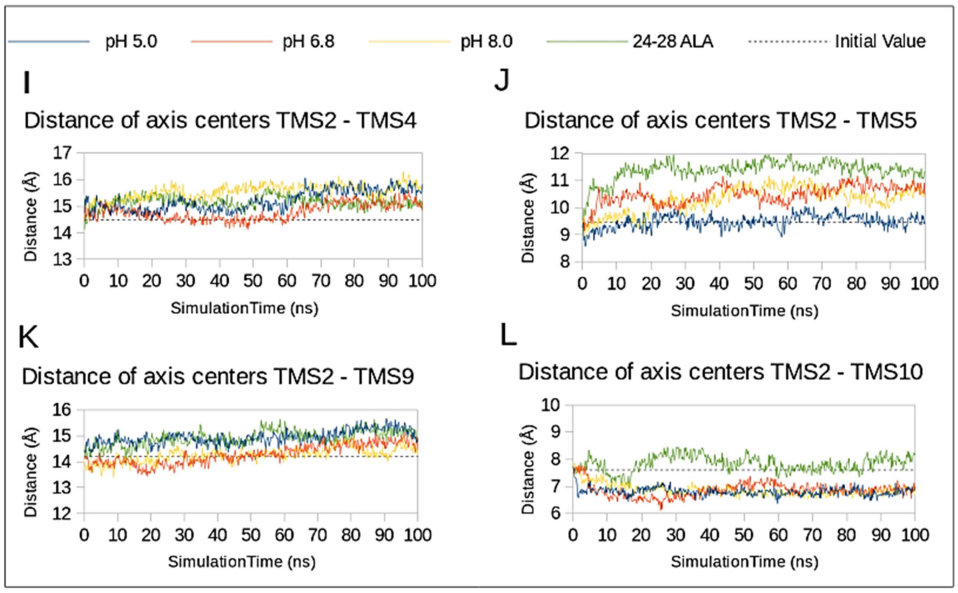

Figure 3.17 *MD simulations monitoring the motion of TMS4, 5, 9 and 10.* ***I-L.*** *Distance of axis centers of each specific helix and TMS2.*

In Figure 3.18A-B, the final structures of each one of the four MD calculations were superimposed together with the inward-open Mhp1 structure (PDB 2X79). In all four cases,

TMS5 showed a propensity to bend towards the inward conformation, with the simulation of pH 8.0 approaching closer to the open structure of Mhp1. In the extracellular interface, TMS9 showed the highest deviation with the LID mutant exhibiting a tendency to remain in the outward-open conformation, while at all pH simulations L9 was bent quite similarly to the Mhp1 inward-open structure.

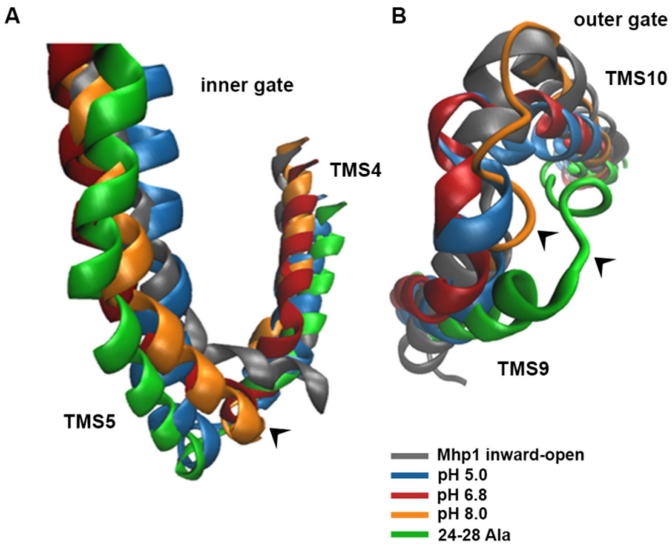

Figure 3.18 A-B. *Comparison of the Mhp1 crystal structure (grey) in the inward-open form (PDB 2X79) with the final structures of the four MD simulations of FurE. The two gates are indicated by arrow heads: intracellular gate L4 between TMS4-TMS5* ***(A)*** *and extracellular gate L9 between TMS9-TMS10* ***(B)****. Notice that the outer gate L9 bends covering the binding cavity at pH 5.0 and 6.8, while it remains in open position in the Ala 24-28 mutant. Also, the intracellular TMS5 segment shows a propensity to bend opening the inner gate in the LID mutant, but this is less apparent in the other three simulated structures.*

Overall, MD simulations suggested that the N-terminal LID exhibits relatively high flexibility at the initial part of the calculations, more pronounced in the case of pH 8.0 and in the LID mutant, mainly driven from the stronger Coulomb interactions between positively charged residues and negatively charged lipids. These interactions mostly influence putative contacts with L8 and TMS9, as shown in Figure 3.18A-B. The proximity of TMS9 to TMS4 appears to be the main reason of a concerted influence to TMS4 and TMS5. The main conclusion from the above MD calculations is that LID motions can influence, in a pH-dependent manner, both the exterior and interior gates and thereby the substrate translocation and transporter specificity. What is also notable is that when the LID motions are higher, as in the case of pH 8.0 or in the LID mutant, FurE acts as a promiscuous transporter recognizing all possible substrates. On the other hand, it becomes more specific for uracil and allantoin as shown from lower pH simulations performed with the wild-type protein.

3.2.8 Specific C-terminal elements are necessary for endocytosis, transport activity and substrate specificity

We have previously shown (Papadaki et al., 2017) that truncation of the 30 last residues of the FurE C-terminus has a dual effect blocking endocytosis and leading to loss of uric acid transport. The first was also achieved when we replaced the two most distal lysines in the C-tail (K521, K522) with arginine residues (Papadaki et al., 2019), suggesting that block of endocytosis in FurE-Δ30 is primarily due to the lack of these two lysines that apparently act as ubiquitin acceptor residues (not shown). In order to better define the limits of the C-terminal segments that affect endocytosis versus substrate specificity, we performed systematic alanine replacements of the last 30 residues of the FurE C-tail (Figure 3.19A).

In Figures 3.19B-C, it is shown that triple Ala replacements in the C-terminus affect transport activity, specificity and endocytic turnover of FurE. More specifically, Ala substitutions of 504-506, 507-509 and 510-512 abolished the ability for growth on uric acid. The triplet 504-506 had additionally a strong reducing effect on growth on allantoin and led to partial resistance to 5FU, showing that the sequence G-M-E is absolutely essential for transport activity *per se*. Ala substitutions in 513-515 had a moderate effect on uric acid growth. Finally, Ala mutations in the distal C-tail (516-524) had no apparent effect on FurE function. These findings showed that the C-tail is critical for both transport activity (504-506) and specificity 507-512. In respect to NH_4^+-elicited endocytosis, Ala mutations in 501-503 were sufficient to totally block endocytosis, similar to FurE-Δ30. Partial abolishment of endocytosis was also observed in mutants 504-506 and 513-518, which might be due to an indirect effect on the topology of 501-503 (Figure 3.19B).

Moreover, we performed radiolabel uracil uptake or competition assays for mutants 501-503, 504-506, 507-509 and 510-512, which seemed to define functional or specificity elements in FurE. Mutants 501-503 and 510-512 conserved 68-80% of the wild-type FurE transport activity, but mutants 504-506 and 507-509 showed significantly reduced activities (~11-20%) [See grey bars in Figure 3.19D].

In competition assays mutant 501-503 behaved similar to the strain expressing wild-type FurE and reflected a significant (~75%) inhibition by excess uric acid (i.e. a high affinity substrate), moderate (~39%) inhibition by allantoin (i.e. a low affinity substrate), and no inhibition by xanthine (i.e. not a substrate). Somehow, mutant 510-512 showed reduced inhibition by either uric acid or allantoin, compared to wild-type FurE. Finally, mutants 504-506 and 507-509 showed practically no measurable inhibition by uric acid, allantoin or xanthine, which is in agreement with growth tests showing no or very little growth on these purines. Thus, direct uptake measurements further

confirmed that residues 504-512 are important for the function and specificity of FurE, while residues that affect endocytosis (501-503) are not critical for function or specificity.

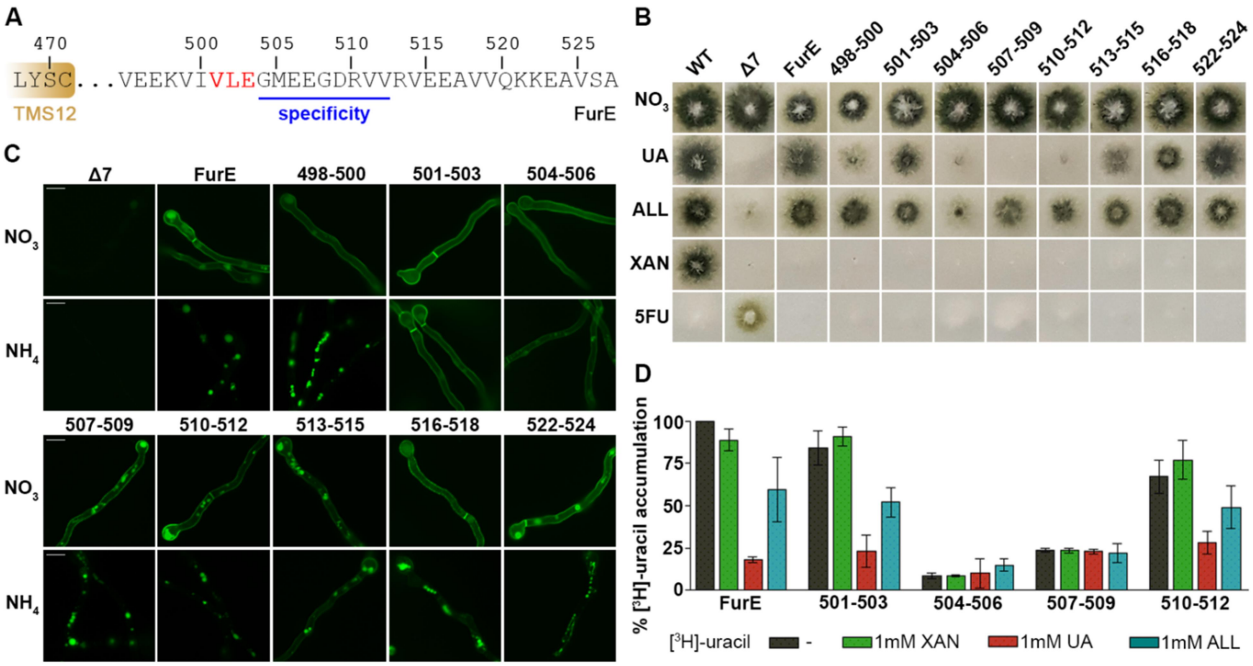

Figure 3.19 Systematic mutational analysis of the C-terminus defines the limits of elements necessary for endocytosis, transport activity and substrate specificity. A. *Sequence of the cytosolic distal C-terminal region of FurE (495-527). The residues involved in endocytosis are highlighted in red and the region involved in substrate specificity determination is underlined, as evidenced in B and C.* ***B.*** *Growth tests of control strains and FurE mutants expressing triple Ala substitutions in the FurE C-terminal region. Each mutant is named after the position of residues replaced. Notice that mutants 504-506, 507-509 and 510-512 have totally lost the ability to grow on UA, while 513-515 has reduced growth on UA. Mutant 504-506 has also significantly reduced ability to grow on ALL and is partially resistant to 5FU, signifying that this mutant is a nearly loss-of-function mutant overall.* ***C.*** *Epifluorescence microscopy of the mutants shown in A. Notice that in the absence of an endocytic signal (NO_3 panel), all FurE mutants are normally localized in the PM. However, in mutants 501-503 and 504-506, FurE shows increased stability with no sign of steady state vacuolar turnover, as in the wild-type FurE or the other mutants. This is in line with the observation that in these mutants, and particularly in 501-503, FurE is also resistant to NH_4^+-elicited endocytosis, suggesting the sequence V-L-E is a primary element necessary for endocytosis. Finally, the fact that the following sequence G-M-E (504-506) is critical for the transport of all substrates (as shown in B), reveals that this element is absolutely essential for the transport mechanism of FurE per se. Scale bars; 5 μm.* ***D.*** *Accumulation of [^{3}H]-uracil in the simultaneous presence of excess (1 mM) of various substrates as indicated. Standard deviation is depicted with error bars.*

3.3 Characterization of the substrate translocation trajectory of the FurE/NCS1 transporter

3.3.1 Mutational analysis confirms the functional importance of specific residues in substrate translocation trajectory

To investigate the validity of the modeled substrate translocation trajectory proposed by MDs, we performed relative mutational analysis of specific residues that most probably form dynamic interacting networks or are elements of the alternating inward- and outward- facing pore cavities. Using standard directed mutagenesis protocols, we constructed the following mutations of FurE: W39A, Q59A, T63A and S64A (in TMS1); R123A (in TMS3); R193A, F196A and K199A (in TMS5); D261A and R264A (in TMS6); N437A (in TMS8); and S384A, F385A and S386A (in TMS10) (see Figure 3.20). Among those residues, W39-R193, Q59-S386 and R123-D261-N345 were predicted to specifically interact with each other (marked in the same color in Figure 3.20). All mutant alleles were fused C-terminally with *gfp* and introduced in the *A. nidulans* Δ7 strain. The strong *gpdA* promoter was used for their overexpression, as previously described (Papadaki et al., 2019, 2017).

Figure 3.21 summarizes the growth phenotypes of control strains and all FurE mutants that could be classified into three major types in respect to their FurE-dependent growth. Type I includes loss-of-function mutants (i.e. similar to the negative control Δ7 strain; Type II includes mutants with partial loss-of-function and/or modification of substrate specificity; and Type III includes mutants that have a similar to the positive control strain expressing the wild-type FurE growth phenotype. Based on this, we can say that most FurE mutants were significantly affected as they belong in Type I (R123A, D261A, R264A and F385A) or II (W39A, R193A, Q59A, T63A, S64A, S386A, F196A, K199A). Only mutants N347A and S384A conserved a wild-type profile of FurE-dependent growth on all three major substrates, a picture reflected to strong growth on uric acid and allantoin and sensitivity to 5FU. All mutants affected in FurE transport activity lost significantly their capacity of uric acid transport, while conserving detectable, albeit variable capacity for allantoin or 5FU transport. Among mutants scoring as total loss-of-function, only R264A was due to a gross defect in stable localization in the PM, as in all other cases the mutant FurE versions were located in the periphery of the cells, in septa and some vacuoles (the latter reflects the normal constitutive turnover of the (Figure 3.21 right panel).

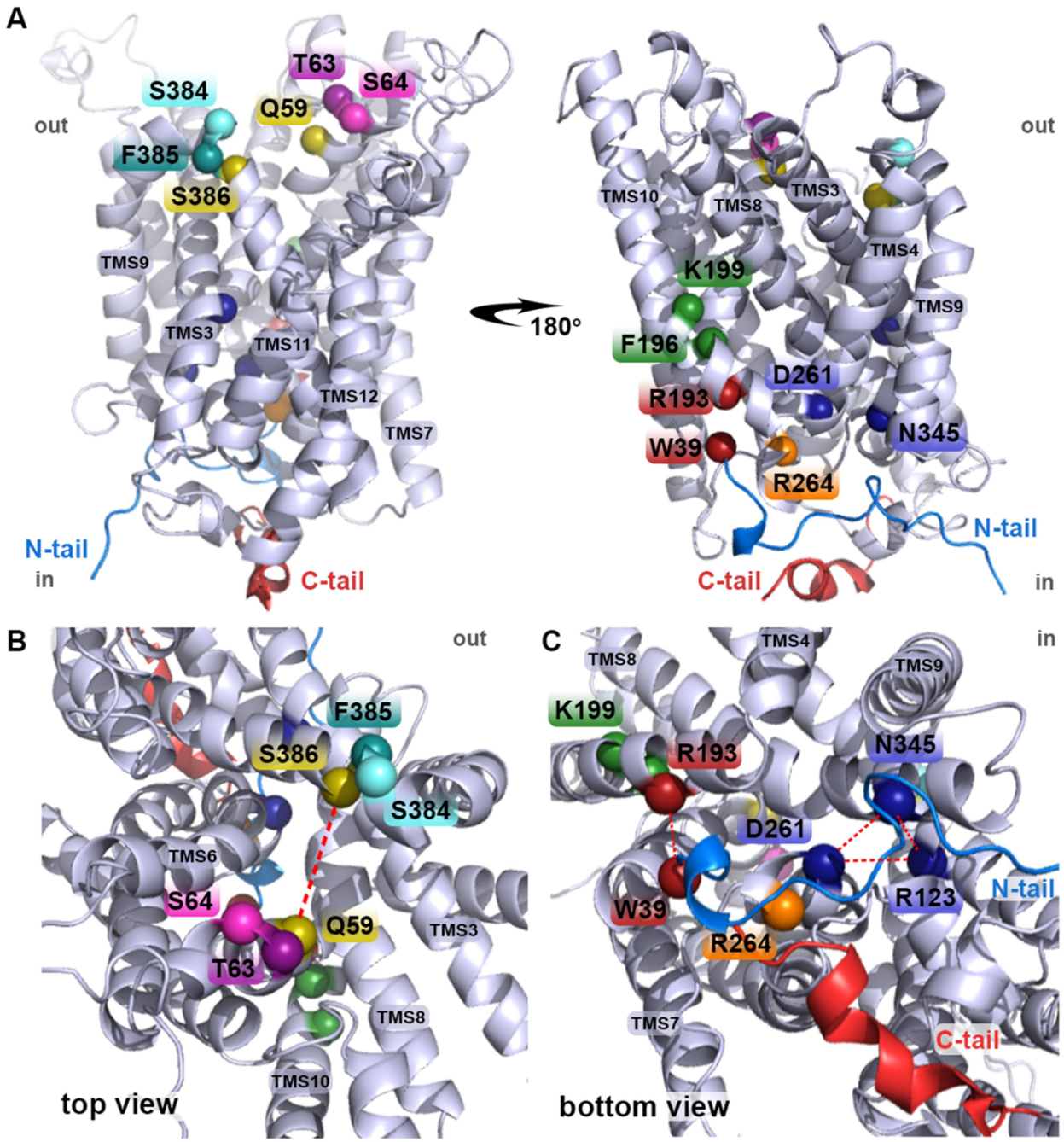

Figure 3.20 A. *FurE outward model where the residues proposed to be elements of the substrate translocation pathway are depicted as spheres.* ***B.*** *Top view of FurE where putative interactions between residues Q59 and S386 (in yellow) are depicted.* ***C.*** *Bottom view of FurE. Putative interactions of residues W39 and R193 (in red) and R123-D261-N345 (in blue) are marked. Most residues are located in the alternating inward- and outward-facing pore cavities and the triplet R123/D261/N345 in the substrate binding site.*

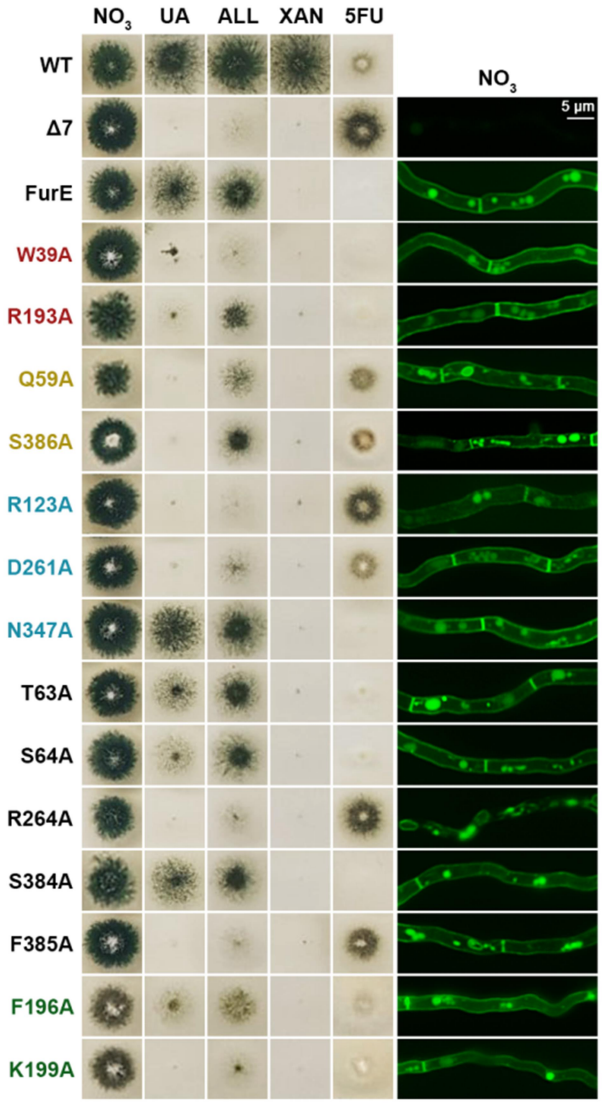

Figure 3.21 *Functional analysis of substrate translocation trajectory mutants. Growth test* ***(left panel)*** *of control strains and strains expressing FurE carrying mutations in specific residues that are proposed to be involved in the substrates translocation trajectory. Colors indicate residues that are elemets of specific, dynamic interactions (see also Figure 3.20) and showed very similar defects in the apparent FurE transport activity and specificity.* ***(right panel)*** *Subcellular localization of the same strains grown until the stage of young hyphae. Notably, all mutants except R264A are normally localized in the PM. Details are as in Figure 3.6A and B.*

Notably, mutations in residues proposed to be elements of specific dynamic interactions along the substrates trajectory (see Figure 3.20 and 3.21) showed similar defects in FurE apparent transport activity and specificity. In particular, Q59A and S386A both led to loss of uric acid transport and reduced allantoin and 5FU accumulation. T63A and S64A, which affect residues that are proposed to interact with S386, also showed specific loss of uric acid transport, but retained allantoin and 5FU accumulation. W39A and R193A led to loss of uric acid transport, conserved significant 5FU transport (sensitivity) and differ only in allantoin transport. R123A and D261A led to a dramatic loss

of transport of all three substrates; F196A and K199A that were proposed to affect residues along the cation (H^+) trajectory led to significantly reduced FurE transport activity for all three substrates. Given their proposed involvement in H^+ coupling, mutants F196A and K199A were also tested on different pHs (i.e. pH 5.0 and 8.0). At pH 5.0, F196A showed reduced apparent growth on all substrates tested, similar to the wild-type FurE, while K199A showed no growth at all. At pH 8.0, the growth test was similar to that at neutral pH (Figure 3.22).

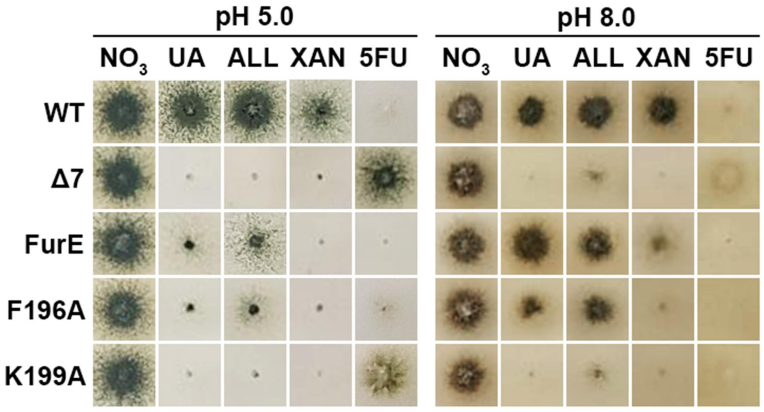

Figure 3.22 *Growth tests of control strains and strains expressing FurE carrying mutations F196A and K199A that are proposed to be elements of the cation (H^+) trajectory, in pH 5.0 and 8.0.*

3.3.2 The sequence identity of TMSs 11 and 12 is not important for FurE function

Crystal structures and relative Molecular Dynamics of NCS1-similar transporters, including those regarding the bacterial homologue Mhp1, supported that TMS11 and TMS12 do not participate in transport catalysis. Although distinct crystal structures of Mhp1 correspond to monomeric forms, some of the structurally similar transporters conforming to the 5+5 inverted repeat fold were shown to exist as dimers. In some cases, as in SERT, DAT or LeuT, a role of TMS11 and TMS12 in dimerization has been proposed, however there is no formal proof for dimerization of these transporters *in vivo*. A prominent example where dimerization is experimentally supported in an APC protein, is the arginine:agmatine antiporter of *E. coli*, namely the AdiC transporter, which has been crystallized as a homodimer (Fang et al., 2009; Gao et al., 2009; Kowalczyk et al., 2011). Despite lack of sequence similarity, AdiC exhibits the same fold of the sodium-coupled symporters LeuT, Mhp1, vSGLT, BetP etc. It consists of 12 transmembrane domains arranged in a 5+5 inverted repeat. TMSs 1, 3, 6, 8 and 10 form a central cavity that is considered to be the substrate binding site, while the last two transmembrane domains of AdiC seem to be involved in its homodimerization and particularly, hydrophobic amino acids from TMS11 of one AdiC molecule interact with non-polar residues from TMS12 of the adjacent molecule. Additional interactions are mediated by residues in TMS3 and TMS10 (Gao et al., 2009).

Previous studies concerning NCS1 transporters failed to show a specific functional role of residues of the last two TMSs in transport kinetics and/or specificity. In FurE, we have employed several unbiased genetic screens to select functional mutants located in TMS11 or TMS12 without success and we never obtained any evidence of dimerization by *in vivo* bifluorescence complementation assays (BiFC) or experiments detecting *trans-endocytosis*. The latter has been successfully performed for the extensively studied UapA transporter of *A. nidulans* which is now known to form a tight homodimer (Alguel et al., 2016; Martzoukou et al., 2015). In particular, it has been demonstrated that a UapA mutant which cannot be ubiquitylated and thus is not internalized, exhibited vacuolar localization upon co-expression with the wild-type UapA transporter under conditions that elicited endocytosis. This phenomenon of the so called *in-trans* endocytosis of provided evidence for the association of UapA transporter in homo- or oligo-dimers (Gournas et al., 2010). Moreover, typical intragenic complementation related to dimerization has been observed in UapA, when two different mutant versions that were retained in the ER, were partially re-localized in the PM after co-expression (Martzoukou et al., 2015). We did not obtain similar evidence of apparent intragenic complementation at the level of subcellular localization for FurE, when we performed relative experiments (i.e. co-expressing wild-type FurE and FurE mutants that could not be internalized). Additionally, as previously described for UapA BiFC assays (Martzoukou et al., 2015), we constructed FurE molecules tagged with each of the two halves of the Yellow Fluorescent Protein (YFP). Strains co-expressing FurE-YFP_N/FurE-YFP_C and isogenic strains expressing solely FurE-YFP_N or FurE-YFP_C (negative controls) were observed *in vivo*, by epifluorescence microscopy. YFP reconstitution signal indicates topological proximity of the two differentially tagged molecules and thus indication for homo- or oligo-dimerization. Yet no reconstituted YFP signal was obtained in the case of FurE.

In order to investigate whether TMS11 or TMS12 of FurE play a role in transport activity, substrate specificity, subcellular trafficking and/or PM localization or turnover, we constructed triple alanine substitutions in residues predicted to be part of the last two TMSs. As shown in Figure 3.23, none of the mutations, except the one in residues 484-486 (Y-Y-L) at the cytoplasmic side of TMS12 significantly affected the FurE-dependent growth on uric acid, allantoin or sensitivity to 5FU. Alanine replacements of residues 487-489 (L-F-F) and 490-492 (V-W-P) led to a change in specificity, reflected in loss of uric acid transport but retention of allantoin and 5FU accumulation. The apparent loss-of-function by Ala substitution of 484-486 was shown to be due to defective localization of FurE in the PM due to blockage of trafficking at the level of the ER. To better understand the nature of this defect, we constructed single Phe or Met replacements of Tyr484, the only well conserved residue of the triplet 484-486. We chose Phe as it is an amino acid with similar chemical properties (aromatic)

and Met as it is the residue found in Mhp1 in the same position. Both these mutations led to a similar defect in FurE localization in the PM due to ER retention, similar to the triple Ala replacement. Thus, we identified Tyr484 as a functionally irreplaceable residue due its essential role in ER exit and PM translocation of FurE. Given that Tyr also has a hydroxyl group, Ser should also be tested in order to address whether it is the aromaticity or the –OH group (or both) that is necessary for FurE proper localization. Relative to the essential role of Tyr484, it is noticeable that very little is known on whether tyrosine kinases are present in fungi.

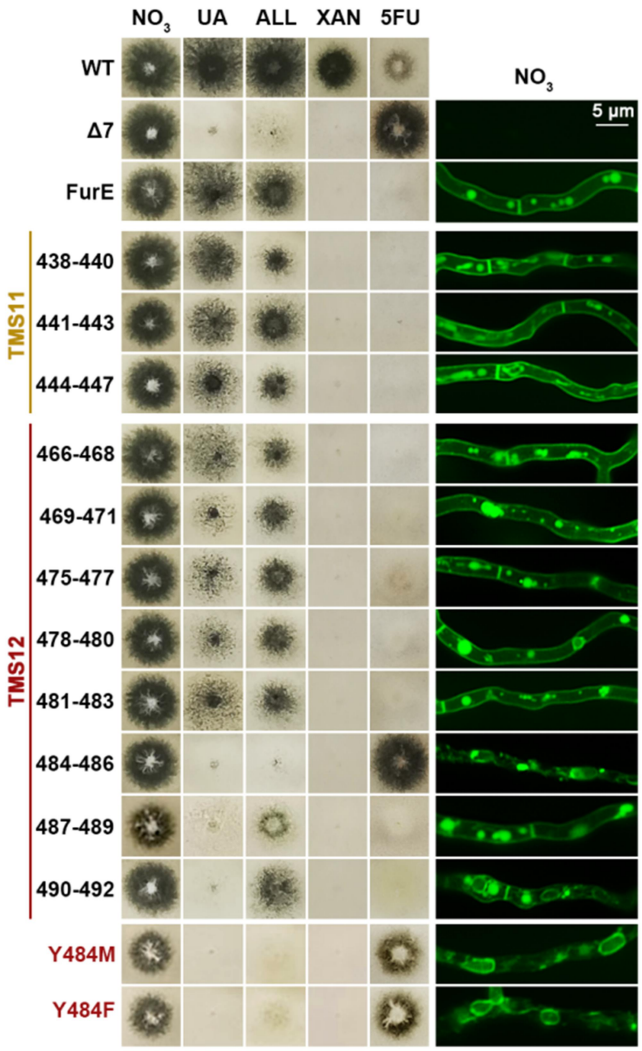

Figure 3.23. (left panel) *Growth test of control strains and strains expressing FurE mutants with triple alanine substitutions in the last two transmembrane domains. Each mutant is named after the position of residues replaced.* ***(right panel)*** *Subcellular localization of the FurE mutants. Noticeably, only the triplets* ^{484}*-YYL-*^{486} *and to a less extend* ^{490}*-VWP-*^{492} *affect the PM localization of FurE, as well as the single mutations in Y484. Details are as in Figure 3.6A and B. Scale bar: 5 µm.*

Altogether, our analysis shows that the sequence identity of TMSs 11 and 12 is not important for FurE transport activity. However, we did identify a specific, conserved Tyr residue in TMS12 that is structurally and/or functionally important, leading to an inability for proper trafficking to the PM. Whether Tyr484 affects proper intrinsic folding or/and is part of an element necessary for ER-exit via interaction with COPII proteins is interesting to be examined. Finally, we discovered that Ala replacements in the last two triplets in TMS12 (487-489 and 490-492) can affect specificity, in line with previous findings that the C-terminal region downstream from TMS12 (498-512) also affects specificity and in particular the capacity for uric acid transport (Papadaki et al., 2019).

3.4 Integrative structural approaches for understanding the mechanism underlying the control of gating and specificity by cytoplasmic termini of transporters

We have previously shown that the cytoplasmic terminal regions of the fungal NCS1 transporter FurE, control specificity from a distance (Papadaki et al., 2017). Using MDs and mutational analysis we postulated that this occurs via interactions of the tails with the cytoplasmic loops, which in turn affect the gating process at the extracellular side of the PM. Interestingly, the crystal structure of the *Drosophila melanogaster* dopamine transporter dDAT, as well as, *ab initio* structure prediction tools and extensive MD simulations of the mammalian hDAT transporter (Khelashvili et al., 2015; Penmatsa et al., 2013; Razavi et al., 2018), have shown similar possible interactions of the N- and C terminal regions with internal loops, with each other and with charged membrane lipids. Thus, although phosphorylation and interactions with membrane lipids emerge as key players governing the role of cytoplasmic regions of eukaryotic LeuT like transporters (Coleman et al., 2016; Penmatsa et al., 2013), we basically ignore the details of this 'long-distance' effect of transporter tails on function and specificity (Mikros and Diallinas, 2019). The main bottleneck leading to this critical gap in our understanding is the fact that structural information concerning the tails of eukaryotic APC transporters is lacking.

X-ray crystallography provides structural information at high resolution, however structures represent only one snapshot of their highly dynamic behavior during transport cycle and a significant amount of time is required to resolve each one of them. Moreover, we cannot obtain information on the tails of the transporters, as they often contain intrinsically disordered parts that cannot be captured and resolved by crystallography. An emerging powerful method that can provide information on the dynamic properties of these systems in their native environment is the Electron

paramagnetic resonance (EPR) spectroscopy which has gained increased importance in structural biology. The method is relied on the magnetic dipole coupling between two unpaired electrons and is used to unravel secondary structure elements, domain arrangements, complex formations on the nanometer scale, or interactions between biomolecules. The pulsed method capable of recovering dipolar couplings is called electron-electron double resonance (PELDOR) or double electron-electron resonance (DEER) (Schiemann and Prisner, 2007). Some of the great advantages of this technique are that there is no restriction to the size of the biomolecule, low concentration samples can be analyzed and most importantly, not only in cryogenic conditions, but also in liquid state at physiological temperatures, allowing measurements with higher relevance to biological conditions. Results obtained, when combined with MD simulations can be extremely accurate. On the other hand, successful isolation of the protein of interest, introduction of paramagnetic labels on desired sites and eventually access to specialized technical equipment and expertise will be required and can prove challenging.

In order for the method to be applied in biological systems, the biomolecule must contain either stable or transient paramagnetic centers such as metal ions, amino acid radicals, or organic co factor radicals. The most commonly used spin-label for site-directed labeling of proteins is MTSSL, a methanethiosulfonate-functionalized nitroxide which interacts specifically with the thiol group of cysteines, forming a disulfide bridge. The label site can be varied by site-directed mutagenesis, provided that the structure and function of the protein are not disturbed.

3.4.1 The rationale behind mutant selection

To this direction, FurE mutants were constructed for future electron paramagnetic resonance (EPR) experiments, carrying cysteine residues at predicted interacting domains of the transporter. These residues were carefully selected and tested in the model of FurE, as they should conform to certain requirements that a) ensure the accessibility of these sites to spin labels, b) should not interfere with the binding site(s), c) the expected distances are within the method range (between 15-70 Å) and d) do not affect the proper folding of the transporter (Pliotas, 2017).

In particular, to examine LID interaction with the internal loops and the C-tail, we selected Ser23 as the amino acid just before the conserved motif. Mutations in Gly112 (L2), Leu187 (L4), Ala266 (L6), Pro354 (L8) and Leu502 (C-tail) were constructed for testing the loop interactions, also taking into consideration previous experimental results obtained from targeted loop mutations (see 3.2.5). In cases where loop residues have proved crucial for FurE folding or function, we selected their neighboring residues. To examine possible interactions in residues that might act as outer or inner gates, we selected to introduce Cys in the pair Thr63 (TMS1) - Ala383 (TMS10) at the

extracellular part of FurE, and in the pair Thr38 (TMS1) - Lys188 (L4), at the cytoplasmic side of FurE (Figure 3.24).

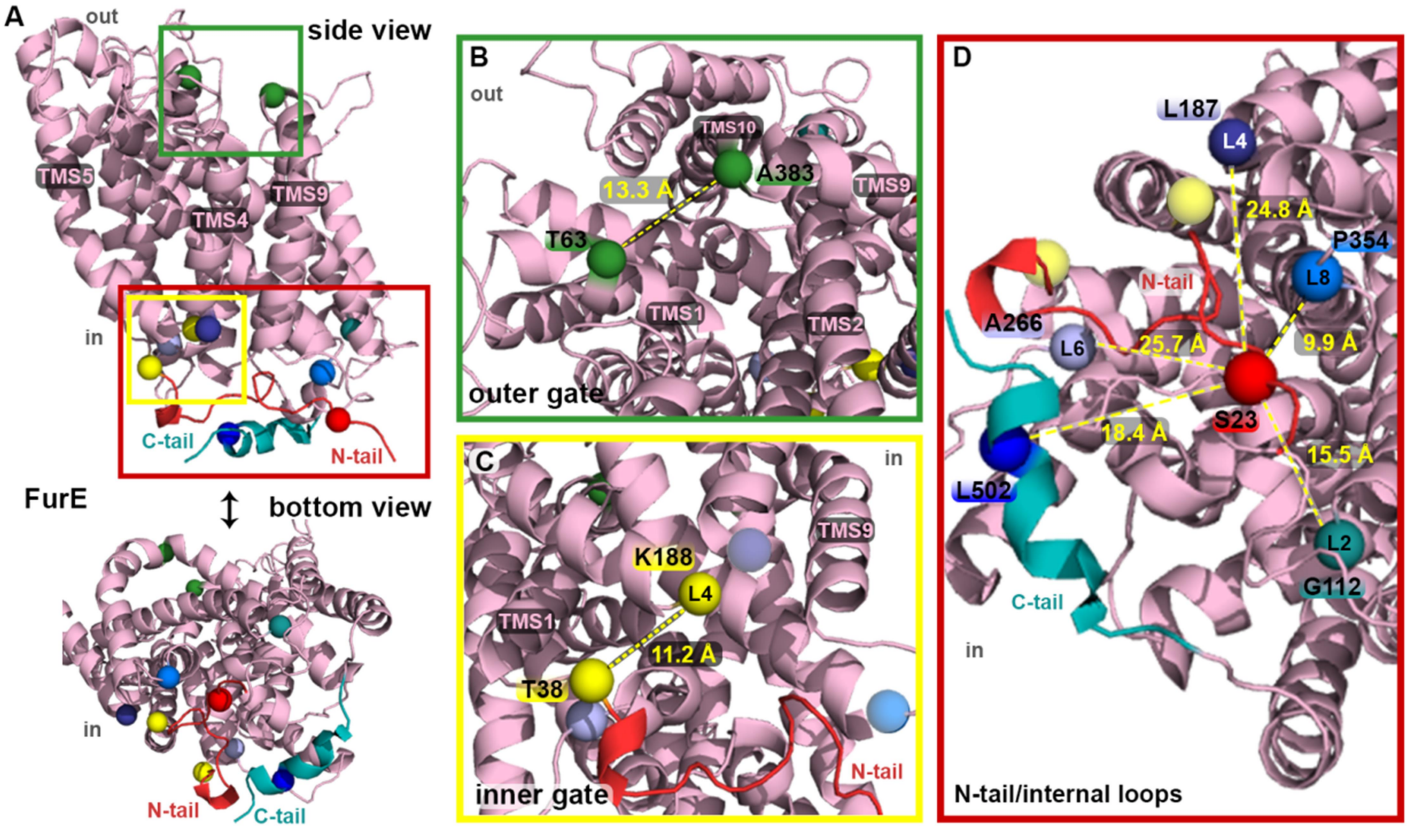

Figure 3.24. A. *Side and bottom view of FurE model where selected residues for future EPR analysis are depicted as spheres.Putative residues that act as* ***B.*** *outer gate (T63 in TMS1 and A383 in TMS10) or* ***C.*** *inner gate (T38 in TMS1 and K188 in L4) of the transporter, are marked in green and yellow, respectively.* ***D.*** *Interactions of the LID (S23), marked in red, with the internal cytosolic loops L2 (G112), L4 (L187), L6 (A266), L8 (P354) and the C-tail (L502) in blue. Measured distances are shown in yellow dashed lines.*

3.4.2 Protein stability and function of cysteine mutants in Aspergillus nidulans

In order to test the protein stability and function of the transporter carrying the selected cysteine mutations for EPR experiments, strains expressing the different FurE versions were first tested in the *A. nidulans* Δ7 strain, as shown in Figure 3.25. From growth tests and epifluorescence microscopy observation, we distinguished those mutations that affect the proper folding, localization and function of the transporter and subsequently excluded mutants expressing G112C and S23C/G112C due to misfolding. Strains expressing mutations S23C, T63C, K188C, P354C, L502C and the double T63C/A383C, S23C/L187C, S23C/A266C and S23C/P354C seem to present altered apparent transport activities, but still localize in the PM. So, eventually, all interactions except the LID/L2 can in principle be used for EPR experiments.

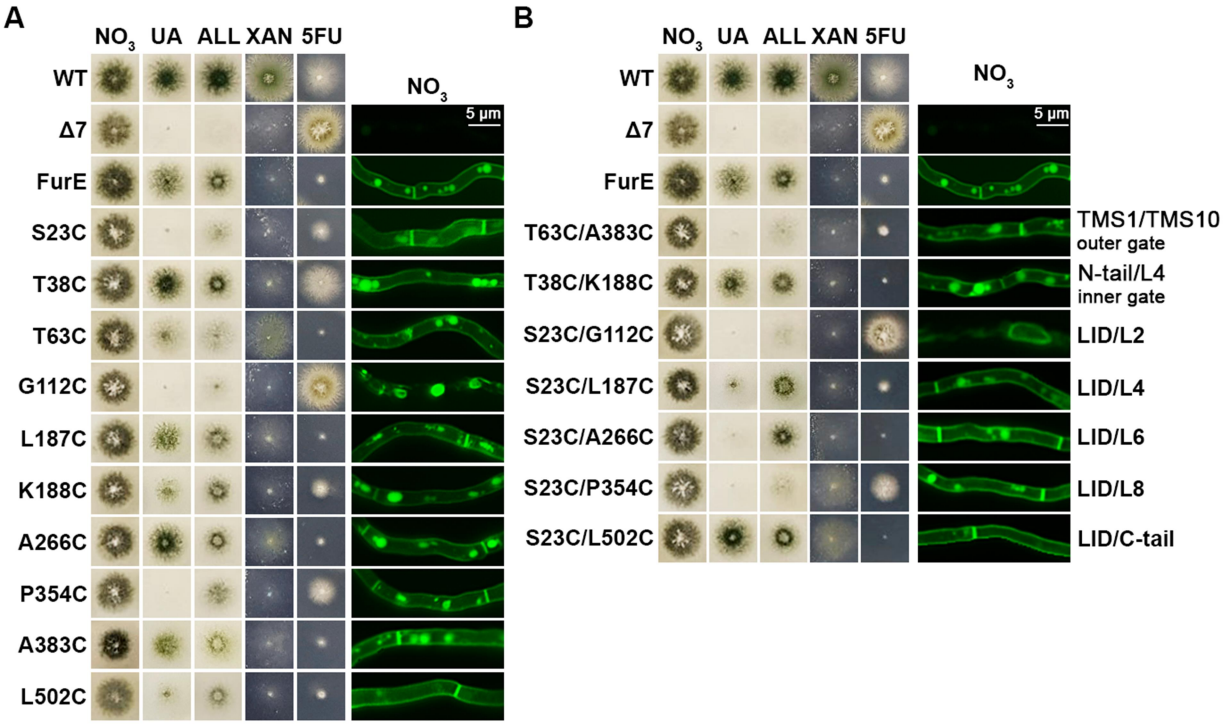

Figure 3.25 *Growth tests of control strains and FurE mutants expressing* ***(A)*** *single and* ***(B)*** *double cysteine mutations located in predicted interacting domains of the transporter. Only mutation G112C and subsequently the double S23C/G112C lead to complete loss-of-function of the transporter and thus cannot be used for further analysis.* ***(A and B right panel)*** *Subcellular localization of the FurE mutants located in the PM except from the mutants G112C and S23C/G112C. Details are as in Figure 3.6A and B. Scale bars: 5 μm.*

3.4.3 Yeast as the expression system

Even though we have previously achieved the expression and purification of another purine transporter (UapA) in *A. nidulans* (Leung et al., 2010), the amount produced was not sufficient for downstream biophysical experiments. Thus, heterologous expression in an appropriate system, such as *S. cerevisiae*, could provide the best alternative for obtaining higher FurE protein yields. For this reason, constructs of the cDNA of FurE carrying the same mutations were fused with *gfp* gene, introduced in the *S. cerevisiae* pDDGFP-2 vector and expressed by the GAL-promoter in a MATa ura3-1 strain. This system was successfully used for biophysical experiments concerning UapA (Alguel et al., 2016). The subcellular localization of the heterologously expressed FurE transporter is shown in Figure 3.26, where most mutants, after overnight galactose induction, are properly localized at the PM of the yeast cells. This work is still in progress, thus only four out of six double mutants were expressed in yeast and observed by epifluorescence microscopy. It is worth noting that overexpressed proteins are often susceptible to proteolysis either due to misfolding or problematic trafficking, thus the proper subcellular targeting of transporters is a good indication of their stability

and function. The conditions in which our protein will be overexpressed and purified will be tested as previously performed for the purine transporter UapA (Leung et al., 2013).

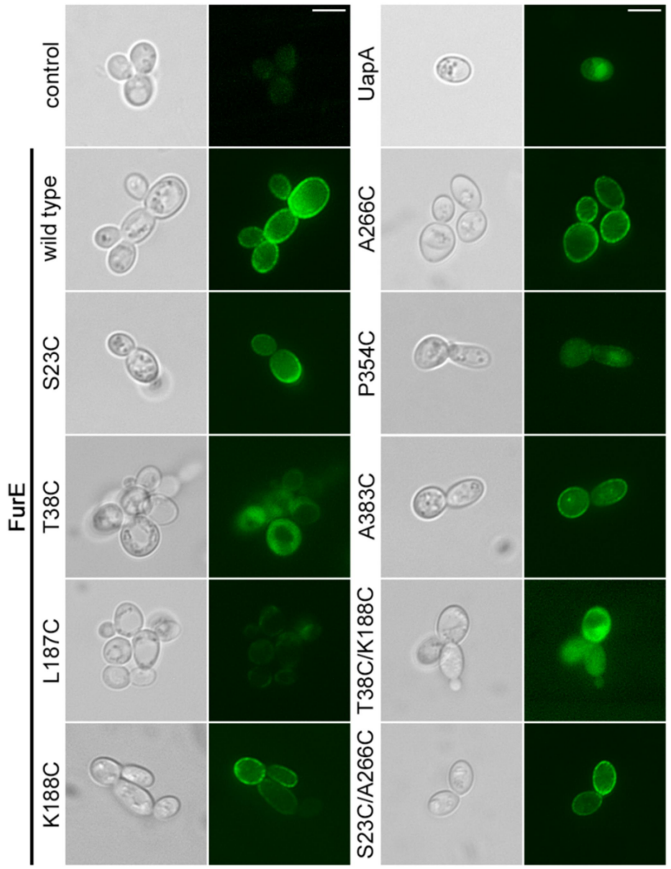

Figure 3.26. *Subcellular topology of control strains and different FurE-GFP single or double mutants. The pDDGFP-2 empty vector was expressed in the S288C strain as negative control and an isogenic strain expressing UapA-GFP was used as a positive control. After overnight galactose induction, most mutants were principally expressed in the plasma membrane. Scale bars: 5 μm.*

CHAPTER 4

CONCLUSIONS AND FUTURE RESEARCH

In recent years, the collection of structural data on transport proteins has become easier, making a decisive contribution to the study and understanding of secondary transport. Much of this information comes from the study of bacterial transporters, which however do not share all structural features characterizing their eukaryotic homologues, such as the elongated termini that appeared later in evolution and offer a variety of additional functional properties. For this reason, direct assessment of structural data of eukaryotic transporters is an emerging need, otherwise erroneous conclusions and misinterpretations could be drawn.

Crystal structures of a small number of eukaryotic solute transporters have been determined with prominent examples being the *Drosophila melanogaster* dopamine transporter dDAT (Penmatsa et al., 2013), the human serotonin transporter hSERT (Coleman et al., 2016), the human glucose transporters hGLUT1 and hGLUT3 (Deng et al., 2014; 2015), and the fungal purine transporter UapA (Alguel et al., 2016). The importance of the termini in membrane trafficking processes and transporters activity has been documented before (for a review see Mikros and Diallinas, 2019). For example, in the bacterial LeuT transporter, the N-terminal region controls the transition of the transporter from the intracellular to the outer facing conformation, resuming the transport cycle (Cheng and Bahar, 2014) and in hDAT transporter the N-terminus is directly associated with the intracellular gates regulation and water penetration into the binding side which is required for uptake and efflux, as well as with the PIP2 lipids (Guptaroy et al., 2009; Khelashvili et al., 2015; Khoshbouei et al., 2004; Razavi et al., 2018). Moreover, in SERT the N-terminus interactions with the internal loops and PIP2 lipids and possible modifications such as phosphorylation are required for the amphetamine-induced efflux (Kern et al., 2017; Sucic et al., 2010). Concerning the C-terminal region, in the *Drosophila melanogaster* dDAT a C-terminal latch is formed that is possibly subjected to phosphorylation altering its conformation or its accessibility to the internalization machinery and has a functional relevance (Penmatsa et al., 2013).

In this thesis, we studied the molecular basis underlying the role of cytoplasmic terminal regions of the fungal NCS1 transporter, namely the uracil-allantoin-uric acid transporter FurE, and provided new evidence on how the selective gating is performed. Using unbiased genetic and reverse genetic approaches, we showed that both terminal regions of FurE are needed for its proper endocytic turnover via a dynamic cross-talk mechanism (Papadaki et al., 2017). We also obtained structural, biochemical and genetic evidence that elongated termini of FurE are involved in substrate

specificity (Papadaki et al., 2019). In more detail, we delimited specific elements in FurE termini crucial for determining substrate specificity and not overall transport activity, namely residues 15-17 in the N-terminus and 504-512 in the C-terminus. MD simulations provided evidence that the conserved LID motif in the N-terminal region interacts with the internal loops and the C-terminus, affecting the relative topology of TMS4-TMS5 (inner gate) and TMS9-TMS10 (outer gate) and eventually the substrate translocation trajectory. Additionally, these interactions are pH-dependent as shown from the influence of the charges on the lipid bilayer of the simulation, emulating the different pH environments. More precisely, at lower pH FurE proved to function as a rather specific 5FU/uracil transporter and at higher pH became progressively promiscuous, eventually transporting xanthine which was not among its known substrates, suggesting that tighter interactions restrict specificity whereas relaxed gating leads to increased number of substrates.

Overall, our work strengthens the emerging concept supporting that elongated cytoplasmic termini acquired through evolution play new fine roles in determining the function of eukaryotic transporters. The next step is to understand the mechanism underlying this regulation and combination of computational and experimental techniques will provide us new insights on how dynamics at the elongated terminal regions are involved in transporter function through allowing transitions between multiple conformations with distinct gating properties.

Membrane proteins pose two distinct challenges in the transition from static structures to mechanism. Firstly, while crystal structures are generally very accurate representations of the tertiary fold, are often crystallized under conditions that may obscure their position in the functional energy landscape and therefore require rigorous validation to assign their mechanistic identities. The second challenge arises from their dynamic nature that requires an understanding under biochemical conditions that mimic the context they are active *in vivo.* Spectroscopic approaches like nuclear magnetic resonance (NMR), electron paramagnetic resonance (EPR) and fluorescence energy transfer (FRET) can provide different timescales and amplitudes of structural changes and are thus suitable for this purpose (Figure 4.1). In particular, NMR describes dynamic properties with high sensitivity, however most membrane proteins are not amenable to this analysis due to size restrictions. FRET has the distinct advantage of monitoring the kinetics of conformational changes at the level of individual molecules, but requires large probes that could compromise the identification of the nature and magnitude of these changes. EPR has numerous advantages that are well suited for the studies on membrane proteins. It has no size limitations on the biomolecule of interest and experiments can be conducted in a variety of conditions (reconstitution in detergent micelles, proteoliposomes, nanodiscs) providing insights into conformational dynamics and protein lipids

interactions. Additionally, low concentration samples are sufficient for EPR analysis, due to the relatively high signal to noise ratios compared to NMR.

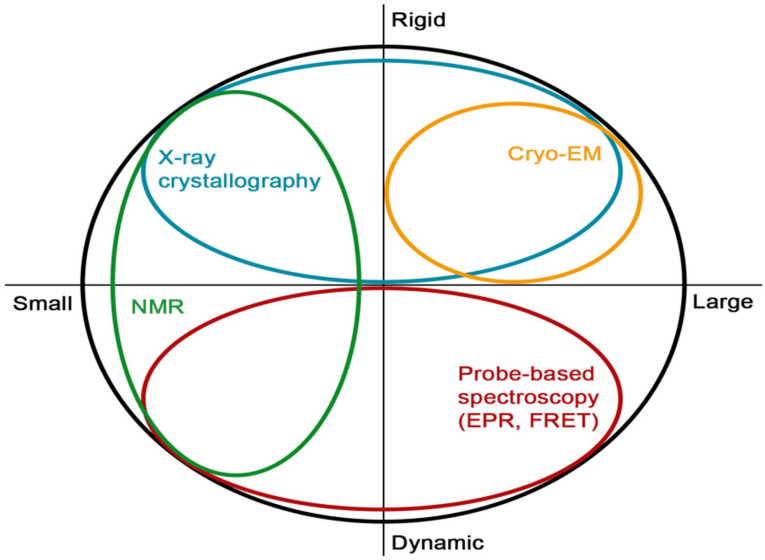

Figure 4.1 *Biophysical methods to study protein structure and dynamics. Whereas X-ray crystallography is the most robust method to determine high-resolution structures of small and large proteins, cryoelectron microscopy is best suited for large proteins and protein complexes. Despite its utility to investigate dynamic properties, current molecular size constraints limit the applicability of liquid-state NMR to <50,000 MW. In contrast, EPR and fluorescence spectroscopies can interrogate dynamic processes regardless of size or complexity. The application of these probe-based methods to proteins of known structure amplifies the interpretation of data toward understanding mechanism (adapted from Claxton et al., 2015).*

The functional role of cytoplasmic terminal regions of FurE seems to reflect a more general mechanism that controls APC transporters, thus we aim to provide new evidence and a mechanistic rationale on how cytosolic termini affect specificity through regulation of selective gating. For this purpose and taking into account the advantages of EPR, we designed a strategy to apply this method on FurE. The final step to perform the EPR analysis is the reconstitution of the proteins and is critical for the correct interpretation of the results. Analysis of membrane proteins in non-destabilizing detergents is an appropriate starting point for assessing conformational dynamics. From previous studies, it has been shown that EPR spectra of membrane-exposed sites are similar in detergent and lipid environments (Claxton et al., 2010; Dong, 2005). However, a more native-like environment where the protein will be reconstituded into lipids, will add a new dimension to the investigation of specific lipid interactions on the conformational equilibria during the transport cycle (Claxton et al., 2015). Liposomes are commonly used for such experiments, but nanodiscs or bicelles (Bayburt and Sligar, 2010; Poulos et al., 2015; Rigaud and Lévy, 2003) are a most promising alternative. In all cases, the phospholipid content can be controlled to reflect the optimal conditions for the stability and

activity of each protein. Putative interactions of FurE with the membrane lipids and especially with the charged PIP2 phospholipids should be also addressed, given results from our laboratory concerning the UapA transporter (Kourkoulou et al., 2019). This is expected to shed new light on our previous finding concerning the pH-dependent activity and substrate profile of FurE (Papadaki et al., 2019). On the computational level, the full-length model of FurE transporter could be built, by using structure prediction tools (i.e. the Rosetta software; Das and Baker, 2008) in combination with extensive Molecular Dynamics simulations.

One major question that should be addressed is how the termini control the fine regulation of gating at the opposite side of the membrane, determining specificity. Elucidating the precise gating mechanism will not only fill significant gaps in basic scientific knowledge, but also has important biomedical applications, as a large number of diseases and pathologies are associated with dysfunction of transporters. Finally, a detailed structural knowledge of transporter dynamic gating mechanisms holds great promise for rational design of emerging pharmacological therapeutics to combat microbial and parasitic infections.

CHAPTER 5

REFERENCES

Abramson, J., 2003. Structure and Mechanism of the Lactose Permease of *Escherichia coli*. Science 301, 610–615.

Alberts, B. (Ed.), 1994. Molecular biology of the cell, 3rd ed. ed. Garland Pub, New York.

Alexopoulos, C.J., Mims, C.W., Blackwell, M., 1996. Introductory mycology, 4th ed. ed. Wiley, New York.

Alguel, Y., Amillis, S., Leung, J., Lambrinidis, G., Capaldi, S., Scull, N.J., Craven, G., Iwata, S., Armstrong, A., Mikros, E., Diallinas, G., Cameron, A.D., Byrne, B., 2016. Structure of eukaryotic purine/H^+ symporter UapA suggests a role for homodimerization in transport activity. Nat. Commun. 7, 11336.

Amara, S.G., Sonders, M.S., 1998. Neurotransmitter transporters as molecular targets for addictive drugs. Drug Alcohol Depend. 51, 87–96.

Amillis, S., Hamari, Z., Amillis, S., Hamari, Z., Roumelioti, K., Scazzocchio, C., Diallinas, G., 2007. Regulation of expression and kinetic modeling of substrate interactions of a uracil transporter in *Aspergillus nidulans*. Mol. Membr. Biol. 24, 206–214.

Aryal, P., Sansom, M.S.P., Tucker, S.J., 2015. Hydrophobic Gating in Ion Channels. J. Mol. Biol. 427, 121–130.

Bayburt, T.H., Sligar, S.G., 2010. Membrane protein assembly into Nanodiscs. FEBS Lett. 584, 1721–1727.

Bayram, Ö., Braus, G.H., Fischer, R., Rodriguez-Romero, J., 2010. Spotlight on *Aspergillus nidulans* photosensory systems. Fungal Genet. Biol. 47, 900–908.

Bosshart, P.D., Fotiadis, D., 2019. Secondary Active Transporters, in: Kuhn, A. (Ed.), Bacterial Cell Walls and Membranes, Subcellular Biochemistry. Springer International Publishing, Cham, pp. 275–299.

Brethes, D., Chirio, M.-C., Napias, C., Chevallier, M.-R., Lavie, J.L., Chevallier, J., 1992. *In vivo* and *in vitro* studies of the purine-cytosine permease of *Saccharomyces cerevisiae*. Functional analysis of a mutant with an altered apparent transport constant of uptake. Eur. J. Biochem. 204, 699–704.

Cheng, M.H., Bahar, I., 2014. Complete Mapping of Substrate Translocation Highlights the Role of LeuT N-terminal Segment in Regulating Transport Cycle. PLoS Comput. Biol. 10, e1003879.

Claxton, D.P., Kazmier, K., Mishra, S., Mchaourab, H.S., 2015. Navigating Membrane Protein Structure, Dynamics, and Energy Landscapes Using Spin Labeling and EPR Spectroscopy, in: Methods in Enzymology. Elsevier, pp. 349–387.

Claxton, D.P., Quick, M., Shi, L., de Carvalho, F.D., Weinstein, H., Javitch, J.A., Mchaourab, H.S., 2010. Ion/substrate-dependent conformational dynamics of a bacterial homolog of neurotransmitter:sodium symporters. Nat. Struct. Mol. Biol. 17, 822–829.

Coleman, J.A., Green, E.M., Gouaux, E., 2016. X-ray structures and mechanism of the human serotonin transporter. Nature 532, 334–339.

Cove, D.J., 1966. The induction and repression of nitrate reductase in the fungus *Aspergillus nidulans*. Biochim. Biophys. Acta BBA - Enzymol. Biol. Oxid. 113, 51–56.

Das, R., Baker, D., 2008. Macromolecular Modeling with Rosetta. Annu. Rev. Biochem. 77, 363–382.

DeChancie, J., Shrivastava, I.H., Bahar, I., 2011. The mechanism of substrate release by the aspartate transporter Glt Ph : insights from simulations. Mol BioSyst 7, 832–842.

Deng, D., Sun, P., Yan, C., Ke, M., Jiang, X., Xiong, L., Ren, W., Hirata, K., Yamamoto, M., Fan, S., Yan N., 2015. Molecular basis of ligand recognition and transport by glucose transporters. Nature. 526(7573):391-6.

Deng, D., Xu, C., Sun, P., Wu, J., Yan, C., Hu, M., Yan, N., 2014. Crystal structure of the human glucose transporter GLUT1. Nature 510, 121–125.

Diallinas, G., 2016. Dissection of Transporter Function: From Genetics to Structure. Trends Genet. 32, 576–590.

Diallinas, G., 2014. Understanding transporter specificity and the discrete appearance of channel-like gating domains in transporters. Front. Pharmacol. 5.

Diallinas, G., Gournas, C., 2008. The ubiquitous Nucleobase-Ascorbate Transporter (NAT) family: Lessons from model microbial genetic systems. Channels 2, 363–372.

Diallinas, G., Scazzocchio, C., 1989. A gene coding for the uric acid-xanthine permease of *Aspergillus nidulans*: inactivational cloning, characterization, and sequence of a cis-acting mutation. Genetics 122, 341–350.

Dong, J., 2005. Structural Basis of Energy Transduction in the Transport Cycle of MsbA. Science 308, 1023–1028.

Drew, D., Boudker, O., 2016. Shared Molecular Mechanisms of Membrane Transporters. Annu. Rev. Biochem. 85, 543–572.

Dupré, S., Urban-Grimal, D., Haguenauer-Tsapis, R., 2004. Ubiquitin and endocytic internalization in yeast and animal cells. Biochim. Biophys. Acta BBA - Mol. Cell Res. 1695, 89–111.

Engel, A., Gaub, H.E., 2008. Structure and Mechanics of Membrane Proteins. Annu. Rev. Biochem. 77, 127–148.

Faham, S., Watanabe, A., Besserer, G.M., Cascio, D., Specht, A., Hirayama, B.A., Wright, E.M., Abramson, J., 2008. The Crystal Structure of a Sodium Galactose Transporter Reveals Mechanistic Insights into Na^+/Sugar Symport. Science 321, 810–814.

Fang, Y., Jayaram, H., Shane, T., Kolmakova-Partensky, L., Wu, F., Williams, C., Xiong, Y., Miller, C., 2009. Structure of a prokaryotic virtual proton pump at 3.2 A resolution. Nature 460, 1040–1043.

Forrest, L.R., Rudnick, G., 2009. The Rocking Bundle: A Mechanism for Ion-Coupled Solute Flux by Symmetrical Transporters. Physiology 24, 377–386.

Gadsby, D.C., 2009. Ion channels versus ion pumps: the principal difference, in principle. Nat. Rev. Mol. Cell Biol. 10, 344–352.

Galagan, J.E., Calvo, S.E., Cuomo, C., Ma, L.-J., Wortman, J.R., Batzoglou, S., Lee, S.-I., Baştürkmen, M., Spevak, C.C., Clutterbuck, J., Kapitonov, V., Jurka, J., Scazzocchio, C., Farman, M., Butler, J., Purcell, S., Harris, S., Braus, G.H., Draht, O., Busch, S., D'Enfert, C., Bouchier, C., Goldman, G.H., Bell-Pedersen, D., Griffiths-Jones, S., Doonan, J.H., Yu, J., Vienken, K., Pain, A., Freitag, M., Selker, E.U., Archer, D.B., Peñalva, M.Á., Oakley, B.R., Momany, M., Tanaka, T., Kumagai, T., Asai, K., Machida, M., Nierman, W.C., Denning, D.W., Caddick, M., Hynes, M., Paoletti, M., Fischer, R., Miller, B., Dyer, P., Sachs, M.S., Osmani, S.A., Birren, B.W., 2005. Sequencing of *Aspergillus nidulans* and comparative analysis with A. fumigatus and A. oryzae. Nature 438, 1105–1115.

Gao, X., Lu, F., Zhou, L., Dang, S., Sun, L., Li, X., Wang, J., Shi, Y., 2009. Structure and Mechanism of an Amino Acid Antiporter. Science 324, 1565–1568.

Garaeva, A.A., Slotboom, D.J., 2020. Elevator-type mechanisms of membrane transport. Biochem. Soc. Trans. 48, 1227–1241.

Gavriil, E.-S., Dimitrakis, S., Papadaki, G., Balaska, S., Lambrinidis, G., Lougiakis, N., Marakos, P., Diallinas, G., Pouli, N., Mikros, E., 2018. Structure-activity relationships in fungal nucleobases transporters as dissected by the inhibitory effects of novel purine analogues. Eur. J. Med. Chem. 156, 240–251.

Gournas, C., Amillis, S., Vlanti, A., Diallinas, G., 2010. Transport-dependent endocytosis and turnover of a uric acid-xanthine permease. Mol. Microbiol. 75, 246–260.

Gournas, C., Papageorgiou, I., Diallinas, G., 2008. The nucleobase–ascorbate transporter (NAT) family: genomics, evolution, structure–function relationships and physiological role. Mol. Biosyst. 4, 404.

Guptaroy, B., Zhang, M., Bowton, E., Binda, F., Shi, L., Weinstein, H., Galli, A., Javitch, J.A., Neubig, R.R., Gnegy, M.E., 2009. A Juxtamembrane Mutation in the N Terminus of the Dopamine Transporter Induces Preference for an Inward-Facing Conformation. Mol. Pharmacol. 75, 514–524.

Hahn, M.K., Blakely, R.D., 2002. Monoamine transporter gene structure and polymorphisms in relation to psychiatric and other complex disorders. Pharmacogenomics J. 2, 217–235.

Hamari, Z., Amillis, S., Drevet, C., Apostolaki, A., Vágvölgyi, C., Diallinas, G., Scazzocchio, C., 2009. Convergent evolution and orphan genes in the Fur4p-like family and characterization of a general nucleoside transporter in *Aspergillus nidulans*. Mol. Microbiol. 73, 43–57.

Hamilton, P.J., Belovich, A.N., Khelashvili, G., Saunders, C., Erreger, K., Javitch, J.A., Sitte, H.H., Weinstein, H., Matthies, H.J.G., Galli, A., 2014. PIP2 regulates psychostimulant behaviors through its interaction with a membrane protein. Nat. Chem. Biol. 10, 582–589.

Harry de Koning, George Diallinas, 2000. Nucleobase transporters. Mol. Membr. Biol. 17, 75–94.

Hein, C., Springael, J. Y., Volland, C., Haguenauer-Tsapis, R., André, B., 1995. NPl1, an essential yeast gene involved in induced degradation of Gap1 and Fur4 permeases, encodes the Rsp5 ubiquitin-protein ligase. Mol Microbiol. 18(1):77-87.

Houbraken, J., de Vries, R.P., Samson, R.A., 2014. Modern Taxonomy of Biotechnologically Important *Aspergillus* and *Penicillium* Species, in: Advances in Applied Microbiology. Elsevier, pp. 199–249.

Jack, D.L., Paulsen, I.T., Saier, M.H., 2000. The amino acid/polyamine/organocation (APC) superfamily of transporters specific for amino acids, polyamines and organocations. Microbiology 146, 1797–1814.

Karachaliou, M., Amillis, S., Evangelinos, M., Kokotos, A.C., Yalelis, V., Diallinas, G., 2013. The arrestin-like protein ArtA is essential for ubiquitination and endocytosis of the UapA transporter in response to both broad-range and specific signals: UapA transporter regulation by ArtA. Mol. Microbiol. 88, 301–317.

Kazmier, K., Sharma, S., Islam, S.M., Roux, B., Mchaourab, H.S., 2014. Conformational cycle and ion-coupling mechanism of the Na^+/hydantoin transporter Mhp1. Proc. Natl. Acad. Sci. 111, 14752–14757.

Keener, J.M., Babst, M., 2013. Quality Control and Substrate-Dependent Downregulation of the Nutrient Transporter Fur4: Fur4 Downregulation. Traffic 14, 412–427.

Kern, C., Erdem, F.A., El-Kasaby, A., Sandtner, W., Freissmuth, M., Sucic, S., 2017. The N Terminus Specifies the Switch between Transport Modes of the Human Serotonin Transporter. J. Biol. Chem. 292, 3603–3613.

Khelashvili, G., Doktorova, M., Sahai, M.A., Johner, N., Shi, L., Weinstein, H., 2015. Computational modeling of the N-terminus of the human dopamine transporter and its interaction with PIP 2 -containing membranes: Modeling of DAT N-Terminus/PIP 2 Interactions. Proteins Struct. Funct. Bioinforma. 83, 952–969.

Khoshbouei, H., Sen, N., Guptaroy, B., Johnson, L., Lund, D., Gnegy, M.E., Galli, A., Javitch, J.A., 2004. N-Terminal Phosphorylation of the Dopamine Transporter Is Required for Amphetamine-Induced Efflux. PLoS Biol. 2, e78.

Kilic, F., Rudnick, G., 2000. Oligomerization of serotonin transporter and its functional consequences. Proc. Natl. Acad. Sci. U. S. A. 97, 3106–3111.

Kirk, P.M., Cannon, P.F., Minter, D.W., Stalpers, J.A., 2008. Dictionary of the Fungi, 10th ed.

Koukaki, M., Giannoutsou, E., Karagouni, A., Diallinas, G., 2003. A novel improved method for *Aspergillus nidulans* transformation. J. Microbiol. Methods 55, 687–695.

Koukaki, M., Vlanti, A., Goudela, S., Pantazopoulou, A., Gioule, H., Tournaviti, S., Diallinas, G., 2005. The Nucleobase-ascorbate Transporter (NAT) Signature Motif in UapA Defines the Function of the Purine Translocation Pathway. J. Mol. Biol. 350, 499–513.

Kourkoulou, A., Grevias, P., Lambrinidis, G., Pyle, E., Dionysopoulou, M., Politis, A., Mikros, E., Byrne, B., Diallinas, G., 2019. Specific Residues in a Purine Transporter Are Critical for Dimerization, ER Exit, and Function. Genetics 213, 1357–1372.

Kowalczyk, L., Ratera, M., Paladino, A., Bartoccioni, P., Errasti-Murugarren, E., Valencia, E., Portella, G., Bial, S., Zorzano, A., Fita, I., Orozco, M., Carpena, X., Vázquez-Ibar, J.L., Palacín, M., 2011. Molecular basis of substrate-induced permeation by an amino acid antiporter. Proc. Natl. Acad. Sci. U. S. A. 108, 3935–3940.

Krishnamurthy, H., Gouaux, E., 2012. X-ray structures of LeuT in substrate-free outward-open and apo inward-open states. Nature 481, 469–474.

Krogsgaard-Larsen, P., Frolund, B., Frydenvang, K., 2000. GABA Uptake Inhibitors. Design, Molecular Pharmacology and Therapeutic Aspects. Curr. Pharm. Des. 6, 1193–1209.

Krypotou, E., Diallinas, G., 2014. Transport assays in filamentous fungi: Kinetic characterization of the UapC purine transporter of *Aspergillus nidulans*. Fungal Genet. Biol. 63, 1–8.

Krypotou, E., Evangelidis, T., Bobonis, J., Pittis, A.A., Gabaldón, T., Scazzocchio, C., Mikros, E., Diallinas, G., 2015. Origin, diversification and substrate specificity in the family of NCS1/FUR transporters: Origin and specificity of Fur transporters. Mol. Microbiol. 96, 927–950.

Krypotou, E., Kosti, V., Amillis, S., Myrianthopoulos, V., Mikros, E., Diallinas, G., 2012. Modeling, Substrate Docking, and Mutational Analysis Identify Residues Essential for the Function and Specificity of a Eukaryotic Purine-Cytosine NCS1 Transporter. J. Biol. Chem. 287, 36792–36803.

Lauwers, E., Erpapazoglou, Z., Haguenauer-Tsapis, R., André, B., 2010. The ubiquitin code of yeast permease trafficking. Trends Cell Biol. 20, 196–204.

Leung, J., Cameron, A.D., Diallinas, G., Byrne, B., 2013. Stabilizing the heterologously expressed uric acid-xanthine transporter UapA from the lower eukaryote *Aspergillus nidulans* . Mol. Membr. Biol. 30, 32–42.

Lin, C.H., MacGurn, J.A., Chu, T., Stefan, C.J., Emr, S.D., 2008. Arrestin-Related Ubiquitin-Ligase Adaptors Regulate Endocytosis and Protein Turnover at the Cell Surface. Cell 135, 714–725.

Lockington, R.A., Kelly, J.M., 2001. Carbon catabolite repression in *Aspergillus nidulans* involves deubiquitination. Mol Microbiol. 40(6):1311-21.

Lougiakis, N., Gavriil, E.-S., Kairis, M., Sioupouli, G., Lambrinidis, G., Benaki, D., Krypotou, E., Mikros, E., Marakos, P., Pouli, N., Diallinas, G., 2016. Design and synthesis of purine analogues as highly specific ligands for FcyB, a ubiquitous fungal nucleobase transporter. Bioorg. Med. Chem. 24, 5941–5952.

Lu, F., Li, S., Jiang, Y., Jiang, J., Fan, H., Lu, G., Deng, D., Dang, S., Zhang, X., Wang, J., Yan, N., 2011. Structure and mechanism of the uracil transporter UraA. Nature 472, 243–246.

Luckey, M., 2008. Membrane Structural Biology: With Biochemical and Biophysical Foundations. Cambridge University Press, Cambridge.

Lutzoni, F., Kauff, F., Cox, C.J., McLaughlin, D., Celio, G., Dentinger, B., Padamsee, M., Hibbett, D., James, T.Y., Baloch, E., Grube, M., Reeb, V., Hofstetter, V., Schoch, C., Arnold, A.E., Miadlikowska, J., Spatafora, J., Johnson, D., Hambleton, S., Crockett, M., Shoemaker, R., Sung, G.-H., Lücking, R., Lumbsch, T., O'Donnell, K., Binder, M., Diederich, P., Ertz, D., Gueidan, C., Hansen, K., Harris, R.C., Hosaka, K., Lim, Y.-W., Matheny, B., Nishida, H., Pfister, D., Rogers, J., Rossman, A., Schmitt, I., Sipman, H., Stone, J., Sugiyama, J., Yahr, R., Vilgalys, R., 2004. Assembling the fungal tree of life: progress, classification, and evolution of subcellular traits. Am. J. Bot. 91, 1446–1480.

Marger, M.D., Saier, M.H., 1993. A major superfamily of transmembrane facilitators that catalyse uniport, symport and antiport. Trends Biochem. Sci. 18, 13–20.

Martzoukou, O., Karachaliou, M., Yalelis, V., Leung, J., Byrne, B., Amillis, S., Diallinas, G., 2015. Oligomerization of the UapA Purine Transporter Is Critical for ER-Exit, Plasma Membrane Localization and Turnover. J. Mol. Biol. 427, 2679–2696.

Masson, J., Sagné, C., Hamon, M., El Mestikawy, S., 1999. Neurotransmitter transporters in the central nervous system. Pharmacol. Rev. 51, 439–464.

Mazei-Robison, M.S., Blakely, R.D., 2006. ADHD and the Dopamine Transporter: Are There Reasons to Pay Attention?, in: Sitte, H.H., Freissmuth, M. (Eds.), Neurotransmitter Transporters, Handbook of Experimental Pharmacology. Springer-Verlag, Berlin/Heidelberg, pp. 373–415.

Mikros, E., Diallinas, G., 2019. Tales of tails in transporters. Open Biol. 9, 190083.

Miranda, M., Sorkin, A., 2007. Regulation of receptors and transporters by ubiquitination: new insights into surprisingly similar mechanisms. Mol. Interv. 7, 157–167.

Mitchell, P., 1990. Osmochemistry of solute translocation. Res. Microbiol. 141, 286–289.

Mitchell, P., 1957. A General Theory of Membrane Transport From Studies of Bacteria. Nature 180, 134–136.

Moran, Y., Barzilai, M.G., Liebeskind, B.J., Zakon, H.H., 2015. Evolution of voltage-gated ion channels at the emergence of Metazoa. J. Exp. Biol. 218, 515–525.

Nelson, N., 2002. The Family of Na+/Cl− Neurotransmitter Transporters. J. Neurochem. 71, 1785–1803.

Nikko, E., Pelham, H.R.B., 2009. Arrestin-Mediated Endocytosis of Yeast Plasma Membrane Transporters. Traffic 10, 1856–1867.

Ohtake, F., Tsuchiya, H., Saeki, Y., & Tanaka, K., 2018. K63 ubiquitylation triggers proteasomal degradation by seeding branched ubiquitin chains. Proc. Natl. Acad. Sci. U.S A. 115(7):E1401-E1408.

Ozaki, N., Goldman, D., Kaye, W.H., Plotnicov, K., Greenberg, B.D., Lappalainen, J., Rudnick, G., Murphy, D.L., 2003. Serotonin transporter missense mutation associated with a complex neuropsychiatric phenotype. Mol. Psychiatry 8, 933–936.

Pantazopoulou, A., Diallinas, G., 2007. Fungal nucleobase transporters. FEMS Microbiol. Rev. 31, 657–675.

Pao, S.S., Paulsen, I.T., Saier, M.H., 1998. Major Facilitator Superfamily. Microbiol. Mol. Biol. Rev. 62, 1–34.

Papadaki, G.F., Amillis, S., Diallinas, G., 2017. Substrate Specificity of the FurE Transporter Is Determined by Cytoplasmic Terminal Domain Interactions. Genetics genetics.300327.2017.

Papadaki, G.F., Lambrinidis, G., Zamanos, A., Mikros, E., Diallinas, G., 2019. Cytosolic N- and C-Termini of the *Aspergillus nidulans* FurE Transporter Contain Distinct Elements that Regulate by Long-Range Effects Function and Specificity. J. Mol. Biol. 431, 3827–3844.

Papadaki, G.F., Ma, P., Ahmad, I., Calabrese, A.N., Baldwin, S.A., Henderson, P.J.F., Diallinas, G., 2018. Membrane Transport Proteins: The Nucleobase-Cation-Symport-1 Family, in: European Biophysical Societies, Roberts, G., Watts, A. (Eds.), Encyclopedia of Biophysics. Springer Berlin Heidelberg, Berlin, Heidelberg, pp. 1–7.

Papageorgiou, I., Gournas, C., Vlanti, A., Amillis, S., Pantazopoulou, A., Diallinas, G., 2008. Specific Interdomain Synergy in the UapA Transporter Determines Its Unique Specificity for Uric Acid among NAT Carriers. J. Mol. Biol. 382, 1121–1135.

Patlak, C.S., 1957. Contributions to the theory of active transport: II. The gate type non-carrier mechanism and generalizations concerning tracer flow, efficiency, and measurement of energy expenditure. Bull. Math. Biophys. 19, 209–235.

Patlak, C.S., 1956. Contributions to the theory of active transport. Bull. Math. Biophys. 18, 271–315.

Patwari, P., Lee, R.T., 2012. An expanded family of arrestins regulate metabolism. Trends Endocrinol. Metab. TEM 23, 216–222.

Pedersen, B.P., Kumar, H., Waight, A.B., Risenmay, A.J., Roe-Zurz, Z., Chau, B.H., Schlessinger, A., Bonomi, M., Harries, W., Sali, A., Johri, A.K., Stroud, R.M., 2013. Crystal structure of a eukaryotic phosphate transporter. Nature 496, 533–536.

Peñalva, M.A., Galindo, A., Abenza, J.F., Pinar, M., Calcagno-Pizarelli, A.M., Arst, H.N., Pantazopoulou, A., 2012. Searching for gold beyond mitosis: Mining intracellular membrane traffic in *Aspergillus nidulans*. Cell. Logist. 2, 2–14.

Penmatsa, A., Wang, K.H., Gouaux, E., 2013. X-ray structure of dopamine transporter elucidates antidepressant mechanism. Nature 503, 85–90.

Pliotas, C., 2017. Ion Channel Conformation and Oligomerization Assessment by Site-Directed Spin Labeling and Pulsed-EPR, in: Methods in Enzymology. Elsevier, pp. 203–242.

Poulos, S., Morgan, J.L.W., Zimmer, J., Faham, S., 2015. Bicelles Coming of Age, in: Methods in Enzymology. Elsevier, pp. 393–416.

Punt, P.J., Zegers, N.D., Busscher, M., Pouwels, P.H., van den Hondel, C.A.M.J.J., 1991. Intracellular and extracellular production of proteins in Aspergillus under the control of expression signals of the highly expressed *Aspergillus nidulans gpd*A gene. J. Biotechnol. 17, 19–33.

Radestock, S., Forrest, L.R., 2011. The Alternating-Access Mechanism of MFS Transporters Arises from Inverted-Topology Repeats. J. Mol. Biol. 407, 698–715.

Razavi, A.M., Khelashvili, G., Weinstein, H., 2018. How structural elements evolving from bacterial to human SLC6 transporters enabled new functional properties. BMC Biol. 16, 31.

Ressl, S., Terwisscha van Scheltinga, A.C., Vonrhein, C., Ott, V., Ziegler, C., 2009. Molecular basis of transport and regulation in the Na^+/betaine symporter BetP. Nature 458, 47–52.

Reyes, N., Ginter, C., Boudker, O., 2009. Transport mechanism of a bacterial homologue of glutamate transporters. Nature 462, 880–885.

Richerson, G.B., Wu, Y., 2004. Role of the GABA Transporter in Epilepsy, in: Binder, D.K., Scharfman, H.E. (Eds.), Recent Advances in Epilepsy Research, Advances in Experimental Medicine and Biology. Springer US, Boston, MA, pp. 76–91.

Rigaud, J.-L., Lévy, D., 2003. Reconstitution of Membrane Proteins into Liposomes, in: Methods in Enzymology. Elsevier, pp. 65–86.

Saier, M.H., Reddy, V.S., Tamang, D.G., Västermark, Å., 2014. The Transporter Classification Database. Nucleic Acids Res. 42, D251–D258.

Sambrook, J., Russell, D.W., 2001. Molecular cloning: a laboratory manual, 3rd ed. ed. Cold Spring Harbor Laboratory Press, Cold Spring Harbor, N.Y.

Scazzocchio, C., 2006. *Aspergillus* genomes: secret sex and the secrets of sex. Trends Genet. 22, 521–525.

Scazzocchio, C., Sdrin, N., Ong, G., 1982. Positive regulation in a eukaryote, a study of the uaY gene of Aspergillus nidulans: I. Characterization of alleles, dominance and complementation studies, and a fine structure map of the uaY--oxpA cluster. Genetics 100, 185–208.

Schiemann, O., Prisner, T.F., 2007. Long-range distance determinations in biomacromolecules by EPR spectroscopy. Q. Rev. Biophys. 40, 1–53.

Shimamura, T., Yajima, S., Suzuki, S., Rutherford, N.G., O'Reilly, J., Henderson, P.J.F., Iwata, S., 2008. Crystallization of the hydantoin transporter Mhp1 from *Microbacterium liquefaciens*. Acta Crystallograph. Sect. F Struct. Biol. Cryst. Commun. 64, 1172–1174.

Simmons, K.J., Jackson, S.M., Brueckner, F., Patching, S.G., Beckstein, O., Ivanova, E., Geng, T., Weyand, S., Drew, D., Lanigan, J., Sharples, D.J., Sansom, M.S., Iwata, S., Fishwick, C.W., Johnson, A.P., Cameron, A.D., Henderson, P.J., 2014. Molecular mechanism of ligand recognition by membrane transport protein, Mhp1. EMBO J. 33, 1831–1844.

Singh, S.K., Pal, A., 2015. Biophysical Approaches to the Study of LeuT, a Prokaryotic Homolog of Neurotransmitter Sodium Symporters, in: Methods in Enzymology. Elsevier, pp. 167–198.

Sioupouli, G., Lambrinidis, G., Mikros, E., Amillis, S., Diallinas, G., 2017. Cryptic purine transporters in *Aspergillus nidulans* reveal the role of specific residues in the evolution of specificity in the NCS1 family: Cryptic purine transporters in *A. nidulans*. Mol. Microbiol. 103, 319–332.

Sitte, H.H., 2004. Sodium-Dependent Neurotransmitter TRANSPORTERS: OLIGOMERIZATION as a Determinant of Transporter Function and Trafficking. Mol. Interv. 4, 38–47.

Smirnova, I., Kasho, V., Kaback, H.R., 2011. Lactose Permease and the Alternating Access Mechanism. Biochemistry 50, 9684–9693.

Sonders, M.S., Quick, M., Javitch, J.A., 2005. How did the neurotransmitter cross the bilayer? A closer view. Curr. Opin. Neurobiol. 15, 296–304.

Springael, J.Y., De Craene, J.O., André, B., 1999. The yeast Npi1/Rsp5 ubiquitin ligase lacking its N-terminal C2 domain is competent for ubiquitination but not for subsequent endocytosis of the gap1 permease. Biochem. Biophys. Res. Commun. 257, 561–566.

Sucic, S., Dallinger, S., Zdrazil, B., Weissensteiner, R., Jørgensen, T.N., Holy, M., Kudlacek, O., Seidel, S., Cha, J.H., Gether, U., Newman, A.H., Ecker, G.F., Freissmuth, M., Sitte, H.H., 2010. The N Terminus of Monoamine Transporters Is a Lever Required for the Action of Amphetamines. J. Biol. Chem. 285, 10924–10938.

Sun, J., Bankston, J.R., Payandeh, J., Hinds, T.R., Zagotta, W.N., Zheng, N., 2014. Crystal structure of the plant dual-affinity nitrate transporter NRT1.1. Nature 507, 73–77.

Sun, L., Zeng, X., Yan, C., Sun, X., Gong, X., Rao, Y., Yan, N., 2012. Crystal structure of a bacterial homologue of glucose transporters GLUT1–4. Nature 490, 361–366.

Swaminathan, S., Amerik, A.Y., Hochstrasser, M., 1999. The Doa4 deubiquitinating enzyme is required for ubiquitin homeostasis in yeast. Mol Biol Cell. 10(8):2583-94.

Todd, R.B., Davis, M.A., Hynes, M.J., 2007. Genetic manipulation of *Aspergillus nidulans*: meiotic progeny for genetic analysis and strain construction. Nat. Protoc. 2, 811–821.

Torres, G.E., Carneiro, A., Seamans, K., Fiorentini, C., Sweeney, A., Yao, W.-D., Caron, M.G., 2003. Oligomerization and Trafficking of the Human Dopamine Transporter: MUTATIONAL ANALYSIS IDENTIFIES CRITICAL DOMAINS IMPORTANT FOR THE FUNCTIONAL EXPRESSION OF THE TRANSPORTER. J. Biol. Chem. 278, 2731–2739.

Turk, E., Wright, E.M., 2004. The sodium/glucose cotransport family SLC5. Pflgers Arch. Eur. J. Physiol. 447, 510–518.

Valdez-Taubas, J., Harispe, L., Scazzocchio, C., Gorfinkiel, L., Rosa, A.L., 2004. Ammonium-induced internalisation of UapC, the general purine permease from *Aspergillus nidulans*. Fungal Genet. Biol. 41, 42–51.

Västermark, Å., Saier, M.H., 2014. Evolutionary relationship between 5+5 and 7+7 inverted repeat folds within the amino acid-polyamine-organocation superfamily: Evolutionary Relationship of Inverted Repeat Folds. Proteins Struct. Funct. Bioinforma. 82, 336–346.

Vlanti, A., Diallinas, G., 2008. The *Aspergillus nidulans* FcyB cytosine-purine scavenger is highly expressed during germination and in reproductive compartments and is downregulated by endocytosis. Mol. Microbiol. 68, 959–977.

Wagner, R., Montigny, J., Wergifosse, P., Souciet, J.L., Potier, S., 1998. The ORF YBL042 of *Saccharomyces cerevisiae* encodes a uridine permease. FEMS Microbiol. Lett. 159, 69–75.

Wang, S.C., Davejan, P., Hendargo, K.J., Javadi-Razaz, I., Chou, A., Yee, D.C., Ghazi, F., Lam, K.J.K., Conn, A.M., Madrigal, A., Medrano-Soto, A., Saier, M.H., 2020. Expansion of the Major Facilitator Superfamily (MFS) to include novel transporters as well as transmembrane-acting enzymes. Biochim. Biophys. Acta BBA - Biomembr. 1862, 183277.

Weyand, S., Shimamura, T., Yajima, S., Suzuki, S., Mirza, O., Krusong, K., Carpenter, E.P., Rutherford, N.G., Hadden, J.M., O'Reilly, J., Ma, P., Saidijam, M., Patching, S.G., Hope, R.J., Norbertczak, H.T., Roach, P.C.J., Iwata, S., Henderson, P.J.F., Cameron, A.D., 2008. Structure and Molecular Mechanism of a Nucleobase-Cation-Symport-1 Family Transporter. Science 322, 709–713.

Yamashita, A., Singh, S.K., Kawate, T., Jin, Y., Gouaux, E., 2005. Crystal structure of a bacterial homologue of Na^+/Cl^--dependent neurotransmitter transporters. Nature 437, 215–223.

Yan, N., 2015. Structural Biology of the Major Facilitator Superfamily Transporters. Annu. Rev. Biophys. 44, 257–283.

Yin, Y., He, X., Szewczyk, P., Nguyen, T., Chang, G., 2006. Structure of the Multidrug Transporter EmrD from *Escherichia coli.* Science 312.

Yu, X., Yang, G., Yan, C., Baylon, J.L., Jiang, J., Fan, H., Lu, G., Hasegawa, K., Okumura, H., Wang, T., Tajkhorshid, E., Li, S., Yan, N., 2017. Dimeric structure of the uracil:proton symporter UraA provides mechanistic insights into the SLC4/23/26 transporters. Cell Res. 27(8):1020-1033.

CHAPTER 6

APPENDIX

6.1 Design of novel purine analogues in understanding structure-activity relationships in fungal nucleobase transporters

Adapted from Gavriil ES, Dimitrakis S, Papadaki et al. 2018. ***Eur J Med Chem.*** *156: 240-251*

Solute transport is associated with major changes in the structure of transporters and recent high-resolution structures shed light in the mechanisms behind these transitions. The *A. nidulans* purine/H^+ symporters FcyB and AzgA belong to evolutionary and structurally distinct transporter families (NCS1 and NAT/NCS2 respectively), but display very similar high-affinity binding for adenine, hypoxanthine and guanine. On the contrary, UapA and AzgA are structurally similar (NAT family) but they transport entirely different substrates and drugs. The only rigorous way to functionally distinguish AzgA from FcyB is via their relative capacity to transport cytosine or specific purine or pyrimidine analogues. These observations suggest that divergent and convergent evolution events led to the architecture of the binding site in these two families. *A. nidulans* is the ideal model organism to study structure-function relationships in nucleobase transporters via classical and reverse genetics and modeling, using the available crystal structures of bacterial homologues (Diallinas, 2016, 2014) and by analyzing the crystal structure of UapA (Alguel et al., 2016).

In a different but complementary approach, chemical biology methodologies were developed in order to better understand how specificity is determined in different nucleobase transporters. More specifically, through virtual screenings and semi-rational approaches we identified compounds that might interact with the substrate binding site of a specific transporter and then tested if they could be recognized by a functionally similar transporter. For this purpose, FcyB ligands based on 3-deazapurines were synthesized and then tested whether they interact with AzgA (i.e. a functional analogue) or UapA (i.e. a structural homologue). However, only one of these compounds proved to be moderately toxic for *A. nidulans* (Lougiakis et al., 2016).

In order to further understand the molecular details of structure-activity relationships in all three major nucleobase transporters of fungi, more 3-deazapurine analogues were synthesized and tested (Gavriil et al., 2018). Initially, they were tested as competitive inhibitors of FcyB- or AzgA-mediated [^{3}H]-radiolabeled adenine uptake, or UapA-mediated [^{3}H]-radiolabeled xanthine uptake as previously described (Krypotou and Diallinas, 2014), in strains expressing the specific transporter studied in a genetically 'clean' background lacking all functionally similar transporters. As

summarized in Figure 6.1A-B, compounds 12a-f and 13 did not show any inhibitory activity. The derivatives 10a, 10d, 10e, 11d, 11e and 11f reduced FcyB-mediated [^{3}H]-adenine accumulation rate to <10%, compared to the control. The compounds 10c, 11d, 11e and 11f also showed a relative significant inhibition of AzgA-mediated [^{3}H]-adenine accumulation rate, which however was lower than the one observed with FcyB. None of the compounds tested showed any inhibitory activity on UapA-mediated transport of xanthine (data not shown).

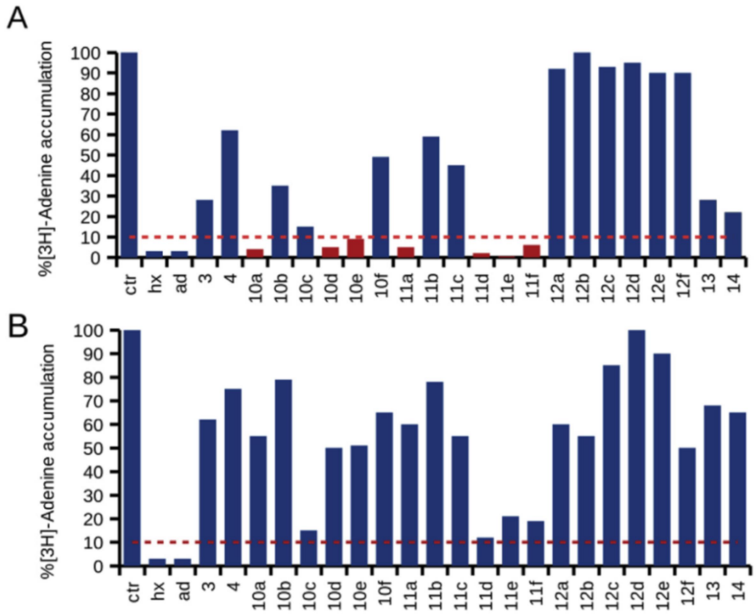

Figure 6.1. *Competition of FcyB-* ***(A)*** *or AzgA-* ***(B)*** *mediated [^{3}H]-adenine uptake by 1000-fold excess (0.5 mM) of unlabeled 3-deazapurine analogues.*

Compounds that proved to be active inhibitors of FcyB were further evaluated by estimating their K_i using IC50 measurments. As shown in Table 6.1, all compounds exhibited values lower than 110 μM for FcyB, with the analogues 10a and 11e being the most potent exhibiting K_is of 19 and 42 μM respectively. As compound 11d showed the higher inhibitory activity against AzgA, the corresponding K_i value was also determined and found to be 58 μM.

Table 6.1 *3-deazapurine analogue binding profile of FcyB. Results are averages of at least three independent experiments with three replicates for each concentration point. SD was <10%.*

Compound	***K*$_i$ (μM)**	**Compound**	***K*$_i$ (μM)**
10a	19 ± 3	**11f**	72 ± 4
10c	106 ± 12	**11e**	42 ± 6
10d	49 ± 10	**1**	5 ± 1
10e	100 ± 5	**2**	38 ± 6
11a	74 ± 6	**Adenine**	7 ± 1
11d	82 ± 8	**Hypoxanthine**	11 ± 1

Overall, seven new compounds with high affinity (19-106 μM) for the FcyB binding site were identified. Interestingly, three of them could also efficiently inhibit AzgA but none of them had any effect on the uric acid-xanthine transporter UapA. It is very important to understand how nucleobase transporters specificity is determined in a molecular lever but at the same time this work might constitute a critical step for novel purine-related antifungals design.

6.2 Curriculum vitae

Georgia F. Papadaki

Birthdate: 27/04/1994 Birthplace: Chania, Crete, Greece
Current Address: Samou 30-32, 10438, Athens, Greece
Permanent Address: E. Pateraki 16, 73133, Chania, Greece
Email: gfpapadaki@biol.uoa.gr Mobile: +30 697 6767 163

Education & Training

PhD Student - S. Niarchos Foundation Scholar, Department of Biology, School of Science, National and Kapodistrian University of Athens, Greece.

November 2017 – January 2021

Research project title: 'Mechanisms of subcellular membrane trafficking'. Subtitle: 'The unexpected pleiotroptic functional role of cytoplasmic tails of the Fur transporters' Supervisor: George Diallinas, Professor of Molecular Microbiology, Laboratory of Molecular Biology and Fungi Genetics, Faculty of Botany, Department of Biology, NKUA, Greece.

Erasmus+ Traineeship, Stockholm University, Department of Molecular Biosciences, The Wenner-Gren Institute, Stockholm, Sweden.

February – August 2017

Research project title: 'Quality control of Inner Nuclear Membrane Proteins'. Supervisor: Per O. Ljungdahl, Professor of Cell Biology, Departmental Head.

B.Sc. in Biology, Department of Biology, School of Science, National and Kapodistrian University of Athens, Greece. Grade: 8.0/10, 'Very Good'.

October 2012 – February 2017

Undergraduate Thesis title: 'The cytoplasmic C-terminal region of NCS1/FUR transporters has a dual role in endocytosis and transport'. Supervisor: George Diallinas, Professor of Molecular Microbiology, Laboratory of Molecular Biology and Fungi Genetics, Faculty of Botany, Department of Biology, NKUA, Greece.

High School degree, 4th General High School, Amperia, Chania, Greece. Grade: 19.5/20, 'Excellent'.

September 2009 – June 2012

Publications

Papadaki G.F., G. Lambrinidis, A. Zamanos, E. Mikros, and G. Diallinas (2019) Cytosolic N- and C-Termini of the *Aspergillus nidulans* FurE Transporter Contain Distinct Elements that Regulate by Long-Range Effects Function and Specificity. *J Mol Biol,* doi: 10.1016/j.jmb.2019.07.013.

Papadaki G.F., P. Ma, I. Ahmad, A. N. Calabrese, S. A. Baldwin, P. J. F. Henderson, and G. Diallinas (2018) Membrane Transport Proteins: The Nucleobase-Cation-Symport-1 Family. In: Roberts G., Watts A., European Biophysical Societies (eds) Encyclopedia of Biophysics. Springer, Berlin, Heidelberg (DOI: https://doi.org/10.1007/978-3-642-35943-9)

Gavriil E. S., S. Dimitrakis, G. Papadaki, S. Balaska, G. Lambrinidis, N. Lougiakis, P. Marakos, G. Diallinas, N. Pouli, and E. Mikros. (2018) Structure-activity relationships in fungal nucleobases transporters as dissected by the inhibitory effects of novel purine analogues. *Eur J Med Chem*. doi: 10.1016/j.ejmech.2018.06.038.

Papadaki G.F., S. Amillis, and G. Diallinas (2017) Substrate specificity of the FurE transporter is determined by cytoplasmic terminal domain interactions. *Genetics*, doi: 10.1534/genetics.117.300327.

Scholarships

EMBO Short Term Fellowship (2020), scholarship for a three-mont research exchange in CHOP, Philadelphia, US.

Stavros Niarchos Foundation (2018-2021), scholarship for postgraduate study.

Erasmus+ Traineeship programme (2017), funding for a six-month work placement in Stockholm University, Sweden.

Conferences

Oral presentations

Georgia Papadaki, George Diallinas, 2016**.** 'The cytoplasmic C-terminal region of NCS1/FUR transporters has a dual role in endocytosis and transport'.
38th Scientific Conference *of the Hellenic Society of Biological Sciences, Kavala, Greece.*

Posters

Georgia F. Papadaki, George Lambrinidis, Emmanuel Mikros and George Diallinas, 2020. 'Roles of the cytosolic tails and the last two transmembrane domains in NCS1/FUR family of transporters'. *15th European Conference on Fungal Genetics 15 (ECFG15) and Asperfest, Rome, Italy.*

Georgia F. Papadaki, George Lambrinidis, Andreas Zamanos, Emmanuel Mikros and George Diallinas, 2019. 'The cytosolic N- and C-termini of the FurE transporter control ER-exit, pH-dependent substrate specificity and endocytosis'.
Gordon Research Conference & Gordon Research Seminar on Mechanisms of Membrane Transport, Colby-Sawyer College, New London, NH United States.

Georgia F. Papadaki, Andreas Zamanos, Vassiliki A. Iconomidou and George Diallinas, 2018. 'A surprising tripartite functional role of the cytosolic N-terminus in the FurE transporter'.
36th Small Meeting on Yeast Transport *and Energetics, Martina Franca, Italy.*

Georgia Papadaki, George Diallinas, 2016. 'The cytoplasmic C-terminal region of NCS1/FUR transporters has a dual role in endocytosis and transport'.
38th Scientific Conference of the Hellenic Society of Biological Sciences, Kavala, Greece.

Georgia Papadaki, George Diallinas, 2016. 'The cytoplasmic C-terminal region of NCS1/FUR transporters has a dual role in endocytosis and transport'.
34th Small Meeting on Yeast *Transport and Energetics, Chania, Greece.*

Georgia Papadaki, George Diallinas, 2016. 'The cytoplasmic C-terminal region of NCS1/FUR transporters has a dual role in endocytosis and transport'.
67th Panhellenic Conference of the Hellenic Society of Biochemistry and Molecular Biology, Ioannina, Greece.

Languages

Greek (Native)

English – Excellent (*Cambridge CPE, Michigan ECPE*)

French – Very good (*DELF B2*)

Working experience

Organizing committee, 34th Small Meeting on Yeast Transport and Energetics, 29/08- 02/09/2016, Chania, Crete, Greece.

Secretary assistant (volunteer), WWF Greece, Athens, Greece.

Volunteer, Mouries Farm, Skyrian Horse Conservation Centre, Skyros, Greece.

Other Skills & Activities

IT literacy: Excellent knowledge of Microsoft Office, Adobe Photoshop Software, GraphPad Prism Software, PyMol, ZEN, Perl programming language and bioinformatics tools (BLAST, MultiAlin, ExPASy)

Other interests: Coast Lifeguard, Swimming, Windsurfing, Biking, Bouldering, playing the Accordion, Travelling, Reading, playing Chess

6.3 List of oligonucleotides used in this study

Oligonucleotides	Sequence 5'-3'
GFP NotI R	CGCGCGGCCGCTTACTTGTACAGCTCGTCC
FurD SpeI F	GCGACTAGTATGCGTTTCGGTCGCTTTCACC
FurA SpeI F	GCGACTAGTATGTCAGCTATTAAACGATGGATC
FurE SpeI F	GCGACTAGTATGGGACTACGAGAAAGACTCC
FurA ΔC NS NotI R	GCGGCGGCCGCGCCGGTGTGGATATCTTCCG
FurD ΔC NS NotI R	GCGGCGGCCGCGCTCTCCCCCAACTCCTCCC
FurE ΔC NS NotI R	GCGGCGGCCGCCTCTTCAACATCAAACGGCCAG
gpdA (1000) AatII F	GCGGACGTCGGTTGACCGGTGCCTGGATC
YFPn XbaI F	CGCGTCTAGAATGGTGAGCAAGGGCGAGGAGCTG
YFPn SpeI R	CGCGACTAGTTTACATGATATAGACGTTGTGGCTGTTG
YFPc BamHI F	CGCGGGATCCATGGCCGACAAGCAGAAGAAC
YFPc NS BamHI R	CGCGGGATCCCTTGTACAGCTCGTCCATG
YFPn BamHI F	CGCGGGATCCATGGTGAGCAAGGGCGAGGAGCTG
YFPn NS BamHI R	CGCGGGATCCCATGATATAGACGTTGTGGCTGTTG
FurD BglII F	GCCGAGATCTATGCGTTTCGGTCGCTTTCACC
FurD XbaI NS R	GCGCTCTAGATAAACAGCAAAACCCTTCTCC
FurE BamHI F	GCCGGGATCCATGGGACTACGAGAAAGACTCC
FurE XbaI NS R	GCGCTCTAGAGCAGAGACAGCCTCCTTCTTCTGCACC
FurE DN12-14A R	CTTCGGTGGCCAGGCTGGCGGCCGCTTGTTTTACTTGGAGTCTTTC
FurE DN15-17A F	GTAAAACAAGGCGACGCCGCGGCCGCCACCGAAGCCGTTGCCTC
FurE DN15-17A R	GAGGCAACGGCTTCGGTGGCGGCCGCGGCGTCGCCTTGTTTTAC
FurE DN18-20A F	GCGACGCCAGCCTGGCCGCGGCCGCCGTTGCCTCCAACAAAGAC
FurE DN18-20A R	GTCTTTGTTGGAGGCAACGGCGGCCGCGGCCAGGCTGGCGTCGC
FurE DN21-23A F	GCCTGGCCACCGAAGCCGCGGCCGCCAACAAAGACCTCGACCCG
FurE DN21-23A R	CGGGTCGAGGTCTTTGTTGGCGGCCGCGGCTTCGGTGGCCAGGC
FurE DN24-26A F	CGAAGCCGTTGCCTCCGCGGCCGCCCTCGACCCGATCCCGCTCG
FurE DN24-26A R	CGAGCGGGATCGGGTCGAGGGCGGCCGCGGAGGCAACGGCTTCG
FurE DN27-29A F	GTTGCCTCCAACAAAGACGCGGCCGCGATCCCGCTCGACTCGCC
FurE DN27-29A R	GGCGAGTCGAGCGGGATCGCGGCCGCGTCTTTGTTGGAGGCAAC
FurE DN24-29A F	CCGTTGCCTCCGCGGCAGCCGCAGCCGCGATCCCGCTCGACTCG
FurE DN24-29A R	CGAGTCGAGCGGGATCGCGGCTGCGGCTGCCGCGGAGGCAACGG
FurE DN30-32A F	CCAACAAAGACCTCGACCCGGCGGCCGCCGACTCGCCCAAACGC
FurE DN30-32A R	GCGTTTGGGCGAGTCGGCGGCCGCCGGGTCGAGGTCTTTGTTGG
FurE DN33-35A F	CTCGACCCGATCCCGCTCGCGGCCGCCAAACGCACGTGGAGATG
FurE DN33-35A R	CATCTCCACGTGCGTTTGGCGGCCGCGAGCGGGATCGGGTCGAG
FurE DN36-38A F	GATCCCGCTCGACTCGCCCGCGGCCGCGTGGAGATGGCCGTCAC
FurE DN36-38A R	GTGACGGCCATCTCCACGCGGCCGCGGGCGAGTCGAGCGGGATC
FurE R108A F	GCATCAACTTCCCCGTCTACACTGCAGCCAGCTTCGGTATGAAGGG
FurE R108A R	CCCTTCATACCGAAGCTGGCTGCAGTGTAGACGGGGAAGTTGATGC
FurE K188A F	CAAGCGCCACTGCTATGGCTCGCAGTGTCCAAGCTACGATACC
FurE K188A R	GGTATCGTAGCTTGGACACTGCGAGCCATAGCAGTGGCGCTTG
FurE Y265A F	CATGCCGGATTTCACGCGGGCCGCCAAAACTCCCAGGGAGGTG
FurE Y265A R	CACCTCCCTGGGAGTTTTGGCGGCCCGCGTGAAATCCGGCATG
FurE K355R F	CGACCTGGCCCTCTGGTTTCCCAgGTACGTCGATACCCGTCGCG
FurE K355R R	CGCGACGGGTATCGACGTACcTGGGAAACCAGAGGGCCAGGTCG
FurE T359A F	GGTTTCCCAAGTACGTCGATGCCCGTCGCGGGGCGTATATC
FurE T359A R	GATATACGCCCCGCGACGGGCATCGACGTACTTGGGAAACC
FurE D498-500A F	CCGTTTGATGTTGAAGAGGCGGCCGCTGTGCTTGAGGGAATGGAGG
FurE D498-500A R	CCTCCATTCCCTCAAGCACAGCGGCCGCCTCTTCAACATCAAACGG
FurE D501-503A F	GATGTTGAAGAGAAAGTCATTGCGGCCGCGGGAATGGAGGAGGGAG
FurE D501-503A R	CTCCCTCCTCCATTCCCGCGGCCGCAATGACTTTCTCTTCAACATC
FurE D504-506A F	AAGTCATTGTGCTTGAGGCGGCCGCGGAGGGAGATAGGGTTGTTAG
FurE D504-506A R	CTAACAACCCTATCTCCCTCCGCGGCCGCCTCAAGCACAATGACTT

Oligonucleotides	Sequence 5'-3'
FurE D507-509A F	GTGCTTGAGGGAATGGAGGCGGCCGCTAGGGTTGTTAGGGTTGAG
FurE D507-509A R	CTCAACCCTAACAACCCTAGCGGCCGCCTCCATTCCCTCAAGCAC
FurE D510-512A F	GGAATGGAGGAGGGAGATGCGGCCGCTAGGGTTGAGGAGGCGG
FurE D510-512A R	CCGCCTCCTCAACCCTAGCGGCCGCATCTCCCTCCTCCATTCC
FurE D513-515A F	GGAGGGAGATAGGGTTGTTGCGGCCGCGGAGGCGGTGGTGCAGAAG
FurE D513-515A R	CTTCTGCACCACCGCCTCCGCGGCCGCAACAACCCTATCTCCCTCC
FurE D516-518A F	GATAGGGTTGTTAGGGTTGAGGCGGCCGCGGTGCAGAAGAAGGAGG
FurE D516-518A R	CCTCCTTCTTCTGCACCGCGGCCGCCTCAACCCTAACAACCCTATC
FurE D522-524A F	GGAGGCGGTGGTGCAGAAGGCGGCCGCTGTCTCTGCAGCGGCCG
FurE D522-524A R	CGGCCGCTGCAGAGACAGCGGCCGCCTTCTGCACCACCGCCTCC
FurE K521/522R F	GTTGAGGAGGCGGTGGTGCAGAGGAGGGAGGCTGTCTCTGCATAG
FurE K521/522R R	CTATGCAGAGACAGCCTCCCTCCTCTGCACCACCGCCTCCTCAAC
FurE W39A F	GCTCGACTCGCCCAAACGCACGGCGAGATGGCCGTCACTACTGG
FurE W39A R	CCAGTAGTGACGGCCATCTCGCCGTGCGTTTGGGCGAGTCGAGC
FurE Q59A F	GCGTTTAGTATTAGCATGTATGCAGTGACCTCGACTTCGGTCAG
FurE Q59A R	CTGACCGAAGTCGAGGTCACTGCATACATGCTAATACTAAACGC
FurE T63A F	GCATGTATCAAGTGACCTCGGCTTCGGTCAGTAAGGGCCTAAG
FurE T63A R	CTTAGGCCCTTACTGACCGAAGCCGAGGTCACTTGATACATGC
FurE S64A F	GCATGTATCAAGTGACCTCGACTGCAGTCAGTAAGGGCCTAAGTGC
FurE S64A R	GCACTTAGGCCCTTACTGACTGCAGTCGAGGTCACTTGATACATGC
FurE R123A F	GCTACTTCGCCGTCTTCGTTGCAGGGATTGTCGCTATTATCTGG
FurE R123A R	CCAGATAATAGCGACAATCCCTGCAACGAAGACGGCGAAGTAGC
FurE R193A F	GGCTCAAAGTGTCCAAGCTAGCATACCTCTTTATCGTGAAAACG
FurE R193A R	CGTTTTCACGATAAAGAGGTATGCTAGCTTGGACACTTTGAGCC
FurE D261A F	GCTGGCCCTGAACATGCCGGCTTTCACGCGGTACGCCAAAACTCC
FurE D261A R	GGAGTTTTGGCGTACCGCGTGAAAGCCGGCATGTTCAGGGCCAGC
FurE R264A F	CCTGAACATGCCGGATTTCACGGCGTACGCCAAAACTCCCAGGGAG
FurE R264A R	CTCCCTGGGAGTTTTGGCGTACGCCGTGAAATCCGGCATGTTCAGG
FurE N347A F	GCGAATAGCGTCTCCTTCTCGGCCGACCTGGCCCTCTGGTTTCC
FurE N347A R	GGAAACCAGAGGGCCAGGTCGGCCGAGAAGGAGACGCTATTCGC
FurE S384A F	GTACATTCAAAACAGCGCGGCCGCCTTTTCATCTTTTCTAGGTGGG
FurE S384A R	CCCACCTAGAAAAGATGAAAAGGCGGCCGCGCTGTTTTGAATGTAC
FurE F385A F	CATTCAAAACAGCGCGGCGAGCGCTTCATCTTTTCTAGGTGGG
FurE F385A R	CCCACCTAGAAAAGATGAAGCGCTCGCCGCGCTGTTTTGAATG
FurE S386A F	CAAAACAGCGCGGCGAGCTTTGCATCTTTTCTAGGTGGGTACAGC
FurE S386A R	GCTGTACCCACCTAGAAAAGATGCAAAGCTCGCCGCGCTGTTTTG
FurE Y484F F	CATTGTTGTTTCTGGGATGGTCTTTTACTTGCTGTTTTTTGTCTGG
FurE Y484F R	CCAGACAAAAAACAGCAAGTAAAAGACCATCCCAGAAACAACAATG
FurE Y484M F	CATTGTTGTTTCTGGGATGGTCATGTACTTGCTGTTTTTTGTCTGG
FurE Y484M R	CCAGACAAAAAACAGCAAGTACATGACCATCCCAGAAACAACAATG
FurE K199A F	GCTACGATACCTCTTTATCGTGGCAACGTGCATCATGCCGATCTTC
FurE K199A R	GAAGATCGGCATGATGCACGTTGCCACGATAAAGAGGTATCGTAGC
FurE F196A F	GTGTCCAAGCTACGATACCTCGCTATCGTGAAAACGTGCATCATG
FurE F196A R	CATGATGCACGTTTTCACGATAGCGAGGTATCGTAGCTTGGACAC
FurE d466-468 F	GCGTGCCGAAGGGAGCGGCGGCCGCGTACAGCTGCAGTTGGTTGG
FurE d466-468 R	CCAACCAACTGCAGCTGTACGCGGCCGCCGCTCCCTTCGGCACGC
FurE d469-471 F	GAAGGGAGCGAATTACTTGGCGGCCGCCAGTTGGTTGGTGAGCATTG
FurE d469-471 R	CAATGCTCACCAACCAACTGGCGGCCGCCAAGTAATTCGCTCCCTTC
FurE d472-474 F	GAATTACTTGTACAGCTGCGCGGCCGCGGTGAGCATTGTTGTTTCTG
FurE d472-474 R	CAGAAACAACAATGCTCACCGCGGCCGCGCAGCTGTACAAGTAATTC
FurE d475-477 F	GTACAGCTGCAGTTGGTTGGCGGCCGCTGTTGTTTCTGGGATGGTC
FurE d475-477 R	GACCATCCCAGAAACAACAGCGGCCGCCAACCAACTGCAGCTGTAC
FurE d478-480 F	CAGTTGGTTGGTGAGCATTGCGGCCGCTGGGATGGTCTATTACTTG
FurE d478-480 R	CAAGTAATAGACCATCCCAGCGGCCGCAATGCTCACCAACCAACTG
FurE d481-483 F	GGTGAGCATTGTTGTTTCTGCGGCCGCCTATTACTTGCTGTTTTTTG
FurE d481-483 R	CAAAAAACAGCAAGTAATAGGCGGCCGCAGAAACAACAATGCTCACC

Oligonucleotides	Sequence 5'-3'
FurE d484-486 F	GTTGTTTCTGGGATGGTCGCGGCCGCGCTGTTTTTTGTCTGGCCG
FurE d484-486 R	CGGCCAGACAAAAAACAGCGCGGCCGCGACCATCCCAGAAACAAC
FurE d487-489 F	CTGGGATGGTCTATTACTTGGCGGCCGCTGTCTGGCCGTTTGATG
FurE d487-489 R	CATCAAACGGCCAGACAGCGGCCGCCAAGTAATAGACCATCCCAG
FurE d490-492 F	CTATTACTTGCTGTTTTTTGCGGCCGCGTTTGATGTTGAAGAGAAAG
FurE d490-492 R	CTTTCTCTTCAACATCAAACGCGGCCGCAAAAAACAGCAAGTAATAG
FurE d438-440 F	GGTGTGAATATACGCGCCGCGGCCGCGTTTGTCTGCGGCATCG
FurE d438-440 R	CGATGCCGCAGACAAACGCGGCCGCGGCGCGTATATTCACACC
FurE d441-443 F	GAATATACGCGCCATGATCTCGGCGGCCGCCGGCATCGCGCCGAATC
FurE d441-443 R	GATTCGGCGCGATGCCGGCGGCCGCCGAGATCATGGCGCGTATATTC
FurE d444-447 F	CATGATCTCGTTTGTCTGCGCGGCCGCGGCGAATCTGCCTGGTTTG
FurE d444-447 R	CAAACCAGGCAGATTCGCCGCGGCCGCGCAGACAAACGAGATCATG
FurE d448-450 F	GTTTGTCTGCGGCATCGCGCCGGCGGCCGCTGGTTTGGCTGCGGTG
FurE d448-450 R	CACCGCAGCCAAACCAGCGGCCGCCGGCGCGATGCCGCAGACAAAC
FurE S23C F	CTGGCCACCGAAGCCGTTGCCTGCAACAAAGACCTCGACCCGATCC
FurE S23C R	GGATCGGGTCGAGGTCTTTGTTGCAGGCAACGGCTTCGGTGGCCAG
FurE T38C F	CCGCTCGACTCGCCCAAACGCTGCTGGAGATGGCCGTCACTACTGG
FurE T38C R	CCAGTAGTGACGGCCATCTCCAGCAGCGTTTGGGCGAGTCGAGCGG
FurE T63C F	GACTCGCGATGCTAGTGACCTCGTGTTCGGTCAGTAAGGGCCTAAG
FurE T63C R	CTTAGGCCCTTACTGACCGAACACGAGGTCACTAGCATCGCGAGTC
T63C on cDNA F	GCATGTATCAAGTGACCTCGTGTTCGGTCAGTAAGGGCCTAAG
T63C on cDNA R	CTTAGGCCCTTACTGACCGAACACGAGGTCACTTGATACATGC
FurE G112C F	CGTCTACACTCGAGCCAGCTTCTGTATGAAGGGGAGCTACTTCGC
FurE G112C R	GCGAAGTAGCTCCCCTTCATACAGAAGCTGGCTCGAGTGTAGACG
FurE L187C F	CCTGCAAGCGCCACTGCTATGGTGCAAAGTGTCCAAGCTACGATAC
FurE L187C R	GTATCGTAGCTTGGACACTTTGCACCATAGCAGTGGCGCTTGCAGG
FurE K188C F	GCAAGCGCCACTGCTATGGCTCTGTGTGTCCAAGCTACGATACCTC
FurE K188C R	GAGGTATCGTAGCTTGGACACACAGAGCCATAGCAGTGGCGCTTGC
FurE A266C F	CATGCCGGATTTCACGCGGTACTGCAAAACTCCCAGGGAGGTGTTC
FurE A266C R	GAACACCTCCCTGGGAGTTTTGCAGTACCGCGTGAAATCCGGCATG
FurE P354C F	GAACGACCTGGCCCTCTGGTTTTGCAAGTACGTCGATACCCGTCGC
FurE P354C R	GCGACGGGTATCGACGTACTTGCAAAACCAGAGGGCCAGGTCGTTC
FurE A383C F	GTGGTACATTCAAAACAGCGCGTGTAGCTTTTCATCTTTTCTAGGT
FurE A383C R	ACCTAGAAAAGATGAAAAGCTACACGCGCTGTTTTGAATGTACCAC
FurE L502C F	GTTGAAGAGAAAGTCATTGTGTGTGAGGGAATGGAGGAGGGAGATAG
FurE L502C R	CTATCTCCCTCCTCCATTCCCTCACACACAATGACTTTCTCTTCAAC
FurE XmaI F	CGCCCCGGGATGGGACTACGAGAAAGACTCC
FurE XmaI R	CGCCCCGGGCTATGCAGAGACAGCCTCCTTC
FurE NS XmaI R	CGCCCCGGGTGCAGAGACAGCCTCCTTC
FurE seq 1	CGCCGTCTTCGGTATGCTTCC
FurE seq 2	CGCGGTACGCCAAAACTCCCAG
FurE seq 3	GCTGCAGTTGGTTGGTGAGC
FurE seq 1 cDNA	GCTATTATCTGGTTTGGCACG

6.4 Reprints of original publications

Substrate Specificity of the FurE Transporter Is Determined by Cytoplasmic Terminal Domain Interactions

Georgia F. Papadaki, Sotiris Amillis, and George Diallinas[1]
Department of Biology, National and Kapodistrian University of Athens, Panepistimioupolis, Athens 15784, Greece
ORCID ID: 0000-0002-3426-726X (G.D.)

ABSTRACT FurE, a member of the Nucleobase Cation Symporter 1 transporter family in *Aspergillus nidulans*, is specific for allantoin, uric acid (UA), uracil, and related analogs. Herein, we show that C- or N-terminally-truncated FurE transporters (FurE-ΔC or FurE-ΔN) present increased protein stability, but also an inability for UA transport. To better understand the role of cytoplasmic terminal regions, we characterized genetic suppressors that restore FurE-ΔC-mediated UA transport. Suppressors map in the periphery of the substrate-binding site [Thr133 in transmembrane segment (TMS)3 and Val343 in TMS8], an outward-facing gate (Ser296 in TMS7, Ile371 in TMS9, and Tyr392 and Leu394 in TMS10), or in flexible loops (Asp26 in L_N, Gly222 in L5, and Asn308 in L7). Selected suppressors were also shown to restore the wild-type specificity of FurE-ΔN, suggesting that both C- and/or N-terminal domains are involved in intramolecular dynamics critical for substrate selection. A direct, substrate-sensitive interaction of C- and/or N-terminal domains was supported by bimolecular fluorescence complementation assays. To our knowledge, this is the first case where not only the function, but also the specificity, of a eukaryotic transporter is regulated by its terminal cytoplasmic regions.

KEYWORDS nucleobase; purine; allantoin; Mhp1; genetics; gating

Years of research have led to a model where solute transmembrane transporters operate by an alternating access mechanism that exhibits at least two structurally distinct conformations, outward (extracellular)-facing and inward (cytoplasmic)-facing, the alternation of which is promoted by substrate binding and release (Forrest *et al.* 2011; Kaback *et al.* 2011). More recent genetic, functional, and structural evidence has supported the idea that during transport catalysis, transporters acquire multiple distinct conformations, a distinction based not only on whether the binding site is facing the extracellular or cytoplasmic side of the cell, but also on whether specific domains of the protein allow or occlude substrate access to, or release from, the binding site. These distinct domains seem to function as gates, gating elements, or selectivity filters (Diallinas 2008, 2016). Thus, current models consider that during substrate translocation, transporters obtain at least four structurally distinct sequential conformations: an outward-facing "open" conformation that provides access to substrates; an outward-facing "closed" conformation, where the substrate is bound in the major substrate-binding site while a domain (*e.g.*, an external gate) moves to occlude further access of substrates from the extracellular side or leakage of the substrate from the binding site; an inward-facing closed conformation, where the substrate is still bound in the major substrate-binding site while a distinct domain (*e.g.*, an internal gate) occludes substrate release into the cytoplasm; and an inward-facing open conformer, where the internal gate is displaced to allow the release of the substrate into the cytoplasm (Shi 2013; Diallinas 2014, 2016; Penmatsa and Gouaux 2014; Colas *et al.* 2016; Quistgaard *et al.* 2016).

Interestingly, genetic, functional, and structural approaches have shown that mutations altering the specificity of transporters are preferably located at gating elements or selectivity filters, rather than within the major binding site. Such gating or selectivity elements can be located at the periphery of the major binding site, but also at flexible transmembrane-α-helices or hydrophilic loops that act as dynamic hinges

doi: https://doi.org/10.1534/genetics.117.300327
Manuscript received July 21, 2017; accepted for publication October 3, 2017; published Early Online October 4, 2017.
Supplemental material is available online at www.genetics.org/lookup/suppl/doi:10.1534/genetics.117.300327/-/DC1.
[1]Corresponding author: Department of Biology, National and Kapodistrian University of Athens, Panepistimioupolis, Athens 15784, Greece. E-mail: diallina@biol.uoa.gr

(Papageorgiou *et al.* 2008; Weyand *et al.* 2008; Kosti *et al.* 2010; Shimamura *et al.* 2010; Adelman *et al.* 2011; Kazmier *et al.* 2014; Simmons *et al.* 2014; Alguel *et al.* 2016a; Diallinas 2016). The independent action of gating or selectivity elements has been further supported by the fact that specific mutations in these elements often do not alter the transport kinetics for physiological substrates, and may lead to additive or synthetic transport activities and specificities when combined with substrate-binding mutations (Papageorgiou *et al.* 2008; Kosti *et al.* 2010; Alguel *et al.* 2016a). Overall, these findings strongly suggest that transporter specificity might be determined through molecular and functional synergy of multiple domains (Diallinas 2014, 2016). Recently, homo-oligomerization was also found to be important for transporter specificity (Alguel *et al.* 2016a,b; Diallinas 2016).

In this work, we present genetic and biochemical evidence supporting the idea that transporter specificity in the NCS1 (Nucleobase Cation Symporter 1) transporter family (Pantazopoulou and Diallinas 2007; Weyand *et al.* 2008; Krypotou *et al.* 2012, 2015; Sioupouli *et al.* 2017) is determined via dynamic intramolecular interactions of multiple domains. More specifically, we show that cytoplasmic N- and C-terminal segments of FurE, an allantoin–uric acid–uracil transporter of the fungus *Aspergillus nidulans* (Krypotou *et al.* 2015), interact with each other and that this interaction is critical for substrate specificity. Our results are discussed in the context of available knowledge from crystallographic and *in silico* approaches to study NSC1 transporters.

Materials and Methods

Media, strains, and growth conditions

Standard complete (CM) and minimal media (MM) for *A. nidulans* growth were used. Media and supplemented auxotrophies were used at the concentrations given in the Fungal Genetics Stock Centre (FGSC; http://www.fgsc.net). Glucose 1% (w/v) or Fructose 0.1% (w/v) was used as carbon sources. For nitrogen sources, 10 mM ammonium tartrate (NH_4) or sodium nitrate (NO_3) was used. Nucleobases and analogs were used at the following final concentrations: 5-fluorouracil (5FU) 100 μM, 5-fluorocytosine (5FC) 50 μM, 5-fluorouridine (5FUd) 10 μM, uric acid (UA) 0.5 mM, xanthine [XAN 1mM, uracil (URA) 1mM and allantoin (ALL)] 1 mM. For induction of genes under the *alcA*p promoter, 50 mM ethanol was also added to the MM. All media and chemical reagents were obtained from Sigma [Sigma Chemical] (St. Louis, MO) or AppliChem (Bioline Scientific SA, Hellas). A Δ*uapA* Δ*uapC*::*AfpyrG* Δ*azgA pabaA1 argB2* mutant (Pantazopoulou *et al.* 2007) was the recipient strain in transformations with plasmids carrying the *furE* and *yfp* fusions. Selection was based on complementation of arginine auxotrophy *argB2* and p-aminobenzoic acid auxotrophy *pabaA1*. A Δ*furD*::*riboB* Δ*furA*::*riboB* Δ*fcyB*::*argB* Δ*azgA* Δ*uapA* Δ*uapC*::*AfpyrG* Δ*cntA*::*riboB pabaA1 pantoB100* mutant strain, named Δ7, was the recipient strain in transformations with plasmids carrying *fur* genes or alleles based on complementation of the pantothenic acid auxotrophy *pantoB100* (Krypotou and Diallinas 2014). Derivatives of mutant strains were obtained through genetic crosses based on auxotrophic markers for heterokaryon establishment and, if needed, identified by relevant PCR. *A. nidulans* protoplast isolation and transformation was performed as previously described (Koukaki *et al.* 2003). Growth tests were performed at 37° for 48 hr, at pH 6.8.

Standard molecular biology manipulations and plasmid construction

Genomic DNA extraction from *A. nidulans* was performed as described in FGSC. Plasmids, prepared in *Escherichia coli*, and DNA restriction or PCR fragments were purified from agarose 1% gels with a Nucleospin Plasmid Kit or Nucleospin ExtractII kit, according to the manufacturer's instructions (Macherey-Nagel, Lab Supplies Scientific SA, Hellas). Standard PCR reactions were performed using KAPATaq DNA polymerase (Kapa Biosystems). PCR products used for cloning, sequencing, and reintroduction by transformation in *A. nidulans* were amplified by a high-fidelity KAPA HiFi HotStart Ready Mix (Kapa Biosystems) polymerase. DNA sequences were determined by VBC-Genomics (Vienna, Austria). Site-directed mutagenesis was carried out according to the instructions accompanying the Quik-Change Site-Directed Mutagenesis Kit (Agilent Technologies, Stratagene, La Jolla, CA). The principal vector used for most *A. nidulans* mutants is a modified pGEM-T-easy vector carrying a version of the *gpdA* promoter, the *trpC* 3′ termination region, and the *panB* selection marker (Krypotou *et al.* 2015). For bimolecular fluorescence complementation (BiFC) analyses, the N-terminal half of yellow fluorescent protein (YFP_n; 154 amino acids of YFP), or the C-terminal half of YFP (YFP_c; 86 amino acids of YFP) was amplified from plasmids PDV7 and PDV8 (Takeshita *et al.* 2008) and cloned into pAN510exp-alcAp or pAN520exp-alcAp (Martzoukou *et al.* 2015), followed by cloning of the *furE* ORF. Mutations and segment truncations in Fur transporters were constructed by oligonucleotide-directed mutagenesis or appropriate forward and reverse primers (Supplemental Material, Table S1 in File S1). Transformants arising from single-copy integration events with intact Fur ORFs were identified by Southern and PCR analysis.

Protein extraction and western blotting

Cultures for membrane protein extraction were grown in MM supplemented with $NaNO_3$ at 25° for 14 hr prior to the addition of NH_4^+ or substrate. Membrane protein extraction was performed as previously described (Evangelinos *et al.* 2016). Equal sample loading was estimated by Bradford assays. Total proteins (30–50 μg) were separated by SDS-PAGE (8% w/v polyacrylamide gel) and electroblotted (Mini Protean Tetra Cell, Bio-Rad, Hercules, CA) onto PVDF membranes (Macherey-Nagel). Immunodetection was performed with a primary mouse anti-GFP monoclonal antibody (Roche Diagnostics), or a mouse anti-actin monoclonal (C4) antibody (MP Biomedicals Europe) and a secondary goat anti-mouse IgG HRP-linked antibody (Cell Signaling Technology). Blots were developed by

Table 1 Profile of the mutations suppressing the inability of FurE-ΔC to grow on uric acid. The relevant nucleobase substitution is underlined.

Mutation	Codon Change	Number of Isolates	Location	Putative Domain
D26N	GAC > AAC	1	N-tail	Flex loop
T133V	ACG > GTG	4	TMS3	Binding site filter
G222K	GGG > AAG	1	L5	Flex loop
	GGG > AAG	4		
N308T	AAC > ACC	7	L7	Flex loop
	AAC > ACA	1		
	AAC > ACT	1		
S296R	AGC >CGC	4	TMS7	Gate
V343I	GTC > ATC	1	TMS8	Binding site filter
I371L	ATC > CTC	1	TMS9	Gate
I371F	ATC > TTC	3	TMS9	Gate
I371P	ATC > CCC	1	TMS9	Gate
Y392N	TAC > AAC	6	TMS10	Gate
Y392C	TAC > TGC	5	TMS10	Gate
Y392E	TAC > GAA	1	TMS10	Gate
L394P	CTG > CCG	4	TMS10	Gate

TMS, transmembrane segment.

the chemiluminescent method using the LumiSensor Chemiluminescent HRP Substrate kit (Genscript USA) and SuperRX Fuji medical X-Ray films (FujiFILM Europe).

Uptake assays

Kinetic analysis of Fur transporter activity was measured by estimating uptake rates of [^{3}H]-uracil (40 Ci mmol^{-1}, Moravek Biochemicals, CA), as previously described in Krypotou and Diallinas (2014). In brief, [^{3}H]-uracil uptake was assayed in *A. nidulans* conidiospores germinating for 4 hr at 37°, at 140 rpm, in liquid MM (pH 6.8). Initial velocities were measured on 10^7 conidiospores/100 μl by incubation with concentrations of 0.2–2.0 μM of [^{3}H]-uracil at 37°. The time of incubation was defined through time course experiments and the period of time when each transporter showed linear increased activity was chosen, respectively. $K_{m/i}$ values were obtained using radiolabeled uracil at 0.2–0.5 μM in the presence of various concentrations (0.5–2000 μM) of nonlabeled substrates. K_i values were calculated by satisfying the criteria for use of the Cheng and Prusoff equation, $K_i = IC50 / [1 + (L / K_m)]$, in which L is the permeant concentration. In our assays, K_i values equal IC50 values as the L is very low (at least 10-fold lower than the K_m value). Background counts are subtracted from the values obtained in strains expressing the relevant transporter. K_m, K_i, and V_{max} determination is carried out using standard Lineweaver–Burk or Eadie–Hofstee equation formulae, or relevant software (*e.g.*, GraphPad Prism). All transport assays were carried out in triplicate. SD was < 20%.

Isolation and characterization of suppressor mutations

Mutagenesis was performed at a standard distance of 20 cm from an Osram HNS30 UV-B/C lamp. Suppressor mutations were obtained after 3 min 45 sec UV mutagenesis of 10^9 conidiospores of the strain FurE-ΔC and subsequent selection of colonies capable of growing on MM containing UA as a sole nitrogen source, at 25°. Spores from positive colonies were collected after 6–8 days and isolated colonies were obtained by standard purification on the same selective medium that was used to obtain the original colonies. Genomic DNA from 45 purified colonies was isolated and the ORF of FurE-ΔC was amplified and sequenced. In all cases, the amplified fragments contained a new mutation (Table 1). Strains carrying suppressor mutations were outcrossed with the original non-mutagenized strain to show that suppressor phenotypes cosegregate with sequenced FurE mutations.

Epifluorescence microscopy

Samples for inverted epifluorescence microscopy were prepared as previously described (Valdez-Taubas *et al.* 2004; Gournas *et al.* 2010; Karachaliou *et al.* 2013). In brief, sterile 35-mm 1-liter dishes with glass bottoms (Ibidi, Germany), containing liquid minimal media supplemented with $NaNO_3$ and 0.1% glucose or fructose, were inoculated from a spore solution and incubated for 16–22 hr at 25°. The samples were observed on an Axioplan Zeiss ([Carl Zeiss], Thornwood, NY) phase contrast epifluorescent microscope and the resulting images were acquired with a Zeiss-MRC5 digital camera using AxioVs40 V4.40.0 software. FM4-64 terminal vacuolar staining was as described in Evangelinos *et al.* (2016). Image processing, contrast adjustment, and color combining were made using Adobe Photoshop CS3 software or ImageJ software. To quantify transporter endocytosis, Vacuolar Surface (Total surface of vacuoles containing GFP/hypha) and Vacuolar GFP Fluorescence (Total fluorescence intensity of vacuoles containing GFP/hypha) were measured using the Area Selection Tool of the ICY application (Martzoukou *et al.* 2017). Tukey's Multiple Comparison Test (one-way ANOVA) was performed to test the statistical significance of the results for five Regions of Interest using Graphpad Prism3. Images were further processed and annotated in Adobe Photoshop CS3 (Martzoukou *et al.* 2017).

Data availability

Strains constructed in this work are available upon request.

Results

C-terminally-truncated Fur transporters show modified apparent substrate specificities

Members of the NCS1 transporter family are present in prokaryotes, fungi, and some plants. Fungal, and especially *A. nidulans*, NCS1 transporters have been extensively studied in respect to their function, specificity, regulation of expression, and evolution, and are classified into two distinct subfamilies: the Fcy- and the Fur-like transporters (de Koning and Diallinas 2000; Pantazopoulou and Diallinas 2007; Krypotou *et al.* 2015). *A. nidulans* possesses seven Fur transporters (FurA–G): two function as major uracil (FurD) or allantoin (FurA) transporters (Amillis *et al.* 2007; Hamari *et al.* 2009); one is a secondary, low-affinity, promiscuous transporter specific for uracil, allantoin, UA, and related analogs (FurE), and the rest function as cryptic, very low-efficiency uracil transporters (Krypotou *et al.* 2015).

Using functional GFP-tagged Fur versions, we have previously shown that Fur transporters are differentially sensitive to endocytic turnover in response to two well-characterized endocytic triggers (Krypotou *et al.* 2015), those elicited by either an excess of substrate or the presence of a primary nitrogen source (Gournas *et al.* 2010). In particular, FurE is highly sensitive to endocytosis, showing a degree of internalization and turnover even in the absence of endocytic signals (*e.g.*, constitutive endocytosis), FurD is mostly sensitive to ammonium-elicited and less so to substrate-elicited internalization, and FurA is sensitive solely to ammonium-elicited endocytosis. Some of the other Fur transporters (FurC and FurG) do not respond to any known endocytic trigger. In all cases studied, fungal transporter downregulation via endocytosis necessitates prior Lys63-ubiquitylation by Hect-type ubiquitin ligases (Lauwers *et al.* 2010; Gournas *et al.* 2016).

To investigate the basis of the differential response of Fur transporters to endocytosis and turnover, and based on the observation that all Fur proteins possess several Lys residues as candidates for ubiquitylation at their C-terminal cytoplasmic regions (Gournas *et al.* 2010; Karachaliou *et al.* 2013), we constructed and functionally analyzed strains expressing truncated versions of FurA, FurD, and FurE transporters, all lacking a C-terminal region (CTR) including the three most terminally located Lys residues (Figure S1 in File S1). We also constructed a C-terminally-truncated version of a specific allele of FurE, FurE-K252F, which increases FurE-mediated transport activity and thus permits better assessment of the wild-type FurE function (Krypotou *et al.* 2015). All truncated *fur* gene versions were fused C-terminally with the *gfp* ORF, while the constitutive $gpdA_p$ promoter was used to drive their transcription (see *Materials and Methods*).

The truncated Fur versions (named FurA-ΔC-GFP, FurD-ΔC-GFP, FurE-ΔC-GFP, and FurE-K252F-ΔC-GFP) were introduced by standard genetic transformation in an *A. nidulans* strain, called Δ7, lacking all seven major transporters specific for nucleobases, allantoin, or nucleosides, as previously performed for the nontruncated FurA-GFP, FurD-GFP, and FurE-GFP transporters (Krypotou *et al.* 2015). Selected purified transformants arising from intact single-copy plasmid integration events were further analyzed by growth tests, radiolabeled substrate uptake assays, and epifluorescence microscopy.

Figure 1A shows a growth test of selected transformants and isogenic controls on MM containing UA or allantoin as sole nitrogen sources, or nitrate plus toxic nucleobase analogs known to be transported by the Fur transporters. A wild-type positive control strain grows on UA or allantoin and is sensitive to all nucleobase/nucleoside toxic analogs tested (*e.g.*, 5FU, 5FC, and 5FUd), because it expresses all relevant transporters. A negative control strain, Δ7, lacking all major nucleobase transporters, does not grow on UA or allantoin, and is resistant to all toxic nucleobase/nucleoside analogs tested. It should be noted that the Δ7 strain carries, among other transporter null mutations, total deletions of *furA* and *furD*, but not *furE* gene. However, *furE* expression driven by its native promoter is extremely low, so that no FurE-dependent growth on UA or allantoin—or no sensitivity to 5FU, 5FC, or 5FUd—is detected. The transport activity of FurE is only observed when FurE is expressed from the strong $gpdA_p$ promoter in Δ7 (Krypotou *et al.* 2015). Isogenic Δ7 strains expressing the nontruncated GFP-tagged Fur versions from the $gpdA_p$ promoter confer distinct growth profiles on UA, allantoin, or toxic analogs as follows. Strains expressing FurA grow on allantoin, albeit the relevant colonies are very compact due to over-accumulation of this toxic metabolite and show sensitivity to all toxic nucleobase/nucleoside analogs. Strains expressing FurD grow weakly on UA and are sensitive to 5FU, 5FC, or 5FUd. Strains expressing FurE grow well on allantoin, weakly on UA, and are sensitive to 5FU, 5FC, or 5FUd. Strains expressing the hyperactive FurE-K252F grow equally well on allantoin or UA, and are sensitive to 5FU or 5FC, but not to 5FUd. These growth phenotypes are in agreement with what has been reported before (Krypotou *et al.* 2015). Strains expressing the corresponding truncated versions of FurD, FurE, or FurE-K252F (*i.e.*, FurD-ΔC, FurE-ΔC, or FurE-K252F-ΔC) showed distinct growth phenotypes when compared to their nontruncated equivalents. The strain expressing the truncated FurD transporter shows stronger growth on UA and allantoin, but is more resistant to 5FC. More impressively, the strain expressing the truncated FurE transporter could not grow at all on UA, despite retaining full capacity to grow on allantoin or being sensitive to 5FU, 5FC, or 5FUd. The strain expressing the truncated FurE-K252F showed reduced capacity to grow on UA, especially at 37°, but was equally sensitive to all toxic analogs tested with the nontruncated version. In contrast, no apparent growth differences could be detected between strains expressing FurA or FurA-ΔC. Thus, deletion of the C-terminal part of at least FurD and FurE, or FurE-K252F, led to a modification of the apparent substrate specificity of these transporters. The molecular rational behind this

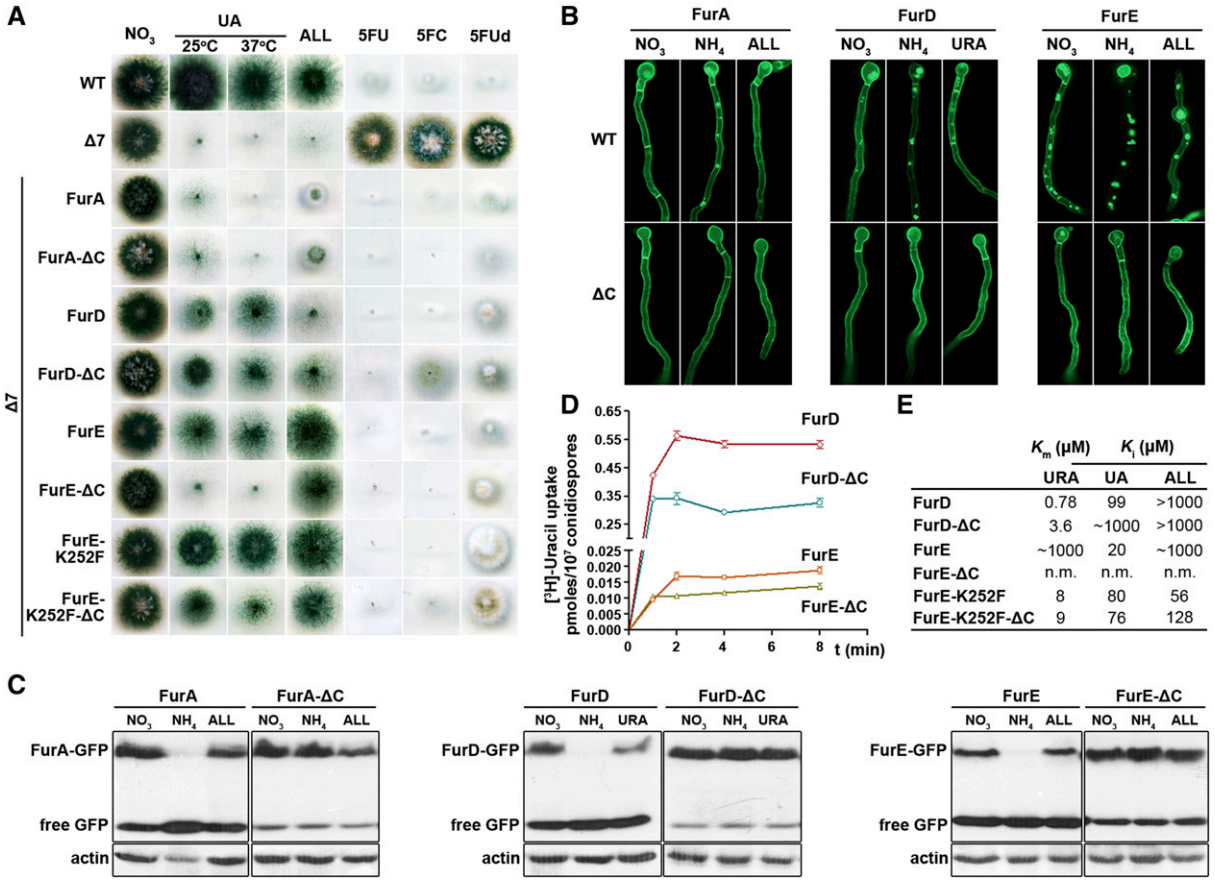

Figure 1 Functional characterization of truncated Fur transporters. (A) C-terminally-truncated Fur transporters show modified apparent substrate specificities. Growth test of strains expressing, from *gpdA*$_p$ promoter, nontruncated (WT) and truncated Fur-GFP transporters. The test is performed at 37° on MM media containing as sole nitrogen source nitrate (control), UA, or ALL, or on nitrate media containing a nucleobase toxic analog (5FU, 5FC, or 5FUd). The growth on UA is recorded at both 37 and 25°. WT stands for a standard *A. nidulans* wild-type strain. Δ7 is a mutant strain carrying total deletions in all seven major transporters for nucleobases, nucleosides, and ALL (*uapAΔ uapCΔ azgAΔ furDΔ furAΔ fcyBΔ cntAΔ*). The Δ7 strain has an intact endogenous *furE* gene transporter, but this is very little expressed under standard conditions and thus does not contribute to detectable transport of its potential substrates (UA, URA, or ALL). All other strains are single-copy isogenic transformants of Δ7 expressing the indicated nontruncated or truncated Fur transporter. K252F is a missense mutation increasing the activity of FurE (Krypotou *et al.* 2015). (B) C-terminally-truncated Fur transporters do not undergo endocytosis. Subcellular localization of nontruncated (WT) and truncated GFP-tagged Fur transporters, expressed from the *gpdA*$_p$ promoter, as analyzed by *in vivo* inverted epifluorescence microscopy. Samples are grown for 18 hr at 25° under control (MM with nitrate as N source), or substrate-elicited (ALL or URA) or ammonium-elicited endocytic conditions (MM with nitrate as N source plus addition of substrate or ammonium for the last 2 hr of the culture). Endocytic turnover is identified by the appearance of cytoplasmic structures corresponding to endosomes and vacuoles and the progressive diminution of the peripheral fluorescent signal (Gournas *et al.* 2010; Krypotou *et al.* 2015). Notice that different Fur transporters have distinct sensitivities to endocytosis (FurE > FurD, FurA), but truncation of the C-terminus stabilizes the Fur-GFP chimeras in all cases. (C) C-terminally-truncated Fur transporters show dramatically reduced turnover. Western blot analysis of total protein extracts of strains expressing WT and truncated Fur-GFP versions, using anti-GFP (upper panel) or anti-actin (control, lower panel) antibody. Growth conditions are as in (B). Free GFP levels reflect vacuolar degradation of Fur-GFP proteins. (D and E) C-terminally-truncated Fur transporters show modified transport kinetics. (D) Time course of [^{3}H]-URA uptake by truncated (FurD-ΔC and FurE-ΔC) and nontruncated (FurD and FurE) transporters. SD is depicted with error bars. (E) $K_{i/m}$ values (micromolar) for truncated and nontruncated FurD and FurE transporters determined using [^{3}H]-URA uptake competition. Results are averages of three measurements for each concentration point. SD was < 20%. 5FC, 5-fluorocytosine; 5FU, 5-fluorouracil; 5FUd, 5-fluorouridine; ALL, allantoin; MM, minimal media; n.m., nonmeasurable; URA, uracil; UA, uric acid; WT, wild-type.

rather unexpected observation became the major theme of this work.

C-terminally-truncated Fur transporters show increased protein stability and modified transport kinetics

To investigate the effects of C-terminal truncation in different Fur transporters, we followed the subcellular localization and turnover of the truncated versions by *in vivo* epifluorescence microscopic and western blot analysis. First, we tested both the rate of constitutive endocytosis and that triggered by either an excess of substrate or the addition of a primary nitrogen source (*e.g.*, ammonium). Figure 1B shows that, in all cases, C-terminal truncation of the Fur proteins stabilizes the Fur transporters in the plasma membrane. As a consequence, very little, if any, fluorescence is associated within vacuoles, unlike what is observed for the nontruncated Fur versions. Vacuolar GFP fluorescence is a standard measure to detect endocytosis of GFP-tagged transporters in fungi and mammalian cells, as transporters, following internalization from the plasma membrane, are sorted into vacuoles via the

endosomal/multivesicular bodies (MVB) pathway. Once in the vacuolar lumen, GFP remains rather stable for a sufficient period of time, which permits quantification of fluorescence (Gournas *et al.* 2010). Figure S2 in File S1 depicts the colocalization of the GFP fluorescent signal, coming from degradation of the Fur-GFP chimaeras, with the endosome/vacuole-specific FM4-64 molecular stain. Quantification and statistical analyses of the surface and intensity of vacuolar GFP fluorescence confirmed the essential role of the CTR in Fur endocytosis (Figure S3 in File S1). Western blot analysis (Figure 1C) confirmed that the steady-state levels of truncated Fur proteins are similar and remain high in all conditions tested, including conditions triggering endocytosis. This contrasts with the picture of the nontruncated Fur proteins, where the relevant steady-state levels show a dramatic reduction in the presence of ammonium and a significant drop in the presence of substrate (allantoin or uracil), when compared to nonendocytic conditions (*i.e.*, NO_3^-). Notice also that in the strains expressing the truncated versions free GFP polypeptide levels, which arise from the turnover of Fur-GFP, remain low, whereas in strains expressing the nontruncated Fur proteins free GFP polypeptide levels are significantly higher (Figure 1C). In general, the western blot analysis is in perfect line with the results observed from *in vivo* epifluorescence microscopy.

The increased stability of the truncated versions could, in principle, explain the observation that FurD-ΔC grows better on UA or allantoin compared to the nontruncated FurD, but could not explain the increased resistance to 5FC of the former *vs.* the latter. More importantly, the increased stability of the truncated FurE-ΔC contrasted with its specific inability to transport UA. Thus, the apparent changes in the specificity of FurD and FurE could not be rationalized on a quantitative basis of increased protein levels.

We also measured directly the transport activity of the truncated *vs.* the nontruncated versions of FurD and FurE by standard uptake assays using radiolabeled uracil (Krypotou and Diallinas 2014). FurA activity cannot be assayed as there is no commercially available radiolabeled allantoin. Figure 1D shows that truncated FurD and FurE had similar initial uptake rates (see values at 1 min uptake), albeit 40–50% reduced steady-state accumulation of uracil compared to the nontruncated equivalents. This suggests that the absence of the C-tail has a moderate, but detectable, reduction in the steady-state uptake capacity of Fur transporters. We do not have an explanation for this finding, but it seems that stabilization of truncated versions might lead to their overaccumulation in the plasma membrane, and that this in turn might have a negative effect on transport activity.

To further dissect the role of the CTR of FurD and FurE in transport, we determined the K_m or K_i values of FurD-ΔC and FurE-K252F-ΔC for uracil, UA, or allantoin, and compared them with those of the nontruncated proteins (the low transport activity of FurE-ΔC does not allow rigorous kinetic analysis). Figure 1E shows that truncation of FurD reduces the affinity for uracil (4.6-fold) and UA ($>$ 10-fold), but seemingly does not affect the very low affinity for allantoin. Truncation of FurE-K252F did not affect the affinity for uracil and UA, but led to a moderate 2.5-fold reduction in allantoin binding. Overall, these results show that truncation of the C-tail of Fur transporters not only increases their stability in the plasma membrane (PM), but also leads to differential modification of the relevant transport kinetics, in addition to changes in specificity.

Genetic suppressors of the C-terminal truncation restore substrate specificity in FurE

To better understand how the CTR might affect FurE specificity, we selected genetic suppressors of the C-terminal truncation that restore substrate specificity in FurE by direct selection of revertants on media containing UA as the sole nitrogen source, after standard UV mutagenesis of the strain expressing FurE-ΔC (see *Materials and Methods*). We obtained $>$ 50 revertants able to grow on UA, and the *furE-ΔC* ORF of 45 of them was amplified by PCR and sequenced. In nearly all cases, we detected a single-codon change, while in a single case two nearby codons were modified. Table 1 summarizes the profile of the suppressor mutations obtained. Selected strains carrying suppressors corresponding to different mutations were outcrossed with the original nonmutagenized strain, and the progeny analyzed showed that the suppressor phenotype cosegregated with the sequenced FurE mutation. Overall, suppressor mutations mapped in several transmembrane segments (TMS) 3, 7, 8, 9 and 10, but also in external loops (L5 or L7), and in the N-terminal protein region. Growth tests of relevant mutant strains showed that they are all able to grow on UA and allantoin, and that all are sensitive to relevant toxic nucleobase analogs (Figure 2A, *upper panel*). Importantly, T133V, and to a lesser degree some of the other mutants (*e.g.*, Y392N, Y392E, V343I, or L349P), could also grow moderately on xanthine, which is not a physiological substrate of either FurE or FurE-ΔC. None of the mutants acquired the capacity to grow on other purines that are not substrates of Fur transporters, such as adenine, hypoxanthine, or guanine (data not shown). Thus, all suppressor mutations restored the ability of FurE-ΔC to transport UA, but additionally, some specific mutations enlarged the FurE or FurE-ΔC specificity profile to include xanthine. The suppressor mutations did not significantly affect the stable localization of FurE-ΔC in the plasma membrane (Figure 2A, *lower panel*), despite some retention in the ER or very moderately increased turnover in specific cases, suggesting that the suppressor mutations do not affect the folding of the transporters.

Comparative uptake assays further showed that most suppressors have a moderate positive effect on the generally low rate of accumulation of radioactive uracil mediated by FurE or FurE-ΔC (Figure 2B). The most prominent case was mutation T133V, which led to more than a sevenfold increase in uracil uptake, and to lower degree mutations V343I, L349P, I371P, Y392C, Y392N, or Y392E, which led to 3–4.5-fold increases. Western blot analysis of two selected suppressor mutants

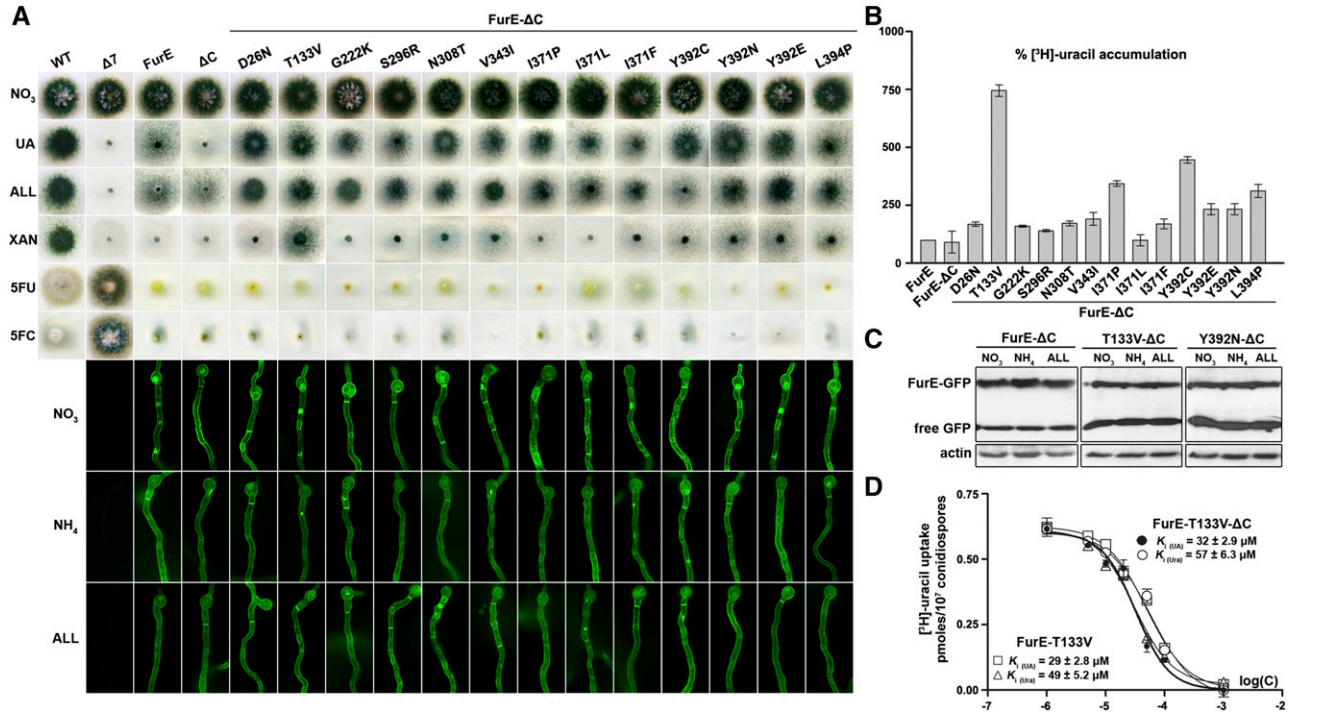

Figure 2 Functional characterization of FurE-ΔC suppressors. (A) Upper panel: growth tests of FurE-ΔC suppressors. FurE-ΔC suppressors and control strains (WT, Δ7, FurE, and FurE-ΔC) were grown in MM containing nitrate (control), UA, ALL, or XAN as N sources, or on nitrate media containing 5FU or 5FC. All growth tests shown were performed at 37°. Lower panel: subcellular localization of FurE-ΔC suppressors. FurE-ΔC suppressors and control strains were analyzed by *in vivo* epifluorescence microscopy. Notice that some suppressor mutations lead to partial retention of FurE-ΔC in internal structures resembling the ER (open rings), or to moderate sorting in the vacuole, but still the majority of FurE is sorted in the PM. Cultures are grown in MM containing nitrate as nitrogen source for 18 hr at 25°. (B) Transport kinetics of FurE-ΔC suppressors. Comparative [^{3}H]-URA accumulation (4 min) in strains expressing FurE-ΔC suppressor mutations and control strains (FurE and FurE-ΔC). SD is depicted with error bars. (C) Steady-state protein levels of selected FurE-ΔC suppressors showing increased apparent transport activity. Western blot analysis of total protein extracts of strains expressing truncated FurE-ΔC (the same as that shown in Figure 1), FurE-ΔC-T133V, or FurE-ΔC-Y392N, using anti-GFP (upper panel) or anti-actin (control, lower panel) antibody. Growth conditions are as for microscopy. Free GFP levels reflect vacuolar degradation of the intact Fur-GFP proteins. (D) Transport kinetics of FurE-T133V and FurE-T133V-ΔC. Dose response curve of [^{3}H]-URA uptake by FurE-T133V or FurE-T133V-ΔC in the presence of increasing concentration of nonradiolabeled URA or UA, respectively. The IC_{50} (equal to $K_{i/m}$) values measured are depicted as inserts (for details see *Materials and Methods*). Results are averages of three measurements for each concentration point. SD was < 20%. 5FC, 5-fluorocytosine; 5FU, 5-fluorouracil; ALL, allantoin; MM, minimal media; PM, plasma membrane; URA, uracil; UA, uric acid; WT, wild-type; XAN, xanthine.

showing increased transport capacity, namely T133V and Y392N, showed that this is not justified by an analogous increase in FurE protein steady-state levels (Figure 2C). In fact, these mutations slightly increase the turnover of FurE-ΔC (notice a two- to fourfold increase in the accumulation of free GFP). Thus, the results of uptake and western blot analyses together confirm that mutations T133V and Y392N do lead to a significant increase in FurE-ΔC-mediated transport capacity *per se*.

The generally low uracil uptake rates of most suppressors did not permit a rigorous estimation of affinity constants for FurE substrates, and thus we could not test whether suppressors generally reconferred UA transport by increasing UA binding. However, the K_i for UA could be measured in mutant FurE-T133V-ΔC, which is the only suppressor that showed sufficient transport activity for the performance of rigorous kinetic analysis. Figure 2D shows that FurE-T133V-ΔC has an affinity constant of 32 μM for UA and 57 μM for uracil. These values cannot be directly compared to the original FurE-ΔC, as this showed accumulation of these radiolabeled substrates that was too low to be analyzed kinetically. However, similar affinity constants for UA (29 μM) and uracil (49 μM) have been obtained in a strain expressing a nontruncated version carrying the suppressor mutation FurE-T133V, suggesting that the effect of mutation T133V on transport kinetics is independent of the truncated C-tail segment. Thus, comparing wild-type FurE (Krypotou *et al.* 2015 and Figure 1D) to FurE-T133V we detect a significant increase (~20-fold) in the affinity for uracil (K_m from 1000 to 49 μM), which could explain the apparent sevenfold increase in uracil accumulation, but practically no change in the affinity for UA (K_i from 20 to 29 μM). In other words, the restoration of UA transport in FurE-T133V-ΔC is, in principle, not due to an increase in the binding affinity for UA, but rather to a change related to the dynamics of transport catalysis.

Overall, the functional analysis of FurE suppressors showed that the relevant mutations do not affect the expression, folding, and turnover of FurE, but that they differentially modify the transport kinetics and specificity of the transporter.

N-terminal truncation of FurE leads to growth phenotypes mimicking those of C-terminal truncation

We also constructed and studied an N-terminally-truncated version of the FurE transporter (Figure S4 in File S1). This includes a deletion of the first 21 amino acid residues of the cytoplasmic N-terminal region of FurE (FurE-ΔN). The deleted segment does not show any sequence conservation in members of the NCS1 family and is thus not expected to affect the proper ER-exit and further exocytosis of the transporter. FurE-ΔN led to specific loss of apparent FurE-mediated transport of UA, and to a very moderate increase in 5FC resistance, a phenotype similar to the one obtained with a strain expressing the C-terminally-truncated version of FurE. Similarly to FurE-ΔC, FurE-ΔN did not affect the ability of FurE to transport allantoin or 5FU (Figure 3A). Transport assays further showed that FurE-ΔN confers a detectable rate of uracil accumulation (Figure 3B), confirming that this truncation has not abolished the transport of substrates other than UA or 5FC. Microscopic analysis showed that the FurE-ΔN version is stably localized in the PM and remains integrated in it, even after imposing conditions triggering wild-type FurE endocytosis, exactly as is the case for the C-terminally-truncated FurE version (Figure 3C, *upper panel*). The observation that truncation of the N-terminal region stabilizes FurE under endocytic conditions was confirmed by western blot analysis (Figure 3D, *left panel*). Thus, both N- and C-terminal truncations of FurE lead to specific loss of UA transport and a block of endocytosis.

Given the similarity of phenotypes caused by the N- and C-truncations, we next examined whether selected suppressors of the C-terminal truncation might also suppress the N-terminal truncation phenotypes. The mutations selected, T133V and Y392N, were examined in the context of either FurE-ΔN or nontruncated FurE. When these mutations were included in a nontruncated FurE, both conferred growth on allantoin, UA, or xanthine, sensitivity to relevant toxic substrates, and increased FurE endocytosis very slightly, judging from an increased number of fluorescent vacuoles (Figure 3, A and C, *middle and lower panels*). Most importantly, both suppressors restored growth in UA in strains expressing the truncated FurE-ΔN version, and in addition, T133V also conferred growth on xanthine of a FurE-ΔN strain (Figure 3A). Somewhat surprisingly, mutations T133V and Y392N also increased FurE-ΔN endocytosis, more evident in response to the presence of ammonium (Figure 3C), in contrast to what was observed when these mutations were present in the FurE-ΔC-truncated version (as shown in Figure 2A, *lower panel*). Relevant western blot analysis (Figure 3D) showed that mutations T133V or Y392N do increase the turnover of the nontruncated protein under all conditions tested, but that the N-terminal truncation partially counteracts this effect, especially when cells grow under nonendocytic conditions (*i.e.*, NO_3^-).

Overall, our results suggested that both the C- and N-terminally-truncated segments of FurE contain *cis*-acting elements that are critical for endocytosis. This further suggested that the two cytoplasmic terminal regions might synergize in determining a FurE topology necessary for recruiting the endocytic machinery. This hypothesis gained further support though the independent experiments described in the next section.

The N- and C-terminal cytoplasmic segments of FurE come into close proximity in the absence of substrate

The similarity of phenotypes arising from truncations of either the N-terminal regions or CTRs prompted us to test whether these two domains interact, and whether this interaction is part of a mechanism regulating FurE function and stability. To test this interaction, we employed intramolecular BiFC (see *Materials and Methods*). Figure 4A shows that expression of YFP_n-FurE-YFP_c reconstitutes YFP fluorescence at the plasma membrane, whereas expression of each chimera by itself (FurE-YFP_c or FurE-YFP_n) does not produce any detectable fluorescent signal. Importantly, when the same assay was performed in the presence of substrates (*e.g.*, allantoin) added for increasing time periods, the fluorescent signal was practically lost in a time-dependent manner (Figure 4B). The latter observation suggests that when FurE is actively transporting its substrates, its two terminal cytoplasmic tails do not stably reconstitute split-YFP, unlike what is observed in the absence of transport activity (*i.e.*, the absence of substrates).

Of note, strains expressing FurE-YFP_n or/and FurE-YFP_c grow on allantoin and are sensitive to 5FU, but do not grow on UA (results not shown). This suggests that FurE molecules tagged at their termini with either of the two parts of YFP are generally functional, but have lost their ability to specifically transport UA, similarly to the truncated versions. This observation further supports the idea that modifications of the two cytoplasmic terminal regions of FurE are critical for UA transport and FurE specificity in general.

A doubly N- and C-terminally-truncated version of FurE does not respond to endocytosis and shows wild-type function and specificity

We also constructed and tested a doubly truncated FurE version (FurE-ΔN/ΔC). Surprisingly, a strain expressing FurE-ΔN/ΔC could grow on UA in addition to allantoin, and was sensitive to toxic analogs, an apparent specificity profile that is similar to wild-type FurE (Figure S5A in File S1). Transport assays confirmed that FurE-ΔN/ΔC was capable of uracil accumulation, with an apparent measured rate of uracil accumulation very similar to that of a wild-type nontruncated FurE (data not shown). FurE-ΔN/ΔC was stably localized in the PM and did not respond to endocytosis (Figure S5, B and C in File S1). In other words, simultaneous truncation of both cytoplasmic terminal regions, which when truncated individually lead to functional modification of FurE, seems to restore the wild-type FurE transport function. In the absence of relevant structural data, this result is not easy to explain. However, it is

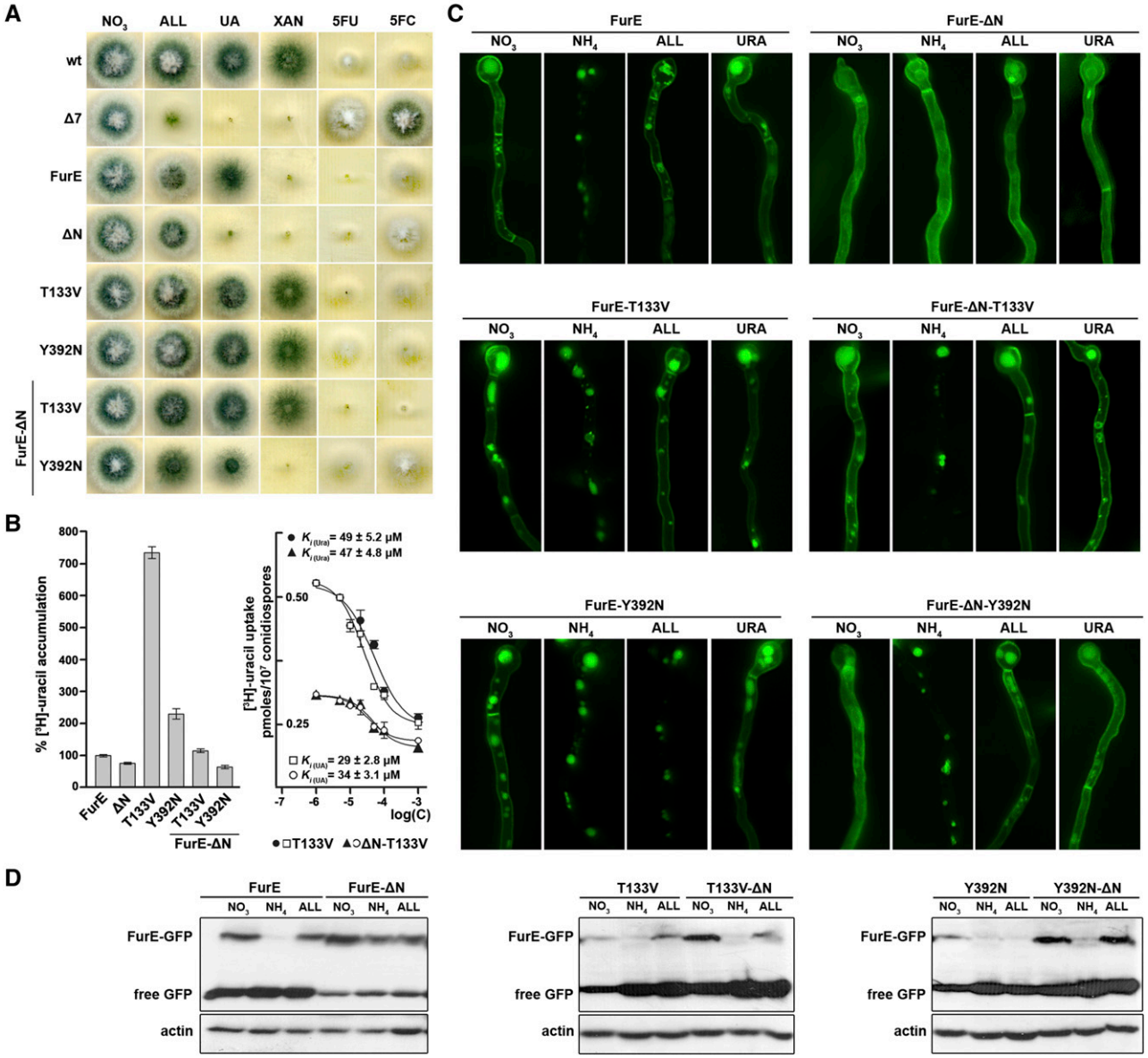

Figure 3 Functional characterization of the FurE-ΔN truncation. (A) Truncation of the N-terminal region confers growth phenotype mimicking C-terminal truncation. Growth tests of strains expressing FurE-ΔN, selected FurE-ΔC suppressors (T133V, Y392N), versions of FurE-ΔN carrying the selected suppressor mutations (FurE-T133V-ΔN and FurE-Y392N-ΔN), and control strains. Growth conditions and labeling are as in the legend of Figure 1A. (B) Transport kinetics of different versions of FurE-ΔN. Left panel: comparative radiolabeled URA accumulation rates in strains expressing the different versions of FurE and control strains, which were tested in (A and B). Right panel: dose response curve of [^{3}H]-URA uptake in the presence of increasing concentration of nonradiolabeled URA or UA, respectively, in strains expressing FurE-T133V or FurE-T133V-ΔN. The IC_{50} (equal to $K_{i/m}$) values measured are depicted as inserts (for details see *Materials and Methods*). Results are averages of three measurements for each concentration point. SD was $< 20\%$. (C) Subcellular localization of different versions of FurE-ΔN analyzed by *in vivo* epifluorescence microscopy. Details are as in Figure 1B. Notice that FurE-ΔN does not undergo endocytosis in response to either ammonium, ALL or URA, whereas FurE-T133V-ΔN and FurE-Y392N-ΔN are normally endocytosed in response to ammonium, but less in response to ALL or URA. Nontruncated versions, FurE-ΔN, FurE-T133V, and FurE-Y392N-ΔN, included as controls, are also normally endocytosed. (D) Steady-state protein levels of different versions of FurE-ΔN. Western blot analysis of total protein extracts of strains expressing FurE, FurE-T133V, or FurE-Y392N, as well as truncated FurE-ΔN, FurE-ΔN-T133V, or FurE-ΔN-Y392N, using anti-GFP (upper panel) or anti-actin (control, lower panel) antibody. Growth conditions are as in (C). Notice that both mutations studied reduce the steady-state levels of FurE, but truncation of the N-terminal region partially counteracts this effect. Free GFP levels reflect vacuolar degradation of the intact Fur-GFP proteins. 5FC, 5-fluorocytosine; 5FU, 5-fluorouracil; ALL, allantoin; MM, minimal media; URA, uracil; UA, uric acid; wt, wild-type; XAN, xanthine.

an important observation as it strongly suggests that the basic mechanism of transport in NCS1 transporters does not require the extended N- and C-terminal domains that are uniquely present in eukaryotic homologs, which in the context of the present work further establishes that the acquisition of specific cytoplasmic termini in eukaryotic NCS1 members serves a fine regulatory role in determining transport kinetics and specificity.

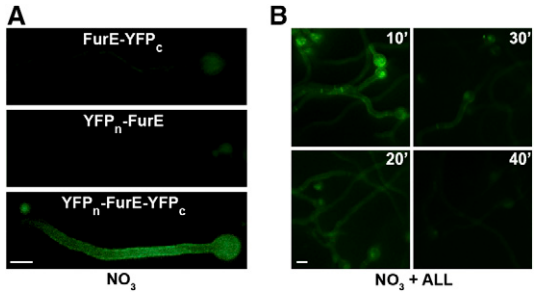

Figure 4 The N- and C-terminal cytoplasmic segments of FurE come into close proximity. (A) Isogenic strains expressing YFP$_n$-FurE-YFP$_c$, FurE-YFP$_c$, or YFP$_n$-FurE were analyzed by *in vivo* epifluorescence microscopy (for details see *Materials and Methods*). Notice that that expression of FurE-YFP$_c$ or YFP$_n$-FurE does not lead to a detectable fluorescent signal, whereas expression of YFP$_n$-FurE-YFP$_c$ leads to clear cortical fluorescence, compatible with reconstitution of the two parts of YFP in the chimeric transporter, apparently expressed in the PM. (B) In the strain expressing YFP$_n$-FurE-YFP$_c$, notice that addition of substrate (ALL), prior to microscopic examination, reduces and eventually turns off the fluorescent signal in a time-dependent manner. ALL, allantoin; PM, plasma membrane; YFP, yellow fluorescent protein.

Suppressors reveal a critical functional role of distinct gating or selectivity elements in FurE

Fur transporters are homologous to the bacterial Mhp1 benzylhydantoin transporter, which also belongs to the NCS1 family. We have previously constructed and validated structural models of FurA, FurD, and FurE based on the crystal structure of Mhp1. Validation included substrate docking, molecular dynamics, and an analysis of mutations that alter the function or specificity of Fur transporters. This work has identified the putative binding site of relative substrates and revealed the importance of TMS10, acting as an external gate critical for the high specificity of FurD (Krypotou *et al.* 2015). Herein, we mapped all characterized residues concerning suppressor mutations in the 3D-modeled structure of FurE (Figure 5). Based on this, we could classify suppressors as one of three types. Type I suppressors concern amino acids proximal to substrate-binding residues, as these were defined genetically, functionally, and by *in silico* docking (Krypotou *et al.* 2015). These are suppressors T133V (TMS3) and V343I (TMS8), which are very close to the major substrate-binding residues Trp130 and Gln134, or Asn341, respectively. Thr133 seems to be an essential element of the major binding site, whereas, Val343 lies "one-step down" in the theoretical trajectory from the binding site toward the cytoplasm. These residues can act as selectivity filters. Type II suppressors concern amino acids Ser296 in TMS7, Ile371 in TMS9, and Tyr392 and Leu394 in TMS10. TMS10 is a flexible transmembrane segment that has been shown to act as an outward-facing gate not only in FurD, but also in Mhp1 (Kazmier *et al.* 2014; Simmons *et al.* 2014). Molecular dynamics have indeed shown that TMS10 participates in an occlusion mechanism via its dramatic movement over the major substrate-biding site, while specific mutations in this segment modify (mostly enlarge) the specificity of the transporters, apparently by compromising the occlusion mechanism (Shimamura *et al.* 2010; Adelman *et al.* 2011; Kazmier *et al.* 2014; Simmons *et al.* 2014). In FurD, mutation M389A (in TMS10) converts this uracil transporter to a transporter capable of recognizing all purines and pyrimidines (Krypotou *et al.* 2015). Mutations in Leu363 (in TMS10) also affect the substrate specificity of Mhp1 (Simmons *et al.* 2014). The evidence from molecular dynamics in Mhp1 further suggests that TMS10 acts as a dynamic outward gate in concert with TMS9 and the extracellular hydrophilic segment linking TMS7 and TMS8 (EL4 in Mhp1) (Kazmier *et al.* 2014; Simmons *et al.* 2014). Thus, the FurE-ΔC suppressors related to residues Ser296 in TMS7 and Ile371 in TMS9 might also affect the dynamics of the outward-facing gate in FurE. Type III suppressors concern amino acids located in flexible loops, distantly located from the substrate-binding site or the translocation trajectory. Asp26 is at the border of TMS1 with the N-terminal cytoplasmic loop, Gly222 is in the extracellular loop L5, and Asn308 is in extracellular loop L7. Although there are no genetic or functional data related to these residues, molecular dynamics in Mhp1 have shown that substrate binding triggers the movement of TMS1, TMS5, and TMS7, consistent with the closing or opening of the intracellular (TMS1 and TMS5) and extracellular (TMS7) vestibules that lead to the major substrate-binding site (Kazmier *et al.* 2014; Simmons *et al.* 2014).

Overall, the suppressors isolated concern residues mapping either in or close to the major substrate-binding site (TMS3 and TMS8; type I), in an outward-facing gate (TMS7, TMS9, and TMS10; type II), or in dynamic loops that might act as hinges to control gating or the alteration from inward to outward and vice versa (N-terminal-TMS1, L5, and L7; type III).

Discussion

The N- and C-terminal cytoplasmic segments of FurE proved to be important in determining transport kinetics and substrate specificity. A critical but less pronounced role in transport activity and specificity of the CTR of FurD was also implied by growth tests, but this was not analyzed further. No apparent functional modification was detected in the version lacking the CTR of FurA. Thus, the specificity of Fur transporters, and possibly other eukaryotic NCS1 transporters, seems to be differentially dependent on molecular interactions involving domains located at their cytoplasmic N- or CTRs. Although truncations of N- and/or C-terminal segments led to blocks in endocytosis, this could not explain the observed changes in transport kinetics and specificity. Furthermore, transport kinetic analysis has shown that specificity changes cannot always be directly related to analogous modifications in substrate-binding affinities or apparent transport rates. This is best exemplified in the case of FurE-K252F-ΔC, where the specific reduction of UA transport cannot be assigned to a change in the affinity for UA, as this remains practically identical to that of the nontruncated FurE-K252F version. Finally, the cytoplasmic location of the truncated regions makes it rather improbable that the segments deleted are parts of

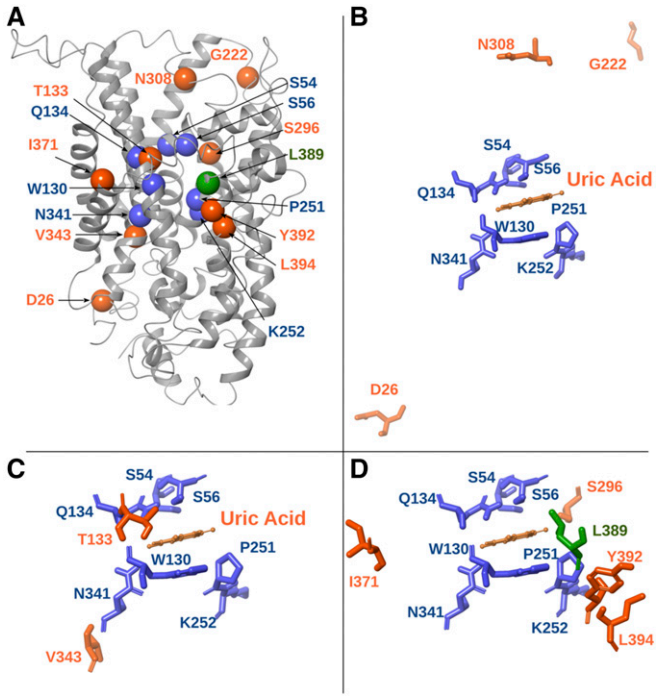

Figure 5 Location of suppressor mutations in the modeled FurE structure. (A) Model structure of FurE highlighting the residues altered in suppressor mutations (orange spheres) in relation to the substrate-binding site residues (blue spheres), and a critical residue in the putative outer gate (green sphere) (Krypotou *et al.* 2015). (B) Topology of amino acids (Asp26 in L_N, Asn308 in L7, and Gly222 in L5) modified in type III suppressors, located in loops that may function as flexible hinges (see text). (C) Topology of amino acids [Thr133 in transmembrane segment (TMS)3 and Val343 in TMS8] modified in type I suppressors (see text), located proximal to residues shown to interact with substrates in the major substrate-binding pocket of FurE (Ser54 and Ser56 in TMS1, Gln134 and Trp130 in TMS3, Pro251 and Lys252 in TMS6, and Asn342 in TMS8). (D) Topology of amino acids (Ser296 in TMS7, Ile371 in TMS9, and Tyr392 and Leu394 in TMS10) modified in type II suppressors, located next to or in the periphery of a major residue of the outer gate (Leu389 in TMS10).

the substrate-binding site or even of the substrate translocation trajectory, as these were previously defined by genetic, *in silico*, and structural analyses in NCS1 transporters. Of note, the deleted segments in the Fur proteins are "naturally" absent in the prokaryotic members of the NCS1 family. These findings indicate that the cytoplasmic terminal truncations affect the specificity of certain Fur transporters without modifying their *bona fide* substrate-binding site or translocation trajectory. In a most rational scenario, terminal truncations modify the transport dynamics of FurE due to the role of the deleted segments in critical intramolecular interactions affecting distinct gating or selectivity elements (Shimamura *et al.* 2010; Adelman *et al.* 2011; Kazmier *et al.* 2014; Simmons *et al.* 2014; Krypotou *et al.* 2015; Sioupouli *et al.* 2017).

Using an unbiased genetic approach, we fortified the above conclusion by selecting suppressors "restoring" the loss of UA transport in the truncated FurE-ΔC transporter. We obtained several suppressor mutations in residues located at the periphery of the substrate-binding site, in a tentative external gate, and in flexible loops that might act as hinges during conformational changes associated with transport catalysis. Notably, we did not obtain any mutations affecting residues that bind substrates directly, which supports our previous notion that specificity in transporters is principally determined by gating elements or peripheral selectivity filters, rather than the substrate-binding site (Amillis *et al.* 2001; Papageorgiou *et al.* 2008; Diallinas 2014, 2016; Krypotou *et al.* 2015; Alguel *et al.* 2016a).

BiFC analysis strongly suggested that the cytoplasmic N- and C-termini of FurE interact physically in the absence of substrates, but that this interaction is practically lost when the transporter is actively transporting substrates. These findings further suggest that, in the absence of substrates, the cytoplasmic N- and C-termini are in close contact, compatible with a rather "immobilized" outward-facing conformation. This idea is in agreement with reports stating that once the two parts of split-YFP interact, they tend to remain associated (Horstman *et al.* 2014). In the presence of substrates the transporter becomes active, so that upon substrate entry into the binding cavity, exposed in the outward-facing conformation, induced-fit phenomena will force the alteration of the transporter to an inward-facing conformation, and thus the loss of interaction of the split-YFP parts attached to the two cytoplasmic termini. Subsequent dynamic cycles of transport will hinder the stable association of the two cytoplasmic termini, compatible with lack of detection of YFP fluorescent signal.

The interaction of the N- and C-termini, detected genetically and by BiFC for FurE, is apparently not essential for the alternation of outward- and inward-facing conformations that accompany transport catalysis. This conclusion arises from the observation that the singly-truncated versions do transport substrates other than UA, and mostly because the doubly-truncated FurE behaves, unexpectedly, similarly to wild-type FurE. Thus, it seems more probable that the interaction of the N- and C-termini regulates the fine functioning of gating or selectivity elements along the substrate translocation trajectory. In a speculative model for the functioning of FurE, the order of events might be as follows (Figure 6). In the non-truncated version found in the outward-facing conformation, an interaction of the N- and C-termini opens the external gate "fully" and thus all physiological substrates (UA, allantoin, or uracil) fit in the major substrate-binding site. Proper substrate binding triggers occlusion of the outward-facing gate. Closure of the outward-facing gate elicits a major conformational change leading to the inward-closed structure. This will subsequently disrupt the interaction of the N- and C-termini, followed by opening of the internal gate and the release of substrate into the cytoplasm. Lack of the C- or N-terminal region alleviates the full opening of the external gate, in a way that only smaller or specific substrates (*e.g.*, uracil and allantoin) can have access to the binding site. Thus, UA is excluded either because the outer gate is not sufficiently open or because the closure of the gate has not occurred properly. Suppressor mutations modify the action of

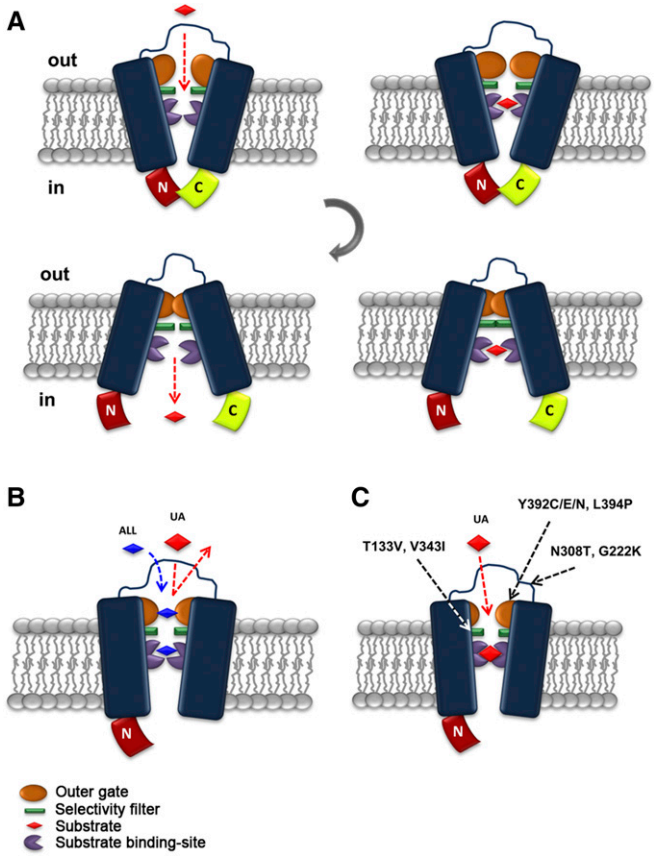

Figure 6 Highly speculative scheme of the role of the interaction of the N- and C-terminal regions in FurE functioning. (A) In the nontruncated version found in the outward-facing conformation, an interaction of the N- and C-termini opens "fully" the external gate and thus all physiological substrates [uric acid (UA), allantoin (ALL), or uracil: red rhomboid] fit within the major substrate-binding site. Proper substrate binding triggers occlusion of the outward-facing gate (in orange). Closure of the outward-facing gate elicits a gross conformational change leading to the inward-closed structure. This will subsequently disrupt of the N- and C-termini interaction, open the internal gate, and lead to release of substrate into the cytoplasm. (B) Lack of the C- (or N-terminal) region restricts the full opening of the outer gate, in a way that allows only smaller or specific substrates (*e.g.*, ALL or uracil) to have access to the binding site. Thus, UA is excluded either because the outer gate is not sufficiently open or because the closure of the gate does not occur properly. (C) Suppressor mutations indirectly modify the outer gate action, or other filtering or gating elements (in green), so that UA regains access to the binding site and is transported.

gating elements so that all substrates regain access to the binding site and are transported.

A similar mechanism, proposing that intramolecular interactions of cytoplasmic domains are critical for proper transporter functioning, has been described in a number of recently reported cases. One such case concerns the *Saccharomyces cerevisiae* Fur4p uracil transporter, which is homologous to the *A. nidulans* Fur transporters studied herein. In Fur4p, an N-terminal domain called LID (Loop Interaction Domain) has been shown to regulate ubiquitylation and endocytic turnover in response to transport activity or stress conditions that promote unfolding (Keener and Babst 2013). It seems that this domain senses conformational alterations in the transporter, in a way that renders a region adjacent to it accessible for ubiquitylation, a prerequisite for Fur4p endocytosis and turnover. Evidence based on crystal structures of the prokaryotic homolog Mhp1 has shown that in an outward-facing conformation, the LID interacts tightly with all of the cytoplasmic loops and the C-terminus of the transporter via a series of hydrogen bonds. In contrast, when the transporter acquires an inward-facing conformation, the interaction of LID with the other cytoplasmic domains is loosened. The LID–loop interactions also seem to play an important role in stabilizing the basic fold of Fur4p, as N-terminal deletions that remove it cause ER retention and degradation (Keener and Babst 2013). However, in the case of Fur4, cytoplasmic interactions affect the turnover of the protein, rather than its transport function directly.

In the case of the fungal Mep2 ammonium transporters, which also act as receptors and are thus called transceptors (Diallinas 2017), a CTR has been shown, using both structural and genetic evidence, to act as a domain that dynamically interacts with the main body of the transporter, and is thus directly involved in a mechanism that regulates the opening and closing of the substrate translocation pathway (van den Berg *et al.* 2015). Under nitrogen-sufficient conditions, where Mep2 is not phosphorylated and transport is inactive, the CTR makes relatively few contacts with the main body of the transporter. Under nitrogen-limited conditions, Mep2 is activated via Npr1 kinase-dependent phosphorylation of Ser457 in the CTR. Interestingly, in the *Arabidopsis thaliana* homologous Amt-1 ammonium transporters, phosphorylation of the CTR under conditions of high ammonium inhibits transport activity; that is, the nonphosphorylated state of the plant transporter is active (Loqué *et al.* 2007; Lanquar and Frommer 2010; Boeckstaens *et al.* 2014). This means that phosphorylation can either lead to channel closing (in the case of ammonium transporters) or channel opening (in the case of Mep2). Overall, the results on Mep2/Amt1 lead to a model for the regulation of transition between closed and open states of eukaryotic ammonium transporters involving the phosphorylation-dependent dynamic interaction of CTRs with specific cytoplasmic loops (*e.g.*, ICL1/ICL3) (Boeckstaens *et al.* 2014). However, how exactly the substrate translocation pathway in Mep2/Amt1 opens and closes remains elusive.

Another interesting case where cytoplasmic regions control transport functioning directly occurs in prokaryotic ATP-binding cassette (ABC) transporters or the homologous human cystic fibrosis transmembrane conductance regulator (CFTR) chloride channel involved in cystic fibrosis [Gadsby *et al.* 2006; Mihályi *et al.* 2016, for a review see Locher (2016)]. In particular, in CFTR and other ABC transporters, ATP-binding-dependent dimerization of two cytosolic nucleotide-binding domains (NBDs) opens the pore, whereas dimer disruption following ATP hydrolysis closes it. Spontaneous openings without ATP are rare in wild-type, but not in mutant versions of CFTR, but are still strictly coupled to NBD dimerization. Coordinated NBD/pore movements are therefore intrinsic to CFTR, suggesting that ATP alters the stability, but not the fundamental

structural architecture, of open- and closed-pore conformations. The apparently cyclic, dynamic restructuring of the intramolecular domain made of two NBD domains might be mechanistically analogous to the N- and C-tail interaction, which we propose to be the basis of the gating cycle in FurE.

Phosphorylation is likely to be a common mechanism for the regulation of eukaryotic transporters and channels in response to environmental or stress signals, or transport activity. Prominent examples, besides Fur4p and Mep2/Amt-1 discussed above, include transporters specific for urea (Klein 2014), nitrate (Parker and Newstead 2014; Jacquot *et al.* 2017), amino acids (Gournas *et al.* 2016), or aquaporins (Törnroth-Horsefield *et al.* 2010). Our work has not investigated a possible functional role of phosphorylation of cytoplasmic terminal regions in FurE or other Fur transporters. The only Fur-like transporter studied with respect to phosphorylation is the Fur4p of *S. cerevisiae*. In this transporter, an N-terminal cytoplasmic PEST-like sequence seems to be essential for transporter turnover, via ubiquitylation and endocytosis (Marchal *et al.* 1998, 2000). However, no direct effect of N-terminal phosphorylation on the function of Fur4p has been identified.

In conclusion, the present work adds another transporter family to a handful of eukaryotic transporters that have been shown to be regulated by dynamic interactions of their cytoplasmic tails. What is novel in our work is that cytoplasmic terminal regions affect not simply transporter activity or turnover, but can finely regulate substrate specificity. This, in turn, allows us to propose that transporter-specific interactions of terminal cytoplasmic regions provide a flexible mechanism for the generation of novel specificities over the course of evolution. Given that most prokaryotic homologs of eukaryotic transporters do not possess long cytoplasmic terminal regions, it seems that the acquisition of such extended terminal cytoplasmic regions served as a molecular novelty that allowed fine transporter neo-functionalization. Additionally, given that terminal regions of transporters are little conserved, even among close eukaryotic homologs, it is becoming evident that we cannot predict substrate specificities *a priori* simply by comparing similarities in substrate-binding sites. Thus, after the recent discovery of dynamic gating elements and oligomerization (Diallinas 2017), terminal cytoplasmic regions, acting as allosteric switches, have come to add an extra level of complexity regarding what determines transporter function and specificity.

Acknowledgments

We are grateful to George Lambrinidis for his help in making Figure 6. This work was supported by a Stavros S. Niarchos Foundation for Charity grant.

Literature Cited

Adelman, J. L., A. L. Dale, M. C. Zwier, D. Bhatt, L. T. Chong *et al.*, 2011 Simulations of the alternating access mechanism of the sodium symporter Mhp1. Biophys. J. 101: 2399–2407.

Alguel, Y., A. D. Cameron, G. Diallinas, and B. Byrne, 2016a Transporter oligomerization: form and function. Biochem. Soc. Trans. 44: 1737–1744.

Alguel, Y., S. Amillis, J. Leung, G. Lambrinidis, S. Capaldi *et al.*, 2016b Structure of eukaryotic purine/H $^{(+)}$ symporter UapA suggests a role for homodimerization in transport activity. Nat. Commun. 7: 11336.

Amillis, S., M. Koukaki, and G. Diallinas, 2001 Substitution F569S converts UapA, a specific uric acid-xanthine transporter, into a broad specificity transporter for purine-related solutes. J. Mol. Biol. 313: 765–774.

Amillis, S., Z. Hamari, K. Roumelioti, C. Scazzocchio, and G. Diallinas, 2007 Regulation of expression and kinetic modeling of substrate interactions of a uracil transporter in *Aspergillus nidulans*. Mol. Membr. Biol. 24: 206–214.

Boeckstaens, M., E. Llinares, P. Van Vooren, and A. M. Marini, 2014 The TORC1 effector kinase Npr1 fine tunes the inherent activity of the Mep2 ammonium transport protein. Nat. Commun. 5: 3101.

Colas, C., P. M. Ung, and A. Schlessinger, 2016 SLC transporters: structure, function, and drug discovery. Medchemcomm 7: 1069–1081.

de Koning, H., and G. Diallinas, 2000 Nucleobase transporters. Mol. Membr. Biol. 17: 75–94.

Diallinas, G., 2008 Biochemistry. An almost-complete movie. Science 322: 1644–1645.

Diallinas, G., 2014 Understanding transporter specificity and the discrete appearance of channel-like gating domains in transporters. Front. Pharmacol. 5: 207.

Diallinas, G., 2016 Dissection of transporter function: from genetics to structure. Trends Genet. 32: 576–590.

Diallinas, G., 2017 Transceptors as a functional link of transporters and receptors. Microb. Cell 4: 69–73.

Evangelinos, M., O. Martzoukou, K. Chorozian, S. Amillis, and G. Diallinas, 2016 BsdA(Bsd2)-dependent vacuolar turnover of a misfolded version of the UapA transporter along the secretory pathway: prominent role of selective autophagy. Mol. Microbiol. 100: 893–911.

Forrest, L. R., R. Krämer, and C. Ziegler, 2011 The structural basis of secondary active transport mechanisms. Biochim. Biophys. Acta 1807: 167–188.

Gadsby, D. C., P. Vergani, and L. Csanády, 2006 The ABC protein turned chloride channel whose failure causes cystic fibrosis. Nature 440: 477–483.

Gournas, C., S. Amillis, A. Vlanti, and G. Diallinas, 2010 Transport-dependent endocytosis and turnover of a uric acid-xanthine permease. Mol. Microbiol. 75: 246–260.

Gournas, C., M. Prévost, E. M. Krammer, and B. André, 2016 Function and regulation of fungal amino acid transporters: insights from predicted structure. Adv. Exp. Med. Biol. 892: 69–106.

Hamari, Z., S. Amillis, C. Drevet, A. Apostolaki, C. Vágvölgyi *et al.*, 2009 Convergent evolution and orphan genes in the Fur4p-like family and characterization of a general nucleoside transporter in *Aspergillus nidulans*. Mol. Microbiol. 73: 43–57.

Horstman, A., I. A. Tonaco, K. Boutilier, and R. G. Immink, 2014 A cautionary note on the use of split-YFP/BiFC in plant protein-protein interaction studies. Int. J. Mol. Sci. 15: 9628–9643.

Jacquot, A., Z. Li, A. Gojon, W. Schulze, and L. Lejay, 2017 Post-translational regulation of nitrogen transporters in plants and microorganisms. J. Exp. Bot. 68: 2567–2580.

Kaback, H. R., I. Smirnova, V. Kasho, Y. Nie, and Y. Zhou, 2011 The alternating access transport mechanism in LacY. J. Membr. Biol. 239: 85–93.

Karachaliou, M., S. Amillis, M. Evangelinos, A. C. Kokotos, V. Yalelis *et al.*, 2013 The arrestin-like protein ArtA is essential for ubiquitination and endocytosis of the UapA transporter in response

to both broad-range and specific signals. Mol. Microbiol. 88: 301–317.
Kazmier, K., S. Sharma, S. M. Islam, B. Roux, and H. S. Mchaourab, 2014 Conformational cycle and ion-coupling mechanism of the Na^+/hydantoin transporter Mhp1. Proc. Natl. Acad. Sci. USA 111: 14752–14757.
Keener, J. M., and M. Babst, 2013 Quality control and substrate-dependent downregulation of the nutrient transporter Fur4. Traffic 14: 412–427.
Klein, J. D., 2014 Expression of urea transporters and their regulation. Subcell. Biochem. 73: 79–107.
Kosti, V., I. Papageorgiou, and G. Diallinas, 2010 Dynamic elements at both cytoplasmically and extracellularly facing sides of the UapA transporter selectively control the accessibility of substrates to their translocation pathway. J. Mol. Biol. 397: 1132–1143.
Koukaki, M., E. Giannoutsou, A. Karagouni, and G. Diallinas, 2003 A novel improved method for *Aspergillus nidulans* transformation. J. Microbiol. Methods 55: 687–695.
Krypotou, E., and G. Diallinas, 2014 Transport assays in filamentous fungi: kinetic characterization of the UapC purine transporter of *Aspergillus nidulans*. Fungal Genet. Biol. 63: 1–8.
Krypotou, E., V. Kosti, S. Amillis, V. Myrianthopoulos, E. Mikros *et al.*, 2012 Modeling, substrate docking, and mutational analysis identify residues essential for the function and specificity of a eukaryotic purine-cytosine NCS1 transporter. J. Biol. Chem. 287: 36792–36803.
Krypotou, E., T. Evangelidis, J. Bobonis, A. A. Pittis, T. Gabaldón *et al.*, 2015 Origin, diversification and substrate specificity in the family of NCS1/FUR transporters. Mol. Microbiol. 96: 927–950.
Lanquar, V., and W. B. Frommer, 2010 Adjusting ammonium uptake via phosphorylation. Plant Signal. Behav. 5: 736–738.
Lauwers, E., Z. Erpapazoglou, R. Haguenauer-Tsapis, and B. André, 2010 The ubiquitin code of yeast permease trafficking. Trends Cell Biol. 20: 196–204.
Locher, K. P., 2016 Mechanistic diversity in ATP-binding cassette (ABC) transporters. Nat. Struct. Mol. Biol. 23: 487–493.
Loqué, D., S. Lalonde, L. L. Looger, N. von Wirén, and W. B. Frommer, 2007 A cytosolic trans-activation domain essential for ammonium uptake. Nature 446: 195–198.
Martzoukou, O., M. Karachaliou, V. Yalelis, J. Leung, B. Byrne *et al.*, 2015 Oligomerization of the UapA purine transporter is critical for ER-exit, plasma membrane localization and turnover. J. Mol. Biol. 427: 2679–2696.
Martzoukou, O., S. Amillis, A. Zervakou, S. Christoforidis, and G. Diallinas, 2017 The AP-2 complex has a specialized clathrin-independent role in apical endocytosis and polar growth in fungi. Elife 21: 6.
Marchal, C., R. Haguenauer-Tsapis, and D. Urban-Grimal, 1998 A PEST-like sequence mediates phosphorylation and efficient ubiquitination of yeast uracil permease. Mol. Cell. Biol. 18: 314–321.
Marchal, C., R. Haguenauer-Tsapis, and D. Urban-Grimal, 2000 Casein kinase I-dependent phosphorylation within a PEST sequence and ubiquitination at nearby lysines signal endocytosis of yeast uracil permease. J. Biol. Chem. 275: 23608–23614.
Mihályi, C., B. Töröcsik, and L. Csanády, 2016 Obligate coupling of CFTR pore opening to tight nucleotide-binding domain dimerization. Elife 5: e18164.
Pantazopoulou, A., and G. Diallinas, 2007 Fungal nucleobase transporters. FEMS Microbiol. Rev. 31: 657–675.
Pantazopoulou, A., N. D. Lemuh, D. G. Hatzinikolaou, C. Drevet, G. Cecchetto *et al.*, 2007 Differential physiological and developmental expression of the UapA and AzgA purine transporters in *Aspergillus nidulans*. Fungal Genet. Biol. 44: 627–640.
Papageorgiou, I., C. Gournas, A. Vlanti, S. Amillis, A. Pantazopoulou *et al.*, 2008 Specific interdomain synergy in the UapA transporter determines its unique specificity for uric acid among NAT carriers. J. Mol. Biol. 382: 1121–1135.
Parker, J. L., and S. Newstead, 2014 Molecular basis of nitrate uptake by the plant nitrate transporter NRT1.1. Nature 507: 68–72.
Penmatsa, A., and E. Gouaux, 2014 How LeuT shapes our understanding of the mechanisms of sodium-coupled neurotransmitter transporters. J. Physiol. 592: 863–869.
Quistgaard, E. M., C. Löw, F. Guettou, and P. Nordlund, 2016 Understanding transport by the major facilitator superfamily (MFS): structures pave the way. Nat. Rev. Mol. Cell Biol. 17: 123–132.
Shi, Y., 2013 Common folds and transport mechanisms of secondary active transporters. Annu. Rev. Biophys. 42: 51–72.
Shimamura, T., S. Weyand, O. Beckstein, N. G. Rutherford, J. M. Hadden *et al.*, 2010 Molecular basis of alternating access membrane transport by the sodium-hydantoin transporter Mhp1. Science 328: 470–473.
Simmons, K. J., S. M. Jackson, F. Brueckner, S. G. Patching, O. Beckstein *et al.*, 2014 Molecular mechanism of ligand recognition by membrane transport protein, Mhp1. EMBO J. 33: 1831–1844.
Sioupouli, G., G. Lambrinidis, E. Mikros, S. Amillis, and G. Diallinas, 2017 Cryptic purine transporters in *Aspergillus nidulans* reveal the role of specific residues in the evolution of specificity in the NCS1 family. Mol. Microbiol. 103: 319–332.
Takeshita, N., Y. Higashitsuji, S. Konzack, and R. Fischer, 2008 Apical sterol-rich membranes are essential for localizing cell end markers that determine growth directionality in the filamentous fungus *Aspergillus nidulans*. Mol. Biol. Cell 19: 339–351.
Törnroth-Horsefield, S., K. Hedfalk, G. Fischer, K. Lindkvist-Petersson, and R. Neutze, 2010 Structural insights into eukaryotic aquaporin regulation. FEBS Lett. 584: 2580–2588.
Valdez-Taubas, J., L. Harispe, C. Scazzocchio, L. Gorfinkiel, and A. L. Rosa, 2004 Ammonium-induced internalisation of UapC, the general purine permease from *Aspergillus nidulans*. Fungal Genet. Biol. 41: 42–51.
van den Berg, B., A. Chembath, D. Jefferies, A. Basle, S. Khalid *et al.*, 2015 Structural basis for Mep2 ammonium transceptor activation by phosphorylation. Nat. Commun. 7: 11337.
Weyand, S., T. Shimamura, S. Yajima, S. Suzuki, O. Mirza *et al.*, 2008 Structure and molecular mechanism of a nucleobase-cation-symport-1 family transporter. Science 322: 709–713.

Communicating editor: J. Heitman

European Journal of Medicinal Chemistry 156 (2018) 240–251

Contents lists available at ScienceDirect

European Journal of Medicinal Chemistry

journal homepage: http://www.elsevier.com/locate/ejmech

Research paper

Structure-activity relationships in fungal nucleobases transporters as dissected by the inhibitory effects of novel purine analogues

Efthymios-Spyridon Gavriil [a], Spyridon Dimitrakis [a], Georgia Papadaki [b], Sophia Balaska [b], George Lambrinidis [a], Nikolaos Lougiakis [a], Panagiotis Marakos [a], George Diallinas [b, **], Nicole Pouli [a], Emmanuel Mikros [a, *]

[a] Division of Pharmaceutical Chemistry, Department of Pharmacy, National and Kapodistrian University of Athens, Panepistimiopolis, Zografou, 15771, Greece
[b] Department of Biology, National and Kapodistrian University of Athens, Panepistimiopolis, Athens, 15784, Greece

ARTICLE INFO

Article history:
Received 7 March 2018
Received in revised form
13 June 2018
Accepted 13 June 2018
Available online 18 June 2018

Keywords:
Purine isosters
Imidazo[4,5-*c*]pyridine
Rational design
Aspergillus nidulans
Purine transporters
Molecular dynamics

ABSTRACT

We have previously rationally designed, synthesized and tested a number of 3-deazapurine analogues, which inhibit the ubiquitous fungal nucleobase transporter FcyB, through binding in its major substrate binding site, by specifically interacting with Asn163. Here, in an effort to further understand the molecular details of structure-activity relationships in all three major nucleobase transporters of fungi, we extend this study by designing, based on our previous experience, synthesizing and testing further 3-deazapurine analogues. We thus identify seven new compounds with relatively high affinity (19–106 μM) for the FcyB binding site. Importantly, four of these compounds can also efficiently inhibit AzgA, a structurally and evolutionary distinct, but functionally similar, purine transporter. Contrastingly, none of the new compounds tested had any effect on the transport activity of the uric acid-xanthine transporter UapA, albeit this being a structural homologue of AzgA. Besides the apparent importance for understanding how nucleobase transporter specificity is determined at the molecular level, our work might constitute a critical step in the design of novel purine-related antifungals.

1. Introduction

Early genetic and biochemical studies established the presence of highly specific nucleobase transporters in fungi. The lack of growth on purines or the use of purine or pyrimidine toxicity, caused either by an excess of a base (e.g. uracil, uric acid), or by a cytotoxic analogue (e.g. oxypurinol, allopurinol, 8-azaguanine, 5-fluorouracil, 5-fluorocytosine), provided a powerful tool to select mutants and identify the corresponding genes [1,2]. Out of work performed mostly in *Aspergillus nidulans,* but also in *Aspergillus fumigatus, Saccharomyces cerevisiae* and *Candida albicans*, we now know that there are four specific nucleobase uptake systems that belong to two structurally and evolutionary distinct protein families [3]. The first, called NAT (Nucleobase Ascorbate Transporters, also called Nucleobase Cation Symporters 2 or NCS2) includes two sub-groups, with totally non-overlapping specificities, the UapA/C-like and the AzgA-like transporters [4–6]. UapA/C transporters are specific for uric acid and xanthine, whereas AzgA transporters are specific for adenine-hypoxanthine-guanine. In addition, UapA/C and AzgA transport totally different purine analogues and drugs, namely oxypurinol and allopurinol versus 8-azaguanine and 6-mercaptourine, respectively. The second major family is called NCS1 (Nucleobase Cation Symporters 1) and also includes two subgroups with totally non-overlapping specificities, the Fcy-like [7,8] and the Fur-like transporters [9,10]. Fcy-like transporters are specific for adenine-hypoxanthine-guanine-cytosine, whereas Fur-like transporters are highly specific for either uracil or allantoin, the latter being a purine catabolic metabolite. All these transporter groups function as H^+- dependent secondary transporters or H^+ symporters. All filamentous fungi, including the major pathogens, *A. fumigatus* and *A. flavus*, possess all four subgroups of the two families, while several yeasts, including *S. cerevisiae*, lack the UapA/C subgroup.[3] The distinction of nucleobase transporters in two major families, initially based simply on functional assays, was confirmed by structural approaches, including x-ray

* Corresponding author.
** Corresponding author.
E-mail addresses: diallina@biol.uoa.gr (G. Diallinas), mikros@pharm.uoa.gr (E. Mikros).

https://doi.org/10.1016/j.ejmech.2018.06.038
0223-5234/

crystallography and relative modeling approaches of bacterial homologues [11–15], but also of the UapA transporter of *A. nidulans* [16]. The sub-group distinction of the NAT and NCS1 families is supported by prominent differences in their substrate specificities and the presence of characteristic amino acid sequence motifs.

What seems to be an apparent paradox is that while UapA and AzgA are structurally similar (NAT family), they transport entirely different substrates and drugs, while FcyB which belongs to a different major family (NCS1) has very similar specificity profile and similar binding affinities for purines with AzgA. The only rigorous way to functionally distinguish AzgA from FcyB is via their relative capacity to transport cytosine or specific purine or pyrimidine analogues. These observations suggest that the architecture of the binding site of NAT and NCS1 transporter is shaped via both divergent and convergent evolution events. While functional details for substrate binding and transport have been elucidated by genetic and *in vivo* transport kinetic approaches for several fungal members of the NCS1 family (see references above), direct structural information comes only from the bacterial benzyl-hydantoin Mhp1 transporter [12–14]. Mhp1, but also all studied fungal NCS1 homologues modeled on the Mh1 structure, are characterized by a core of ten transmembrane helices divided in two symmetric sets oppositely orientated with respect to the membrane, termed the 5-helix inverted repeat (5HIR) motif. There are additionally two C-terminal transmembrane helices (TMH11 and TMH12), which apparently do not participate in transport activity, and their role is unknown. Importantly, as the structure of Mhp1 has been previously solved in three different conformations, this has provided insights into the molecular basis of the alternating access mechanism of transport. Briefly, sodium ions bind and favor the formation of an outward-facing state and the consequent substrate binding in a cavity formed between a “bundle” (TMHs 1, 2, 6 and 7) and a “hash” motif (TMHs 3, 4, 8 and 9). Upon substrate binding TMH10 bends over the substrate in the occluded state triggering the rotation of the one motif relative to the other towards the inward-facing conformation, accompanied by a bend of TMH5 which opens the cavity further to the intracellular and enables substrate transport.

In *A. nidulans* we have developed tools to study rigorously structure-function relationships in nucleobase transporters. These include the construction of strains expressing a single nucleobase transporter in a genetically ‘clean’ background lacking all functionally similar transporters due to multiple null mutations, and efficient cellular and functional assays measuring transporter expression, turnover and activity [17,18]. Additionally, all nucleobase transporters of *A. nidulans* have been extensively analyzed via classical and reverse genetics and modeling using available crystal structures of bacterial homologues [18]. Thus, we have defined, at the molecular level, transporter-substrate interactions and identified the major elements of substrate binding sites. Furthermore, we have identified elements located outside the major binding site that affect nucleobase transporter specificity, collectively named gating elements [17–19]. Most importantly, we obtained direct evidence of structure-function relationships in UapA by analyzing the crystal structure of a genetically stabilized version of UapA in complex with xanthine [19].The crystal structure validated conclusions drawn by genetic and biochemical approaches and further showed dimerization is critical for UapA function and specificity [16–18].

In a different but complementary approach, we recently developed chemical biology methodologies to better understand how specificity is determined in different nucleobase transporters [20]. In particular, we used a virtual screening and semi-rational approaches to identify compounds that might interact with the substrate binding site of a specific nucleobase transporter, and then test whether positive-scoring compounds can also be recognized by a functionally similar transporter. More specifically, we looked for FcyB ligands and then tested whether they interact with AzgA (i.e. a functional analogue) or UapA (i.e. a structural homologue). We thus identified a number of 3-deazapurines substituted in the corresponding 6- and 9-positions of the original purine scaffold, which proved highly specific solely for FcyB [20]. One of these compounds proved to be moderately toxic for *A. nidulans* growth. In the present work, we exploited findings of our original approach to identify further purine analogues that might act differentially on the relative *A. nidulans* transporters. We identified seven new compounds recognized with high affinity by the FcyB, and among them, four were also recognized by AzgA, but none by UapA. This work complements in our understanding of the transporter-substrate interactions and could also be considered as an important step towards developing purine-related analogues as potentially novel highly targeted antifungals.

2. Results

2.1. Rationale for 3-deazapurine analogue design

In order to design new chemical probes allowing better understanding the FcyB function, a structural model for the protein was required. In this study we have de novo constructed an FcyB structure by homology modeling, using as template the most recent Mhp1 occluded crystal structure (pdb 4d1d), which is in the outward conformation in complex with an hydantoin derivative acting as inhibitor [13]. The new model displays only few differences within the binding cavity of the transporter when compared to a previously constructed model based on the occluded Mhp1 topology (pdb 2jlo) [7]. The integrity of the transmembrane helices is improved when compared with the previous model. The major difference is related to the first part of TMH10 between Glu401 and Tyr409, which is tilted moving away from the cavity forming the outward conformation. For exploring possibilities of modifying further the 3-deazapurine scaffold, we were guided by the structure-activity relationships of the recently reported series of 1,4-substituted-3-deazapurine analogues [20], which can be summarized as follows. The most potent analogue has been found to be the 4-benzylamine substituted derivative **1** (Fig. 1A), interacting with Glu397 on TMH9-10 at the edge of the transporter outward cavity along with the main interaction between N3 and Asn163.

Additionally, compound **2** bearing at position 4- a methylpiperazino-group, containing a quaternary nitrogen positively charged at the physiological pH conditions, has proved to possess interesting activity as well. The corresponding mono-substituted parent analogues **3** and **4** respectively (Fig. 1A), albeit not highly potent, maintain a certain degree of inhibitory activity against both AzgA and FcyB. In order to further investigate the different substitutions of this scaffold, we examined the possibilities for an additional interaction with an important residue in the vicinity, namely Asn354 by introducing at position 2- an enolic OH or SH group, maintaining the optimum substitution pattern at position 4-. With the aim of facilitating the interpretation of the resulting data, we have decided to preserve only the 4-substituent of the previously studied compounds, and thus deal with 2,4-disubstituted analogues. This would also provide the possibility to investigate the effect of both imidazole nitrogen atoms in the molecular level. Furthermore, no substitution at position 1- together with the enolic OH at position 2- which is expected to be in its carbonyl form will generate correspondingly a hydrogen bond (HB) -donor and -acceptor that could better match the targeted interaction with amide side chains of Asn163 or Asn354. Finally, in order to further investigate substitution at position 2- and more specifically the hydrophobic cavity existing around Pro353 (Fig. 1B), a number of analogues bearing both a hydrophobic surface and a

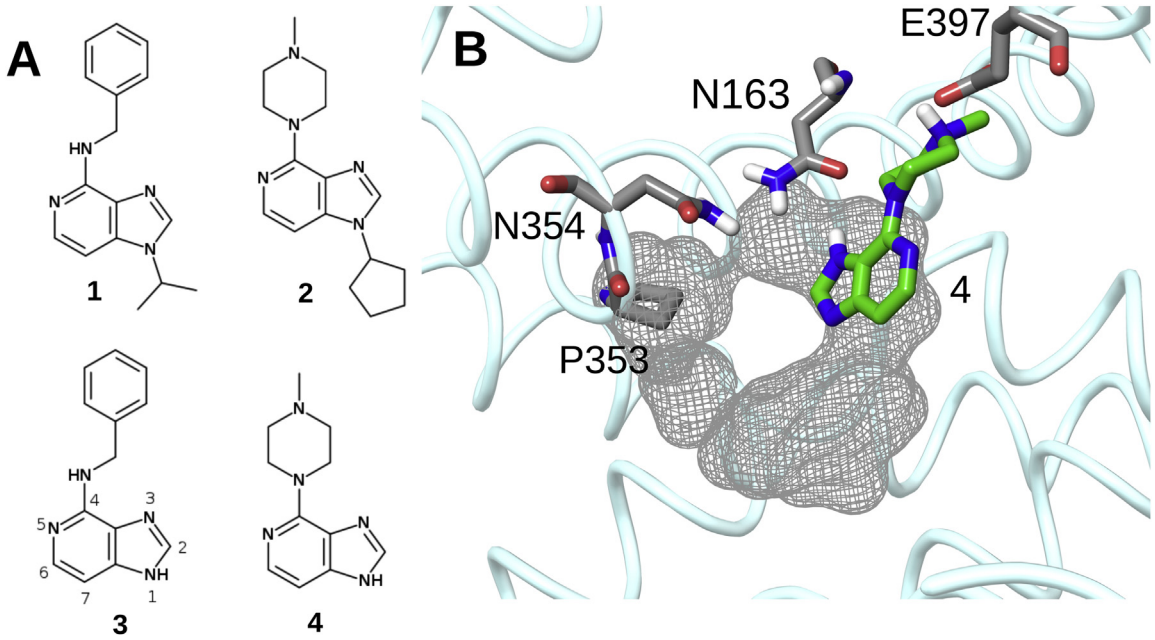

Fig. 1. A. Structures of Compounds 1–4. **B.** Global minimum energy structure of compound 4 in complex with FcyB model. In grey the hydrophobic surface of the protein binding pocket near Pro353 forming a cavity that is targeted by the synthesized compounds.

functional group that could interact with Asn354 have also been designed and synthesized.

2.2. Chemical synthesis of novel 3-deazapurine analogues

The target compounds were prepared using 4-amino-2-chloropyridine (**5,** Scheme 1), which was nitrated to result into a mixture of the nitroderivatives **6** and **7.** [21] The appropriate 3-nitroderivative **6** underwent nucleophilic substitution using *N*-methylpiperazine or benzylamine and provided the intermediate nitropyridines **8** and **9** [20]. These derivatives were first reduced and the resulting diamines were cyclized using CDI, tCDI or selected aromatic aldehydes to result in the desired 2-substituted imidazopyridines **10a-f** and **11a-f**. Concerning the benzylamino-derivatives **8**, the cyclization reaction provided the isomeric imidazopyridines **12a-f** as well (Scheme 1). Additionally, during the preparation of compounds **10d** and **10f**, a second product was also isolated, that identified to be **13** and **14** respectively (Fig. 2). These compounds should have derived from the concomitant formation of arylimines on both aminogroups of the intermediate pyridodiamines, followed by ring-closure.

2.3. Evaluation of novel 3-deazapurine analogues as inhibitors of purine transporters

The new 3-deazapurine analogues were tested as competitive inhibitors of FcyB- or AzgA-mediated ^{3}H-radiolabelled adenine uptake, or UapA-mediated ^{3}H-radiolabelled xanthine uptake. In all cases, assays were performed, as already described [22], in strains expressing the specific transporter studied in the absence of other

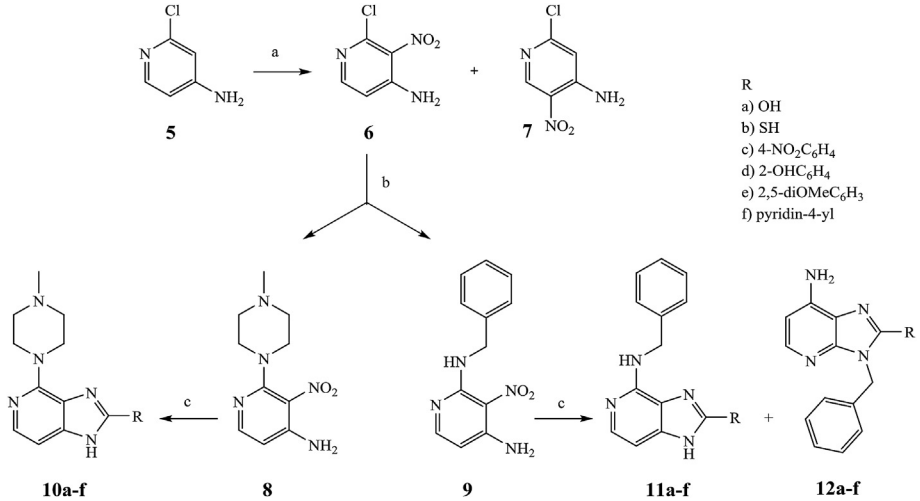

Scheme 1. Reagents and conditions: a) $HNO_{3\,(f.)}$, $H_2SO_{4\,(c.)}$, 90 °C; b) N-methylpiperazine (for **8**), or benzylamine (for **9**), EtOH, reflux; c) (1) H_2, Pd/C, EtOH, 35psi, r.t.; (2) CDI or tCDI, THF, reflux, or R-CHO, toluene, montmorillonite K-10, reflux.

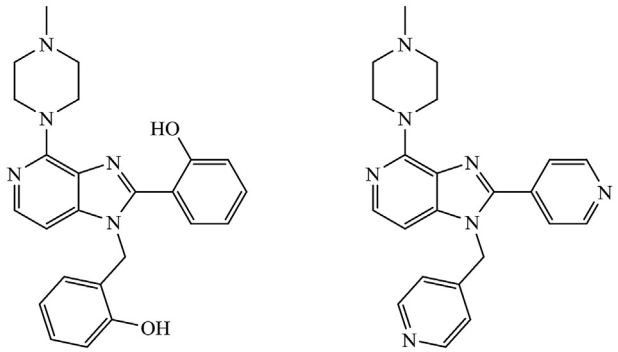

Fig. 2. Structure of compounds **13**–**14**.

transporters of similar specificity [20]. The competition results for FcyB and AzgA are summarized in Fig. 3, along with the previously reported compounds **3** and **4,** as well as, unlabeled adenine or hypoxanthine (physiological substrates of FcyB and AzgA), as controls.

Compounds **12a-f**, and **13** did not show any inhibitory activity. Among the derivatives, **10a, 10d, 10e, 11d, 11e** and **11f** reduced FcyB-mediated ^{3}H-adenine accumulation rate to <10%, compared to the control (absence of any inhibitor). The compounds **10c, 11d, 11e** and **11f** also showed a relative significant inhibition of AzgA-mediated ^{3}H-adenine accumulation rate, which however was lower than the one observed with FcyB. None of the compounds tested showed any inhibitory activity on UapA-mediated transport of xanthine (data not shown).

2.4. Kinetic characterization of competing analogues

Compounds that proved to be active as inhibitors of FcyB were further evaluated by estimating their K_i, using IC_{50} measurements. Results are shown in Table 1. All compounds exhibited values lower than 110 μM for FcyB, with the methylpiperazine analogue **10a** being the most potent followed by the benzylamine analogue **11e**, exhibiting K_i of 19 and 42 μM respectively. As compound **11d** showed the higher inhibitory activity against AzgA the corresponding K_i value was also determined and found to be 58 μM.

2.5. Molecular modeling FcyB-ligand interactions

In order to further develop a structure-activity relationship model and gain insight in FcyB-ligand interactions, MD and docking calculations have been carried out. First, we present the models derived by docking calculations for the most active compounds namely compounds **10a** and **11e.** Each one of these two compounds contains different substitutions at positions 4- and 2- thus exemplifying the basic characteristics for the protein-ligand interactions as derived by theoretical calculations. The synthesized analogues were submitted to docking calculations using the Induced Fit Docking algorithm as implemented in Maestro 10 (Schrodinger

Table 1
3-deazapurine analogue binding profile of FcyB.

Compound	K_i (μM)
10a	19 ± 3
10c	106 ± 12
10d	49 ± 10
10e	100 ± 5
11a	74 ± 6
11d	82 ± 8
11f	72 ± 4
11e	42 ± 6
1	5 ± 1
2	38 ± 6
Adenine	7 ± 1
Hypoxanthine	11 ± 1

Results are averages of at least three independent experiments with three replicates for each concentration point. SD was <10%.

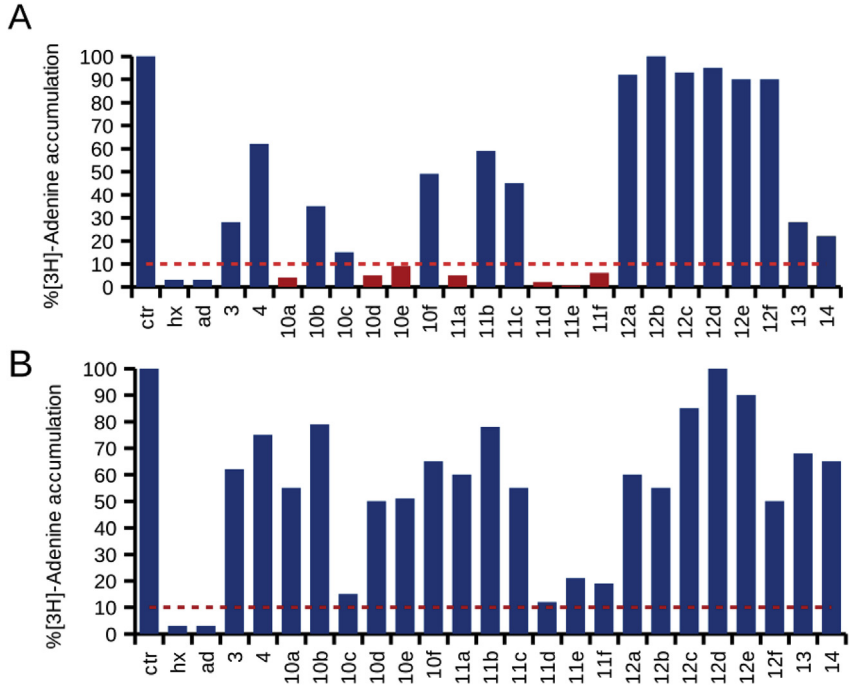

Fig. 3. Competition of FcyB- (**A**) or AzgA- (**B**) mediated [^{3}H]-adenine uptake by 1000-fold excess (0.5 mM) of unlabeled 3-deazapurine analogues.

Inc). The most active compound the piperazine-substituted **10a** was considered as positively charged, since the pKa value of N-methyl-piperazino group was calculated to be 8.6 using Jaguar Software. The resulted low energy structures show that the ligand was stabilized inside the binding pocket mainly in a similar position as described previously [20]. Upon binding to FcyB, the protonated tertiary nitrogen forms salt bridge with Glu397. Additionally, two other hydrogen bonds are formed between N3H and Asn163 amide carbonyl group, while C2=O interacts with NH2 of Asn354 side chain. Finally, an extra H-bond seems to be possible between N1H and Ser261. Trp159 shows π-π stacking interactions with 3-deaza aromatic ring. (Fig. 4A, C). In the case of compound **11e,** the bulky 2-[(2,5-dimethoxy)phenyl] group forms the π-π stacking interactions with Trp159 while two hydrogen bonds are formed one between Glu397 and the N4H and the second between Ser85 side chain and the methoxy group of the 2-substituent (Fig. 4B, D).

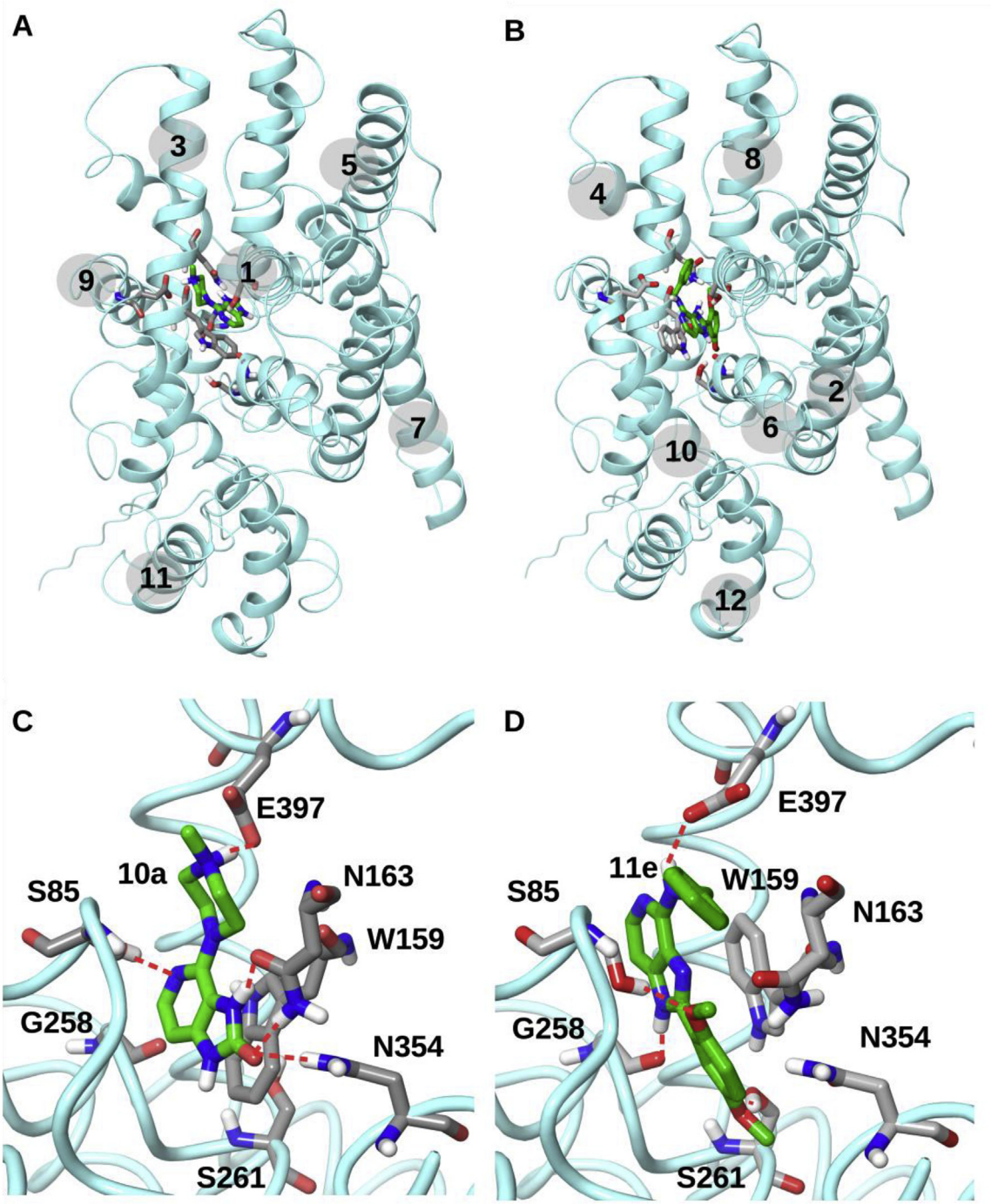

Fig. 4. Low energy binding mode of compounds 10a (**A**) and 11e (**B**) in complex with FcyB as resulted by docking calculations. **C** and **D** detailed presentation of the interactions in the binding cavity for **10a** and **11e** (in green) correspondingly. Hydrogen bonds are depicted with red dashed lines. (For interpretation of the references to colour in this figure legend, the reader is referred to the Web version of this article.)

2.6. Molecular dynamics of FcyB in complex with analogue ***10a***

To further address aspects of molecular recognition and dynamic behavior, a study of the protein-ligand interactions has been undertaken for FcyB in complex with compound **10a** using molecular dynamics. Initially the ligand was positioned in a location similar to the corresponding to the hydantoin derivative in the parent Mhp1 crystal structure used for template (pdb: 4d1d) and a 90 ns simulation was carried out. The MD trajectory shows that the protein remains relatively stable as depicted by the small variations of the overall Ca RMSD from the 30th ns till the end of the simulation (Fig. S1A). The residue RMS fluctuations ranged from 0.8 Å for rigid secondary structural elements to 6 Å for mobile loops (Fig. S1B). The most important conformational change of the protein seems to be the reorientation of TMH10, taking place mainly till the 30th ns. This reorientation of TMH10 displaces the Glu401 of ~4 Å and all residues 386–400 in the loop between TMH9-TMH10 (Fig. 5A).

The ligand **10a** remains in the binding cavity although during of the simulation is displaced by ~3 Å towards the protein surface (Fig. 5B). During the initial part till the 40th ns the ligand forms HB mainly with Asn163 and Asn354 while it displays weaker interactions with Tyr262 and Ser85. It is then relocated losing contact with Asn354 and Tyr262. During the whole simulation the ligand forms a π-π interaction with Trp159 and till the end it remains between Asn163, Trp159 and Ile89 (Fig. 5C). It is interesting that Trp259 remains parallel to the ligand however interactions are rare specifically between 0 and 30 ns then the ligand moves away and there is no interaction after. The charged quaternary piperazine nitrogen initially forms contacts with Glu397 and Glu401 (the later through a water molecule). However its displacement and the simultaneous shift of TMH10 reorients the residues' side chains weakening and finally eliminating those interactions, leaving the piperazine moiety mainly surrounded by water molecules (data not shown).

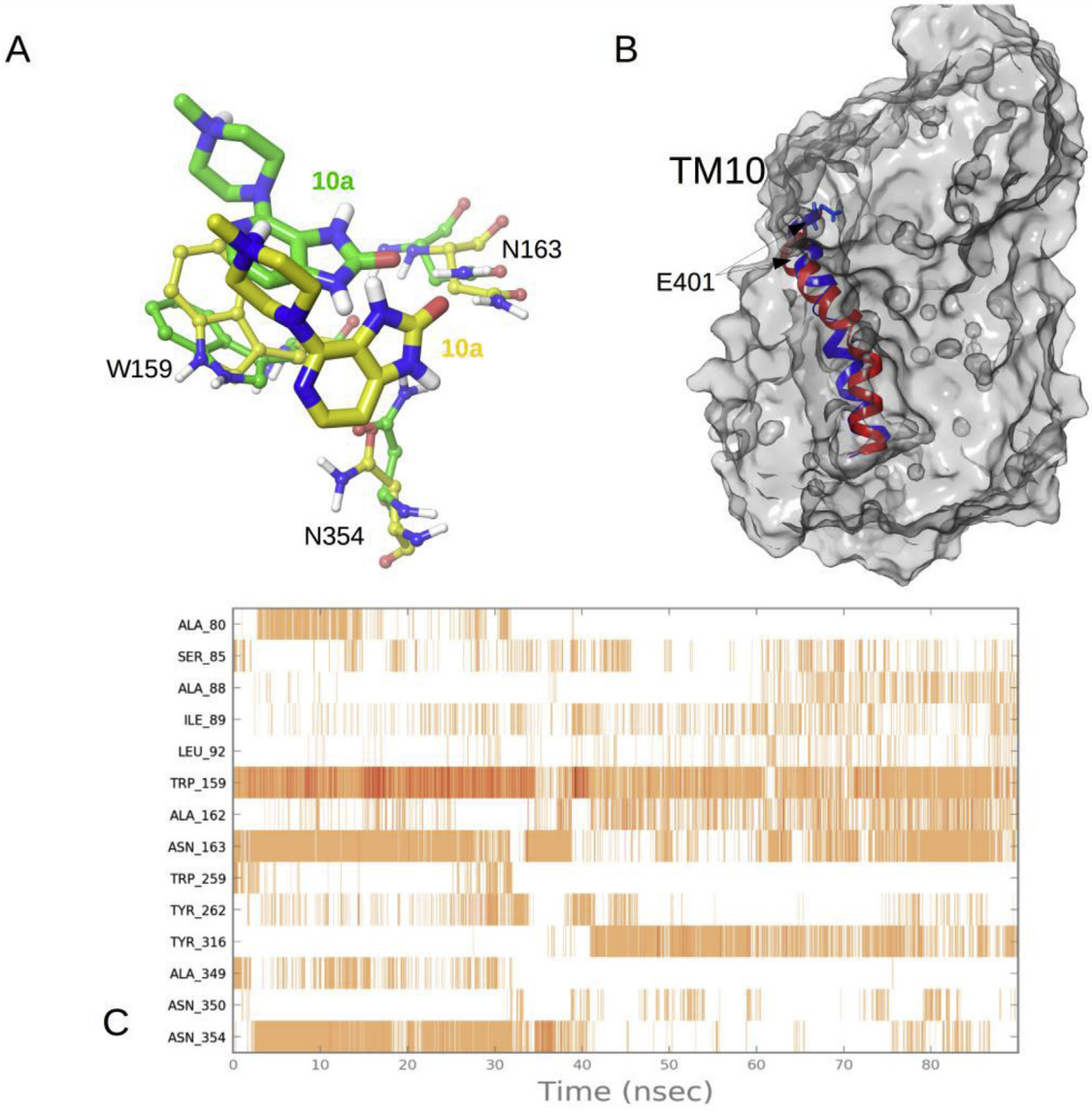

Fig. 5. Molecular Dynamic Analysis of Fcyb in complex with compound 10a. A. Superposition of the binding site of FcyB in complex with compound **10a**: Initial pose of MD simulation (t = 0 ns, yellow) and final pose of MD simulation (t = 90 ns, green). B. Superposition of starting (cyan) and ending (red) position of TMH10 after 90ns of simulation time. C. Timeline representation of interactions of compound **10a** during the MD simulation. The panel shows which residue interacts with the ligand in each trajectory frame. Dark shades of orange indicate more than one specific contact. (For interpretation of the references to colour in this figure legend, the reader is referred to the Web version of this article.)

3. Discussion

The *A. nidulans* purine/H^+ symporters FcyB and AzgA belong to evolutionary and structurally distinct transporter families (NCS1 and NAT/NCS2, respectively), but display very similar, high-affinity, binding for adenine, hypoxanthine and guanine. However, their substrate binding sites should be significantly different, as revealed by their binding affinities for cytosine (recognized only by FcyB) or other, non-physiological substrates, such as the drugs 5-fluorocytosine (FcyB) or 8-azaguanine (AzgA). We have previously reported a model of FcyB based on the first crystal structure of the bacterial homologue Mhp1 [7]. In the same report we identified, via substrate docking approaches and rational mutational analysis, residues essential for the function and specificity that seem to define the substrate-binding site of FcyB. Furthermore, we have subsequently shown that 3-deazaadenine derivatives bearing substitutions on positions 1 and 4, inhibit the transport of physiological substrates [20].

Here we present a refined model of FcyB structure built upon homology threading to the updated, outward-facing, crystal structure of Mhp1. This new FcyB model shows that the side chains of all five residues that have been shown previously to be critical for transport activity, namely Ser85 (TMH1), Trp159, Asn163 (TMH3), Trp259 (TMH6) and Asn354 (TMH8), protrude to the substrate-binding cavity of the transporter. Using the improved FcyB model, we evaluated, as inhibitors of FcyB and two other *A. nidulans* purine transporters, novel 3-deazaadenine analogues, which were rationally designed based on our previous relative experience.

The synthesized compounds tested in this work expand the study on FcyB-ligand interactions. They firstly show that substitution at both positions 2 and 4 can antagonize adenine uptake, with similar inhibitory activities to some of the previously tested 3-deazaadenine derivatives. The introduction of a carbonyl group in position 2 of 3-deazaadenine scafold enhances dramatically binding to FcyB, since compounds **10a** and **11a** exhibit 10- and 5-fold higher inhibitory activity when compared to the parent molecules **4** and **3**. This suggests that the carbonyl group participates actively in protein-ligand interactions, confirming the model proposed in Fig. 4A, C, which shows that the major interaction of FcyB with the purine ring occurs via H-bonding with residues Asn163 and Asn354. A very similar pattern has been observed in the crystal structure of hydantoin bound to Mhp1 forming H-bonds with the corresponding Glu121 and Asn318 [13]. This is also in agreement with the observation that conversion of carbonyl oxygen to sulfur in the thiourea analogues **10b** and **11b** decreases the inhibitory activity, as the corresponding interactions formed by sulfur are expected to be weaker. The carbonyl substitution is also advantageous when comparing derivative **10a** to **2**, both bearing a 4-methylpiperazine substituent at position 4. This trend is inversed in the case of the **11a** and **1** pair bearing a benzylamino substitution at the same position. In this case the carbonyl substitution is detrimental, decreasing the inhibitory activity ten-fold. According to the models derived by docking calculations this is probably due to the fact that in **1** the contribution for the protein-ligand interaction stems from the bidentate H-bonding formation between the NH at position 4 and N3 with the Asn163 amide, while this not the case in **11a** where interactions involving C2=O and N3H with Asn163 are apparently weaker. Other substitutions than the OH at position 2 can still produce interesting activities with most surprising the 2,5-dimethoxyphenyl substitution that proved to be the most active derivative of the **11a-f** series. Compound **11e** seems to be displaced in the outer part of the binding cavity in such orientation that can form appropriate hydrophobic interactions via the 2,5-dimethoxyphenyl moiety and H-bonding between all different nitrogen atoms with surrounding residue side chains (Fig. 4B, D) resulting in an increased activity.

A critical point of our present work, but also of our previous relative work, concerns the specificity of the compounds tested against FcyB. All compounds exhibiting important inhibitory activity display significantly increased specificity for FcyB, compared to AzgA (Fig. 3). Although AzgA and FcyB fold in completely different structures, they both transport adenine, hypoxanthine or guanine. The major interaction in the AzgA cavity is between the substrate and two carboxylates from Glu339 and Asp394 [6]. In this case, interactions are completely different and specificity is driven by a complex multiplicity of interactions. It is noticeable that the parent compounds **4** and **3** do not show any significant inhibitory activity to either AzgA or FcyB, however the urea compounds **10a** and **11a** do exhibit significant binding specificity. Interestingly substitution at position 2 by a 4-NO_2-phenyl moiety abolishes specificity, compound **10c** being one of the most active against AzgA along with the 2-(2-OH-phenyl)-substituted **11d**. Those compounds form the basis for further development of new optimized structures targeting AzgA. Although from the point of view of basic science, the distinct FcyB selectivity over AzgA is important as it shows that highly specific transporter drugs can indeed be rationally designed, for the purpose of a therapeutic antifungal activity, the discovery or design of dual inhibitors acting on several fungal-specific transporters might prove even more valuable. In this direction, analogues **10c** or **11d** (see Fig. 3) seem as promising starting compounds to inhibit both FcyB and AzgA fungal nucleobase transporters.

Solute transport is associated with major changes in the structure of transporters. High-resolution structures of the Mhp1 transporter suggest that during the transport cycle the transition from the outward-open to occluded and then to the inward-open conformation, a semi-rigid body rotation occurs between hash and bundle motifs while TMH10 bends as an extracellular gate to close the binding cavity, accompanied by a bending of TMH5 operating as an intracellular gate. Upon binding of the substrate TMH10 twists over the substrate closing the extracellular gate and occluding it in the binding cavity. The importance of the TMH10 reorientation is also shown in the well-studied 5HIR transporter LeuT, where the extracellular gate is closed through the formation of a salt-bridge between Arg30 (TMH1b) and Asp404 (TMH10) along with other interactions between the two helices. The importance of TMH10 in transport has also been shown in the case of FurD, where site-specific mutations in TMH10 result in enlarged specificity [10]. In the comlplex of FcyB with the most active compound of these series, namely **10a**, MD simulations suggested that the ligand is stabilized in a position different than the corresponding one in the case of hydantoin-Mhp1 complex. After 90 ns of simulation the ligand is displaced ~3 Å towards the outer part of the cavity. In this position, **10a** is stabilized by forming HBs with Asn163 and Ser85 as well as π-π stacking with Trp159, while the "rest" of the analogue is mainly solvated by a sphere of water molecules. Although the starting structure was constructed upon the outward-facing conformation of Mhp1, the new position of **10a** in the cavity tilts the TMH10 further away. This dynamic behavior confirms that this compound acts as a competitive inhibitor of transport. In that sense scaffolds based on **10a** are interesting not only as chemical biology tools for the study of similar purine transporters, but also can be considered for further development of specific transporter-targeted antifungal drugs.

In conclusion, we have identified seven new compounds with relatively high affinity for the FcyB binding site. Importantly three of these compounds can also efficiently inhibit AzgA, a structurally and evolutionary distinct, but functionally similar, fungal purine transporter. None of the new compounds had any effect on the transport activity of the uric acid-xanthine transporter UapA, albeit

this being a structural homologue of AzgA. Besides the apparent importance for understanding how nucleobase transporter specificity is determined at the molecular level, our work might constitute a critical step in the design of novel purine-related antifungals.

4. Methods

4.1. Chemistry

Melting points were determined on a Büchi apparatus and are uncorrected. ^{1}H NMR spectra and 2D spectra were recorded on a Bruker Avance III 600 or a Bruker Avance DRX 400 instrument, whereas ^{13}C NMR spectra were recorded on a Bruker Avance III 600 or a Bruker AC 200 spectrometer in deuterated solvents and were referenced to TMS (δ scale). The signals of ^{1}H and ^{13}C spectra were unambiguously assigned by using 2D NMR techniques: ^{1}H^{1}H COSY, NOESY, HMQC, and HMBC. Mass spectra were recorded with a LTQ Orbitrap Discovery instrument, possessing an Ionmax ionization source. Flash chromatography was performed on Merck silica gel 60 (0.040–0.063 mm). Analytical thin layer chromatography (TLC) was carried out on precoated (0.25 mm) Merck silica gel F-254 plates.

4.1.1. Synthesis and characterization of compounds 10a-f, 11a-f, 12a-f

*4.1.1.1. 4-(4-Methylpiperazin-1-yl)-1,3-dihydroimidazo[4,5-c]pyridin-2-one **(10a)**.* A solution of the nitro derivative **8** (240 mg, 1.0 mmol) in absolute ethanol (60 mL) was hydrogenated in the presence of 10% Pd/C (90 mg) at 35 psi for 4 h. The solution was filtered through a celite pad to remove the catalyst and the filtrate was evaporated to dryness. To a solution of the resulting diamine (210 mg, 1.0 mmol) in tetrahydrofuran (10 mL), 1,1′-carbonyldiimidazole was added (325 mg, 2.0 mmol) and the mixture was heated at reflux for 24 h. Then, the organic solvent was evaporated under vacuo and the residue was purified using silica gel column chromatography (dichloromethane/methanol: 8/2). White solid, 230 mg (98%), m.p. >250 °C (methanol/ether). ^{1}H NMR (400 MHz, DMSO-d_6) δ 10.97 (s, 1H, NH), 10.75 (s, 1H, NH), 7.75 (d, J = 5.3 Hz, 1H, H-6), 6.60 (d, J = 5.3 Hz, 1H, H-7), 3.20 (m, 4H, piperazine H-2,6), 2.45 (m, 4H, piperazine H-3,5), 2.21 (s, 3H, NCH_3). ^{13}C NMR (151 MHz, DMSO-d_6) δ 154.70 (C-2), 145.26 (C-4), 139.46 (C-6), 136.49 (C-7a), 114.93 (C-3a), 99.55 (C-7), 54.60 (piperazine C-3,5), 47.35 piperazine (C-2,6), 45.84 (NCH_3). HRMS-ESI(−) ($C_{11}H_{14}N_5O$) [M-H]$^-$ m/z calcd 232.1193, found 232.1198.

*4.1.1.2. 4-(4-Methylpiperazin-1-yl)-1,3-dihydroimidazo[4,5-c]pyridine-2-thione **(10b)**.* This compound was synthesized using a procedure analogous to that of **10a**, using 1,1′-thiocarbonyldiimidazole. The residue was purified using silica gel column chromatography (dichloromethane/methanol: 9/1). Beige solid, yield 68%, m.p. >250 °C (methanol/ether). ^{1}H NMR (400 MHz, DMSO-d_6) δ 13.25–12.45 (brs, 2H, NH), 7.87 (d, J = 5.4 Hz, 1H, H-6), 6.75 (d, J = 5.4 Hz, 1H, H-7), 3.33 (m, 4H, piperazine H-2,6), 2.50 (m, 4H, piperazine H-3,5), 2.25 (s, 3H, NCH_3). ^{13}C NMR (151 MHz, DMSO-d_6) δ 168.21 (C-2), 145.87 (C-4), 140.60 (C-6), 139.01 (C-7a), 118.19 (C-3a), 99.29 (C-7), 54.49 (piperazine C-3,5), 47.36 (piperazine C-2,6), 45.75 (NCH_3). HRMS-ESI(−) ($C_{11}H_{14}N_5S$) [M-H]$^-$ m/z calcd 248.0964, found 248.0969.

*4.1.1.3. 4-(4-Methylpiperazin-1-yl)-2-(4-nitrophenyl)-1H-imidazo[4,5-c]pyridine **(10c)**.* To a solution of **8** (210 mg, 1.0 mmol) in toluene (10 mL), was added montmorillonite K-10 (300 mg) followed by 4-nitrobenzaldehyde (166 mg, 1.1 mmol) and the mixture was heated at reflux for 24 h. Then, the organic solvent was evaporated under vacuo and the residue was purified using silica gel column chromatography (dichloromethane/methanol: 9/1) to provide **10c** as a brown solid, 200 mg (59%), m.p.>250 °C (ethanol/ether). ^{1}H NMR (400 MHz, DMSO-d_6) δ 13.64–13.34 (brs, 1H, NH), 8.40 (d, J = 8.9 Hz, 2H, H-3′,5′), 8.35 (d, J = 8.9 Hz, 2H, H-2′,6′), 7.84 (d, J = 5.6 Hz, 1H, H-6), 6.91 (d, J = 5.6 Hz, 1H, H-7), 4.16 (m, 4H, piperazine H-2,6), 2.54 (m, 4H, piperazine H-3,5), 2.28 (s, 3H, NCH_3). ^{13}C NMR (151 MHz, DMSO-d_6) δ 151.12 (C-4), 147.69 (C-4′), 145.91 (C-2), 141.26 (C-7a), 140.73 (C-6), 135.51 (C-1′), 128.87 (C-3a), 127.18 (C-2′,6′), 124.34 (C-3′,5′), 98.52 (C-7), 54.61 (piperazine C-3,5), 45.64 (piperazine C-2,6), 45.51 (NCH_3). HRMS-ESI(−) ($C_{17}H_{17}N_6O_2$) [M-H]$^-$ m/z calcd 337.1408, found 337.1412.

*4.1.1.4. 2-(2-Hydroxyphenyl)-4-(4-methylpiperazin-1-yl)-1H-imidazo[4,5-c]pyridine **(10d)**.* This compound was synthesized using a procedure analogous to that of **10c.** The residue was purified using silica gel column chromatography (dichloromethane/methanol: 9/1) and upon successive preparative thin layer chromatography (chloroform/methanol: 9/1), compound **10d** was isolated as a beige solid, yield 47%, m.p. 224–225 °C (ether), together with a small amount of **13.** Data for **10d**: ^{1}H NMR (600 MHz, DMSO-d_6) δ 13.47–13.02 (brs, 1H, NH), 12.47–12.03 (brs, 1H, OH), 8.05 (d, J = 7.5 Hz, 1H, H-6′), 7.87 (d, J = 5.2 Hz, 1H, H-6), 7.37 (t, J = 7.5 Hz, 1H, H-4′), 7.02 (m, 2H, H-3′,5′), 6.99 (d, J = 5.2 Hz, 1H, H-7), 4.00 (m, 4H, piperazine H-2,6), 2.57 (m, 4H, piperazine H-3,5), 2.30 (s, 3H, NCH_3).^{13}C NMR (151 MHz, DMSO-d_6) δ 157.16 (C-2′), 150.39 (C-4), 148.81 (C-2), 140.21 (C-6), 139.93 (C-7a), 131.54 (C-4′), 126.59 (C-6′), 126.10 (C-3a), 119.35 (C-5′), 116.99 (C-3′), 112.98 (C-1′), 99.14 (C-7), 54.64 (piperazine C-3,5), 46.02 (piperazine C-2,6), 45.86 (NCH_3). HRMS-ESI(−) ($C_{17}H_{18}N_5O$) [M-H]$^-$ m/z calcd 308.1506, found 308.1510.

Data for 1-[(2-hydroxyphenyl)methyl]-2-(2-hydroxyphenyl)-4-(4-methylpiperazin-1-yl)-1*H*-imidazo [4,5-*c*]pyridine **(13):** beige solid, yield 4%, m.p. 165–166 °C (methanol). ^{1}H NMR (600 MHz, DMSO-d_6) δ 10.54–10.10 (brs, 1H, OH), 10.05–9.65 (brs, 1H, OH), 7.76 (d, J = 5.7 Hz, 1H, H-6), 7.33 (d, J = 7.5 Hz, 2H, H-3′,5′) 7.01 (m, 2H, H-6′,4″), 6.89 (m, 1H, H-4′), 6.76 (m, 1H, H-3″), 6.72 (d, J = 5.7 Hz, 1H, H-7), 6.58 (t, J = 7.4 Hz, 1H, H-5″), 6.36 (d, J = 7.4 Hz, 1H, H-6″), 5.23 (s, 2H, CH_2), 4.05 (m, 4H, piperazine H-2,6), 2.44 (m, 4H, piperazine H-3,5), 2.22 (s, 3H, NCH_3). ^{13}C NMR (151 MHz, DMSO-d_6) δ 155.85 (C-2′), 154.58 (C-2″), 150.96 (C-4), 149.14 (C-2), 141.14 (C-7a), 139.56 (C-6), 131.35 (C-3′), 128.35 (C-4″), 127.44 (C-3a), 127.02 (C-6″), 126.80 (C-1′), 122.45 (C-1″), 119.13 (C-4′), 118.80 (C-5″), 117.11 (C-5′), 115.90 (C-6′), 114.88 (C-3″), 97.93 (C-7), 54.59 (piperazine C-3,5), 45.64 (NCH_3), 45.51 (piperazine C-2,6), 42.83 (CH_2). The ^{13}C NMR chemical shifts for this compound were extracted from the corresponding HMBC spectrum. HRMS-ESI(+) ($C_{24}H_{26}N_5O_2$) [M+H]$^+$ m/z calcd 416.2081, found 416.2080.

*4.1.1.5. 2-(2,5-Dimethoxyphenyl)-4-(4-methylpiperazin-1-yl)-1H-imidazo[4,5-c]pyridine **(10e)**.* This compound was synthesized using a procedure analogous to that of **10c.** The residue was purified using silica gel column chromatography (dichloromethane/methanol: 9/1) and the product was obtained as a yellow solid, yield 42%, m.p. 180–181 °C (n-hexane). ^{1}H NMR (600 MHz, DMSO-d_6) δ 12.34–12.20 (brs, 1H, NH), 7.79 (d, J = 5.5 Hz, 1H, H-6), 7.76 (d, J = 3.2 Hz, 1H, H-6′), 7.15 (d, J = 9.0 Hz, 1H, H-3′), 7.05 (dd, J = 9.0, 3.2 Hz, 1H, H-4′), 6.97 (d, J = 5.5 Hz, 1H, H-7), 4.14 (m, 4H, piperazine H-2,6), 3.94 (s, 3H, 2′-OCH_3), 3.78 (s, 3H, 5′-OCH_3), 2.57 (m, 4H, piperazine H-3,5), 2.28 (s, 3H, NCH_3). ^{13}C NMR (151 MHz, DMSO-d_6) δ 153.23 (C-5′), 151.06 (C-2′), 150.78 (C-4), 145.70 (C-2), 140.61 (C-7a), 139.48 (C-6), 127.80 (C-3a), 118.35 (C-1′), 116.27 (C-4′), 114.57 (C-6′), 113.36 (C-3′), 99.48 (C-7), 56.18 (2′-OCH_3), 55.62 (5′-OCH_3), 54.53 (piperazine C-3,5), 45.52 (NCH_3-piperazine C-2,6). HRMS-ESI(−) ($C_{19}H_{22}N_5O_2$) [M-H]$^-$ m/z calcd 352.1768, found 352.1770.

*4.1.1.6. 4-(4-Methylpiperazin-1-yl)-2-(pyridin-4-yl)-1H-imidazo[4,5-c]pyridine **(10f)**.* This compound was synthesized using a procedure analogous to that of **10c.** The residue was purified using silica gel column chromatography (dichloromethane/methanol: 9/2) and upon successive preparative thin layer chromatography (chloroform/methanol: 9/2) compound **10f** was isolated as yellow oil (yield 28%), together with a small amount of **14.** Data for **10f:** ^{1}H NMR (600 MHz, DMSO-d_6) δ 13.80–13.10 (brs, 1H, NH), 8.74 (d, J = 5.7 Hz, 2H, H-2′,6′), 8.04 (d, J = 5.7 Hz, 2H, H-3′,5′), 7.84 (d, J = 5.6 Hz, 1H, H-6), 6.90 (d, J = 5.6 Hz, 1H, H-7), 4.14 (m, 4H, piperazine H-2,6), 2.46 (m, 4H, piperazine H-3,5), 2.23 (s, 3H, NCH_3). ^{13}C NMR (151 MHz, DMSO-d_6) δ 151.22 (C-4), 150.49 (C-2′,6′), 145.66 (C-2), 141.09 (C-7a), 140.66 (C-6), 136.62 (C-4′), 128.61 (C-3a), 120.13 (C-3′,5′), 98.50 (C-7), 54.78 (piperazine C-3,5), 45.90 (NCH_3), 45.69 (piperazine C-2,6). HRMS-ESI(−) ($C_{16}H_{17}N_6$) $[M-H]^-$ m/z calcd 293.1509, found 293.1512.

Data for 4-(4-methylpiperazin-1-yl)-1-[(pyridin-4-yl)methyl]-2-(4-pyridyl)-1*H*-imidazo [4,5-*c*]pyridine **(14):** Yellow oil, Yield 4%. ^{1}H NMR (600 MHz, DMSO-d_6) δ 8.70 (d, J = 6.0 Hz, 1H, H-2′,6′), 8.47 (d, J = 5.8 Hz, 1H, H-2″,6″), 7.86 (d, J = 5.7 Hz, 1H, H-6), 7.66 (d, J = 6.0 Hz, 1H, H-3′,5′), 6.97 (d, J = 5.8 Hz, 1H, H-3″,5″), 6.87 (d, J = 5.7 Hz, 1H, H-7), 5.66 (s, 2H, CH_2), 4.13 (m, 4H, piperazine H-2,6), 2.45 (m, 4H, piperazine H-3,5), 2.22 (s, 3H, NCH_3). ^{13}C NMR (151 MHz, DMSO-d_6) δ 151.32 (C-4), 150.29 (C-2′,6′), 150.10 (C-2″,6″), 147.17 (C-2), 145.36 (C-4″), 142.59 (C-7a), 141.08 (C-6), 136.74 (C-4′), 127.29 (C-3a), 122.96 (C-3′,5′), 121.16 (C-3″,5″), 97.50 (C-7), 54.80 (piperazine C-3,5), 46.75 (CH_2), 45.94 (NCH_3), 45.66 (piperazine C-2,6). HRMS-ESI(+) ($C_{22}H_{24}N_7$) $[M+H]^+$ m/z calcd 386.2088, found 386.2089.

*4.1.1.7. 4-Benzylamino-1,3-dihydroimidazo[4,5-c]pyridin-2-one (11a) and 7-amino-3-benzyl-3H-imidazo[4,5-b]pyridin-2-one **(12a)**.* These compounds were synthesized using a procedure analogous to that of **10a.** The residue was purified using silica gel column chromatography (ethyl acetate/methanol: 9/1) and each isomer was isolated using preparative thin layer chromatography (dichloromethane/methanol 95:5).

Data for **11a:** Yield 15%, white solid, m.p. 197–198 °C (ether), ^{1}H NMR (600 MHz, Acetone-d_6) δ 9.90–9.82 brs, 1H, imidazole NH), 9.48–9.40 (brs, 1H, imidazole NH), 7.73 (d, J = 5.4 Hz, 1H, H-6), 7.40 (d, J = 7.6 Hz, 2H, benzylamine H-2,6), 7.31 (t, J = 7.3 Hz, 2H, benzylamine H-3,5), 7.23 (t, J = 7.3 Hz, 1H, benzylamine H-4), 6.47 (d, J = 5.4 Hz, 1H, H-7), 5.71 (s, 1H, benzylamine NH), 4.71 (d, J = 5.5 Hz, 2H, benzylamine CH_2). ^{13}C NMR (151 MHz, Acetone-d_6) δ 155.12 (C-2), 144.16 (C-4), 141.62 (benzylamine C-1), 141.20 (C-6), 136.06 (C-7a), 129.18 (benzylamine C-3,5), 128.57 (benzylamine C-2,6), 127.62 (benzylamine C-4), 112.10 (C-3a), 97.72 (C-7), 45.55 (benzylamine CH_2). HRMS-ESI(−) ($C_{13}H_{11}N_4O$) $[M-H]^-$ m/z calcd 239.0938, found 239.0945).

Data for **12a:** Yield 35%, brown solid m.p. 256–257 °C (ether), ^{1}H NMR (600 MHz, DMSO-d_6) δ 10.34–10.28 (brs, 1H, NH), 7.56 (d, J = 5.7 Hz, 1H, H-5), 7.29 (m, 4H, benzyl H-2,3,5,6), 7.23 (m, 1H, benzyl H-4), 6.33 (d, J = 5.7 Hz, 1H, H-6), 5.77 (s, 2H, NH_2), 4.93 (s, 2H, benzyl CH_2). ^{13}C NMR (151 MHz, DMSO-d_6) δ 152.68 (C-2), 143.90 (C-3a), 141.31 (C-5), 137.77 (benzyl C-1), 137.35 (C-7), 128.37 (benzyl C-3,5), 127.39 (benzyl C-2,6), 127.13 (benzyl C-4), 107.33 (C-7a), 104.95 (C-6), 42.12 (benzyl CH_2). HRMS-ESI (+) ($C_{13}H_{13}N_4O$) $[M+H]^+$ m/z calcd 241.1084, found 241.1086).

*4.1.1.8. 4-Benzylamino-1,3-dihydroimidazo[4,5-c]pyridine-2-thione (11 b) and 7-amino-3-benzyl-3H-imidazo[4,5-b]pyridine-2-thione **(12b)**.* These compounds were synthesized using a procedure analogous to that of **10a.** The residue was purified using silica gel column chromatography (cyclohexane/ethyl acetate: 1/2) and each isomer was isolated using preparative thin layer chromatography (dichloromethane/methanol 95:5).

Data for **11b:** Yield 15%, brown solid m.p. 250–251 °C (ether), ^{1}H NMR (600 MHz, Acetone-d_6) δ 11.54–11.40 (brs, 1H, imidazole NH), 11.37–11.20 (brs, 1H, imidazole NH), 7.82 (d, J = 5.6 Hz, 1H, H-6), 7.43 (d, J = 7.6 Hz, 2H, benzylamine H-2,6), 7.32 (t, J = 7.6 Hz, 2H, benzylamine H-3,5), 7.25 (t, J = 7.4 Hz, 1H, benzylamine H-4), 6.61 (d, J = 5.6 Hz, 1H, H-7), 6.13–6.10 (brs, 1H, benzylamine NH), 4.75 (d, J = 5.2 Hz, 2H, benzylamine CH_2). ^{13}C NMR (151 MHz, Acetone-d_6) δ 169.64 (C-2), 144.37 (C-4), 142.52 (C-6), 141.00 (benzylamine C-1), 138.78 (C-7a), 129.24 (benzylamine C-3,5), 128.62 (benzylamine C-2,6), 127.77 (benzylamine C-4), 115.96 (C-3a), 97.38 (C-7), 45.55 (benzylamine CH_2). HRMS-ESI(+) ($C_{13}H_{13}N_4S$) $[M+H]^+$ m/z calcd 257.0855, found 257.0861.

Data for **12b:** Yield 30%, white solid m.p. 262–263 °C (ether), ^{1}H NMR (600 MHz, DMSO-d_6) δ 13.07–11.68 (brs, 1H, NH), 7.74 (d, J = 5.5 Hz, 1H, H-5), 7.37 (d, J = 7.3 Hz, 2H, benzyl H-2,6), 7.29 (t, J = 7.4 Hz, 2H, benzyl H-3,5), 7.23 (t, J = 7.1 Hz, 1H, benzyl H-4), 6.43 d, J = 5.5 Hz, 1H, H-6), 6.17 (s, 2H, NH_2), 5.37 (s, 2H, benzyl CH_2). ^{13}C NMR (151 MHz, DMSO-d_6) δ 166.36 (C-2), 145.87 (C-3a), 143.74 (C-5), 138.55 (C-7), 136.85 (benzyl C-1), 128.25 (benzyl C-3,5), 127.74 (benzyl C-2,6), 127.23 (benzyl C-4), 110.89 (C-7a), 104.73 (C-6), 44.92 (benzyl CH_2). HRMS-ESI(+) ($C_{13}H_{13}N_4S$) $[M+H]^+$ m/z calcd 257.0855, found 257.0848).

*4.1.1.9. N-Benzyl-2-(4-nitrophenyl)-1H-imidazo[4,5-c]pyridin-4-amine (11c) and 3-benzyl-2-(4-nitrophenyl)-3H-imidazo[4,5-b]pyridin-7-amine **(12c)**.* These compounds were synthesized using a procedure analogous to that of **10c.** The residue was purified using silica gel column chromatography (ethyl acetate) and each isomer was isolated using preparative thin layer chromatography (ethyl acetate).

Data for **11c:** Yield 25%, yellow solid m.p.: 255–256 °C (ether), ^{1}H NMR (600 MHz, Acetone-d_6) δ 12.23–11.28 (brs, 1H, imidazole NH), 8.40 (d, J = 8.9 Hz, 2H, nitrophenyl H-3,5), 8.36 (d, J = 8.9 Hz, 2H, nitrophenyl H-2,6), 7.80 (d, J = 5.8 Hz, 1H, H-6), 7.46 (d, J = 7.5 Hz, 2H, benzylamine H-2,6), 7.30 (t, J = 7.6 Hz, 2H, benzylamine H-3,5), 7.21 (t, J = 7.4 Hz, 1H, benzylamine H-4), 6.81 (d, J = 5.8 Hz, 1H, H-7), 6.78–6.71 (brs, 1H, benzylamine NH), 4.90 (s, 2H, benzylamine CH_2). ^{13}C NMR (151 MHz, Acetone-d_6) δ 152.30 (C-4), 149.07 (nitrophenyl C-1), 148.14 (nitrophenyl C-4), 142.21 (C-3a), 141.98 (C-6), 137.01 (C-2), 129.09 (benzylamine C-3,5), 128.42 (benzylamine C-2,6), 127.96 (nitrophenyl C-3,5), 127.47 (benzylamine C-4), 125.02 (nitrophenyl C-2,6), 98.62 (C-7), 45.00 (benzylamine CH_2). HRMS-ESI(−) ($C_{19}H_{14}N_5O_2$) $[M-H]^-$ m/z calcd 344.1153, found 344.1141.

Data for **12c:** Yield 35%, yellow solid m.p.: 198–199 °C (methanol), ^{1}H NMR (600 MHz, DMSO-d_6) δ 8.32 (d, J = 8.8 Hz, 2H, nitrophenyl H-3,5), 8.01 (d, J = 8.8 Hz, 2H, nitrophenyl H-2,6), 7.90 (d, J = 5.5 Hz, 1H, H-5), 7.24 (t, J = 7.3 Hz, 2H, benzyl H-3,5), 7.19 (t, J = 7.2 Hz, 1H, benzyl H-4), 6.98 (d, J = 7.3 Hz, 2H, benzyl H-2,6), 6.61 (s, 2H, NH_2), 6.46 (d, J = 5.5 Hz, 1H, H-6), 5.62 (s, 2H, benzyl CH_2). ^{13}C NMR (151 MHz, DMSO-d_6) δ 149.19 (C-2), 147.64 (nitrophenyl C-4), 147.17 (C-3a), 147.00 (C-7), 145.74 (C-5), 137.18 (benzyl C-1), 136.58 (nitrophenyl C-1), 129.70 (nitrophenyl C-2,6), 128.64 (benzyl C-3,5), 127.35 (benzyl C-4), 126.29 (benzyl C-2,6), 123.80 (nitrophenyl C-3,5), 122.95 (C-7a), 102.84 (C-6), 45.94 (benzyl CH_2). HRMS-ESI(+) ($C_{19}H_{16}N_5O_2$) $[M+H]^+$ m/z calcd 346.1299, found 346.1288.

*4.1.1.10. N-Benzyl-2-(2-hydroxyphenyl)-1H-imidazo[4,5-c]pyridin-4-amine (11 d) and 3-benzyl-2-(2-hydroxyphenyl)-3H-imidazo[4,5-b]pyridin-7-amine **(12d)**.* These compounds were synthesized using a procedure analogous to that of **10c.** The residue was purified using silica gel column chromatography (dichloromethane/methanol: 9/1) to provide compounds **11d** and **12d**.

Data for **11d:** Yield 15%, brown solid m.p.: 118–119 °C (ether/n-pentane), ^{1}H NMR (600 MHz, Acetone-d_6) δ 12.54–12.36 (brs, 1H,

imidazole NH), 12.32–12.14 (brs, 1H, OH), 7.94 (dd, $J = 7.8$, 1.3 Hz, 1H, hydroxyphenyl H-3), 7.83 (d, $J = 5.6$ Hz, 1H, H-6), 7.45 (d, $J = 7.5$ Hz, 2H, benzylamine H-3,5), 7.35 (td, $J = 7.8$, 1.3 Hz, 1H, hydroxyphenyl H-5), 7.29 (t, $J = 7.6$ Hz, 2H, benzylamine 2,6), 7.20 (t, $J = 7.4$ Hz, 1H, benzylamine H-4), 7.17–7.11 (brs, 1H, benzylamine NH), 7.01 (dd, $J = 7.8$, 0.9 Hz, 1H, hydroxyphenyl H-6), 6.96 (td, $J = 7.8$, 0.9 Hz, 1H, hydroxyphenyl H-4), 6.79 (d, $J = 5.6$ Hz, 1H, H-7), 4.88 (d, $J = 5.2$ Hz, 2H, benzylamine CH_2). ^{13}C NMR (151 MHz, Acetone-d_6) δ 159.26 (C-2), 151.50 (C-4), 150.60 (hydroxyphenyl C-1), 142.37 (C-6), 142.15 (benzylamine C-1), 138.56 (C-7a), 132.23 (hydroxyphenyl C-5), 129.03 (benzylamine C-2,6), 128.40 (benzylamine C-3,5), 127.37 (benzylamine C-4), 126.38 (hydroxyphenyl C-3), 119.88 (hydroxyphenyl C-4), 118.28 (hydroxyphenyl C-6), 113.56 (hydroxyphenyl C-2), 97.97 (C-7), 44.83 (benzylamine CH_2). HRMS-ESI(+) ($C_{19}H_{17}N_4O$) $[M+H]^+$ m/z calcd 317.1397, found 317.1407.

Data for **12d:** Yield 35%, white solid m.p.: 253–254 °C (ether), ^1H NMR (600 MHz, DMSO-d_6) δ 11.43 (s, 1H, OH), 7.85 (d, $J = 5.5$ Hz, 1H, H-5), 7.41 (dd, $J = 7.7$, 1.4 Hz, 1H, hydroxyphenyl H-6), 7.32 (td, $J = 7.7$, 1.4 Hz, 1H, hydroxyphenyl H-4), 7.22 (t, $J = 7.3$ Hz, 2H, benzyl H-3,5), 7.18 (t, $J = 7.2$ Hz, 1H, benzyl H-4), 7.02 (dd, $J = 7.7$, 0.8 Hz, 1H, hydroxyphenyl H-3), 6.97 (d, $J = 7.3$ Hz, 2H, benzyl H-2,6), 6.84 (td, $J = 7.7$, 0.8 Hz, 1H, hydroxyphenyl H-5), 6.54 (s, 2H, NH_2), 6.43 (d, $J = 5.5$ Hz, 1H, H-6), 5.54 (s, 2H, benzyl CH_2). ^{13}C NMR (151 MHz, DMSO-d_6) δ 156.61 (hydroxyphenyl C-2), 148.26 (C-2), 147.99 (C-7), 146.25 (C-3a), 144.93 (C-5), 137.36 (benzyl C-1), 131.15 (hydroxyphenyl C-4), 129.41 (hydroxyphenyl C-6), 128.48 (benzyl C-3,5), 127.18 (benzyl C-4), 126.40 (benzyl C-2,6), 121.32 (C-7a), 118.88 (hydroxyphenyl C-5), 116.64 (hydroxyphenyl C-3), 115.72 (hydroxyphenyl C-1), 102.79 (C-6), 46.06 (benzyl CH_2). HRMS-ESI(+) ($C_{19}H_{17}N_4O$) $[M+H]^+$ m/z calcd 317.1397, found 317.1392.

*4.1.1.11. N-Benzyl-2-(2,5-dimethoxyphenyl)-1H-imidazo[4,5-c]pyridin-4-amine (11e) and 3-benzyl-2-(2,5-dimethoxyphenyl)-3H-imidazo[4,5-b]pyridin-7-amine **(12e)**.* These compounds were synthesized using a procedure analogous to that of **10c.** The residue was purified using silica gel column chromatography (dichloromethane/methanol: 19/1) to provide compounds **11e** and **12e**.

Data for **11e:** Yield 20%, brown solid m.p.: 190–191 °C (ether/n-pentane), ^1H NMR (600 MHz, Acetone-d_6) δ 11.82–11.76 (brs, 1H, imidazole NH), 8.02 (d, $J = 3.1$ Hz, 1H, dimethoxyphenyl H-6), 7.74 (d, $J = 5.5$ Hz, 1H, H-6), 7.45 (d, $J = 7.5$ Hz, 2H, benzylamine H-2,6), 7.30 (t, $J = 7.5$ Hz, 2H, benzylamine H-3,5), 7.20 (t, $J = 7.3$ Hz, 1H, benzylamine H-4), 7.15 (d, $J = 9.0$ Hz, 1H, dimethoxyphenyl H-3), 7.01 (dd, $J = 9.0$, 3.1 Hz, 1H, dimethoxyphenyl H-4), 6.75 (d, $J = 5.5$ Hz, 1H, H-7), 6.53–6.49 (brs, 1H, benzylamine NH), 4.88 (d, $J = 5.8$ Hz, 2H, benzylamine CH_2), 4.00 (s, 3H, dimethoxyphenyl CH_3O-5), 3.81 (s, 3H, dimethoxyphenyl CH_3O-2). ^{13}C NMR (151 MHz, Acetone-d_6) δ 154.88 (dimethoxyphenyl C-2), 152.16 (dimethoxyphenyl C-5), 152.09 (C-4), 148.02 (C-2), 142.33 (benzylamine C-1), 141.14 (C-6), 139.30 (C-7a), 129.05 (benzylamine C-3,5), 128.42 (benzylamine C-2,6), 128.09 (C-3a), 127.37 (benzylamine C-4), 119.61 (dimethoxyphenyl C-1), 117.45 (dimethoxyphenyl C-4), 114.76 (dimethoxyphenyl C-6), 113.94 (dimethoxyphenyl C-3), 98.72 (C-7), 56.57 (dimethoxyphenyl CH_3O-5), 56.06 (dimethoxyphenyl CH_3O-2), 44.97 (benzylamine CH_2). HRMS-ESI(−) ($C_{21}H_{19}N_4O_2$) $[M-H]^-$ m/z calcd 359.1514, found 359.1498.

Data for **12e:** Yield 45%, orange solid m.p.: 90–91 °C (ether/n-pentane), ^1H NMR (600 MHz, DMSO-d_6) δ 7.83 (d, $J = 5.5$ Hz, 1H, H-5), 7.16 (m, 3H, dimethoxyphenyl H-4, benzyl H-3,5), 7.07 (m, 2H, dimethoxyphenyl H-3, benzyl H-4), 6.88 (d, $J = 6.9$ Hz, 2H, benzyl H-2,6), 6.85 (d, $J = 2.6$ Hz, 1H, dimethoxyphenyl H-6), 6.40 (d, $J = 5.5$ Hz, 1H, H-6), 6.36 (s, 2H, NH_2), 5.21 (s, 2H, benzyl CH_2), 3.66 (s, 3H, dimethoxyphenyl CH_3O-2), 3.62 (s, 3H, dimethoxyphenyl CH_3O-5). ^{13}C NMR (151 MHz, DMSO-d_6) δ 152.80 (dimethoxyphenyl C-2), 151.17 (dimethoxyphenyl C-5), 148.26 (C-2), 147.29 (dimethoxyphenyl C-1), 146.53 (C-3a), 144.59 (C-5), 137.44 (benzyl C-1), 128.14 (dimethoxyphenyl C-4), 126.99 (benzyl C-3,5), 126.79 (benzyl C-2,6), 122.68 (C-7), 120.27 (C-7a), 116.98 (dimethoxyphenyl C-6), 116.65 (dimethoxyphenyl C-3), 112.62 (benzyl C-4), 102.32 (C-6), 55.67 (dimethoxyphenyl CH_3O-2), 55.55 (dimethoxyphenyl CH_3O-5), 45.55 (benzyl CH_2). HRMS-ESI(+) ($C_{21}H_{21}N_4O_2$) $[M+H]^+$ m/z calcd 361.1659, found 361.1655.

*4.1.1.12. N-Benzyl-2-(pyridin-4-yl)-1H-imidazo[4,5-c]pyridin-4-amine (11f) and 3-benzyl-2-(pyridin-4-yl)imidazo[4,5-b]pyridin-7-amine **(12f)**.* These compounds were synthesized using a procedure analogous to that of **6c.** The residue was purified using silica gel column chromatography (dichloromethane/methanol: 9/1) to provide compounds **11f** and **12f**.

Data for **11f:** Yield 25%, brown solid m.p.: 150–151 °C (ether/n-pentane), ^1H NMR (600 MHz, Acetone-d_6) δ 12.78–11.75 (brs, 1H, NH imidazole), 8.71 (dd, J = 4.5, 1,5 Hz, 2H, pyridinyl H-3,5), 8.04 (dd, $J = 4.5$, 1.5 Hz, 2H, pyridinyl H-2,6), 7.81 (d, $J = 5.5$ Hz, 1H, H-6), 7.45 (d, $J = 7.7$ Hz, 2H, benzylamine H-2,6), 7.30 (t, $J = 7.6$ Hz, 2H, benzylamine H-3,5), 7.21 (t, $J = 7.4$ Hz, 1H, benzylamine H-4), 6.79 (d, $J = 5.5$ Hz, 1H, H-7), 6.70–6.65 (brs, 1H, benzylamine NH), 4.89 (d, $J = 4.9$ Hz, 2H, benzylamine CH_2). ^{13}C NMR (151 MHz, Acetone-d_6) δ 152.40 (C-4), 151.45 (pyridinyl C-3,5), 147.78 (C-2), 142.31 (C-6), 142.03 (benzylamine C-1), 140.24 (C-7a), 138.00 (pyridinyl C-1), 129.12 (C-3a), 129.08 (benzylamine C-3,5), 128.41 (benzylamine C-2,6), 127.45 (benzylamine C-4), 120.90 (pyridinyl C-2,6), 98.38 (C-7), 44.96 (benzylamine CH_2). HRMS-ESI(−) ($C_{18}H_{14}N_5$) $[M-H]^-$ m/z calcd 300.1255, found 300.1243.

Data for **12f:** Yield 40%, brown solid m.p.: 222–223 °C (ether), ^1H NMR (600 MHz, DMSO-d_6) δ 8.67 (d, $J = 5.8$ Hz, 2H, pyridinyl H-3,5), 7.90 (d, $J = 5.5$ Hz, 1H, H-5), 7.69 (d, $J = 5.8$ Hz, 2H, pyridinyl H-2,6), 7.25 (t, $J = 7.4$ Hz, 2H, benzyl H-3,5), 7.20 (t, $J = 7.2$ Hz, 1H, benzyl H-4), 6.98 (d, $J = 7.5$ Hz, 2H, benzyl H-2,6), 6.59 (s, 2H, NH_2), 6.46 (d, $J = 5.5$ Hz, 1H, H-6), 5.62 (s, 2H, benzyl CH_2). ^{13}C NMR (151 MHz, DMSO-d_6) δ 150.10 (pyridinyl C-3,5), 149.16 (C-2), 147.18 (C-3a), 146.56 (C-7), 145.77 (C-5), 137.68 (pyridinyl C-1), 137.25 (benzyl C-1), 128.66 (benzyl C-3,5), 127.35 (benzyl C-4), 126.20 (benzyl C-2,6), 122.80 (C-7a), 122.57 (pyridinyl C-2,6), 102.81 (C-6), 45.83 (benzyl CH_2). HRMS-ESI(+) ($C_{18}H_{16}N_5$) $[M+H]^+$ m/z calcd 302.1400, found 302.1408.

4.2. Aspergillus manipulations

Standard complete and minimal media (MM) for *A. nidulans* were used. Media and supplemented auxotrophies were at the concentrations given in http://www.fgsc.net. 10 mM, $NaNO_3$ was used as a nitrogen source. Inhibitors are added in MM dissolved in DMSO at 500 μM. Transformations were performed as described previously. Strains have been described before.[20,23] In brief, the three strains used each expressed either FcyB, or AzgA or UapA, in an otherwise isogenic genetic background that lacked, due to total deletions of the corresponding genes, any other nucleobase-nucleoside-allantoin transporter (*uapAΔ uapCΔ azgAΔ furDΔ furAΔ fcybΔ cntA*). The transporter to be studied in each case was introduced by standard genetic transformation [24] with a plasmid carrying the corresponding gene expressed by its native promoter.

4.3. Transport assays

Transport assays for measuring the activity of purine transporters, such as FcyB, AzgA or UapA, is carried out in germinating conidiospores, as recently described in detail by Krypotou and Diallinas [22]. For transport competition assays, 0.5 μM of ^3H-radiolabelled substrate (adenine or xanthine) is added in a mix

with 1000-fold excess analogues (500 μM). Assays are terminated by freezing, immediate centrifugation and washing of cells. K_i values are estimated from IC_{50} measurements using the Cheng and Prussof equation [Ki = IC50/1+ [S]/Km, where [S] is the fixed concentration of radiolabeled substrate used] and analyzed by the GraphPad Prism software. All experiments are carried out at three times, with each assays performed in triplicate. Standard deviation in all cases is less than 30%. Radiolabeled purines used are: [2,8-^{3}H]-adenine or [8-^{3}H]-xanthine 22.8 Ci/mmol, all from Moravek Biochemicals.

4.4. Homology modeling

The 3D Model of Fcyb was constructed based on the crystal structure of bacterial benzyl-hydantoin Mhp1 transporter (PDB entry 4D1D) [13] and we utilized the alignment already published by our group [7]. The final model was built using Prime software (Schrodinger Release, 2017-4: Prime, Schrödinger, LLC, New York, NY, 2017) and the resulted model was prepared using the Protein Preparation Wizard as implemented on Maestro 10 (Schrödinger Release, 2017-4: Schrödinger Suite, 2017-4 Protein Preparation Wizard; Epik, Schrödinger, LLC, New York, NY, 2017; Impact, Schrödinger, LLC, New York, NY, 2017; Prime, Schrödinger, LLC, New York, NY, 2017).

4.5. Docking calculations

4.5.1. Ligand and protein preparation

All analogues designed were prepared using the ligand preparation wizard as implemented in Maestro 10 (Schrödinger Release, 2017-4: LigPrep, Schrödinger, LLC, New York, NY, 2017).

4.5.2. Induced fit docking

Schrödinger developed and validated an Induced Fit Docking protocol based on Glide and the Refinement module in Prime for accurate prediction of ligand binding modes and concomitant structural changes in the receptor.(Schrödinger Release, 2017-4: Schrödinger Suite, 2017-4 Induced Fit Docking protocol; Glide, Schrödinger, LLC, New York, NY, 2016; Prime, Schrödinger, LLC, New York, NY, 2017) [25]. The IFD protocol models induced fit docking of ligands using the following steps:

1. An optional constrained minimization of the receptor (protein preparation, refinement only) with an RMSD cutoff of 0.18 Å. Normally this is done when preparing the protein with the Protein Preparation Wizard.
2. Initial Glide docking of each ligand using a softened potential (van der Waals radii scaling), and optional removal of side chains and application of constraints. By default, a maximum 20 poses per ligand are retained, and by default poses to be retained must have a Coulomb-vdW score less than 100 and an H-bond score less than −0.05.
3. Prime side-chain prediction for each protein-ligand complex, on residues within a given distance of any ligand pose (default 5 Å), with optional inclusion or exclusion of other residues, and an optional implicit membrane model.
4. Prime minimization of the same set of residues and the ligand for each protein/ligand complex pose. The receptor structure in each pose now reflects an induced fit to the ligand structure and conformation.
5. Glide redocking of each protein-ligand complex structure within a specified energy of the lowest-energy structure (default 30 kcal/mol). The ligand is now rigorously docked, using default Glide settings, into the induced-fit receptor structure.
6. Estimation of the binding energy (IFDScore) for each output pose.

4.6. Molecular dynamics simulations

Molecular Dynamic simulations were conducted with Desmond v.3 software (Schrödinger Release, 2017-3: Desmond Molecular Dynamics System, D. E. Shaw Research, New York, NY, 2017. Maestro-Desmond Interoperability Tools, Schrödinger, New York, NY, 2017.) [26]. First the system was prepared by embedding the protein in a POPC lipid bilayer, solvating the membrane by TIP3P explicit water, neutralizing with counter ions and adding 150 mM salt. Initially a stepwise equilibration protocol was utilized, developed by Desmond for membrane proteins. A 90 ns simulation was performed in the NPT ensemble with Langevin thermostat and barostat and semi isotropic pressure restraints for the substrate studied (compound **10a**). All figures were created with Maestro v10 (Schrödinger Release, 2017-4: Maestro, Schrödinger, LLC, New York, NY, 2017).

Acknowledgements

This research was co-supported by the European Union (European Social Fund) and Greek national funds through the Operational Program “Education and Lifelong Learning” of the National Strategic Reference Framework-Research Funding Program: THALES, investing in knowledge society through the European Social Fund. G. Papadaki was supported by a “Stavros Niarchos Foundation” fellowship within the framework of a research grant to the National and Kapodistrian University of Athens.

Appendix A. Supplementary data

The Supplementary Data contains the 1H NMR and 13C NMR spectra of synthesized compounds, and Supplementary Figure SF1 related to the MD simulations.

Supplementary data related to this article can be found at https://doi.org/10.1016/j.ejmech.2018.06.038.

References

[1] A.J. Darlington, C. Scazzocchio, Use of analogues and the substrate-sensitivity of mutants in analysis of purine uptake and breakdown in Aspergillus nidulans, J. Bacteriol. 93 (1967) 937–940.
[2] G. Diallinas, C. Scazzocchio, A gene coding for the uric acid-xanthine permease of Aspergillus nidulans: inactivational cloning, characterization, and sequence of a cis-acting mutation, Genetics 122 (1989) 341.
[3] A. Pantazopoulou, G. Diallinas, Fungal nucleobase transporters, FEMS (Fed. Eur. Microbiol. Soc.) Microbiol. Rev. 31 (2007) 657–675.
[4] G. Diallinas, C. Gournas, Structure-function relationships in the nucleobase-ascorbate transporter (NAT) family: lessons from model microbial genetic systems, Channels 2 (2008) 363–372.
[5] C. Gournas, I. Papageorgiou, G. Diallinas, The nucleobase–ascorbate transporter (NAT) family: genomics, evolution, structure–function relationships and physiological role, Mol. Biosyst. 4 (2008) 404.
[6] E. Krypotou, G. Lambrinidis, T. Evangelidis, E. Mikros, G. Diallinas, Modelling, substrate docking and mutational analysis identify residues essential for function and specificity of the major fungal purine transporter AzgA, Mol. Microbiol. 93 (2014) 129–145.
[7] E. Krypotou, V. Kosti, S. Amillis, V. Myrianthopoulos, E. Mikros, G. Diallinas, Modeling, substrate docking, and mutational analysis identify residues essential for the function and specificity of a eukaryotic purine-cytosine NCS1 transporter, J. Biol. Chem. 287 (2012) 36792–36803.
[8] G. Sioupouli, G. Lambrinidis, E. Mikros, S. Amillis, G. Diallinas, Cryptic purine transporters in *Aspergillus nidulans* reveal the role of specific residues in the evolution of specificity in the NCS1 family: cryptic purine transporters in *A. nidulans*, Mol. Microbiol. 103 (2017) 319–332.
[9] Z. Hamari, S. Amillis, C. Drevet, A. Apostolaki, C. Vágvölgyi, G. Diallinas, C. Scazzocchio, Convergent evolution and orphan genes in the Fur4p-like family and characterization of a general nucleoside transporter in *Aspergillus nidulans*, Mol. Microbiol. 73 (2009) 43–57.

[10] E. Krypotou, T. Evangelidis, J. Bobonis, A.A. Pittis, T. Gabaldón, C. Scazzocchio, E. Mikros, G. Diallinas, Origin, diversification and substrate specificity in the family of NCS1/Fur transporters: origin and specificity of Fur transporters, Mol. Microbiol. 96 (2015) 927–950.
[11] F. Lu, S. Li, Y. Jiang, J. Jiang, H. Fan, G. Lu, D. Deng, S. Dang, X. Zhang, J. Wang, N. Yan, Structure and mechanism of the uracil transporter UraA, Nature 472 (2011) 243–246.
[12] T. Shimamura, S. Weyand, O. Beckstein, N.G. Rutherford, J.M. Hadden, D. Sharples, M.S.P. Sansom, S. Iwata, P.J.F. Henderson, A.D. Cameron, Molecular basis of alternating access membrane transport by the sodium-hydantoin transporter Mhp1, Science 328 (2010) 470–473.
[13] K.J. Simmons, S.M. Jackson, F. Brueckner, S.G. Patching, O. Beckstein, E. Ivanova, T. Geng, S. Weyand, D. Drew, J. Lanigan, D.J. Sharples, M.S. Sansom, S. Iwata, C.W. Fishwick, A.P. Johnson, A.D. Cameron, P.J. Henderson, Molecular mechanism of ligand recognition by membrane transport protein, Mhp1, EMBO J. 33 (2014) 1831–1844.
[14] S. Weyand, T. Shimamura, S. Yajima, S. Suzuki, O. Mirza, K. Krusong, E.P. Carpenter, N.G. Rutherford, J.M. Hadden, J. O'Reilly, P. Ma, M. Saidijam, S.G. Patching, R.J. Hope, H.T. Norbertczak, P.C.J. Roach, S. Iwata, P.J.F. Henderson, A.D. Cameron, Structure and molecular mechanism of a nucleobase-cation-symport-1 family transporter, Science 322 (2008) 709–713.
[15] X. Yu, G. Yang, C. Yan, J.L. Baylon, J. Jiang, H. Fan, G. Lu, K. Hasegawa, H. Okumura, T. Wang, E. Tajkhorshid, S. Li, N. Yan, Dimeric structure of the uracil:proton symporter UraA provides mechanistic insights into the SLC4/23/26 transporters, Cell Res. 27 (2017) 1020–1033.
[16] Y. Alguel, S. Amillis, J. Leung, G. Lambrinidis, S. Capaldi, N.J. Scull, G. Craven, S. Iwata, A. Armstrong, E. Mikros, G. Diallinas, A.D. Cameron, B. Byrne, Structure of eukaryotic purine/H+ symporter UapA suggests a role for homodimerization in transport activity, Nat. Commun. 7 (2016) 11336.
[17] G. Diallinas, Understanding transporter specificity and the discrete appearance of channel-like gating domains in transporters, Front. Pharmacol. 5 (2014).
[18] G. Diallinas, Dissection of transporter function: from genetics to structure, Trends Genet. 32 (2016) 576–590.
[19] Y. Alguel, A.D. Cameron, G. Diallinas, B. Byrne, Transporter oligomerization: form and function, Biochem. Soc. Trans. 44 (2016) 1737–1744.
[20] N. Lougiakis, E.-S. Gavriil, M. Kairis, G. Sioupouli, G. Lambrinidis, D. Benaki, E. Krypotou, E. Mikros, P. Marakos, N. Pouli, G. Diallinas, Design and synthesis of purine analogues as highly specific ligands for FcyB, a ubiquitous fungal nucleobase transporter, Bioorg. Med. Chem. 24 (2016) 5941–5952.
[21] X. Yin, S.W. Schneller, L-deaza-5'-noraisteromycin, Nucleos Nucleot. Nucleic Acids 23 (2004) 67–76.
[22] E. Krypotou, G. Diallinas, Transport assays in filamentous fungi: kinetic characterization of the UapC purine transporter of Aspergillus nidulans, Fungal Genet. Biol. 63 (2014) 1–8.
[23] D. Shivakumar, J. Williams, Y. Wu, W. Damm, J. Shelley, W. Sherman, Prediction of absolute solvation free energies using molecular dynamics free energy perturbation and the OPLS force field, J. Chem. Theor. Comput. 6 (2010) 1509–1519.
[24] M. Koukaki, E. Giannoutsou, A. Karagouni, G. Diallinas, A novel improved method for Aspergillus nidulans transformation,, J. Microbiol. Meth. 55 (2003) 687–695.
[25] W. Sherman, T. Day, M.P. Jacobson, R.A. Friesner, R. Farid, Novel procedure for modeling ligand/receptor induced fit effects, J. Med. Chem. 49 (2006) 534–553.
[26] D. Shivakumar, J. Williams, Y. Wu, W. Damm, J. Shelley, W. Sherman, Prediction of absolute solvation free energies using molecular dynamics free energy perturbation and the OPLS force field, J. Chem. Theor. Comput. 6 (2010) 1509–1519.

M

Membrane Transport Proteins: The Nucleobase-Cation-Symport-1 Family

Georgia F. Papadaki[1], Pikyee Ma[2,3], Irshad Ahmad[2], Antonio N. Calabrese[2], Stephen A. Baldwin[3], Peter J. F. Henderson[2,3] and George Diallinas[1]

[1]Department of Biology, National and Kapodistrian University of Athens, Panepistimioupolis, Athens, Greece

[2]Astbury Centre for Structural Molecular Biology, School of BioMedical Sciences, University of Leeds, Leeds, UK

[3]Astbury Centre for Structural Molecular Biology, Institute of Membrane and Systems Biology, University of Leeds, Leeds, UK

Synonyms

A group of membrane transport proteins is known as the NCS1 (Nucleobase-Cation-Symport-1) or PRT (Purine-Related Transporter) family; Based on similarities of amino acid sequence; Designated A.2.39 in the Transporter Classification Database [TCDB, Saier et al. 2006, 2009]; Substrate specificity and structural modeling

Introduction

The NCS1 family, designated A.2.39 (Saier et al. 2006, 2009), consists of over 2000 currently sequenced proteins derived from Gram-negative and Gram-positive bacteria, archaea, yeast, fungi, and some plants (Pantazopoulou and Diallinas 2007; Ren et al. 2007; Ren and Paulsen 2007, 2010). Proteins of the NCS1 family are 419–635 aminoacyl residues long and possess 12 transmembrane α-helices (TMHs). Eukaryotic members of the family are also characterized by extended cytoplasmic N- and C-terminal regions, which include *cis*-acting elements critical for their subcellular membrane sorting and endocytic turnover (Lauwers et al. 2010; Keener and Babst 2013; Papadaki et al. 2017). NCS1 proteins are structurally related by a 5-helix/5-helix internal pseudosymmetry to proteins in different subfamilies of the Amino acid–Polyamine–organoCation (APC) superfamily, also called the 5-helix inverted repeat (5HIRT) or LeuT superfamily of ion-coupled transporters (Vastermark et al. 2014), which in humans are involved in neurotransmitter, sugar, amino acid, and drug transport. The NCS1 transporters are components of salvage pathways for nucleobases (purines and pyrimidines), nucleosides, vitamins, and related metabolites, including thiamine, hydantoins, and pyridoxine; they also mediate the uptake of several well-established drugs (e.g., antifungals or antibacterial agents) such as 5-fluorocytosine (5-FC) or 5-fluorouracil (5-FU). The mechanism of action of NCS1

Peter JF Henderson: Deceased.

G. C. K. Roberts, A. Watts (eds.), *Encyclopedia of Biophysics*,
https://doi.org/10.1007/978-3-642-35943-9_684-1

transporters is that of substrate-cation symport. The cation involved can be H^+ (Fur and Fcy transporters in fungi) or Na^+ (Mhp1 transport in bacteria). The substrate:cation stoichiometry is 1:1 in Mhp1, but seems to vary in individual proteins, depending on the presence or absence of positive or negative charges in the organic substrate (Pantazopoulou and Diallinas 2007; Weyand et al. 2010).

Overall, the NCS-1 generalized transport reaction is:

$$\begin{aligned}&\text{Nucleobase or related substrate (out)}\\&\quad + \text{cation}^+ \text{ (out)}\\&\rightarrow \text{Nucleobase or related substrate (in)}\\&\quad + \text{cation}^+ \text{ (in)}\end{aligned}$$

Characterized NCS1 Transporters

In bacteria, the best-characterized NCS1 family member is Mhp1 from *Microbacterium liquefaciens*, the structure of which has been determined in distinct conformational topologies (Weyand et al. 2008, 2010; Shimamura et al. 2008, 2014). Mhp1 is a hydantoin-Na^+ symporter, with a preference for substrates with a hydrophobic substituent at position 5 of the hydantoin such as 5-indolyl methyl hydantoin (IMH) and 5-benzyl hydantoin (BH) and often a preference for the L-isomer over the D-isomer; purines, allantoin, or cytosine are not recognized by Mhp1 (Suzuki and Henderson 2006; Simmons et al. 2014; Calabrese et al. 2017). A similar transporter for hydantoin is found in *Arthrobacter aurescens* (Wiese et al. 2001). Members of the NCS1 family that transport hydantoin are of importance in biotechnology for the conversion of L- or D-hydantoin derivatives to compounds of significant added value for biosynthesis of, e.g., amino acids or drugs (Suzuki et al. 2005; Javier Las Heras-Vázquez et al. 2009). Other characterized bacterial NCS1 family members are the transporters for allantoin in *Bacillus subtilis* (PucI, Schultz et al. 2001; Ma et al. 2016) and *Pseudomonas putida* (AAN69889, Ahmad 2017), for cytosine in *Escherichia coli* and *Vibrio parahaemolyticus* (CodB, Danielsen et al. 1992; Ahmad 2017), probably for uracil in *Pseudomonas aeruginosa* (PA0443, Ma 2010) and *Paracoccus denitrificans* (Pden1111, Ma 2010), and putatively for hydroxyl-methylpyrimidine in *Pseudomonas putida* (CytX, Rodionov et al. 2002).

The available crystal structures of Mhp1 correspond to distinct periplasm-open, cytoplasm-open, and occluded state topologies (Weyand et al. 2010; Shimamura et al. 2010; Simmons et al. 2014), strongly supporting the generally accepted alternating access transport mechanism (Diallinas 2008; Krishnamurthy et al. 2009; Kaback et al. 2011; Drew and Boudker 2016). In Mhp1, TMHs 1, 2, 6, and 7 form a four helix bundle and TMHs 3, 4, 8, and 9 form a motif that resembles a hash sign (Fig. 1). Substrate and Na^+ binding sites are located between the hash and bundle motifs and involve residues in TMHs 1 and 6, where the helices break. Binding of the ligand to the outward-facing conformation causes TMH10 to bend and occlude the substrate-binding site; a subsequent transition to the inward-facing conformation occurs as a result of movement of the hash domain relative to the bundle domain (Simmons et al. 2014; Kazmier et al. 2014). Such important observations illuminate our understanding of the complete transport cycle of Mhp1 and by extension other NCS1 proteins.

In higher fungi (Dikarya), NCS1 transporters can be classified, based on their primary amino acid sequence and specificity profile, into two structurally and functionally distinct subfamilies: the Fcy-like and the Fur-like transporters (Fig. 2; Pantazopoulou and Diallinas 2007). Recent phylogenetic analyses have shown that Fur, Fcy and their plant homologues originate through independent horizontal transfers from prokaryotes and that gene duplication has led to the multiplication and functional diversification of fungal NCS1 (Krypotou et al. 2015; Sioupouli et al. 2017).

Several Fur transporters have been functionally characterized in yeast and *Aspergillus nidulans*. The *Saccharomyces cerevisiae* and *Schizosaccharomyces pombe* Fur4p and the *A. nidulans* Fur orthologues are specific, high-

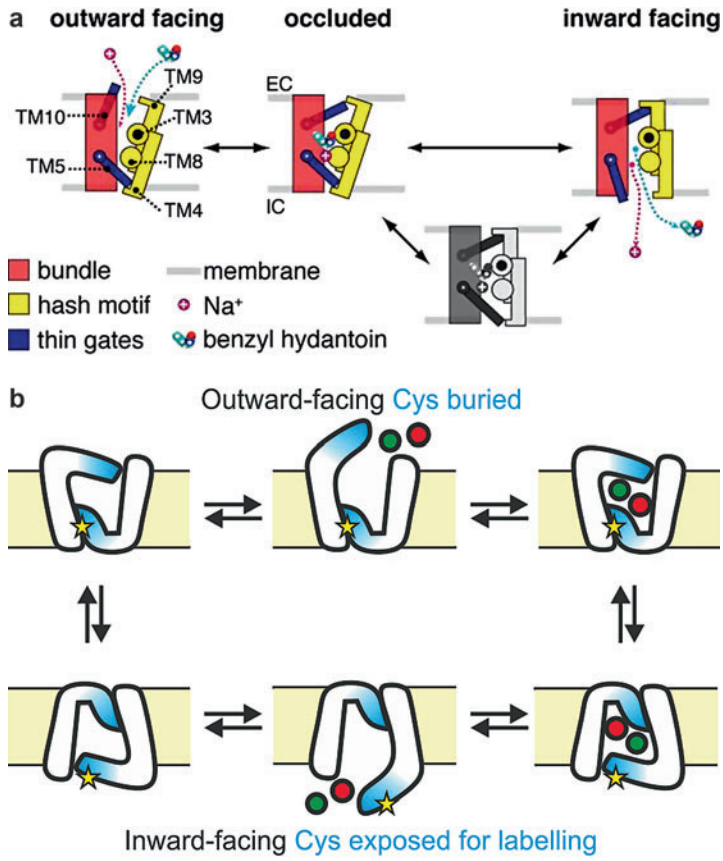

Membrane Transport Proteins: The Nucleobase-Cation-Symport-1 Family, Fig. 1 Schematic representations of the alternating access model for NCS-1 transport proteins highlighting the thick and thin gates. (**a**) The three diagrams represent the outward-facing, occluded, and inward-facing crystal structures of Mhp1. The black and white diagrams show another possible state. Upon sodium and substrate binding the extracellular thin gate (TM 10) closes to form the occluded state. The thick gate then opens with a rigid body rotation of TMs 3, 4, 8, and 9 (the hash motif) relative to TMs 1, 2, 6, 7 (the bundle). Either independently or concomitantly with this the intracellular thin gate (TM 5) also opens to allow the substrates to exit towards the cytoplasm (from Shimamura et al. 2010). (**b**) A generic scheme for the operation of alternating access for all NCS-1 homologues. Green and red circles represent substrate and cation, respectively. The yellow star represents Cys327, which becomes exposed to thiol reagent when Mhp1 is open inwards, and protected when Mhp1 is open outwards (from Calabrese et al. 2017)

affinity (at the lowest μM range), uracil transporters which also transport the highly cytotoxic analogue 5-FU (Pantazopoulou and Diallinas 2007). FurD has also been shown to transport, albeit with moderate-affinity and low-capacity uric acid and xanthine. Yeast and filamentous fungi also possess Fur-like highly specific allantoin transporters (Dal4p and FurA, respectively; Pantazopoulou and Diallinas 2007). *Aspergillus nidulans* additionally possess a low-capacity relatively promiscuous transporter, FurE, capable of mediating the transport of uracil, allantoin, uric acid, and related toxic analogues (Krypotou et al. 2015; Papadaki et al. 2017). Other, more distantly related Fur-like transporters of *S. cerevisiae* have been shown to be specific for uridine (Fui1p), thiamine (Thi7p), or/and nicotinamide riboside (Nrt1p) (Pantazopoulou and Diallinas 2007). Orthologues of Fur-like uracil or allantoin transporters are ubiquitous in all fungi, while Fur-like nucleoside transporters seem to exist solely in yeast, as filamentous fungi employ members of a distinct family (Cnt-like transporters) for nucleoside transport. Interestingly, phylogenetic and

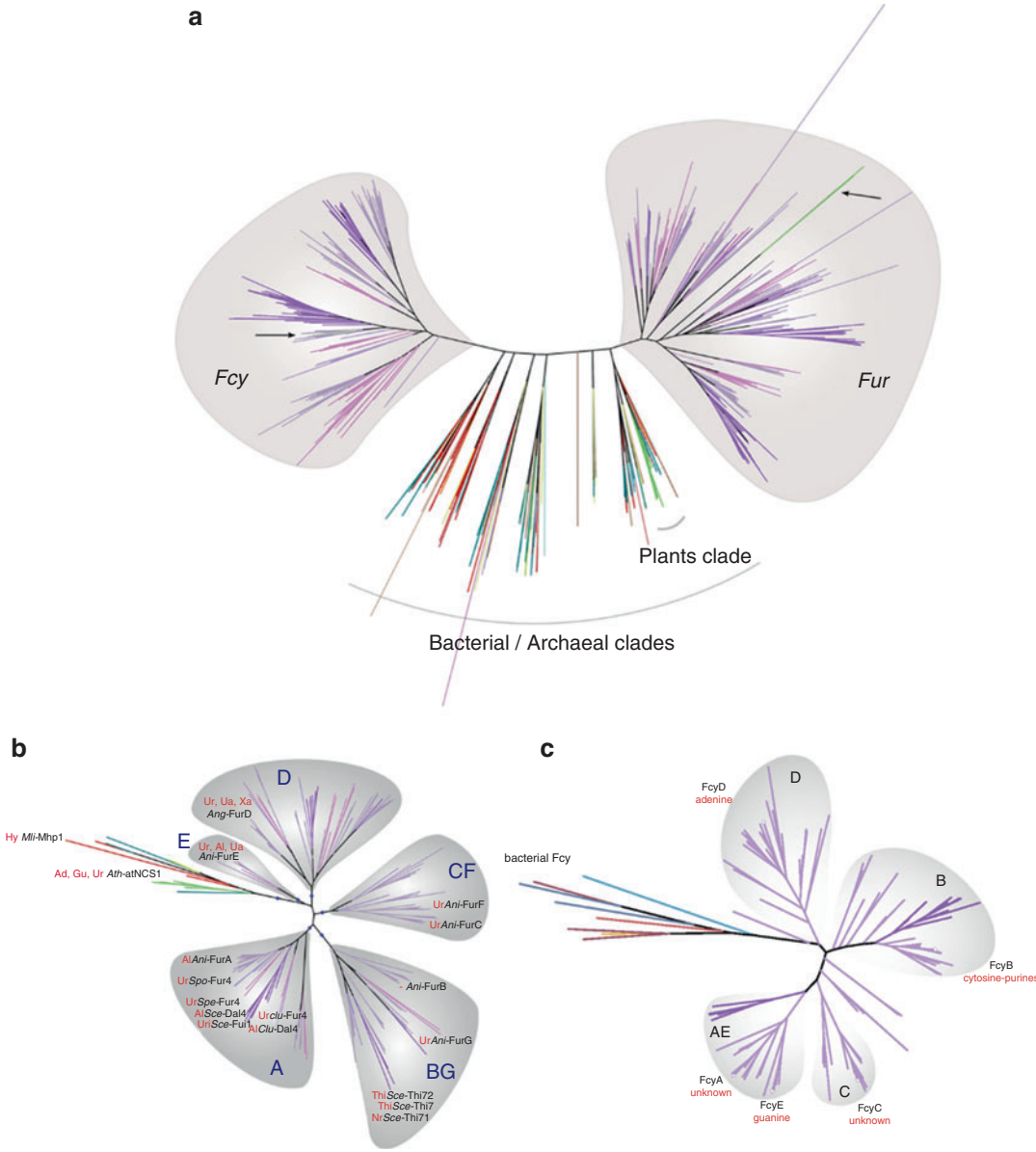

Membrane Transport Proteins: The Nucleobase-Cation-Symport-1 Family, Fig. 2 Phylogenetics of NCS1 transporters. (**a**) Maximum Likelihood phylogenetic tree of all 2248 sequences from 1093 species from all domains carrying the PF_{02133} Pfam domain (NCS1 superfamily). Purple lines correspond to Fcy and Fur fungal proteins, green lines to Plant (Viridiplantae) NCS1 proteins, and Actinobacteria, Proteobacteria, and Firmicutes are in red, blue, and yellow lines, respectively. Maximum Likelihood phylogenetic tree of the fungal. (**b**) Fur family of transporters (190 sequences). Colors are as in A. The sequences from plants cluster with the bacterial ones. Substrate specificities of experimentally characterized transporters are indicated in red. The blue circles in the base of each subfamily clade indicate approximate Likelihood Ratio Test (aLRT) branch support of 100, (**c**) Fcy family of transporters (102 sequences). Subgroups (AE, B, C, and D) contain the Fcy transporters of *A. nidulans* (FcyA-E), and substrate specificities of experimentally characterized transporters are indicated in red. (Adapted from Krypotou et al. 2015; Sioupouli et al. 2017)

functional analyses have suggested that within this subfamily of fungal transporters convergent evolution has occurred multiple times independently, making it impossible to predict the specificity of a Fur transporter a priori, based solely on amino acid sequence similarity (Pantazopoulou and Diallinas 2007; Krypotou et al. 2015; Yoo et al. 1992).

Fcy-like transporters have been functionally characterized in *S. cerevisiae*, *Candida albicans, Candida lusitaniae*, and *A. nidulans* (Pantazopoulou and Diallinas 2007). The best-characterized Fcy-like transporters are the orthologous transporters Fcy2p and FcyB in *S. cerevisiae* and *A. nidulans*, respectively. Both transport adenine, guanine, hypoxanthine, and cytosine with high-affinity and high-capacity, as well as the well-established antifungal 5-FC. The importance of Fcy-like transporters in fungal resistance to 5-FC is highlighted by the fact that nonsense mutations in the corresponding genes are responsible for 5-FC resistance in clinical isolates of *C. lusitaniae* (Florent et al. 2009). Recently, novel purine analogues have been synthesized as highly specific ligands for FcyB, as a first step in developing new antifungals (Lougiakis et al. 2016). The close homologues in *S. cerevisiae (*Fcy21p and Fcy22p) and in *C. albicans* (Fcy21p) seem to have similar specificities but significantly lower apparent activities (Paluszynski et al. 2006; Pantazopoulou and Diallinas 2007), whereas distinct Fcy-like transporters in *A. nidulans* (FcyD or FcyE) have been shown to be cryptic low-capacity adenine or guanine-hypoxanthine transporters (Sioupouli et al. 2017). In contrast to these nucleobase transporters, Tpn1p of *S. cerevisiae* transports vitamin B_6 (pyridoxine) and probably also pyridoxal and pyridoxamine.

The bacterial Mhp1 structure has been used for modeling eukaryotic NCS1 transporters (Fur- and Fcy-like transporters), which together with genetic analyses strongly suggest that specific domains, such as TMH 10, act as gates or gating elements determining substrate specificity in this transporter family (Krypotou et al. 2012, 2015). Interestingly, genetic evidence further showed that the turnover, function, and, intriguingly, the specificity of *A. nidulans* Fur transporters depends on dynamic interactions of the N- and C-terminal cytoplasmic regions with other parts of the protein (Keener and Babst 2013; Papadaki et al. 2017).

Plant NCS1 transporters, which are grouped in a phylogenetic clade closer to Fur-like rather than to the Fcy-like fungal NCS1s (see Fig. 2), have been functionally characterized in *A. thaliana* (AtNCS1) (Mourad et al. 2012; Witz et al. 2012), *Chalmydomonas reinharditii* (CrNCS1), *Zea mays* (ZmNCS1), and *Setaria viridis* (SvNCS1). Their specificity however covers that of both fungal NCS1 subfamilies, that is, includes all purines, uracil, cytosine, allantoin, and several nucleobase analogues (Mourad et al. 2012; Witz et al. 2012, 2014; Schein et al. 2013; Rapp et al. 2015).

Summary

The Nucleobase-Cation-Symport-1 (NCS1) family of membrane transport proteins consists of thousands of currently sequenced proteins derived from bacteria, archaea, fungi, and plants categorized as Family 2.A.39 in the Transport Classification Database. Known substrates include nucleobases, nucleosides, nucleobase-analogues, allantoin, hydantoin derivatives, and vitamins. They are electrochemical potential-driven transporters where translocation of substrate is coupled to the prevailing gradient of Na^+ or H^+. The *Microbacterium* hydantoin permease, Mhp1, is the only member of the NCS-1 family for which the structure has been determined.

Cross-References

- ▶ Membrane Transport, Energetics and Overview
- ▶ Molecular Mechanism and Crystal Structures of the *Microbacterium* Hydantoin Permease, Mhp1

- ▶ The 5-helix Inverted Repeat Superfamily of Membrane Transport Proteins Based on Similarity of Crystal Structures
- ▶ The Nucleobase-Ascorbate-Transporter (NAT) Family

References

Ahmad I (2017) Characterisation of membrane transport proteins of NCS1 and PACE families using biochemical and biophysical techniques. PhD Thesis, University of Leeds

Calabrese AN, Jackson SM, Jones LN, Beckstein O, Heinkel F, Gsponer J, Sans M, Kokkinidou M, Pearson AR, Radford SE, Ashcroft AE, Henderson PJF (2017) Topological dissection of the membrane transport protein Mhp1 derived from cysteine accessibility and mass spectrometry. Anal Chem 89:8844–8852

Danielsen S, Kilstrup M, Barilla K, Jochimsen B, Neuhard J (1992) Characterization of the *Escherichia coli cod*BA operon encoding cytosine permease and cytosine deaminase. Mol Microbiol 6:1335–1344

Diallinas G (2008) Biochemistry. An almost-complete movie. Science 322:1644–1645

Drew D, Boudker O (2016) Shared molecular mechanisms of membrane transporters. Annu Rev Biochem 85:543–572

Florent M, Noël T, Ruprich-Robert G, Da Silva B, Fitton-Ouhabi V, Chastin C, Papon N, Chapeland-Leclerc F (2009) Nonsense and missense mutations in FCY2 and FCY1 genes are responsible for flucytosine resistance and flucytosine-fluconazole cross-resistance in clinical isolates of *Candida lusitaniae*. Antimicrob Agents Chemother 53:2982–2990

Javier Las Heras-Vázquez F, Clemente-Jiménez JM, Martínez-Rodríguez S, Rodríguez-Vico F (2009) Hydantoin racemase: the key enzyme for the production of optically pure α-amino acids, ch12. In: Fessner W-D, Anthonsen T (eds) Modern biocatalysis: stereoselective and environmentally friendly reactions. Wiley-VCH Verlag GmbH & Co. KGaA, Weinheim

Kaback HR, Smirnova I, Kasho V, Nie Y, Zhou Y (2011) The alternating access transport mechanism in LacY. J Membr Biol 239:85–93

Kazmier K, Sharma S, Islam SM, Roux B, Mchaourab HS (2014) Conformational cycle and ion coupling mechanism of the Na^+/hydantoin transporter Mhp1. Proc Natl Acad Sci U S A 111:14752–14757

Keener JM, Babst M (2013) Quality control and substrate-dependent downregulation of the nutrient transporter Fur4. Traffic 14:412–427

Krishnamurthy H, Piscitelli CL, Gouaux E (2009) Unlocking the molecular secrets of sodium-coupled transporters. Nature 459:347–355

Krypotou E, Kosti V, Amillis S, Myrianthopoulos V, Mikros E, Diallinas G (2012) Modeling, substrate docking, and mutational analysis identify residues essential for the function and specificity of a eukaryotic purine-cytosine NCS1 transporter. J Biol Chem 287:36792–36803

Krypotou E, Evangelidis T, Bobonis J, Pittis AA, Gabaldón T, Scazzocchio C, Mikros E, Diallinas G (2015) Origin, diversification and substrate specificity in the family of NCS1/FUR transporters. Mol Microbiol 96:927–950

Lauwers E, Erpapazoglou Z, Haguenauer-Tsapis R, André B (2010) The ubiquitin code of yeast permease trafficking. Trends Cell Biol 20:196–204

Lougiakis N, Gavriil ES, Kairis M, Sioupouli G, Lambrinidis G, Benaki D, Krypotou E, Mikros E, Marakos P, Pouli N, Diallinas G (2016) Design and synthesis of purine analogues as highly specific ligands for FcyB, a ubiquitous fungal nucleobase transporter. Bioorg Med Chem 24:5941–5952

Ma P (2010) Structure-activity relationships of membrane proteins; the NCS-1 family of transporters. PhD Thesis, University of Leeds

Ma P, Patching SG, Ivanova E, Baldwin JM, Sharples D, Baldwin SA, Henderson PJ (2016) Allantoin transport protein, PucI, from *Bacillus subtilis*: evolutionary relationships, amplified expression, activity and specificity. Microbiology 162:823–836

Mourad GS, Tippmann-Crosby J, Hunt KA, Gicheru Y, Bade K, Mansfield TA, Schultes NP (2012) Genetic and molecular characterization reveals a unique nucleobase cation symporter 1 in Arabidopsis. FEBS Lett 586:1370–1378

Paluszynski JP, Klassen R, Rohe M, Meinhardt F (2006) Various cytosine/adenine permease homologues are involved in the toxicity of 5-fluorocytosine in *Saccharomyces cerevisiae*. Yeast 23:707–715

Pantazopoulou A, Diallinas G (2007) Fungal nucleobase transporters. FEMS Microbiol Rev 31:657–675

Papadaki GF, Amillis S, Diallinas G (2017) Substrate specificity of the FurE transporter is determined by cytoplasmic terminal domain interactions. Genetics 207:1387–1400

Rapp M, Schein J, Hunt KA, Nalam V, Mourad GS, Schultes NP (2015) The solute specificity profiles of nucleobase cation symporter 1 (NCS1) from *Zea mays* and *Setaria viridis* illustrate functional flexibility. Protoplasma 253:611–623

Ren Q, Paulsen IT (2007) Large-scale comparative genomic analyses of cytoplasmic membrane transport systems in prokaryotes. J Mol Microbiol Biotechnol 12:165–179

Ren Q, Paulsen IT (2010) TransportDB. http://www.membranetransport.org/

Ren Q, Chen K, Paulsen IT (2007) TransportDB: a comprehensive database resource for cytoplasmic membrane transport systems and outer membrane channels. Nucleic Acids Res 35:D274–D279

Rodionov DA, Vitreschak AG, Mironov AA, Gelfand MS (2002) Comparative genomics of thiamin biosynthesis in procaryotes. J Biol Chem 277:48949–48959

Saier MH Jr, Tran CV, Barabote RD (2006) TCDB: the transporter classification database for membrane transport protein analyses and information. Nucleic Acids Res 34:D181–D186

Saier MH Jr, Yen MR, Noto K, Tamang DG, Elkan C (2009) The transporter classification database: recent advances. Nucl Acids Res 37:D274–D278

Schein JR, Hunt KA, Minton JA, Schultes NP, Mourad GS (2013) The nucleobase cation symporter 1 of *Chlamydomonas reinhardtii* and that of the evolutionarily distant *Arabidopsis thaliana* display parallel function and establish a plant-specific solute transport profile. Plant Physiol Biochem 70:52–60

Schultz AC, Nygaard P, Saxild HH (2001) Functional analysis of 14 genes that constitute the purine catabolic pathway in *Bacillus subtilis* and evidence for a novel regulon controlled by the PucR transcription activator. J Bacteriol 183:3293–3302

Shimamura T, Yajima S, O'Reilly J, Rutherford NG, Henderson PJF, Iwata S (2008) Crystallization of the hydantoin transporter Mhp1 from *Microbacterium liquefaciens*. Acta Crystallog F64:1172–1174

Shimamura T, Weyand S, Beckstein O, Rutherford NG, Hadden JM, Sharples D, Sansom MS, Iwata S, Henderson PJ, Cameron AD (2010) Molecular basis of alternating access membrane transport by the sodium-hydantoin transporter Mhp1. Science 328:470–473

Simmons KJ, Jackson SM, Brueckner F, Patching SG, Beckstein O, Ivanova E, GengT WS, Drew D, Lanigan J, Sharples DJ, Sansom MS, Iwata S, Fishwick CW, Johnson AP, Cameron AD, Henderson PJ (2014) Molecular mechanism of ligand recognition by membrane transport protein, Mhp1. EMBO J 33:1831–1844

Sioupouli G, Lambrinidis G, Mikros E, Amillis S, Diallinas G (2017) Cryptic purine transporters in *Aspergillus nidulans* reveal the role of specific residues in the evolution of specificity in the NCS1 family. Mol Microbiol 103:319–332

Suzuki S, Henderson PJF (2006) The hydantoin transport protein from *Microbacterium liquefacien*. J Bacteriol 188:3329–3336

Suzuki S, Takenaka Y, Onishi N, Yokozeki K (2005) Molecular cloning and expression of the *hyu* genes of *Microbacterium liquefaciens* responsible for the conversion of 5-substituted hydantoins to alpha amino acids, in *Escherichia coli*. Biosci Biotechnol Biochem 69:1473–1482

Vastermark A, Wollwage S, Houle ME, Rio R, Saier MH Jr (2014) Expansion of the APC superfamily of secondary carriers. Proteins 82:2797–2811

Weyand S, Shimamura T, Yajima S, Suzuki S, Mirza O, Krusong K, Carpenter EP, Rutherford NG, Hadden JM, O'Reilly J, Ma P, Saidijam M, Patching SG, Hope RJ, Norbertczak HT, Roach PCJ, Iwata S, Henderson PJF, Cameron AD (2008) Molecular basis of the alternating access model of membrane transport: structure of a nucleobase-cation-symport-1 family transporter. Science 322:709–713

Weyand S, Ma P, Beckstein O, Baldwin J, Jackson S, Suzuki S, Shimamura T, Sansom MSP, Iwata S, Cameron AD, Baldwin SA, Henderson PJF (2010) The nucleobase-cation-symport-1 family of membrane transport proteins. In: Messerschmidt A (ed) Handbook of metalloproteins. Wiley, Chichester, pp 848–864

Wiese A, Mattes R, Syldatk C, Altenbucher J (2001) Organization of genes responsible for the stereospecific conversion of hydantoins to α-amino acids in Arthrobacter aurescens DSM 3747. Arch Microbiol 176:187–196

Witz S, Jung B, Fürst S, Möhlmann T (2012) *De novo* pyrimidine nucleotide synthesis mainly occurs outside of plastids, but a previously undiscovered nucleobase importer provides substrates for the essential salvage pathway in Arabidopsis. Plant Cell 24:1549–1559

Witz S, Panwar P, Schober M, Deppe J, Pasha FA, Lemieux MJ, Möhlmann T (2014) Structure-function relationship of a plant NCS1 member–homology modeling and mutagenesis identified residues critical for substrate specificity of PLUTO, a nucleobase transporter from Arabidopsis. PLoS One 9:e91343

Yoo HS, Cunningham TS, Cooper TG (1992) The allantoin and uracil permease gene sequences of *Saccharomyces cerevisiae* are nearly identical. Yeast 8:997–1006

Cytosolic N- and C-Termini of the *Aspergillus nidulans* FurE Transporter Contain Distinct Elements that Regulate by Long-Range Effects Function and Specificity

Georgia F. Papadaki [1], George Lambrinidis [2], Andreas Zamanos [1], Emmanuel Mikros [2] and George Diallinas [1]

*1 - **Department of Biology,** National and Kapodistrian University of Athens, Panepistimioupolis, Athens 15784, Greece*
*2 - **Department of Pharmacy,** National and Kapodistrian University of Athens, Panepistimioupolis, Athens 15771, Greece*

***Correspondence to Emmanuel Mikros and George Diallinas:** mikros@pharm.uoa.gr, five]diallina@biol.uoa.gr.*
https://doi.org/10.1016/j.jmb.2019.07.013
Edited by I B. Holland

Abstract

FurE, a member of the NCS1 family, is an *Aspergillus nidulans* transporter specific for uracil, allantoin and uric acid. Recently, we showed that C- or N-terminally truncated FurE versions are blocked for endocytosis and surprisingly show modified substrate specificities. Bifluorescence complementation assays and genetic analyses supported the idea that C- and N-termini interact dynamically and through this interaction regulate selective substrate translocation. Here we functionally dissect and define distinct motifs crucial for endocytosis, transport activity, substrate specificity and folding, in both cytosolic termini of FurE. Subsequently, we obtain novel genetic and *in silico* evidence indicating that the molecular dynamics of specific N- and C-terminal regions exert long-range effects on the gating mechanism responsible for substrate selection, via pH-dependent interactions with other internal cytosolic loops and membrane lipids. Our work shows that expanded cytoplasmic termini, acquired through evolution mostly in eukaryotic transporters, provide novel specific functional roles.

Introduction

Transporters are membrane proteins that mediate cellular import and export of nutrients, metabolites, signaling molecules or drugs, and are thus essential for cell communication and life. Despite their evolutionary, structural and functional differences, all transporters appear to use an alternating-access mechanism where a substrate binding site, in "allosteric" cooperation with distinct gating domains, alternates between multiple conformations for receiving and delivering specific substrate(s) from one side of the membrane to the other. This basic mechanism, carried out by dynamic movements of the main transmembrane body and assisted by the flexibility of interconnecting hydrophilic loops, exists in different forms, of the so-called the rocker-switch, the rocking-bundle or the elevator sliding mechanisms [10,25,28,33].

One of the best-studied families of transporters due to a plethora of genetic and biochemical findings concerning fungal members of the family [35,37,55] is the nucleobase cation symporter 1 (NCS1) family. This, together with extensive structural, biophysical and functional data relating to bacterial homologs, principally the benzyl-hydantoin/Na^+ Mhp1 symporter [61],[53],[54] and the allantoin/H^+ PucI symporter [41]. Based on crystal structures of Mhp1, NCS1 proteins consist of 12 transmembrane α-helical segments (TMSs) interconnected with rather short loops and cytosolic N- and C-termini. TMSs 1–10 are arranged as a five-helix intertwined inverted repeat (5HIRT), the LeuT-fold, also found in other transporter families involved in neurotransmitter, sugar, amino acid and drug transport [10,52,59,62]. The last two TMSs (11 and 12) appear crucial for the oligomerization state of some NCS1-like transporters, rather

Please cite this article as: G. F. Papadaki, G. Lambrinidis, A. Zamanos, et al., Cytosolic N- and C-Termini of the *Aspergillus nidulans* FurE Transporter Contain Distinct Elements that Regulat..., Journal of Molecular Biology, https://doi.org/10.1016/j.jmb.2019.07.013

than being involved in the mechanism of transport [22].

The crystal structures available for Mhp1 correspond to conformational distinct outward-facing open, substrate-occluded and cytoplasm-open topologies [53,54,61], indicative of an alternating access rocking-bundle transport mechanism [2,12,29,54]. In all cases, TMSs 1, 2, 6, and 7 form a four-helix bundle, while TMSs 3, 4, 8, and 9 form a "hash sign" motif. The substrate and Na^+ binding sites are found between the hash and bundle motifs and involve residues in TMSs 1 and 6, at helical break-point positions. Ligand binding to the outward-facing conformation causes TMS10, the outer gate, to bend and occlude the binding site. Gate closure elicits a transition to the inward-facing conformation by the movement of the hash domain relative to the bundle domain. The main body movements lead subsequently to opening of an inner gate and release of Na^+ and substrate [6,29,54]. Importantly, structural studies on Mhp1 have been found to be in excellent agreement with functional studies in two homologous subfamilies of NCS1 present in fungi and plants [35,37,48,55]. In particular, mutations affecting transport kinetics and specificity of members of the Fcy and Fur families have been characterized by crystal structures and modeling approaches to be located both in the substrate binding site and also in the outward-facing gate.

We have recently provided genetic evidence that the turnover, function and intriguingly the specificity of an *Aspergillus nidulans* NCS1 homolog, FurE transporter, depend on interactions of the N- and C-terminal cytoplasmic regions with each other and with the main body of the transporter [46]. We showed that C- or N-terminally-truncated versions of FurE (FurE-ΔC30 or FurE-ΔN21) have increased protein stability in conditions that normally trigger ubiquitylation and endocytic turnover [60]. Interestingly, they lose their capacity to import uric acid, while allantoin and uracil are transported normally.

By isolating genetic suppressors of FurE-ΔC30, which restore uric acid transport, we demonstrated that the deleted part of the C-terminus apparently has a long-distance functional effect on the substrate translocation and gating domains. We also obtained direct genetic evidence using bifluorescence complementation assays that the C-terminus interacts with the distal part of the N-terminus. Our results have suggested that both C- and N-terminal domains are involved in intramolecular dynamics critical for the fine regulation of the mechanism that controls substrate transport [44].

Here, we further dissect the function of the N- and C-terminal domains of FurE and identify distinct linear segments that are crucial for endocytic turnover, transport activity, substrate specificity and folding. By using genetics and molecular dynamics (MD), we provide further evidence that specific residues of the N-terminus interact with residues in internal cytoplasmic loops and the C-terminus in a pH-dependent manner, and via these interactions exert long-range control of the gating mechanism and thus substrate specificity. Our results are discussed within the context of how the evolution of extended termini in eukaryotic transporters has provided new molecular paths for the generation of novel functions.

Results

The N-terminus of FurE is crucial for endocytic turnover, specificity and ER-exit

We previously characterized the function of FurE-ΔN21, a truncated version of FurE lacking the first 21 amino acid residues from its N-terminus, tagged with a GFP epitope. FurE-ΔN21 proved insensitive to signals triggering endocytosis [46]. Interestingly, FurE-ΔN21 has lost its transport capacity specifically for uric acid, but retains normal transport of allantoin or uracil, as judged from relevant growth tests [46] (see also Fig. 1).

Although the truncation in FurE-ΔN21 involved a little conserved segment in Fur homologs, a downstream sequence is absolutely conserved in the Fur subfamily, and also well conserved in several prokaryotic NCS1 homologs, including Mhp1. This sequence contains the motif: **N**-X-D/S-L-X-**P** (Fig. 1A). The first Asn and the last Pro are absolutely conserved in all NCS1 members, whereas the D-L sequence is present in fungal Fur homologs, but replaced by S-N/Q in Mhp1 and with various substrate specificities in some other prokaryotic members. Given its presence in prokaryotic NCS1 transporters, we predicted that this N-terminal cytosolic motif might be important for the structure and/or function of this group of transporters, rather than for membrane traffic, endocytosis or other eukaryotic-specific function. We named this motif, the *L*oop *I*nteracting *D*omain (LID) motif, in accordance with a previous publication [30], and for reasons that will become apparent later.

To investigate the function of the LID segment (residues 21–29) and relate this to the already established role of the distal part of the N-terminus (residues 1–21) in endocytosis and substrate specificity, we constructed and analyzed two new truncated FurE versions. The first deleted the entire N-terminus (FurE-ΔN38), for LID, and the second for the first 11 amino acid residues (FurE-ΔN11).

FurE-ΔN38 was retained in the ER membrane and consequently had no apparent transport activity (Fig. 1B, C). In contrast, as judged by growth tests, FurE-ΔN11 possessed normal apparent transport activity and substrate specificity

Please cite this article as: G. F. Papadaki, G. Lambrinidis, A. Zamanos, et al., Cytosolic N- and C-Termini of the *Aspergillus nidulans* FurE Transporter Contain Distinct Elements that Regulat..., Journal of Molecular Biology, https://doi.org/10.1016/j.jmb.2019.07.013

and, when compared to wild-type FurE and FurE-ΔN21 (Fig. 1B, C), showed partial resistance to endocytic internalization. Comparing the effects of the three truncated versions (FurE-ΔN11, FurE-ΔN21 and FurE-ΔN38), it seemed that the distal 10 residues of the N-terminus contribute to endocytosis but not critical for transport activity or specificity, whereas residues within segment 11–20 contribute to endocytosis and are crucial for substrate specificity (compare truncations ΔN11 to ΔN21 in respect to endocytosis and growth on uric acid) (Fig. 1B, C). Finally, segments 21–37 proved critical for ER-exit (compare truncations ΔN21 to ΔN38 in respect to subcellular localization). This analysis was insufficient to define the role of the LID, as ΔN38 deletion was not sorted to the PM.

The LID motif determines substrate specificity but is dispensable for PM localization, transport activity or endocytic turnover

We systemically tested the function of the LID segment, present in the middle part of the N-terminus (residues 21–29), by Ala substitutions of its conserved residues (N24A, D26A, D26A/L27A and P29A). Figure 2A shows that LID mutations allow FurE-mediated growth on uric acid and allantoin and confer sensitivity to 5-fluorouracil (5FU), similar to that of an isogenic strain expressing wild-type FurE. Surprisingly, mutations N24A, D26A and especially D26A/L27A resulted in reduced minimal growth on xanthine, which normally does not support any xanthine-dependent growth by FurE.

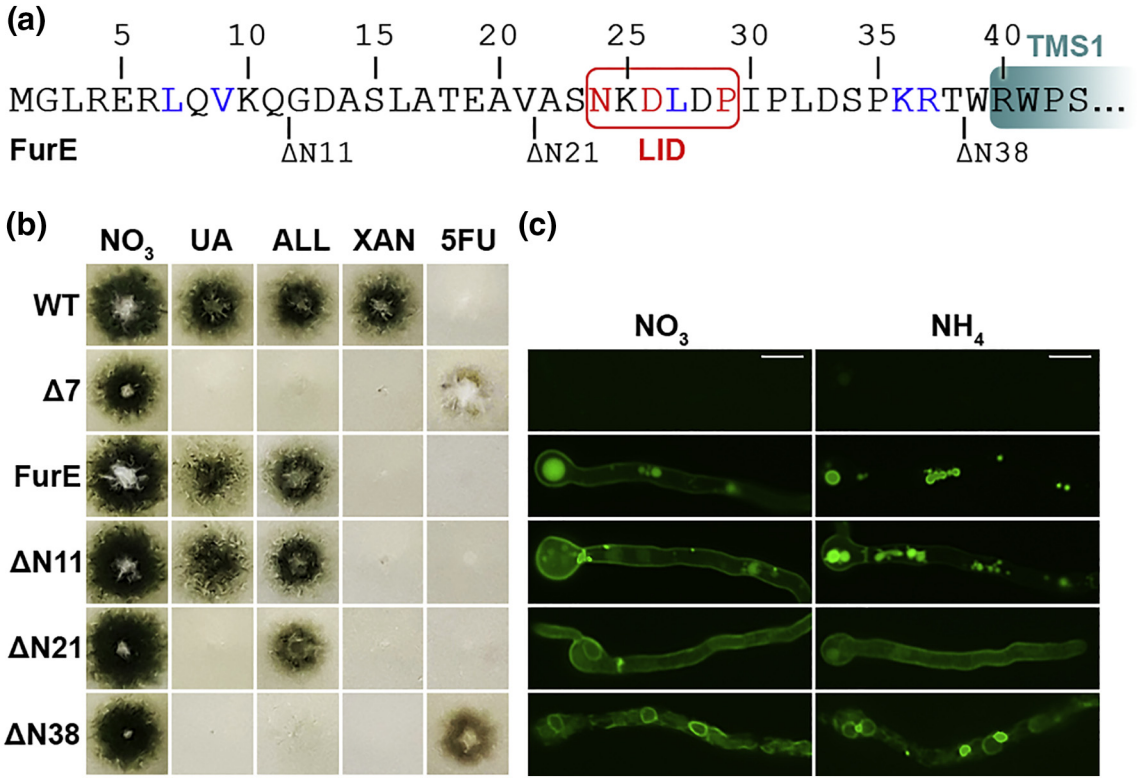

Fig. 1. The N-terminus of FurE is crucial for endocytic turnover, specificity and ER-exit. (A) Schematic representation of the cytosolic N-terminal region of FurE depicting the limits of deletions ΔN11, ΔN21 and ΔN38, and the conserved LID motif (boxed in red). Conserved amino acids in *Aspergilli* and in all fungal homologs are marked in blue and red, respectively. (B) Growth test analysis of a standard wild-type (WT) *A. nidulans* strain, a Δ7 strain lacking all genes encoding nucleobase related transporters [45] (*uapAΔ uapCΔ azgAΔ furDΔ furAΔ fcyBΔ cntAΔ*), and isogenic Δ7 transformants expressing functional GFP-tagged ΔN11, ΔN21, ΔN38 and wild-type FurE versions from the strong *gpdA* promoter. The Δ7 strain has an intact endogenous FurE gene transporter, but this is very little expressed under standard conditions and thus does not contribute to detectable transport of its physiological substrates (UA, ALL) or to sensitivity in 5FU [37]. The test was performed on minimal media (MM) containing nitrate (NO_3^-), uric acid (UA), allantoin (ALL), xanthine (XAN) as sole nitrogen sources, and NO_3 plus the toxic nucleobase analogue 5FU, at 37 °C and pH 6.8. (C) *In vivo* epifluorescence microscopy of the same strains grown until the stage of young hyphae (16–18 h in MM plus NO_3^-). In the right panel, ammonium tartrate (NH_4^+) was added 2 h before microscopic observation. NH_4^+-elicited endocytosis is visible as reduced fluorescent signal from the cell periphery concomitant with the appearance of cytosolic structures, which correspond to vacuoles and endosomes [37,46]. For more details, see Materials and Methods. Scale bars represent 5 μm.

Please cite this article as: G. F. Papadaki, G. Lambrinidis, A. Zamanos, et al., Cytosolic N- and C-Termini of the *Aspergillus nidulans* FurE Transporter Contain Distinct Elements that Regulat..., Journal of Molecular Biology, https://doi.org/10.1016/j.jmb.2019.07.013

In other words, Ala substitutions seem not to affect the capacity for transport, but replacements of N24, D26 and especially D26/L27 enlarged the range of substrate specificity to include xanthine. Figure 2B confirmed that none of the mutations affect stable localization of FurE into the PM (upper panel), and none has an effect on the sensitivity of FurE to endocytosis elicited by NH_4^+ (lower panel).

We performed direct uptake assays to further understand the effect of LID mutations in FurE transport mechanism by measuring radiolabeled uracil accumulation, a low-affinity substrate of FurE [37]. Radiolabeled uracil was used as radiolabeled allantoin is not available commercially and radiolabeled uric acid is very unstable. Radiolabeled uracil accumulation in FurE mutants is similar (D26A) or ~2- to 2.5-fold higher (N24A, D26A/L27A, P29A) to the wild-type FurE (Fig. 2C, gray bars). This not only explains sensitivity to 5FU but also is consistent with normal growth on allantoin or uric acid (Fig. 2A).

Given that mutants N24A, D26A and D26A/L27A also reduced growth on xanthine, we also tested whether this was due to an increase in the affinity for xanthine. Note that wild-type FurE has practically no affinity for xanthine; that is, $K_i > 1$ mM, [37]. To measure xanthine binding, we performed standard competitive inhibition assays that measure radiolabeled uracil accumulation in the presence of excess xanthine (1 mM), as described before [36]. Our results show that FurE single mutants N24A, D26A and P29A have no significant xanthine binding, similarly to wild-type FurE. In contrast, in the double

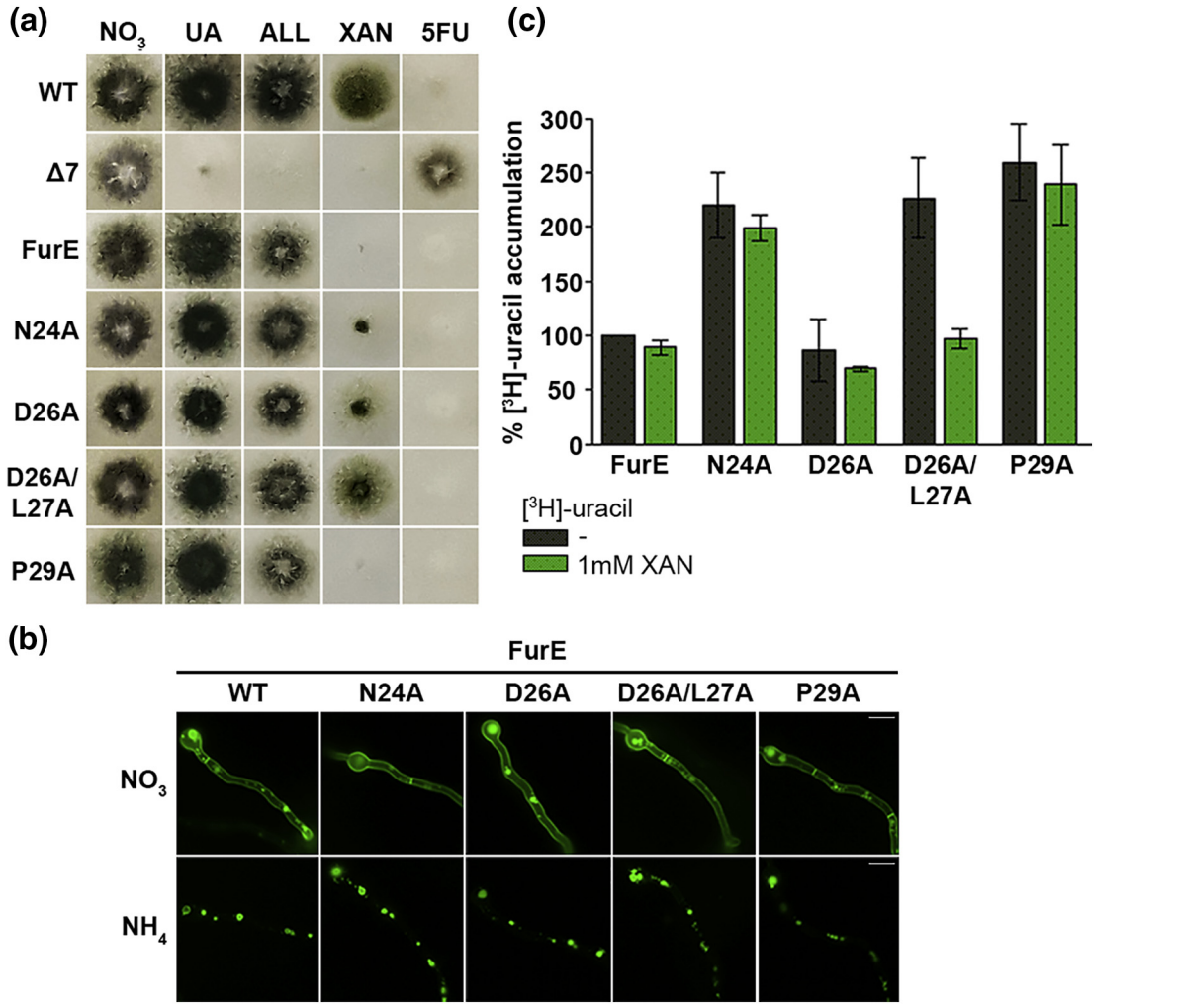

Fig. 2. The LID motif of FurE is crucial for substrate specificity, but dispensable for PM localization, transport activity and endocytic turnover. (A) Growth tests of the control strains (WT, Δ7, FurE) and strains expressing GFP-tagged FurE mutations in the LID (N24A, D26A, D26A/L27A, P29A). Details are as in Fig. 1B. (B) Subcellular localization of the FurE mutants. Noticeably, none of the LID mutations affect the PM localization of FurE (NO_3^- panel) or its endocytosis elicited by NH_4^+. Details are as in Fig. 1C. Scale bars represent 5 μm. (C) Comparative [^{3}H]-uracil (0.5 μM) accumulation and competition assays in the presence of excess (1 mM) of xanthine in strains expressing wild-type FurE, FurE-N24A, FurE-D26A, FurE-D26A/L27A or FurE-P29A. Results shown are averages of three independent assays. Standard deviation is depicted with error bars.

Please cite this article as: G. F. Papadaki, G. Lambrinidis, A. Zamanos, et al., Cytosolic N- and C-Termini of the *Aspergillus nidulans* FurE Transporter Contain Distinct Elements that Regulat..., Journal of Molecular Biology, https://doi.org/10.1016/j.jmb.2019.07.013

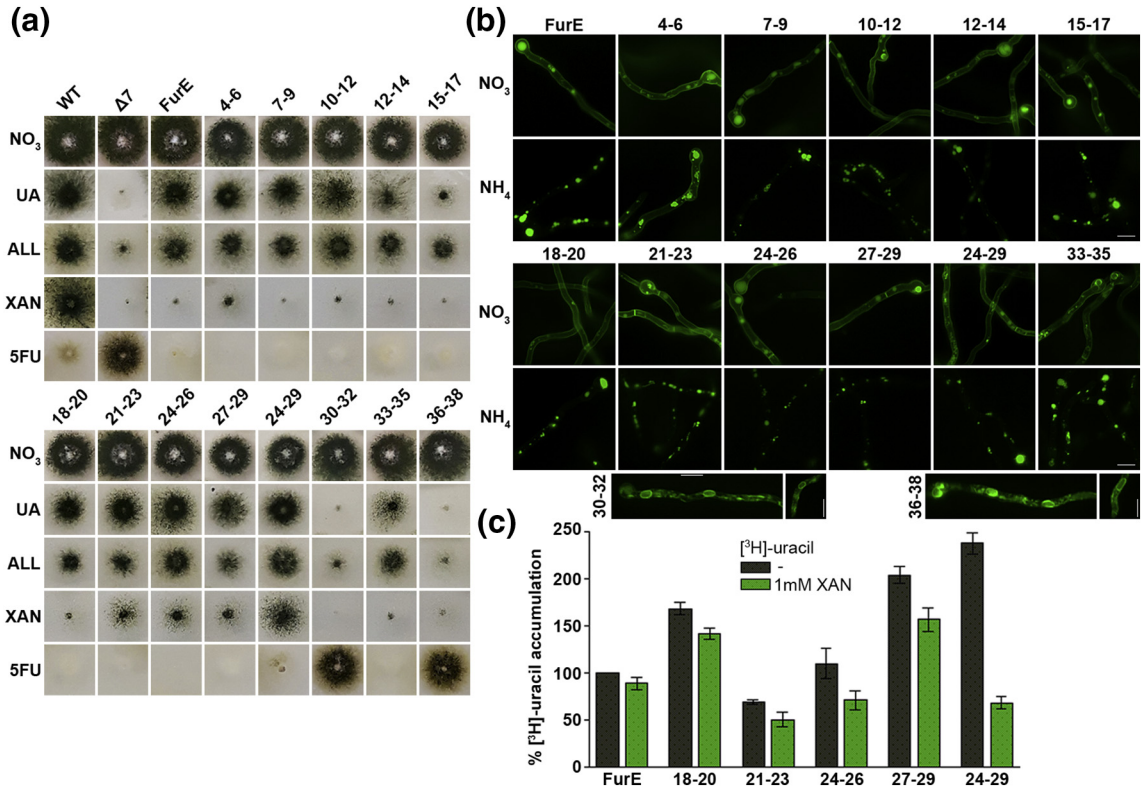

Fig. 3. Delimitation of the N-terminal segments crucial for endocytosis, substrate specificity or ER-exit. (A) Growth tests of control strains and FurE mutants expressing triple Ala substitutions in the FurE N-terminus. Each mutant is named after the position of residues replaced. Notice that mutant 15–17 has significantly reduced capacity to grow on UA, whereas mutants 21–23, 24–26, 27–29 and mostly 24–29 gained the ability to grow on XAN. Details are as in Fig. 1B. (B) Epifluorescence microscopy of the mutants shown in panel A. In the presence of NO_3^- (upper panel), most mutants showed normal PM localization of FurE except mutant 7–9, which showed a degree of instability and increased vacuolar turnover, and mutants 30–32 and 36–38 where FurE was blocked in perinuclear ER rings [46]. Also, all mutants except 4–6 showed the same degree of endocytic turnover as the wild-type FurE after addition of NH_4^+. Mutant 4–6 seems to be partially insensitive to endocytosis, marking the PM even in the presence of NH_4^+. Details are as in Fig. 1C. Scale bars represent 5 μm. (C) Uptake assays measuring accumulation and competition assays by excess substrate of the different strains carrying triple mutations. Details are as in Fig. 2C. Standard deviation is depicted with error bars.

mutant D26A/L27A, uracil uptake was inhibited to >50% by xanthine (Fig. 2C, green bars).

Despite an increase in xanthine binding in the double mutant, FurE-mediated reduced growth, as judged by the single mutants, might not be assigned solely to an increase in xanthine affinity. The growth behavior and transport kinetics of the single mutants, and to a certain degree of the double mutant, are also characteristics of mutations modifying the gating mechanism in other transporters [9,47]. Overall, our results suggested that the LID sequence is critical for specificity by altering the mechanism of gating, rather than by modifying significantly substrate interactions in the bona fide substrate binding site.

Notably, while Ala replacements of N24 and D26/L27 enlarged the specificity range of substrates transported by FurE (allantoin, uracil, uric acid *and* xanthine), deletion of N-terminal residues 1–21 led to restriction of the substrates transported (uracil and allantoin), as described here and previously [46]. A similar restriction of substrates has also been observed by deleting the last 30 amino acid residues of the C-terminus [46]. These observations will be explained later, in context.

Delimitation of N-terminal segments crucial for endocytosis, substrate specificity or ER-exit

To obtain a deeper view on the amino acid residues that are crucial for endocytosis *versus* those that are important for substrate specificity or ER-exit, we systematically mutated, by triple Ala substitutions, the entire N-terminus of FurE. Our results are summarized in Fig. 3. Growth tests on purines, as N sources, or on toxic nucleobase analogues, revealed that the only triple mutations that led to loss of apparent FurE-mediated transport, as judged by lack of growth on allantoin, or uric acid and resistance to 5FU, are those affecting residues

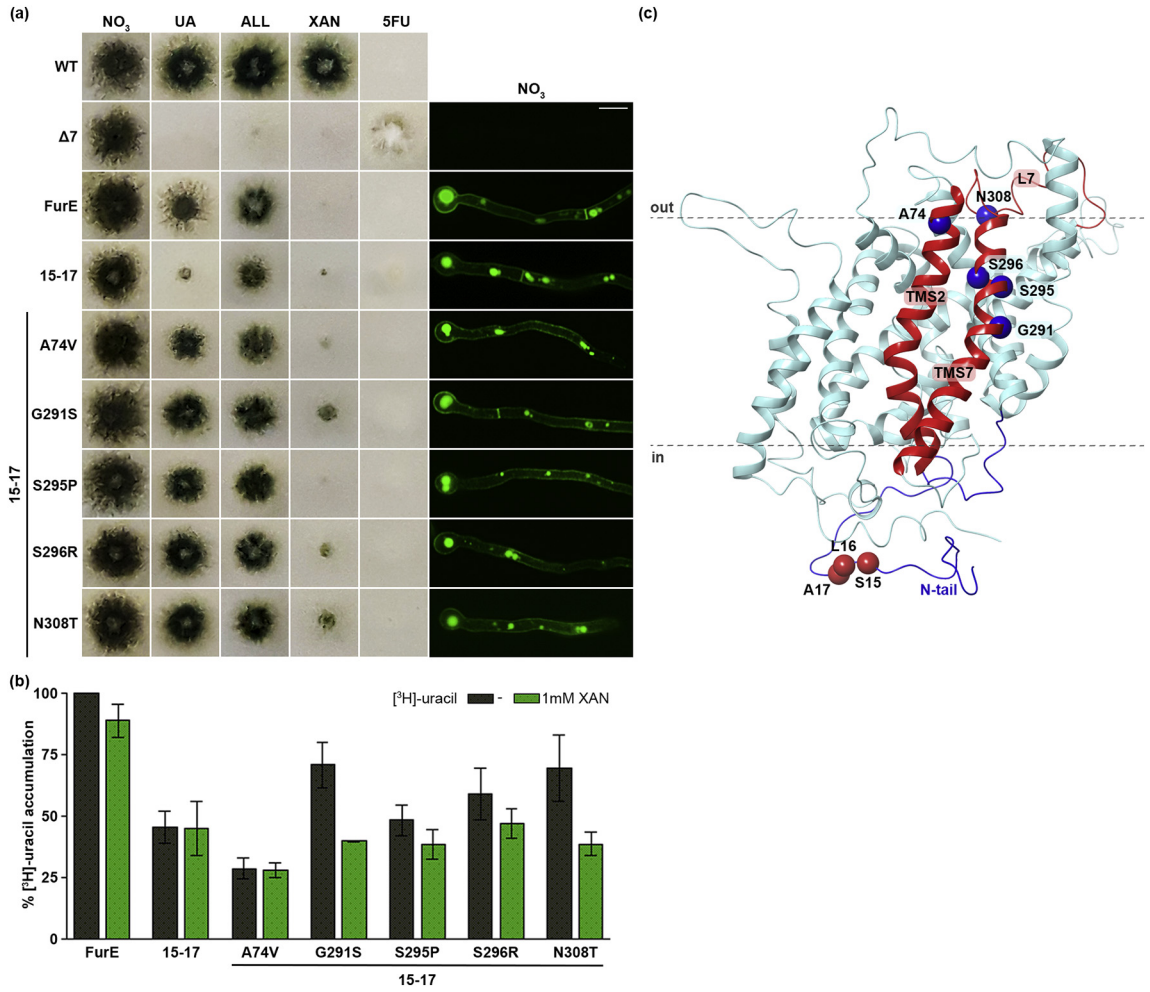

Fig. 4. Genetic evidence for a long-distance effect of the N-terminus on the function of the substrate translocation trajectory. (A) Growth tests (left panel) and subcellular localization (right panel) of the control strains and FurE-S15A/L16A mutant (named 15–17 in the figure) and its suppressor strains. Notice that all suppressors are normally localized in the PM and all have regained the ability of wild-type, FurE-mediated, growth on UA. Details are as in Fig. 1B and C. Scale bar represents 5 μm. (B) Relative accumulation of radiolabeled uracil and competition assays in the presence of excess substrate in different suppressors. Details are as in Fig. 2C. Standard deviation is depicted with error bars. (C) Topology of the suppressor mutations (blue spheres) compared to the original N-terminal S15A/L16A mutation (red spheres).

30–32 and 36–38 (Fig. 3A). This was confirmed by epifluorescence microscopy, which showed that these two mutations led to retention of FurE in the ER membrane, while similarly to wild-type FurE, all other mutant versions of FurE were properly located in the PM and in some vacuoles (Fig. 3B, see NO_3^- panels). Very minor reduction of growth on allantoin, compared to wild-type FurE, was observed in Ala mutations affecting residues 27–29, but this mutant was still highly sensitive to 5FU, suggesting that its transport activity was generally not affected (Fig. 3A). Notably, the triple mutations concerning residues 21–23, 24–26, 27–29 and mostly the hexavalent Ala substitution 24–29 conferred growth on xanthine, which was not seen in the control strain lacking FurE (Δ7) or to that expressing a wild-type FurE (Fig. 3A). This suggests that not only N24 and D26 but also residues 24–29 of the LID are critical for substrate specificity. In addition, growth on uric acid was reduced progressively in mutations affecting residues 10–12, 12–14 and mostly 15–17, and also moderately in mutant 33–35 (Fig. 3A). This means that segments neighboring the LID contribute differentially to substrate selection.

Given that several of the N-terminal triple Ala substitutions conferred growth on xanthine, we tested whether this is due to an increase in the binding affinity for xanthine or is due to a modification in selective gating. We measured accumulation or competition by excess xanthine of radiolabeled uracil in mutants 18–20, 21–23, 24–26, 27–29 and 24–29 (Fig. 3C). Accumulation of radiolabeled uracil was significantly reduced in 27–29 and 24–29 (~20%–25% of wild-type FurE), but little affected or

Please cite this article as: G. F. Papadaki, G. Lambrinidis, A. Zamanos, et al., Cytosolic N- and C-Termini of the *Aspergillus nidulans* FurE Transporter Contain Distinct Elements that Regulat..., Journal of Molecular Biology, https://doi.org/10.1016/j.jmb.2019.07.013

moderately increased in 21–23, 24–26 or 18–20 (75–160% of wild-type FurE; see gray bars). The effect of mutations on the capacity for uracil uptake was not reflected in differences in growth (e.g., sensitivity to 5FU or growth on allantoin). This is not an anomaly, as reduction in transport capacities that are lower than 70%–75% often does not become apparent in growth tests [9,47]. Estimation of the level of inhibition of radiolabeled uracil accumulation by excess xanthine suggested that the mutations studied do not significantly modify the binding affinity for xanthine, despite a trend toward increased inhibition of uracil uptake, seen mostly obvious in mutant 24–26. Thus, growth on xanthine of FurE mutants seemed not to be due to increased xanthine binding, but rather to an alteration of the gating process, as also suggested previously for the single Ala replacements in the LID region.

We also performed uptake and competition assays in mutant 15–17, which showed reduced uric acid growth. Noticeably, uric acid is the only FurE substrate that is recognized by high affinity (K_m = 20 μM; [37]). However, we could not detect any significant effect of mutation 15–17 on the binding affinity of FurE for uric acid (not shown, suggesting that these mutants affect the process of gating rather than modifying the substrate affinities of Fur.

In terms of sensitivity to endocytosis, the only Ala triplet that led to detectable but moderately reduced internalization was the one affecting residues 4–6 (Fig. 3B, lower panel). This contrasts the total block of endocytosis achieved by deleting residues 1–21 and resembles the partial block by deleting residues 1–11 (see Fig. 1). Noticeably, the distal N-terminal segment of Fur transporter is in general little conserved but seems to contain an excess of positively charged residues, two of which are removed in the Ala mutation replacing residues 4–6. Moreover, given that the interaction of N- and C-termini has also been shown to be critical for endocytosis [46], the deletion of the N-terminal residues 1–21 might well hinder this interaction and thus affect FurE turnover (see also later).

Overall, our results showed that distal residues of the N-terminus are essential for endocytosis, middle N-terminus residues affect specificity, and residues proximal to TMS1 are essential for ER-exit, apparently by affecting proper folding of the transporter.

Genetic evidence for an effect of the N-terminus on the functioning of the substrate translocation trajectory

In order to further understand how the N-terminus might affect substrate specificity, we isolated genetic suppressors of mutant S15A/L16A by directly selecting for revertants re-establishing the capacity for FurE-mediated growth on uric acid. Several mutants were selected after U.V. mutagenesis, and 24 of them were purified and characterized in respect to their growth phenotypes on purines and to amino acid changes that occurred within the FurE ORF. Figure 4A shows that all suppressor mutations characterized, namely, A74V, G291S, S295P, S296R and N308T, confer growth phenotypes on uric acid, allantoin or 5FU similarly to that of the isogenic strain expressing wild-type FurE (left panel), but additionally, all except S295P led to weak but clearly detectable growth on xanthine. Furthermore, none of the suppressors affected the proper localization of FurE in the plasma membrane (right panel).

We also performed radiolabeled uracil uptake or competition assays in mutants A74V, G291S, S295P, S296R and N308T, as previously described. Most of them showed ~50%–70% of wild-type FurE uptake capacity, except A74V which showed 30% transport accumulation (Fig. 4B, gray bars). Importantly, mutants that resulted in reduced growth on xanthine (mostly G291S and N308T) also showed increased binding affinity for xanthine, as indicated by the higher level of competition of uracil accumulation by xanthine compared to wild-type FurE or A74G (Fig. 4B, green bars). This suggests that the specific defect in uric acid transport in the original mutant (15–17), proposed to arise from modification of gating process, might be partially restored by an increase in substrate affinity. All suppressors characterized were localized in the TMS7-L7 segment of FurE and concerned missense substitutions in well-conserved amino acids (Fig. 4C). Notably, this region has been suggested to be critical for gating in Mhp1 [29,54].

FurE modeling supports that the N-terminus interacts with specific cytosolic loops and the C-tail

The next question was how truncations of terminal segments or amino acid substitutions within the cytosolic N- or C-termini [46] might be sensed by the transmembrane part of the transporter that hosts the substrate translocation trajectory and carries out transport. Related to this issue, the homologous Mhp1 crystal structure shows that the 20-amino-acid region proximal to TMS1, which includes the LID, is in an extended conformation that runs parallel to the membrane along all cytoplasmic loops. Based on this observation, Keener and Babst [30] have proposed that in *Saccharomyces cerevisiae* the N-terminus of the homologous Fur4p transporter, and in particular its LID region, might functionally and dynamically interact with several cytoplasmic loops when the transporter acquires an outward-facing conformation. This interaction, being dynamic, might then be disrupted by conformational alteration of the transporter to the inward-facing conformation, elicited by substrate binding. These authors further

Please cite this article as: G. F. Papadaki, G. Lambrinidis, A. Zamanos, et al., Cytosolic N- and C-Termini of the *Aspergillus nidulans* FurE Transporter Contain Distinct Elements that Regulat..., Journal of Molecular Biology, https://doi.org/10.1016/j.jmb.2019.07.013

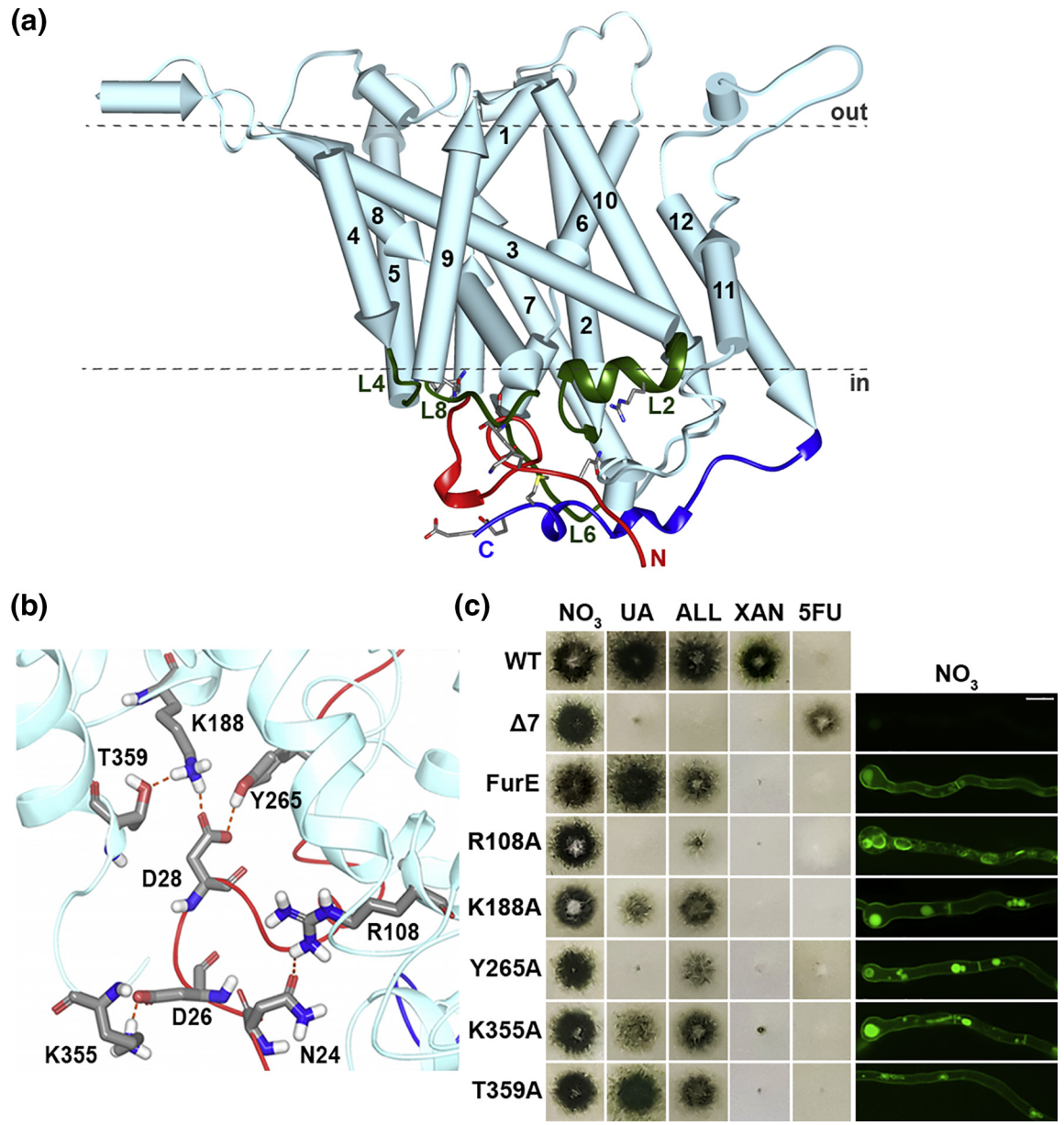

Fig. 5. FurE modeling supports that the N-terminus LID might interact with specific cytosolic loops and the C-tail. (A) FurE model. Notice the close topological distance of the N-terminal region with internal cytosolic loops L2, L4, L6, L8 and the C-tail. (B) Putative major interactions of N-terminal LID with internal cytosolic loops L2, L4 and L8. These interactions were further validated and extended by MD shown in Fig. 7 and Supplementary material. (C) Growth phenotypes (left panel) and subcellular localization (right panel) of loop mutants R108A (L2), K188A (L4), Y265A (L6), K355A and T359A (L8) and control strains. Details are as in previous figures. Notice that all mutant versions of FurE are localized in the PM, except R108A, which is ER-retained. Also, mutations K188A, Y265A and K355A, but not T359A, lead to reduced ability for growth on UA and allantoin, but are still 5FU sensitive, compared to a wild-type FurE. Scale bar represents 5 μm.

proposed that dissociation of the LID from the loops renders the N-terminus accessible for Rsp5/Nedd4-type ubiquitination and degradation, which in turn would explain the phenomenon of transport activity-dependent turnover of Fur4p. They extended this idea to propose that the LID is acting as a conformational-sensitive degron that drives turnover under conditions that lead to partial misfolding of Fur4p. Notably, however, their hypothesis was not supported by targeted mutations in the LID motif, which in their case led to no detectable effect on Fur4p stability or function. Interestingly, Razavi *et al.* [51] very recently also showed that the N-terminus of the mammalian dopamine transporter, which is a

Please cite this article as: G. F. Papadaki, G. Lambrinidis, A. Zamanos, et al., Cytosolic N- and C-Termini of the *Aspergillus nidulans* FurE Transporter Contain Distinct Elements that Regulat..., Journal of Molecular Biology, https://doi.org/10.1016/j.jmb.2019.07.013

structural homolog of NCS1 transporters, interacts dynamically with specific internal loops and the C-terminus, and thus affects the functioning of dopamine transporter. Based on these reports, we tried to obtain evidence as to whether the LID of FurE interacts with the cytosolic loops of the transporter, and thus affects the dynamics of substrate gating and eventual transport specificity.

To identify possible interactions of the N-terminus with internal loops, we built upon homology and validated via MD a refined FurE structural model. Mhp1 benzylhydantoin permease was used as template in the outward-facing crystal structure (PDB entry 2JLN) according to the alignment presented in Supplementary Fig. 1. Similar to the structure of Mhp1, the model represents a 12 α-helix fold with TMS1–10 divided into two symmetric sets oppositely oriented adopting the 5HIRT motif. The overall three-dimensional structure of the FurE model (Fig. 5A) corresponds to an outward-open conformer, with the transmembrane helices connected with rather short loops except the loop between TMS3 and TMS4 with 21 residues, and the loop separating the core and TMS11–12 is longer (26 residues). The model shows that the side chains of residues critical for transport activity [37], namely, W130 ($W117^{Mhp1}$), Q134 ($Q121^{Mhp1}$) in TMS3, and N341 ($N318^{Mhp1}$) in TMS8, superimpose exactly with the corresponding in Mhp1, oriented to the substrate-binding cavity of the transporter. The residues in TMS1 S54 ($Q42^{Mhp1}$) and S56 ($Ala44^{Mhp1}$), although not conserved, but shown to play a critical role in substrate binding [37], protrude to the binding cavity, and the same holds true for K252, which displays a completely different character from the rest of the NCS1 family members. In most members of the family, this residue has aromatic or aliphatic character (W220 in Mhp1), and further studies are needed to fully elucidate the function of this variant [37]. Other residues common to all members of the NCS1 family are W48 (TMS1), which is not oriented toward the translocation pathway, and R108 in L2, which interacts with H427 in L10 and the backbone carbonyl group of L420 in the same loop. R108 is positioned in a hydrophobic crevice between TMS3 and TMS8, which is closed by the LID residues 22–30. A number of specific and putative dynamic contacts of the residues of the N-terminus, and particularly of the LID region, with residues of internal loops and the C-terminus are summarized in Supplementary Table 1, the most important of which are depicted in Fig. 5B. The main interactions identified are as follows: N24 (LID) with R108 (L2), D26 (LID) with K355 (L8), D28 (LID) with K188 (L4) and Y265 (L6). In addition, K188 in L4 seems to interact with L8 (T359). Residues 32–39 of the N-terminus may also contact several residues in L2, L6 and L8 and specific residues of the C-tail, such as M505, and probably E506 and E507. Overall, the LID residues 24–29 are predicted to interact with L2, L4, L6 and L8, while its downstream region (residues 32–39), proximal to TMS1, interacts with L2, L4, L6 and the C-terminus. The C-terminus itself might additionally interact with the FurE core domain, mostly via salt bridges of E497 and E506 with R418 (L10) and R270 (L6). These interactions were further validated by more extensive MD (see later). Noticeably, despite the low similarity of FurE and Mhp1, similar interactions between the N-terminus and L2, L6, L8 and L10 and the C-terminus are also observed in Mhp1 (Supplementary Table 1). It is worth noting that in the case of the outward open conformation of LeuT, the N-terminal $R5^{LeuT}$ interacts with $D369^{LeuT}$ in TMS8 forming a salt bridge, which is disrupted in the inward conformation, as TMS1a and TMS8 move apart [34].

Assuming the above proposed interactions occur, specific mutations in specific loop residues that interact with termini might also affect specificity. To validate experimentally this assumption and the proposed LID-loops interactions, we constructed and functionally analyzed the following loop mutations; R108A in L2, K188R in L4, Y265A in L6, K355A and T359A in L8. Figure 5C shows the growth phenotypes and subcellular localization of the corresponding FurE mutants. Mutation R108A resulted in total ER-retention and thus apparently caused significant FurE misfolding. Thus, no rigorous conclusion on the role of R108 in specificity could be drawn. All other mutants were normally localized in the PM and retained at least an apparent normal capacity to transport 5FU. Y265A resulted in reduced allantoin and no uric acid transport, while mutants K188A and K355A had significantly reduced ability to transport uric acid. Finally, T359A showed wild-type transport level for both substrates. In other words, K188 (L4), Y265 (L6) and K355 (L8) were crucial for determining the specificity profile of FurE. Noticeably, while mutations within the LID (residues 24–29) enlarged the specificity range of substrates to include xanthine, mutations in loops L2, L6 or L8 restricted the set of substrates to mostly 5FU and allantoin, similarly to mutations present just proximal to the LID (residues 12–17). These findings suggest that N-terminus/LID interactions with other internal loops are complex, and thus, the actual outcome in respect to fine changes in specificity of different Ala substitutions is difficult to predict a priori.

The LID is crucial for determining pH-dependent specificity of FurE

Given that FurE is a proton symporter [37], we also tested whether its function, and specifically that of the LID motif, might be differentially affected by the proton or cation gradient of the membrane. We tested FurE-mediated growth phenotypes on relevant substrates or toxic analogues in different pHs, as well as in the presence of a strong Na^+ gradient. The presence of Na^+ gradient was found not to affect the apparent function of wild-type or mutant FurE. Contrastingly, we observed a notable

Please cite this article as: G. F. Papadaki, G. Lambrinidis, A. Zamanos, et al., Cytosolic N- and C-Termini of the *Aspergillus nidulans* FurE Transporter Contain Distinct Elements that Regulat..., Journal of Molecular Biology, https://doi.org/10.1016/j.jmb.2019.07.013

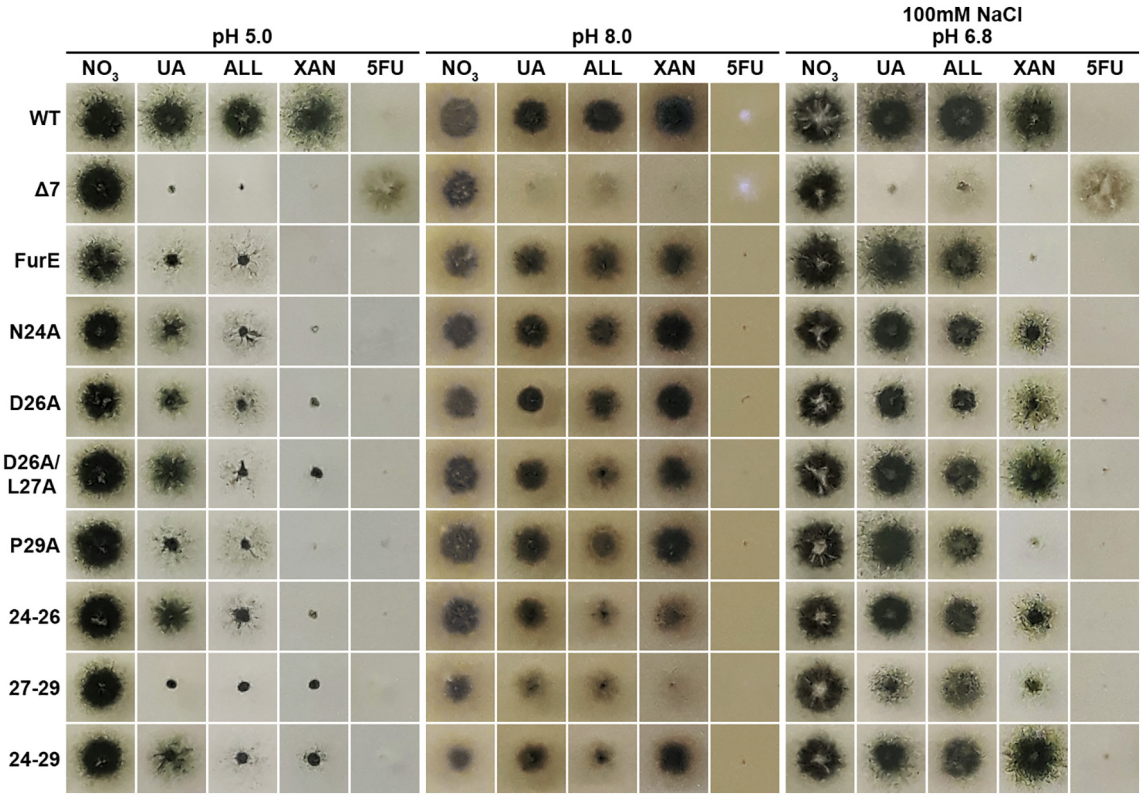

Fig. 6. pH dependence of specificity mutations suggest that ion coupling affects LID interactions and gating. Growth tests of control strains and LID mutations in pH 5.0, 8.0 and 6.8 but in the presence of high Na^+ gradient. For details, see Materials and Methods.

pH-dependence of FurE activity, reflected in growth phenotypes, as highlighted in Fig. 6. In particular, wild-type FurE had significantly reduced apparent transport activity at pH 5.0, as judged by the reduced growth on uric acid and allantoin of the relevant strain, which, however, could still efficiently transport uracil, reflected sensitivity to 5FU. This contrasts the growth phenotypes observed at pH 6.8, the standard pH where *A. nidulans* is tested (see previous figures). At pH 8.0, FurE confers normal growth on uric acid and allantoin, as well as 5FU sensitivity, but unexpectedly, also leads to significant growth on xanthine, which is not a substrate at pH 6.8 or 5.0 (Fig. 6, middle panel). Thus, the overall picture is that FurE has a previously unnoticed pH-dependent substrate profile. At low pH, FurE efficiently transports solely 5FU (and apparently uracil); at neutral pH, FurE also transports uric acid and allantoin; and at pH 8, FurE additionally transports xanthine.

The FurE LID mutants also showed distinct pH-dependent phenotypes. At pH 5.0, most LID mutants (N24A, D26A, D26A/L27A, 24–26 and to a lower degree P29A) grow well on uric acid, unlike the strain expressing the wild-type FurE, while their ability to grow on allantoin or uracil remained similar to that of the wild-type FurE. In other words, at low pH, LID mutants regain wild-type transport capacity for uric acid, but not for allantoin. At pH 8.0, these mutants conserved the wild-type FurE capacity for xanthine transport, which was also apparent at pH 6.8. These findings revealed that at low pH, wild-type FurE functions as a highly specific 5FU (uracil) transporter, incapable for transporting other structurally related substrates, whereas at basic pH, FurE becomes an efficient broad-specificity promiscuous transporter, translocating 5FU, uric acid, allantoin and xanthine.

Given that LID mutations showed a distinct pH behavior compared to wild-type FurE, our results suggested that the protonation state of specific residues in the LID, especially the polar or charged residues N24, D26 or D28, might be responsible for the pH-dependent differences in substrate specificity. Most importantly, Ala mutations in the LID mimic the effect of basic pH, leading to increased promiscuity (i.e., acquisition of the ability to transport xanthine). This observation is discussed further later.

pH-dependent interactions of the LID with intracellular loops affect gating

In order to gain better insight of the interactions between LID and intracellular facing loops, a more detailed structural study was undertaken by running specific MD calculations that would provide

Please cite this article as: G. F. Papadaki, G. Lambrinidis, A. Zamanos, et al., Cytosolic N- and C-Termini of the *Aspergillus nidulans* FurE Transporter Contain Distinct Elements that Regulat..., Journal of Molecular Biology, https://doi.org/10.1016/j.jmb.2019.07.013

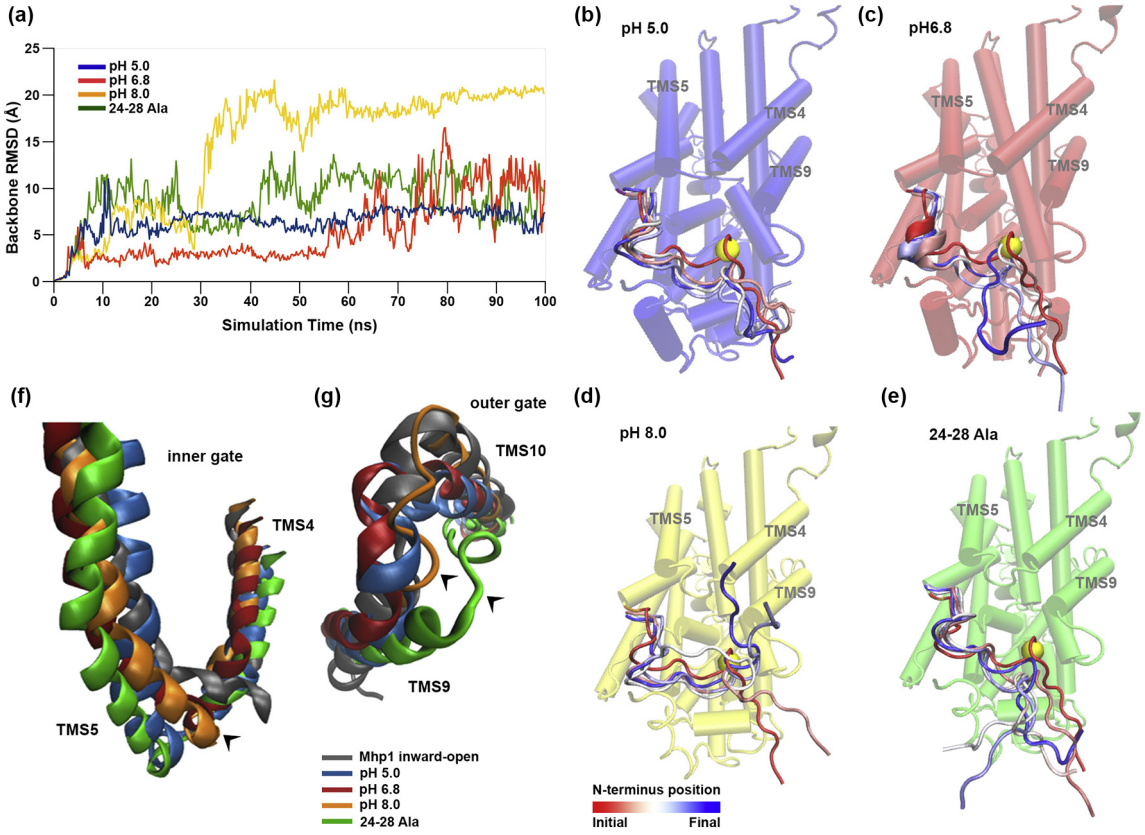

Fig. 7. MD of FurE at different pHs and in the LID mutant (A) RMSD of all Ca atoms of the LID residues 20–40 in respect to the initial structure (blue, pH 5.0; red, pH 6.8; yellow, pH 8; and green, 24–28 Ala mutant). (B–E) Schematic representation of FurE cytoplasmic view together with the conformational transition of the LID residues. Snapshots were taken every 25 ns along the transition pathway and are illustrated color code (red for the initial and blue for the final position). Proline 29 showing the residue of the LID most flexible part is labeled as a yellow sphere. (F–G) Comparison of the Mhp1 crystal structure (gray) in the inward-open form (PDB 2x79) with the final structures of the four MD simulations of FurE. The two gates are indicated by arrow heads: intracellular gate L4 between TMS4–TMS5 and extracellular gate L9 between TMS9-TMS10. Notice that the outer gate L9 bends covering the binding cavity at pH 5.0 and 6.8, while it remains in open position in the Ala 24–28 mutant. Notice also that the intracellular TMS5 segment shows a propensity to bend, opening the inner gate in the LID mutant, but less apparent in the other three simulated structures.

evidence of the flexibility of the LID and the stability of the hydrogen bonds observed in the model. Fundamental to successful MD simulation of a transmembrane protein is the accurate lipid bilayer composition chosen. Here, based on data available for the composition of fungal PM, the lipid bilayer used was composed of 40% phosphatidylcholine 16:1/18:1 (YOPC), 20% Ergosterol (ERG), and 40% phosphatidylinositol lipids (POPI). To specifically address the pH-dependent specificity of FurE, we selected different phosphatidylinositol lipids to emulate different pH environments. For the acidic pH (5.0), POPI lipid models were selected with overall charge −1 (not phosphorylated inositol). For the neutral pH (6.8), 20% POPI and 20% monophosphorylated POPI on position 4 or 5 of inositol with overall charge −3 were mixed (POPI14 or POPI15 equally distributed). Finally, for the basic pH (8.0), we have selected 20% POPI and 20% diphosphorylated POPI on position 4 and 5 of inositol (POPI24 or POPI25 equally distributed), with overall charge −4. In addition, we ran MD simulations of the FurE mutant version where residues 24–28 of the LID were Ala substituted, using the lipid bilayer simulation for neutral pH (6.8). FurE was embedded on each lipid bilayer and solvated by explicit water molecules (TIP3P), and 100 ns of simulation has been calculated in all four cases.

The MD simulations reveal that the N-terminus is highly mobile between residues 20–28, that is, the LID, while the part proximal to TMS1 (residues 30–40) has much less flexibility. The RMSD of the backbone depicted in Fig. 7A shows that in all cases, except at pH 5.0, the LID is flexible after the first 30-ns period of simulation. Figure 7B–E and Supplementary Video 1 illustrate the significant motion of the LID residues 20–28 and the rather fixed position of downstream residues 29–40, which remain at

Please cite this article as: G. F. Papadaki, G. Lambrinidis, A. Zamanos, et al., Cytosolic N- and C-Termini of the *Aspergillus nidulans* FurE Transporter Contain Distinct Elements that Regulat..., Journal of Molecular Biology, https://doi.org/10.1016/j.jmb.2019.07.013

proximity with mostly L8, but also L2 and L10. It is interesting to notice that although the LID mutant (Ala substituted 24–28) was simulated using the lipid bilayer for neutral pH (6.8), it displays different and more flexible dynamic behavior compared to the wild type, which exhibits only minor deviation from the initial structure for more than the first part of the calculation revisiting positions close to it for the rest of the simulated time. The highest RMSD is attained in the simulation at pH 8.0, reaching 15 Å for most of the calculated time period. This might be due to the higher number of interactions of Lys25 with lipid molecules (Supplementary Fig. 2A), in addition to a role of other positively charged residues, such as Lys188 and Arg360, attracted to PIP2 molecules due to the negative charge of the phosphorylated phosphatidylinositol (Supplementary Fig. 2B). The apparent stability of the segment of residues 29–40 was in good agreement with the experimentally defined structures of Mhp1. The comparison between the two crystal structures, outward-open (2jln) and inward-open (2 × 79), presented in Supplementary Fig. 3 shows that only the segment upstream from the small bend at $P15^{Mhp1}$ is re-oriented in the inward position, thus relaxing the interaction between LID and L8 as TMS8 is also slightly bent, similarly to what has been shown for LeuT [34]. Although there are important differences between Mhp1 and LeuT in the mechanism of substrate translocation, it appears that the interruption of the contact between the N-terminus and L8 is common in both cases. Our results suggest that FurE displays the tendency to follow a motion more similar to that observed in Mhp1.

To better visualize and further understand the specific motions of the different helices during the MD simulation, we have investigated (a) the RMSD of each individual helix, (b) the corresponding tilt compared to the *Z*-axis, and (c) the distance of each axis center to that of TMS2, which is the TMS with less motion (Supplementary Fig. 4). The calculations show that at all pHs and for the LID mutant, helices TMS4, 5, 9 and 10 have a higher propensity to bend, specifically at the loops L4 and L9. The RMSD from the initial position calculated during the MD simulation shows that all four TMSs move away from the starting structure between 2 to 5 Å (Supplementary Fig. 4A–D). Differences between the four simulations are more pronounced in the case of TMS5, where it seems that in case of simulation of wild-type FurE at pH 8.0 and for the LID mutant (pH 6.8), the deviations are larger than those of wild-type FurE at pH 5.0 and 6.8. Similarly, highest deviations of the initial value are observed for the tilt of the helices compared to the *Z*-axis observed in the case of TMS5, with the LID mutant tilting in the opposite direction compared to the three different simulations of pH (Supplementary Fig. 4E–H). Finally, when comparing the distance of the axis between the four TMSs 4, 5, 9 and 10 with TMS2, again the highest variation was observed in the case of TMS5, where the mutant displays the highest deviation from the initial value, while the pH 5.0 simulation remains almost stable (Supplementary Fig. 4I–L). Importantly, the specific tendency is clearer when comparing the TMS5 and TMS9 with the inward open structure of Mhp1. In Fig. 7F–G, the final structures of each one of the four MD calculations are superimposed together with the inward-open Mhp1 structure (2 × 79). In all four cases, TMS5 bends toward the inward conformation, with the simulation of pH 8.0 approaching closer to the open structure of Mhp1. In the extracellular interface, TMS9 shows the highest deviation, with the LID mutant tending to remain in the outward-open conformation, while at all pH simulations, L9 is bent, as also found with the Mhp1 inward-open structure.

Overall, MD simulations suggest that the N-terminal LID exhibits relatively high flexibility at the initial part of calculations, more pronounced in the case of pH 8.0 and in the LID mutant, mainly driven from the stronger coulombic interactions between positively charged amino acid residues and negatively charged lipids. These interactions mostly influence putative contacts with L8 and TMS9, as shown in Fig. 7F–G. The proximity of TMS9 to TMS4 appears to be the main reason of a concerted influence to TMS4 and TMS5. The main conclusion from the above MD calculations is that LID motions can influence, in a pH-dependent manner, both the exterior and interior gates and thereby the substrate translocation and transporter specificity. What is also notable is that when the LID motions are higher, as in the case of pH 8.0 or in the LID mutant, FurE acts as a promiscuous transporter recognizing all possible substrates. It becomes more specific for uracil and allantoin as shown from lower pH simulations performed with the wild-type protein.

Specific C-terminal elements are necessary for endocytosis, transport activity and substrate specificity

In Papadaki *et al.* [46], we showed that truncation of the 30 last residues of the FurE C-terminus (FurE-Δ498–528) has a dual effect; it blocks endocytosis and leads to a specificity change, in particular loss of uric acid transport. A block of endocytosis of FurE is also achieved when we replace the most distal two lysines in the C-tail (K521, K522) with arginine residues (Supplementary Fig. 5). This strongly suggests that block in endocytosis in FurE-ΔC30 is primarily due to the lack of these two lysines that apparently act as ubiquitin acceptor residues. To better define the limits of C-terminal segments that affect endocytosis *versus* substrate specificity, we performed systematic Ala replacements of the last 30 residues of the FurE C-tail (Fig. 8A).

Please cite this article as: G. F. Papadaki, G. Lambrinidis, A. Zamanos, et al., Cytosolic N- and C-Termini of the *Aspergillus nidulans* FurE Transporter Contain Distinct Elements that Regulat..., Journal of Molecular Biology, https://doi.org/10.1016/j.jmb.2019.07.013

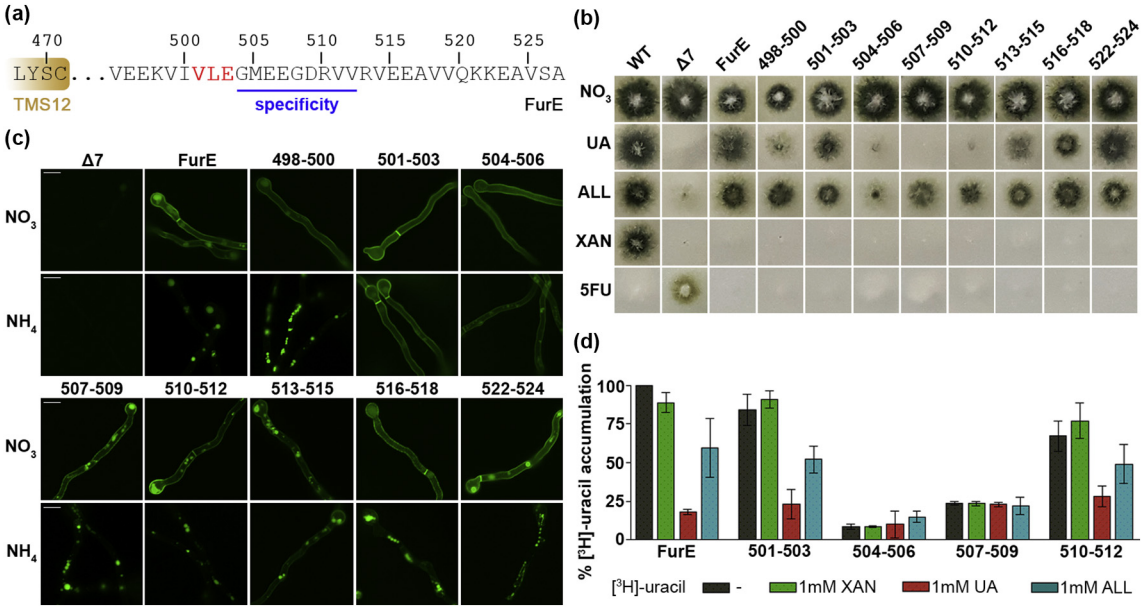

Fig. 8. Systematic mutational analysis of the C-terminus defines the limits of elements necessary for endocytosis, transport activity and substrate specificity. (A) Sequence of the cytosolic distal C-terminal region of FurE (495–527). The residues involved in endocytosis are highlighted in red, and the region involved in substrate specificity determination is underlined, as evidenced in panels B and C. (B) Growth tests of control strains and FurE mutants expressing triple Ala substitutions in the FurE C-terminal region. Each mutant is named after the position of residues replaced. Notice that mutants 504–506, 507–509 and 510–512 have totally lost the ability to grow on UA, while 513–515 has reduced growth on UA. Mutant 504–506 has also significantly reduced ability to grow on ALL and is partially resistant to 5FU, signifying that this mutant is a nearly loss-of-function mutant overall. Details are as in Fig. 1B. (C) Epifluorescence microscopy of the mutants shown in panel A. Notice that in the absence of an endocytic signal (NO_3 panel), all FurE mutants are normally localized in the PM. However, in mutants 501–503 and 504–506, FurE shows increased stability with no sign of steady-state vacuolar turnover, as in the wild-type FurE or the other mutants. This is in line with the observation that in these mutants, and particularly in 501–503, FurE is also resistant to NH_4^+-elicited endocytosis, suggesting that the sequence V-L-E is a primary element necessary for endocytosis. Finally, the fact that the following sequence G-M-E (504–506) is critical for the transport of all substrates (as shown in panel B) reveals that this element is absolutely essential for the transport mechanism of FurE per se. Scale bars represent 5 μm. (D) Accumulation of [^{3}H]-uracil in the simultaneous presence of excess (1 mM) of various substrates as indicated. Details are as in Fig. 2C. Standard deviation is depicted with error bars.

Figure 8B and C shows that triple Ala replacements in the C-terminus affect transport activity, specificity and endocytic turnover of FurE. Ala substitutions of 504–506, 507–509 and 510–512 abolished the ability for growth on uric acid. Mutations in 504–506 also had a strong reducing effect on growth on allantoin and led to partial resistance to 5FU, showing that the sequence G-M-E is absolutely essential for transport activity per se. Ala substitutions in 513–515 had a moderate effect on uric acid growth. Finally, Ala mutations in the distal C-tail (516–524) had no apparent effect on FurE function. These findings showed that the C-tail is critical for both transport activity (504–506) and specificity 507–512 (Fig. 8A). In respect to NH_4^+-elicited endocytosis, Ala mutations in 501–503 were sufficient to totally block endocytosis, similarly to deletion of the C30 segment. Partial abolishment of endocytosis was also observed with Ala mutations in 504–506 and 513–518, which might be due to an indirect effect on the topology of 501–503 (Fig. 8B).

We also performed radiolabel uracil uptake or competition assays for mutations 501–503, 504–506, 507–509 and 510–512, which seemed to define functional or specificity elements in FurE. Mutations 501–503 and 510–512 conserved 68%–80% of the wild-type FurE transport activity, but mutations 504–506 and 507–509 showed significantly reduced activities (~11%–20%; see gray bars in Fig. 8D). In competition assays, mutation 501–503 behaved similarly to the strain expressing wild-type FurE and reflected a significant (~75%) inhibition by excess uric acid (i.e., a high-affinity substrate), moderate (~39%) inhibition by allantoin (i.e., a low-affinity substrate), and no inhibition by xanthine (i.e., a non-substrate). Mutant 510–512 showed reduced inhibition by either uric acid or allantoin compared to wild-type FurE. Finally, mutations 504–506 and 507–509 showed practically no measurable binding of uric acid, allantoin or xanthine, which is in agreement with growth tests showing no or very little growth on these purines. Thus, direct uptake measurements

Please cite this article as: G. F. Papadaki, G. Lambrinidis, A. Zamanos, et al., Cytosolic N- and C-Termini of the *Aspergillus nidulans* FurE Transporter Contain Distinct Elements that Regulat..., Journal of Molecular Biology, https://doi.org/10.1016/j.jmb.2019.07.013

further confirmed that residues 504–512 are important for the function and specificity of FurE, while residues that affect endocytosis (501–503) are not critical for function or specificity.

Discussion

The importance of cytosolic termini in membrane trafficking processes has been well documented in several structurally, functionally and evolutionary distinct eukaryotic transporters, such as those specific for amino acids [8,15,18,50], glucose [4,5,14,26], carboxylic acids [3,13], L-ascorbic acid [38,58], nucleobases [27] or nucleosides [11,49]. In some cases, cytosolic termini are also known to affect the basic transport mechanism [7,14,19,31,40,42,51,56,57,64]. However, in no case, except FurE [46], have cytosolic termini been shown to control substrate *specificity* (for a recent review, see Ref. [44]). Here we provide new evidence and a mechanistic rationale on how cytosolic termini affect specificity through regulation of selective gating. First, using a systematic reverse genetic approach, we topologically and functionally defined the segments of the N- and C-termini that play distinct roles in trafficking, endocytosis or transport function per se. Subsequently, we show, based on unbiased genetic screens and dynamic modeling approaches that the N-terminus of FurE interacts with several internal loops and with the C-terminus, and we identify specific residues crucial for these interactions by systematic mutational analysis. Finally, we show, through extensive MD simulations that interactions of termini with internal loops are "allosterically" transmitted to the opening and closing of gates.

Interestingly, N- and C-terminal elements of FurE affected both endocytosis and transport specificity. A critical point in our study was to uncouple the role of distinct terminal elements in these two processes. Thus, endocytosis was found to require, in addition to K521 and K522 that act as ubiquitylation sites, a short C-terminal sequence M-E–E (residues 501–503) and elements within the distal part of the N-terminus (1–21). The need of both terminal segments of FurE for proper endocytic turnover, apparently via a mechanism that involves their dynamic cross-talk [46], helps to explain how specific conformational changes associated with the transition from an outward to an inward conformation are related with endocytic turnover [9,18]. In a simplified model, when the distal cytosolic termini interact closely with each other and other internal loops, the transporter is found in an outward-facing conformation, while when the interactions of termini and other loops becomes relaxed, the transporter is free to alternate in an inward-facing conformation, open to the cytosolic side. This in turn suggests that relaxation of the tight interaction of the N- and C-terminal regions associated with the inward-facing conformation produces a specific conformation more attractive for endocytic turnover. It seems reasonable to propose that N- and C-terminal sequences co-operatively and dynamically regulate the recruitment of the ubiquitylation machinery (e.g., accessibility of arrestin adaptors), which precedes endocytic turnover.

Delimiting the role of terminal elements in FurE endocytosis helped in defining the exact sequences in the two cytosolic termini that are crucial for determining substrate specificity, namely, residues 15–31 in the N-terminus and 504–512 in the C-terminus. While work from other groups has shown that cytosolic termini might be critical for overall transport activity, apparently through their effect on the alteration from an outward to an inward topology [7,19,31,42,51,56,57], this does not seem to be the case of FurE, where relevant terminal truncations or mutations affect specificity, rather than overall transport activity. This in turn suggests that specific terminal elements finely regulate the process of gating, rather than the basic alteration from outward to inward conformation.

The proposed interactions of the N-terminal region, and in particular of the LID, with specific internal loops provide a rationale on how the role of termini might be transmitted to the opening and closing of gates along the substrate translocating trajectory. More specifically, MD simulations provided evidence that the LID and consequently LID mutations affect, in pH-dependent manner, the relative topology of TMS9-TMS10 (outer gate) and TMS4–TMS5 (inner gate). It should be noted that in our simulations the influence of the charges on the lipid membrane was of crucial importance for approximation of different pHs. Experimental determination of the exact lipid composition of *A. nidulans* PM will be needed to validate our current approach.

Interestingly, FurE proved to function as a rather specific 5FU/uracil transporter at low pH, but as the pH increases, FurE becomes progressively more promiscuous, also transporting uric acid and allantoin, and eventually xanthine. Given that FurE versions carrying LID mutations mimic the specificity profile of the wild-type FurE at high pH, the relevant mutations seem to lead to loosening of gating, and thus to increased promiscuity in substrate selection. The relative MD analysis of the wild-type and mutant versions of FurE further supported the idea that stricter gating, which leads restricted specificity, is associated with tighter interactions of the cytosolic tails with internal loops. On the contrary, relaxed gating, which leads to transport of increased number of substrates, is associated with loosening of the tight interaction of tails with the main body of the transporter.

Please cite this article as: G. F. Papadaki, G. Lambrinidis, A. Zamanos, et al., Cytosolic N- and C-Termini of the *Aspergillus nidulans* FurE Transporter Contain Distinct Elements that Regulat..., Journal of Molecular Biology, https://doi.org/10.1016/j.jmb.2019.07.013

Materials and Methods

Media, strains and growth conditions

Standard complete (CM) and minimal media (MM) for *A. nidulans* growth were used. Media and supplemented auxotrophies were used at the concentrations given in http://www.fgsc.net. Glucose 1% (w/v) was used as carbon source. Ammonium tartrate (NH_4; 10 mM) or sodium nitrate (NO_3) was used as nitrogen source. Nucleobases and analogues were used at the following final concentrations: 5FU 100 μM, uric acid (UA) 0.5 mM, xanthine (XAN) and allantoin (ALL) 1 mM. All media and chemical reagents were obtained from Sigma-Aldrich (Life Science Chemilab SA, Hellas) or AppliChem (Bioline Scientific SA, Hellas). A *ΔfurD::riboB ΔfurA::riboB ΔfcyB::argB ΔazgA ΔuapA ΔuapC::AfpyrG ΔcntA::riboB pabaA1 pantoB100* mutant strain, named Δ7, was the recipient strain in transformations with plasmids carrying *fur* genes or alleles based on complementation of the pantothenic acid auxotrophy *pantoB100* [36]. The Δ7 strain has an intact endogenous FurE gene transporter, but this is very little expressed under standard conditions and thus does not contribute to detectable transport of its physiological substrates (UA, ALL) or to sensitivity in 5FU [37]. *A. nidulans* protoplast isolation and transformation was performed as previously described [32]. Growth tests were performed at 37 °C for 48 h, at pH 6.8 or at pH 5.0 and pH 8.0 where indicated.

Standard molecular biology manipulations and plasmid construction

Genomic DNA extraction from *A. nidulans* was performed as described in FGSC (http://www.fgsc.net). Plasmids, prepared in *Escherichia coli*, and DNA restriction or PCR fragments were purified from agarose 1% gels with the Nucleospin Plasmid Kit or Nucleospin ExtractII kit, according to the manufacturer's instructions (Macherey–Nagel, Lab Supplies Scientific SA, Hellas). Standard PCR reactions were performed using KAPATaq DNA polymerase (Kapa Biosystems). PCR products used for cloning, sequencing and re-introduction by transformation in *A. nidulans* were amplified by a high-fidelity KAPA HiFi HotStart Ready Mix (Kapa Biosystems) polymerase. DNA sequences were determined by VBC-Genomics (Vienna, Austria). Site-directed mutagenesis was carried out according to the instructions accompanying the Quik-Change® Site-Directed Mutagenesis Kit (Agilent Technologies, Stratagene). The principal vector used for most *A. nidulans* mutants is a modified pGEM-T-easy vector carrying a version of the *gpdA* promoter, the *trpC* 3′ termination region and the panB selection marker [37]. Mutations and segment truncations in Fur transporters were constructed by oligonucleotide-directed mutagenesis or appropriate forward and reverse primers (Table S2). Transformants arising from single copy integration events with intact Fur ORFs were identified by Southern and PCR analysis.

Uptake assays

Kinetic analysis of Fur transporters activity was measured by estimating uptake rates of [^{3}H]-uracil uptake (40 Ci mmol^{-1}, Moravek Biochemicals, CA, USA), as previously described by Krypotou and Diallinas [36]. In brief, [^{3}H]-uracil uptake was assayed in *A. nidulans* conidiospores germinating for 4 h at 37 °C, at 140 rpm, in liquid MM (pH 6.8). Initial velocities were measured on 10^7 conidiospores/100 μL by incubation with concentrations of 0.2–2.0 μM of [^{3}H]-uracil at 37 °C. For the competition experiments, initial uptake rates of [^{3}H]-uracil were measured in the simultaneous presence of excess (1 mM) of various putative substrates as indicated. The time of incubation was defined through time-course experiments at 4 min, when the transporter showed linear increased activity. All transport assays were carried out at least in two independent experiments and the measurements in triplicate. Standard deviation was <20%. Results were analyzed in GraphPad Prism software.

Isolation and characterization of suppressor mutations

Suppressor mutations of 10^9 conidiospores of the strain S15A/L16A were obtained after 3-min 45-s exposure at a standard distance of 20 cm from an Osram HNS30 UV-B/C lamp and subsequent selection of colonies capable of growing on MM containing uric acid as sole nitrogen source, at 25 °C. Spores from positive colonies were collected after 6–8 days and further isolated on the same selective medium that was used to obtain the original colonies. Genomic DNA from 24 purified colonies was isolated and the ORF of FurE was amplified and sequenced. In all cases, the amplified fragments contained a new mutation.

Epifluorescence microscopy

Samples for standard epifluorescence microscopy were prepared as previously described [16,27]. In brief, sterile 35-mm l-dishes with a glass bottom (Ibidi, Germany) containing liquid minimal media supplemented with $NaNO_3$ and 0.1% glucose were inoculated from a spore solution and incubated for 18 h at 25 °C. The samples were observed on an Axioplan Zeiss phase contrast epifluorescent microscope, and the resulting images were acquired with

Please cite this article as: G. F. Papadaki, G. Lambrinidis, A. Zamanos, et al., Cytosolic N- and C-Termini of the *Aspergillus nidulans* FurE Transporter Contain Distinct Elements that Regulat..., Journal of Molecular Biology, https://doi.org/10.1016/j.jmb.2019.07.013

a Zeiss-MRC5 digital camera using the AxioVs40 V4.40.0 software. Image processing and contrast adjustment were made using the ZEN 2012 software, while further processing of the TIFF files was made using Adobe Photoshop CS3 software for brightness adjustment, rotation and alignment.

Homology modeling

The construction of a structural model of FurE was based on the crystal structure of the Mhp1 benzylhydantoin permease from *Microbacterium liquefaciens* in the outward-open structure (PDB entry 2JLN). We utilized as starting alignment the one already described by our group [37] and optimized based on mutation analysis data (Supplementary Fig. 1). The final model was built using PRIME software with an energy-based algorithm [23]. A loop refinement routine was also implemented.

Molecular dynamics

FurE was inserted into a lipid bilayer using the CHARMM-GUI tool [63]. The resulting system was explicitly solvated using the TIP3P water model [24] and neutralized by the addition of Na^+ and Cl^- counter ions at concentration of 0.15 M. For the acidic pH (5.0) emulation, the lipid bilayer used was composed of 40% phosphatidylcholine 16:1/18:1 (YOPC), 20% Ergosterol (ERG) and 40% POPI lipid models, which were selected with an overall charge −1 (not phosphorylated inositol). For the neutral pH (6.8) emulation, the lipid bilayer used was composed of 40% phosphatidylcholine 16:1/18:1 (YOPC), 20% Ergosterol (ERG), and 20% POPI and 20% monophosphorilated POPI on position 4 or 5 of inositol (POPI14 or POPI15 was equally distributed), with an overall charge of −3. Finally, for the basic pH (8.0) emulation, the lipid bilayer used was composed of 40% phosphatidylcholine 16:1/18:1 (YOPC), 20% Ergosterol (ERG), 20% POPI and 20% di-phosphorylated POPI on position 4 and 5 of inositol (POPI24 or POPI25 was equally distributed), with an overall charge of −4. For the FurE LID mutant (24–28 Ala substitution), we utilized the pH 6.8 lipid bilayer emulation described above. Starting from wild-type FurE, on CHARMM-GUI's initial step "PDB Manipulation Options," we mutated residues 24–28 to alanines. In all cased, FurE was embedded on each lipid bilayer and solvated by explicit water molecules (TIP3P). The N-terminal residue (Ala20) was methylated and the C-terminus residue (Glu507) was amidated. All MD simulations were performed with GROMACS 2018 [1] using the all-atom force-field CHARMM36 [20]. Periodic boundary conditions were used. Long-range electrostatic interactions were treated with Particle Mesh Ewald method. Non-bonded interactions were described with a Lennard–Jones potential with a cut-off distance of 1 nm, and an integration step of 2 fs was implemented. The system was progressively minimized and equilibrated using the GROMACS input scripts generated by CHARMM-GUI, and the temperature and pressure were held at 303.15 K and 1 bar, respectively [39]. The resulting equilibrated structures were then used as an initial condition for the production runs of 100 ns, with all the constraints turned off. Production runs were subsequently analyzed using GROMACS tools, and all images and videos were prepared using VMD software [21].

Supplementary data to this article can be found online at https://doi.org/10.1016/j.jmb.2019.07.013.

Acknowledgments

We are grateful to Prof. Richard Naftalin for text corrections and scientific comment. This work was supported by a "Stavros S. Niarchos Foundation" grant and by computational time granted from the Greek Research & Technology Network in the National HPC facility—ARIS—under project NCS1_Mechanism (pr006040).

Author Contributions: G.F.P. performed all genetic and molecular experiments. A.Z., G.L. and E.M. performed the *in silico* analysis and the molecular dynamics, and analyzed results. E.M. wrote parts of the article. G.D. conceived and planned experiments analyzed results and wrote the article.

Conflict of Interest: The authors declare that they have no conflict of interest.

Received 3 April 2019;
Received in revised form 4 July 2019;
Accepted 4 July 2019
Available online xxxx

Keywords:
Aspergillus nidulans;
fungi;
transport;
folding;
membrane lipids!

Abbreviations used:
NCS1, nucleobase cation symporter 1; TMS, transmembrane α-helical segment; MD, molecular dynamics; LID, loop interacting domain; 5FU, 5-fluorouracil.

References

[1] M.J. Abraham, T. Murtola, R. Schulz, S. Páll, J.C. Smith, B. Hess, E. Lindahl, GROMACS: high performance molecular

simulations through multi-level parallelism from laptops to supercomputers, SoftwareX 1–2 (2015) 19–25.
[2] J.L. Adelman, A.L. Dale, M.C. Zwier, D. Bhatt, L.T. Chong, D. M. Zuckerman, M. Grabe, Simulations of the alternating access mechanism of the sodium symporter Mhp1, Biophys. J. 101 (2011) 2399–2407.
[3] Becuwe M, Léon S (2014) Integrated control of transporter endocytosis and recycling by the arrestin-related protein Rod1 and the ubiquitin ligase Rsp5. *Elife* 3.
[4] P.D. Brewer, E.N. Habtemichael, I. Romenskaia, C.C. Mastick, A.C. Coster, Insulin-regulated Glut4 translocation: membrane protein trafficking with six distinctive steps, J. Biol. Chem. 289 (2014) 17280–17298.
[5] F.M. Brodsky, Diversity of clathrin function: new tricks for an old protein, Annu. Rev. Cell Dev. Biol. 28 (2012) 309–336.
[6] A.N. Calabrese, S.M. Jackson, L.N. Jones, O. Beckstein, F. Heinkel, J. Gsponer, D. Sharples, M. Sans, M. Kokkinidou, A. R. Pearson, S.E. Radford, A.E. Ashcroft, P.J.F. Henderson, Topological dissection of the membrane transport protein Mhp1 derived from cysteine accessibility and mass spectrometry, Anal. Chem. 89 (2017) 8844–8852.
[7] M.H. Cheng, I. Bahar, Complete mapping of substrate translocation highlights the role of LeuT N-terminal segment in regulating transport cycle, PLoS Comput. Biol. 10 (2014), e1003879.
[8] M. Crapeau, A. Merhi, B. André, Stress conditions promote yeast Gap1 permease ubiquitylation and down-regulation via the arrestin-like Bul and Aly proteins, J. Biol. Chem. 289 (2014) 22103–22116.
[9] G. Diallinas, Dissection of transporter function: from genetics to structure, Trends Genet. 32 (2016) 576–590.
[10] D. Drew, O. Boudker, Shared molecular mechanisms of membrane transporters, Annu. Rev. Biochem. 85 (2016) 543–572.
[11] E. Errasti-Murugarren, F.J. Casado, M. Pastor-Anglada, Different N-terminal motifs determine plasma membrane targeting of the human concentrative nucleoside transporter 3 in polarized and nonpolarized cells, Mol. Pharmacol. 78 (2010) 795–803.
[12] L.R. Forrest, G. Rudnick, The rocking bundle: a mechanism for ion-coupled solute flux by symmetrical transporters, Physiology (Bethesda) 24 (2009) 377–386.
[13] S. Fujita, D. Sato, H. Kasai, M. Ohashi, S. Tsukue, Y. Takekoshi, K. Gomi, T. Shintani, The C-terminal region of the yeast monocarboxylate transporter Jen1 acts as a glucose signal-responding degron recognized by the α-arrestin Rod1, J. Biol. Chem. 293 (2018) 10926–10936.
[14] T. Galochkina, M. Ng Fuk Chong, L. Challali, S. Abbar, C. Etchebest, New insights into GluT1 mechanics during glucose transfer, Sci. Rep. 9 (1) (2019) 998.
[15] K. Ghaddar, A. Merhi, E. Saliba, E.M. Krammer, M. Prévost, B. André, Substrate-induced ubiquitylation and endocytosis of yeast amino acid permeases, Mol. Cell. Biol. 34 (2014) 4447–4463.
[16] C. Gournas, S. Amillis, A. Vlanti, G. Diallinas, Transport-dependent endocytosis and turnover of a uric acid-xanthine permease, Mol. Microbiol. 75 (2010) 246–260.
[18] C. Gournas, M. Prévost, E.M. Krammer, B. André, Function and regulation of fungal amino acid transporters: insights from predicted structure, Adv. Exp. Med. Biol. 892 (2016) 69–106.
[19] B. Guptaroy, M. Zhang, E. Bowton, F. Binda, L. Shi, H. Weinstein, A. Galli, J.A. Javitch, R.R. Neubig, M.E. Gnegy, A juxtamembrane mutation in the N terminus of the dopamine transporter induces preference for an inward-facing conformation, Mol. Pharmacol. 75 (2009) 514–524.
[20] J. Huang, A.D. MacKerell Jr., CHARMM36 all-atom additive protein force field: validation based on comparison to NMR data, J. Comput. Chem. 34 (2013) 2135–2145.
[21] W. Humphrey, A. Dalke, K. Schulten, VMD—visual molecular dynamics, J Molec Graphics 14 (1996) 33–38.
[22] H. Ilgü, J.M. Jeckelmann, V. Gapsys, Z. Ucurum, B.L. de Groot, D. Fotiadis, Insights into the molecular basis for substrate binding and specificity of the wild-type L-arginine/agmatine antiporter AdiC, Proc. Natl. Acad. Sci. U. S. A. 113 (2016) 10358–10363.
[23] Jacobson MP, Pincus DL, Rapp CS, Day TJ, Honig B, Shaw DE, Friesner RA (2004) A hierarchical approach to all-atom protein loop prediction. *Proteins* 55: 351-367
[24] W.L. Jorgensen, J. Chandrasekhar, J.D. Madura, R.W. Impey, M.L. Klein, Comparison of simple potential functions for simulating liquid water, J. Chem. Phys. 79 (1983) 926–935.
[25] H.R. Kaback, I. Smirnova, V. Kasho, Y. Nie, Y. Zhou, The alternating access transport mechanism in LacY, J. Membr. Biol. 239 (2011) 85–93.
[26] K.V. Kandror, P.F. Pilch, The sugar is sIRVed: sorting Glut4 and its fellow travelers, Traffic 12 (2011) 665–671.
[27] M. Karachaliou, S. Amillis, M. Evangelinos, A.C. Kokotos, V. Yalelis, G. Diallinas, The arrestin-like protein ArtA is essential for ubiquitination and endocytosis of the UapA transporter in response to both broad-range and specific signals, Mol. Microbiol. 88 (2013) 301–317.
[28] K. Kazmier, D.P. Claxton, H.S. Mchaourab, Alternating access mechanisms of LeuT-fold transporters: trailblazing towards the promised energy landscapes, Curr. Opin. Struct. Biol. 45 (2017) 100–108.
[29] K. Kazmier, S. Sharma, S.M. Islam, B. Roux, H.S. Mchaourab, Conformational cycle and ion-coupling mechanism of the Na^+/hydantoin transporter Mhp1, Proc. Natl. Acad. Sci. U. S. A. 111 (2014) 14752–14757.
[30] J.M. Keener, M. Babst, Quality control and substrate-dependent downregulation of the nutrient transporter Fur4, Traffic 14 (2013) 412–427.
[31] G. Khelashvili, M. Doktorova, M.A. Sahai, N. Johner, L. Shi, H. Weinstein, Computational modeling of the N-terminus of the human dopamine transporter and its interaction with PIP2-containing membranes, Proteins 83 (2015) 952–969.
[32] M. Koukaki, E. Giannoutsou, A. Karagouni, G. Diallinas, A novel improved method for *Aspergillus nidulans* transformation, J. Microbiol. Methods 55 (2003) 687–695.
[33] H. Krishnamurthy, C.L. Piscitelli, E. Gouaux, Unlocking the molecular secrets of sodium-coupled transporters, Nature 459 (2009) 347–355.
[34] H. Krishnamurthy, E. Gouaux, X-ray structures of LeuT in substrate-free outward-open and apo inward-open states, Nature 481 (2012) 469–474.
[35] E. Krypotou, V. Kosti, S. Amillis, V. Myrianthopoulos, E. Mikros, G. Diallinas, Modeling, substrate docking, and mutational analysis identify residues essential for the function and specificity of a eukaryotic purine-cytosine NCS1 transporter, J. Biol. Chem. 287 (2012) 36792–36803.
[36] E. Krypotou, G. Diallinas, Transport assays in filamentous fungi: kinetic characterization of the UapC purine transporter of *Aspergillus nidulans*, Fungal Genet. Biol. 63 (2014) 1–8.
[37] E. Krypotou, T. Evangelidis, J. Bobonis, A.A. Pittis, T. Gabaldón, C. Scazzocchio, E. Mikros, G. Diallinas, Origin,

Please cite this article as: G. F. Papadaki, G. Lambrinidis, A. Zamanos, et al., Cytosolic N- and C-Termini of the *Aspergillus nidulans* FurE Transporter Contain Distinct Elements that Regulat..., Journal of Molecular Biology, https://doi.org/10.1016/j.jmb.2019.07.013

diversification and substrate specificity in the family of NCS1/FUR transporters, Mol. Microbiol. 96 (2015) 927–950.
[38] S.M. Kuo, L.Y. Wang, S. Yu, C.E. Campbell, S.A. Valiyaparambil, M. Rance, K.M. Blumenthal, The N-terminal basolateral targeting signal unlikely acts alone in the differential trafficking of membrane transporters in MDCK cells, Biochemistry 52 (2013) 5103–5116.
[39] J. Lee, X. Cheng, J.M. Swails, M.S. Yeom, P.K. Eastman, J. A. Lemkul, S. Wei, J. Buckner, J.C. Jeong, Y. Qi, S. Jo, V.S. Pande, D.A. Case, C.L. Brooks 3rd, A.D. MacKerell Jr., J.B. Klauda, W. Im, CHARMM-GUI input generator for NAMD, GROMACS, AMBER, OpenMM, and CHARMM/OpenMM simulations using the CHARMM36 additive force field, J. Chem. Theory Comput. 12 (2016) 405–413.
[40] D. Ma, P. Lu, Y. Shi, Substrate selectivity of the acid-activated glutamate/γ-aminobutyric acid (GABA) antiporter GadC from *Escherichia coli*, J. Biol. Chem. 288 (2013) 15148–15153.
[41] P. Ma, S.G. Patching, E. Ivanova, J.M. Baldwin, D. Sharples, S.A. Baldwin, P.J. Henderson, Allantoin transport protein, PucI, from *Bacillus subtilis*: evolutionary relationships, amplified expression, activity and specificity, Microbiology 162 (2016) 823–836.
[42] L. Malinauskaite, M. Quick, L. Reinhard, J.A. Lyons, H. Yano, J.A. Javitch, P. Nissen, A mechanism for intracellular release of Na^+ by neurotransmitter/sodium symporters, Nat. Struct. Mol. Biol. 21 (2014) 1006–1012.
[44] E. Mikros, G. Diallinas, Tales of tails in transporters, Open Biol. 9 (6) (2019) 190083.
[45] A. Pantazopoulou, N.D. Lemuh, D.G. Hatzinikolaou, C. Drevet, G. Cecchetto, C. Scazzocchio, G. Diallinas, Differential physiological and developmental expression of the UapA and AzgA purine transporters in *Aspergillus nidulans*, Fungal Genet. Biol. 44 (2007) 627–640.
[46] G.F. Papadaki, S. Amillis, G. Diallinas, Substrate specificity of the FurE transporter is determined by cytoplasmic terminal domain interactions, Genetics 207 (2017) 1387–1400.
[47] I. Papageorgiou, C. Gournas, A. Vlanti, S. Amillis, A. Pantazopoulou, G. Diallinas, Specific interdomain synergy in the UapA transporter determines its unique specificity for uric acid among NAT carriers, J. Mol. Biol. 382 (2008) 1121–1135.
[48] S.G. Patching, Recent developments in nucleobase cation symporter-1 (NCS1) family transport proteins from bacteria, archaea, fungi and plants, J. Biosci. 43 (2018) 797–815.
[49] I. Pinilla-Macua, F.J. Casado, M. Pastor-Anglada, Structural determinants for rCNT2 sorting to the plasma membrane of polarized and non-polarized cells, Biochem. J. 442 (2012) 517–525.
[50] D. Popov-Čeleketić, F. Bianchi, S.J. Ruiz, F. Meutiawati, B. Poolman, A plasma membrane association module in yeast amino acid transporters, J. Biol. Chem. 291 (2016) 16024–16037.
[51] A.M. Razavi, G. Khelashvili, H. Weinstein, How structural elements evolving from bacterial to human SLC6 transporters enabled new functional properties, BMC Biol. 16 (2018) 31.
[52] Y. Shi, Common folds and transport mechanisms of secondary active transporters, Annu. Rev. Biophys. 42 (2013) 51–72.
[53] T. Shimamura, S. Weyand, O. Beckstein, N.G. Rutherford, J. M. Hadden, D. Sharples, M.S. Sansom, S. Iwata, P.J. Henderson, A.D. Cameron, Molecular basis of alternating access membrane transport by the sodium-hydantoin transporter Mhp1, Science 328 (2010) 470–473.
[54] K.J. Simmons, S.M. Jackson, F. Brueckner, S.G. Patching, O. Beckstein, E. Ivanova, T. Geng, S. Weyand, D. Drew, J. Lanigan, D.J. Sharples, M.S. Sansom, S. Iwata, C.W. Fishwick, A.P. Johnson, A.D. Cameron, P.J. Henderson, Molecular mechanism of ligand recognition by membrane transport protein, Mhp1, EMBO J. 33 (2014) 1831–1844.
[55] G. Sioupouli, G. Lambrinidis, E. Mikros, S. Amillis, G. Diallinas, Cryptic purine transporters in *Aspergillus nidulans* reveal the role of specific residues in the evolution of specificity in the NCS1 family, Mol. Microbiol. 103 (2017) 319–332.
[56] S. Sucic, S. Dallinger, B. Zdrazil, R. Weissensteiner, T.N. Jørgensen, M. Holy, O. Kudlacek, S. Seidel, J.H. Cha, U. Gether, A.H. Newman, G.F. Ecker, M. Freissmuth, H.H. Sitte, The N terminus of monoamine transporters is a lever required for the action of amphetamines, J. Biol. Chem. 285 (2010) 10924–10938.
[57] C.G. Sweeney, B.P. Tremblay, T. Stockner, H.H. Sitte, H.E. Melikian, Dopamine transporter amino and carboxyl termini synergistically contribute to substrate and inhibitor affinities, J. Biol. Chem. 292 (2017) 1302–1309.
[58] S. Varma, K. Sobey, C.E. Campbell, S.M. Kuo, Hierarchal contribution of N- and C-terminal sequences to the differential localization of homologous sodium-dependent vitamin C transporters, SVCT1 and SVCT2, in epithelial cells, Biochemistry 48 (2009) 2969–2980.
[59] Å. Västermark, M.H. Saier Jr., Evolutionary relationship between 5 + 5 and 7 + 7 inverted repeat folds within the amino acid-polyamine-organocation superfamily, Proteins 82 (2014) 336–346.
[60] A. Vlanti, G. Diallinas, The *Aspergillus nidulans* FcyB cytosine–purine scavenger is highly expressed during germination and in reproductive compartments and is downregulated by endocytosis, Mol. Microbiol. 68 (2008) 959–977.
[61] S. Weyand, T. Shimamura, S. Yajima, S. Suzuki, O. Mirza, K. Krusong, E.P. Carpenter, N.G. Rutherford, J.M. Hadden, J. O'Reilly, P. Ma, M. Saidijam, S.G. Patching, R.J. Hope, H.T. Norbertczak, P.C. Roach, S. Iwata, P.J. Henderson, A.D. Cameron, Structure and molecular mechanism of a nucleobase-cation-symport-1 family transporter, Science 322 (2008) 709–713.
[62] F.H. Wong, J.S. Chen, V. Reddy, J.L. Day, M.A. Shlykov, S. T. Wakabayashi, M.H. Saier Jr., The amino acid-polyamine-organocation superfamily, J. Mol. Microbiol. Biotechnol. 22 (2012) 105–113.
[63] E.L. Wu, X. Cheng, S. Jo, H. Rui, K.C. Song, E.M. Dávila-Contreras, Y. Qi, J. Lee, V. Monje-Galvan, R.M. Venable, J. B. Klauda, W. Im, CHARMM-GUI membrane builder toward realistic biological membrane simulations, J. Comput. Chem. 35 (2014) 1997–2004.
[64] J.V. Busto, A. Elting, D. Haase, F. Spira, J. Kuhlman, M. Schäfer-Herte, R. Wedlich-Söldner, Lateral plasma membrane compartmentalization links protein function and turnover, EMBO J. 37 (16) (2018 Aug 15)https://doi.org/10.15252/embj.201899473.

Please cite this article as: G. F. Papadaki, G. Lambrinidis, A. Zamanos, et al., Cytosolic N- and C-Termini of the *Aspergillus nidulans* FurE Transporter Contain Distinct Elements that Regulat..., Journal of Molecular Biology, https://doi.org/10.1016/j.jmb.2019.07.013